



Synthesis and structural characterization of new alkali metal, alkaline earth metal, and lanthanide complexes with 1,4-diazabutadiene ligands

Dissertation

zur Erlangung des akademischen Grades

doctor rerum naturalium

(Dr. rer. nat.)

von **M.Phil. Ramesh Duraisamy**

geboren am 23.06.1986, in Salem (Indien)

genehmigt durch die Fakultät für Verfahrens- und Systemtechnik
der Otto-von-Guericke-Universität Magdeburg

Promotionskommission: Prof. Dr. rer. nat. habil. Dieter Schinzer (Vorsitz)
Prof. Dr. rer. nat. habil. Frank T. Edlmann (Gutachter)
Prof. Dr. rer. nat. habil. Matthias Westerhausen (Gutachter)

eingereicht am: 06.05.2019

Promotionskolloquium am: 01.08.2019

List of Abbreviations

Me ² DAD ^{Dipp}	<i>N,N'</i> -bis(2,6-diisopropylphenyl)-2,3-dimethyl-1,4-diaza-1,3-butadiene
H ² DAD ^{Dipp}	<i>N,N'</i> -bis(2,6-diisopropylphenyl)-1,4-diaza-1,3-butadiene
H ² DAD ^{Ad}	<i>N,N'</i> -bis(adamantyl)-1,4-diaza-1,3-butadiene
Me ² DAD ^{Mes}	<i>N,N'</i> -bis(2,4,6-trimethylphenyl)-2,3-dimethyl-1,4-diaza-1,3-butadiene
H ² DAD ^{Mes}	<i>N,N'</i> -bis(2,4,6-trimethylphenyl)-1,4-diaza-1,3-butadiene
Cy-Pyr	1-cyclohexyl-5-(cyclohexylimino)-2-methylene-2,5-dihydro-1 <i>H</i> -pyrrol-3-yl
iPr-Pyr	1-isopropyl-5-(isopropylimino)-2-methylene-2,5-dihydro-1 <i>H</i> -pyrrol-3-yl
Dipp	2,6-diisopropylphenyl group
Mes	2,4,6-trimethylphenyl group
Ad	adamantyl group
Me	methyl group
ⁱ Pr	isopropyl group
Cy	cyclohexyl group
Ar	aromatic group
THF	tetrahydrofuran
DME	1,2-dimethoxyethane
TMEDA	tetramethylethylenediamine
TMS	tetramethylsilane
NMR	nuclear magnetic resonance
HSQC	heteronuclear single quantum correlation
MS	mass spectrometry
IR	infrared
EI	electron impact
Cat.	catalyst
δ	chemical shift
ppm	parts per million
s	singlet
d	doublet
t	triplet
sept	septet
m	multiplet
et al.	and others
e.g.	for example

Schreiftliche Erklärung

Ich erkläre hiermit, dass ich die vorliegende Arbeit ohne unzulässige Hilfe Dritter und ohne Benutzung anderer als der angegebenen Hilfsmittel angefertigt habe. Die aus fremden Quellen direkt oder indirekt übernommenen Gedanken sind als solche kenntlich gemacht.

Insbesondere habe ich nicht die Hilfe einer kommerziellen Promotionsberatung in Anspruch genommen. Dritte haben von mir weder unmittelbar noch mittelbar geldwerte Leistungen für Arbeiten erhalten, die im Zusammenhang mit dem Inhalt der vorgelegten Dissertation stehen.

Die Arbeit wurde bisher weder im Inland noch im Ausland in gleicher oder ähnlicher Form als Dissertation eingereicht und ist als Ganzes auch noch nicht veröffentlicht.



Magdeburg, 06.08.2019

Abstract

The aim of this Ph.D. work was to synthesize new alkali metal, alkaline earth metal and lanthanide complexes with 1,4-diaza-1,3-dienes (“DADs”) and to investigate their molecular structures. In the beginning of the Ph.D. work, a series of alkali metal complexes with monoanionic and dianionic 1,4-bis(2,4-diisopropylphenyl)-2,3-dimethyl-1,4-diaza-1,3-butadiene (= $\text{Me}_2\text{DAD}^{\text{Dipp}}$) ligands were synthesized by reduction of $\text{Me}_2\text{DAD}^{\text{Dipp}}$ ligands with alkali metals. Similarly, for the first time, a series of heterobimetallic complexes (Na/Li, K/Li, Rb/Li, Cs/Li, and K/Na) with dianionic $\text{Me}_2\text{DAD}^{\text{Dipp}}$ ligands were synthesized. Moreover, lithium complexes with mono- and dianionic 1,4-Bis(1-adamantyl)-1,4-diaza-1,3-butadiene (= $\text{H}_2\text{DAD}^{\text{Ad}}$) ligands, a heterobimetallic complex (Na/Li) with dianionic $\text{H}_2\text{DAD}^{\text{Ad}}$ ligand, and a series of alkali metal complexes with radical-monoanionic 1,4-bis(2,4-diisopropylphenyl)-1,4-diaza-1,3-butadiene (= $\text{H}_2\text{DAD}^{\text{Dipp}}$) ligand were also prepared by direct metallation. The reduction of the $\text{H}_2\text{DAD}^{\text{Dipp}}$ ligand by KH afforded an unprecedented potassium β -diketimate complex. The reaction between alkali metal complexes with the monoanionic $\text{Me}_2\text{DAD}^{\text{Dipp}}$ ligand and *N,N'*-dicyclohexylcarbodiimide as well as *N,N'*-diisopropylcarbodiimide yielded a new series of heterocyclic compounds. During the course of the Ph.D. work, alkaline earth metal and lanthanide complexes with DADs were also synthesized. In the presence of iodine, $\text{Me}_2\text{DAD}^{\text{Dipp}}$ and $\text{H}_2\text{DAD}^{\text{Ad}}$ ligands were treated with calcium to yield calcium complexes with dianionic $\text{Me}_2\text{DAD}^{\text{Dipp}}$ and radical-monoanionic $\text{H}_2\text{DAD}^{\text{Ad}}$ ligands, respectively. Similarly, $\text{H}_2\text{DAD}^{\text{Dipp}}$ ligand was treated with europium to yield an europium(II) complex with the radical-monoanionic $\text{H}_2\text{DAD}^{\text{Dipp}}$ ligands. A three-component reaction of $\text{Me}_2\text{DAD}^{\text{Dipp}}$, ytterbium, and iodine yielded an iodide-bridged dimeric ytterbium(II) complex with the radical-monoanionic $\text{Me}_2\text{DAD}^{\text{Dipp}}$ ligands, whereas the same combination of $\text{H}_2\text{DAD}^{\text{Dipp}}$, samarium, and iodine yielded a monomeric samarium(III) complex with a dianionic $\text{H}_2\text{DAD}^{\text{Dipp}}$ ligand. All these complexes were thoroughly characterized by NMR, MS, IR, and EPR spectroscopy as well as elemental analyses and X-ray crystallography.

Abstrakt

Das Ziel dieser Promotionsarbeit war es, neue Alkali- und Erdalkalimetall- und Lanthanoid-Komplexe mit 1,4-Diaza-1,3-dienen („DADs“) zu synthetisieren und ihre molekularen Strukturen zu untersuchen. Zu Beginn wurde eine Reihe von Alkalimetallkomplexen mit monoanionischen und dianionischen 1,4-Bis(2,4-diisopropylphenyl)-2,3-dimethyl-1,4-diaza-1,3-butadien-Liganden ($= \text{Me}_2\text{DAD}^{\text{Dipp}}$) durch Reduktion von $\text{Me}_2\text{DAD}^{\text{Dipp}}$ mit Alkalimetallen synthetisiert. In ähnlicher Weise wurde zum ersten Mal eine Reihe von heterobimetallischen Komplexe (Na/Li, K/Li, Rb/Li, Cs/Li, and K/Na) mit dianionischen $\text{Me}_2\text{DAD}^{\text{Dipp}}$ -Liganden synthetisiert. Lithiumkomplexe mit monoanionischen und dianionischen 1,4-Bis(1-adamantyl)-1,4-diaza-1,3-butadien-Liganden ($= \text{H}_2\text{DAD}^{\text{Ad}}$) und ein heterobimetallischer Komplex (Na/Li) mit dianionischem $\text{H}_2\text{DAD}^{\text{Ad}}$ -Liganden sowie eine Reihe von Alkalimetallkomplexen mit radikalisch monoanionischem 4-Bis(2,4-diisopropylphenyl)-1,4-diaza-1,3-butadien-Liganden ($= \text{H}_2\text{DAD}^{\text{Dipp}}$)-Ligand wurden ebenfalls durch direkte Metallierung hergestellt. Die Reduktion von $\text{H}_2\text{DAD}^{\text{Dipp}}$ mit KH lieferte einen unerwarteten Kalium- β -Diketiminat-Komplex. Die Reaktion zwischen Alkalimetallkomplexen mit dem monoanionischen $\text{Me}_2\text{DAD}^{\text{Dipp}}$ -Liganden und *N,N'*-Dicyclohexylcarbodiimid sowie *N,N'*-Diisopropylcarbodiimid führte zu einer neuen Reihe unerwarteter heterocyclischer Verbindungen. Im Laufe der Promotionsarbeit wurden auch Erdalkalimetall- und Lanthanoidkomplexe mit DADs synthetisiert. In Gegenwart von Iod wurden $\text{Me}_2\text{DAD}^{\text{Dipp}}$ und $\text{H}_2\text{DAD}^{\text{Ad}}$ mit Calcium umgesetzt, um Calciumkomplexe mit dem dianionischen $\text{Me}_2\text{DAD}^{\text{Dipp}}$ -Liganden und dem radikalischen $\text{H}_2\text{DAD}^{\text{Ad}}$ -Liganden zu erhalten. In entsprechender Weise lieferte die Reaktion von $\text{H}_2\text{DAD}^{\text{Dipp}}$ mit Europium einen Europium(II)-Komplex mit dem radikalischen, monoanionischen $\text{H}_2\text{DAD}^{\text{Dipp}}$ -Liganden. Eine Dreikomponentenreaktion von $\text{Me}_2\text{DAD}^{\text{Dipp}}$, Ytterbium und Iod ergab einen iodid-verbrückten dimeren Ytterbium(II)-Komplex mit dem radikalischen, monoanionischen $\text{Me}_2\text{DAD}^{\text{Dipp}}$ -Liganden, während die analoge Reaktion von $\text{H}_2\text{DAD}^{\text{Dipp}}$, Samarium und Iod einen einkernigen Samarium(III)-Iodid-Komplex mit einem dianionischen $\text{H}_2\text{DAD}^{\text{Dipp}}$ -Liganden lieferte. Alle diese Komplexe wurden durch NMR-, MS-, IR- und EPR-Spektroskopie sowie Elementaranalysen und Röntgenkristallographie umfassend charakterisiert.

Table of Contents

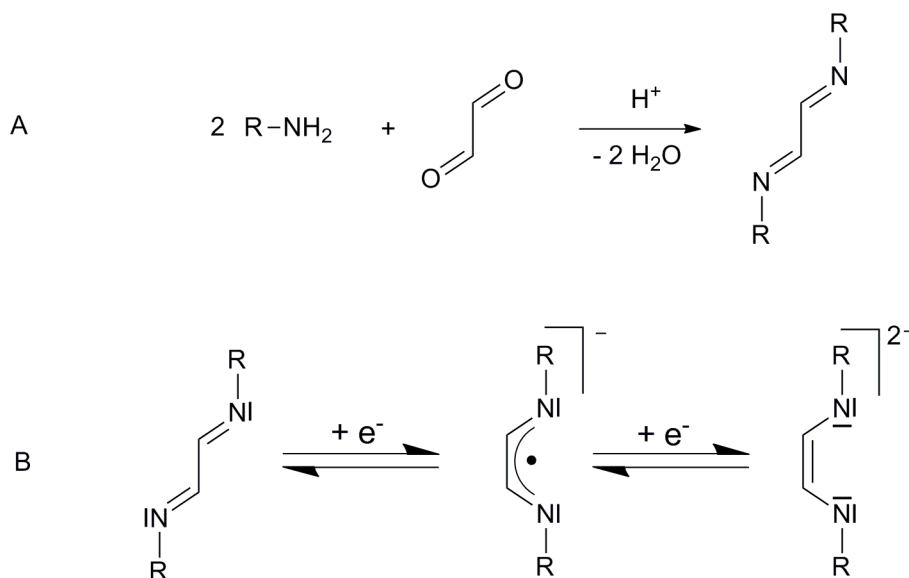
1.	Introduction	1
1.1.	Diazadienes	1
1.2.	The chemistry of alkali metal complexes with DAD ligands	3
1.3.	The chemistry of alkaline earth metal complexes with DAD ligands	11
1.4.	The chemistry of lanthanide complexes with DAD ligands	14
2.	Results and discussion	17
2.1.	Synthesis of DAD ligands (1-3)	17
2.1.1.	Spectroscopic analysis of DAD ligands (1-3)	18
2.2.	Alkali metal complexes with dianionic DAD ligands	20
2.2.1.	Synthesis of alkali metal complexes (4-8) with dianionic $\text{Me}_2\text{DAD}^{\text{Dipp}}$ ligands	20
2.2.2.	Spectroscopic analysis of the complexes (4-8)	22
2.2.3.	Molecular structures of $[\text{Li}_2(\text{Me}_2\text{DAD}^{\text{Dipp}})(\mu\text{-THF})(\text{THF})_2]$ (4) and $[\text{Na}_2(\text{Me}_2\text{DAD}^{\text{Dipp}})(\text{THF})_4]$ (5)	25
2.2.4.	Molecular structure of $\{[\text{K}_2(\text{Me}_2\text{DAD}^{\text{Dipp}})(\mu\text{-THF})(\text{THF})_2] \cdot [\text{K}_2(\text{Me}_2\text{DAD}^{\text{Dipp}})(\mu\text{-THF})(\text{THF})_3]\}_2$ (6)	28
2.2.5.	Molecular structures of $\{[\text{Rb}_2(\text{Me}_2\text{DAD}^{\text{Dipp}})(\text{THF})_4]_2 \cdot \text{THF}\}_n$ (7) and $\{[\text{Cs}_2(\text{Me}_2\text{DAD}^{\text{Dipp}})(\text{THF})_4] \cdot \text{THF}\}_n$ (8)	31
2.2.6.	Synthesis and molecular structure of lithium complex $[\{\text{Li}_2(\text{H}_2\text{DAD}^{\text{Ad}})\}_2(\mu\text{-THF})(\text{THF})_2]$ (9) with dianionic $\text{H}_2\text{DAD}^{\text{Ad}}$ ligand	34
2.3.	Heterobimetallic alkali metal complexes with dianionic DAD ligands	38
2.3.1.	Synthesis of heterobimetallic alkali metal complexes (10-14) with dianionic $\text{Me}_2\text{DAD}^{\text{Dipp}}$ ligands	39
2.3.2.	Spectroscopic analysis of the complexes (10-14)	41
2.3.3.	Molecular structures of $[\text{K}(\text{THF})_2(\text{Me}_2\text{DAD}^{\text{Dipp}})\text{Li}(\text{THF})]$ (11) and $\{[\text{Rb}(\text{THF})(\text{Me}_2\text{DAD}^{\text{Dipp}})\text{Li}(\text{THF})] \cdot \text{THF}\}_n$ (12)	44
2.3.4.	Synthesis and molecular structure of heterobimetallic complex $\{[\text{Na}(\text{H}_2\text{DAD}^{\text{Ad}})\text{Li}(\text{THF})]_4 \cdot \text{THF}\}_n$ (15) with dianionic $\text{H}_2\text{DAD}^{\text{Ad}}$ ligands	48
2.4.	Alkali metal complexes with radical-monoanionic DAD ligands	51
2.4.1.	Synthesis of alkali metal complexes (16-18) with radical-monoanionic $\text{Me}_2\text{DAD}^{\text{Dipp}}$ ligands	51
2.4.2.	Spectroscopic analysis of the complexes (16-18)	53
2.4.3.	Molecular structure of $[\text{Li}(\text{Me}_2\text{DAD}^{\text{Dipp}})(\text{DME})]$ (16)	55
2.4.4.	Synthesis of alkali metal complexes (19-24) with radical-monoanionic $\text{H}_2\text{DAD}^{\text{Ad}}$ and $\text{H}_2\text{DAD}^{\text{Dipp}}$ ligands	57
2.4.5.	Molecular structures of $[\text{Li}(\text{H}_2\text{DAD}^{\text{Ad}})(\text{THF})_2]$ (19) and $[\text{Li}(\text{H}_2\text{DAD}^{\text{Dipp}})(\text{THF})_2]$ (20)	60
2.4.6.	Molecular structures of $[\text{K}(\text{H}_2\text{DAD}^{\text{Dipp}})(\text{THF})_4]$ (22) and $[\text{Rb}(\text{H}_2\text{DAD}^{\text{Dipp}})(\text{THF})_4]$ (23)	62
2.4.7.	Molecular structure of $[\text{Cs}(\text{DippNCHC}(\text{=CHCHN}^{\text{Dipp}})\text{N}^{\text{Dipp}})(\text{THF})_2]_n$ (25)	64

2.5.	Reduction of $\text{H}^2\text{DAD}^{\text{Dipp}}$ ligand with KH	66
2.5.1.	Molecular structure of $[\text{K}(\text{DippNCHC}\{\text{DippNCHN}^{\text{Dipp}}\}\text{CHN}^{\text{Dipp}})(\text{THF})_{1.5}]$ (26)	67
2.6.	Reactions between alkali metal complexes with radical-monoanionic $\text{Me}^2\text{DAD}^{\text{Dipp}}$ ligands and carbodiimides	70
2.6.1.	Spectroscopic analysis of the compounds (27-30)	72
2.6.2.	Molecular structures of $[\text{Li}(\text{DippN}^{\text{Cy-Pyr}})(\text{THF})_3]$ (27), $[\text{Na}(\text{DippN}^{\text{Cy-Pyr}})(\text{THF})_3]$ (28), and $[\text{Na}(\text{DippN}^{\text{iPr-Pyr}})(\text{THF})_3] \cdot \text{THF}$ (30)	76
2.6.3.	Molecular structure of $\{[\text{K}(\text{DippN}^{\text{Cy-Pyr}})(\text{THF})_2]_4 \cdot \text{THF}\}_n$ (29)	79
2.7.	Alkaline earth metal complexes with radical-monoanionic and dianionic DAD ligands	81
2.7.1.	Synthesis of a calcium complex (31) with dianionic $\text{Me}^2\text{DAD}^{\text{Dipp}}$ and (32) with radical monoanionic $\text{H}^2\text{DAD}^{\text{Ad}}$ ligands	81
2.7.2.	Spectroscopic analysis of the complexes 31 and 32	83
2.7.3.	Molecular structures of $[\text{Ca}(\text{Me}^2\text{DAD}^{\text{Dipp}})(\text{THF})_3]$ (31) and $[\text{Ca}(\text{H}^2\text{DAD}^{\text{Ad}})_2(\text{THF})_2] \cdot \text{THF}$ (32)	84
2.8.	Lanthanide complexes with DAD ligands	88
2.8.1.	Synthesis and molecular structure of $[\text{Yb}_2(\mu\text{-I})_2(\text{Me}^2\text{DAD}^{\text{Dipp}})_2(\text{THF})_4] \cdot \text{THF}$ (33)	89
2.8.3.	Synthesis and molecular structure of $[\text{Sm}(\text{H}^2\text{DAD}^{\text{Dipp}})(\text{I})(\text{THF})_3]$ (34)	92
2.8.4.	Synthesis and molecular structure of $[\text{Eu}(\text{H}^2\text{DAD}^{\text{Dipp}})_2(\text{THF})]$ (35)	96
3.	Summary	99
4.	Experimental section	109
5.	Crystal data and refinement details	135
6.	References	184
7.	List of publications	192

1. Introduction

1.1. Diazadienes

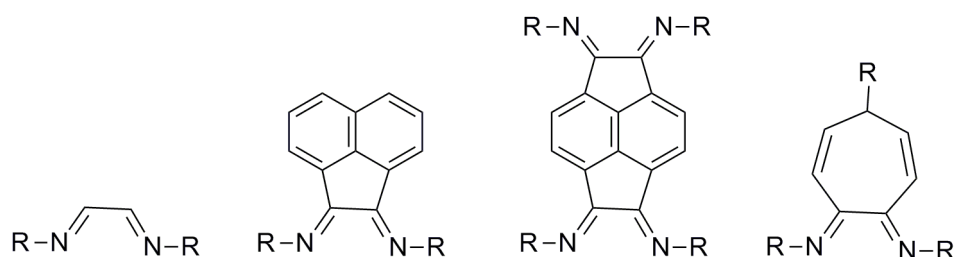
Since the early 1960s, 1,4-disubstituted diazabutadienes have found wide use in the coordination chemistry of transition metals due to their diverse coordination and redox properties.^[1] 1,4-diaza-1,3-dienes (DADs), the bidentate α -diimine ligands chelating through their nitrogen donors, can be easily synthesized by condensation of α -diketones and primary amines under acidic conditions (Scheme 1).^[2] In 1975, tom Dieck et al. demonstrated that the π acceptor capacity of some DAD ligands is about two times higher than that of traditionally used 2,2'-bipyridine.^[2] Since then DADs have been well established as highly versatile ligands for nearly every element in the periodic table.^[1-4] The redox-noninnocent DAD ligands undergo one and two electron reduction processes to yield the corresponding radical anions and enediamide dianions, respectively (Scheme 1).^[3-4] It is important to note that the neutral DADs are in *E*-configuration, whereas the radical anions and enediamide dianions are in *Z*-configuration.



Scheme 1. General synthesis (A) and stepwise reduction (B) of 1,4-diaza-1,3-dienes.

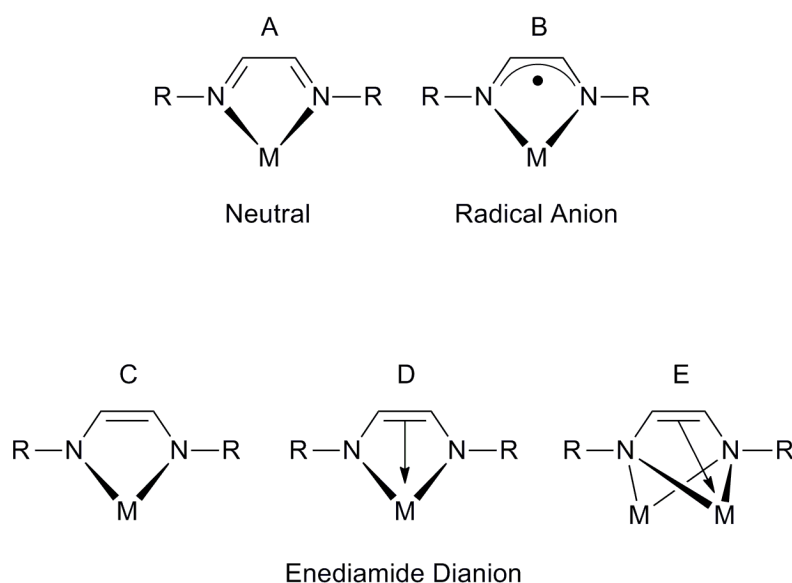
The steric properties of the DAD ligands can be altered by the introduction of various substituents at both C and/or N atoms of the DAD moiety (Scheme 2, page 2). The unique electronic property and the feasibility to modify the steric properties of DAD moiety make the

DADs undoubtedly one of the most versatile ligands in the coordination chemistry. The list of stable DAD complexes comprises main-group metals,^[5-15,32-58] early^[72-87] and late^[88-99] transition metals, as well as the lanthanides and actinides.^[105-126] Important practical applications of metal DAD complexes comprise materials science,^[69,70] synthesis of single-molecule magnets,^[71] homogeneous catalysis,^[88,89,92,142-149] and C-H bond activation.^[91,93,94,119] The well-known DAD ligand systems are listed below.



Scheme 2. Selected literature-known DAD ligand systems.

DAD ligands are able to act both as n - and π -electron donors, due to the lone electron pairs at nitrogen atoms and the π -electrons of the C=N bonds, which provides a variety of coordination modes. Scheme 3 demonstrates the various chelating coordination modes of DAD ligands which have been so far reported in the literature.^[5-15,32-58,72-99,105-126]



Scheme 3. Possible chelating coordination modes of (*Z*)-1,4-diaza-1,3-diene ligands.

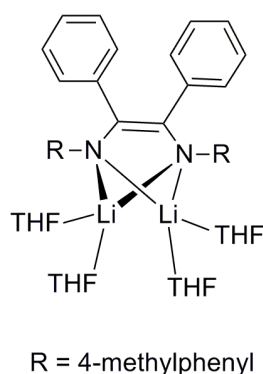
In the vast majority of all metal complexes, the diazadienes act as KN , KN^{\prime} -chelating ligands. Although non-chelating coordination modes are also possible,^[117] well-characterized examples are exceptionally rare. The most common coordination mode with late transition metals is the neutral KN , KN^{\prime} -chelation, particularly in their low oxidation states. Complexes of different s-, p-, and d-block metals have been reported as both the dianionic enediamide derivatives and the radical anions.

1.2. The chemistry of alkali metal complexes with DAD ligands

The chemistry of alkali metal (especially Li, Na and K) DAD complexes has been decently developed.^[5-15] In 1974, alkali metal complexes with a dianionic DAD ligand [$M_2L \cdot L_n$] ($M = Li, Na, K$; $L = [PhN(Ph)C]_2$; $L_n = \text{solvent}$) were synthesized and characterized (by UV-vis spectroscopy) by Walther et al.^[155] In the past decades, a number of alkali metal complexes with mono- or dianionic α -diimine ligands have been synthesized.^[5-15] Most of these complexes were synthesized by direct metallation. The alkali metal complexes with DAD ligands have been used as reducing agents to synthesize different organometallic and organic substrates. Although they have appeared as intermediates in the approaches to other organometallic compounds, structural studies of these complexes are rare.^[156] The heavy alkali metal (Rb and Cs) complexes are exceedingly rare, although they have proven to be valuable ligand transfer reagents where the lighter alkali metal derivatives fail.^[59-61]

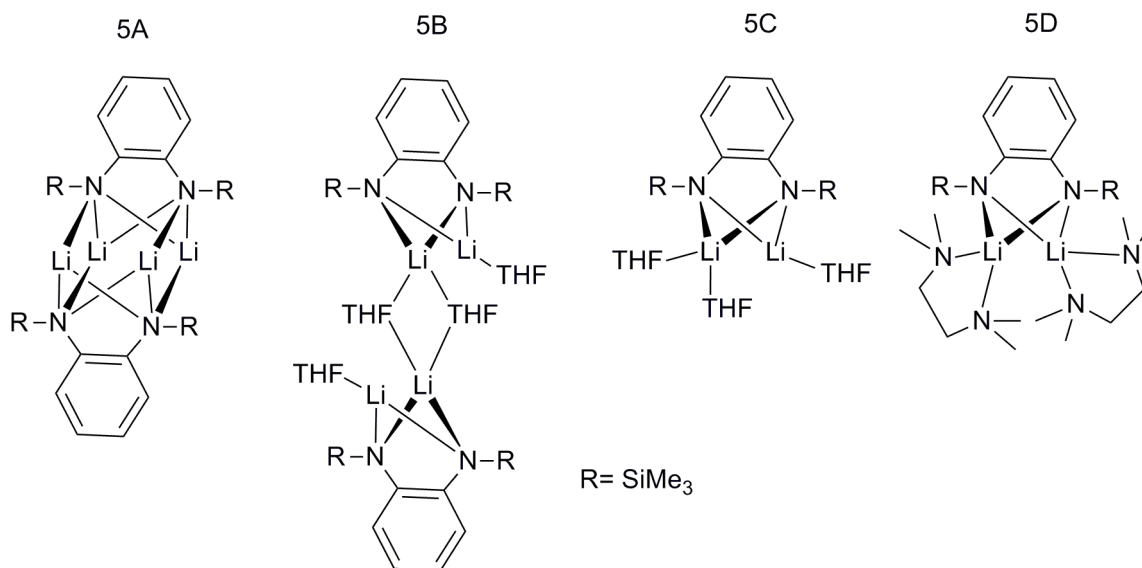
Among the possible coordination modes of DADs (Scheme 3, page 2), the radical-anions (mode B) and enediamide dianions (mode E) are the most common with alkali metals.^[5-15] An exceptional lithium complex (10A) with neutral KN , KN^{\prime} -chelation of DAD ligand is shown in Scheme 10 (page 9).^[13] The lithium, sodium, and potassium complexes with DAD ligands are predominantly used as precursors to synthesize DAD complexes of alkaline earth and transition metals as well as lanthanides by salt metathesis. The synthesis and structures of alkali metal complexes with DAD ligands so far reported are briefly discussed below.

Scholz and co-workers reported the synthesis and structural characterization of a lithium complex with the dianionic DAD ligand (N,N' -bis(4-methylphenyl)-1,4-diaza-2,3-diphenyl-1,3-butadiene). The dilithium complex was synthesized by direct metallation of the DAD ligand in Et_2O/THF . The X-ray structure determination showed that each Li atom is coordinated by two nitrogen atoms from the DAD ligand (in *s-cis*-configuration) and two oxygen atoms from the terminal THF molecules (Scheme 4, page 4).^[5]



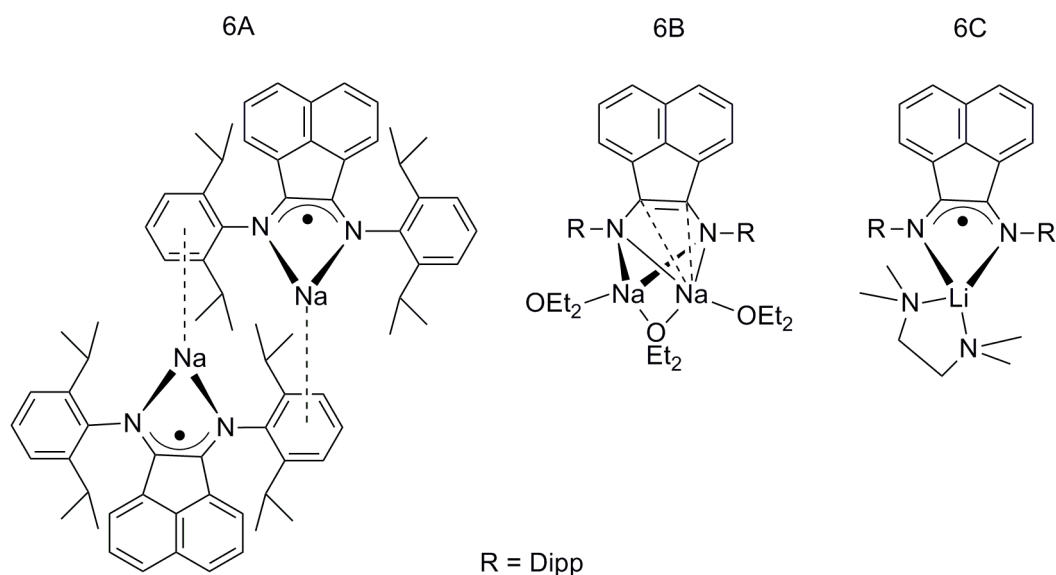
Scheme 4. Lithium DAD complex.^[5]

Lappert and co-workers reported a series of lithium complexes with dianionic DAD ligands. The diamidodilithium complexes 5A-5D (Scheme 5) were synthesized by treating 1,2-bis(trimethylsilylamino)benzene with *n*-butyllithium in a 1:2 molar ratio. The coligand-free tetranuclear complex 5A was prepared in hexane and the THF solvated tetra nuclear complex 5B was obtained by adding THF in stoichiometric amount (Li:THF in a 1:1 molar ratio) to complex 5A. The binuclear complex 5C was obtained with an excess THF, while the binuclear TMEDA adduct 5D was obtained by using TMEDA instead of THF.^[6]



Scheme 5. Solvent influence on the molecular structures of lithium DAD complexes.^[6]

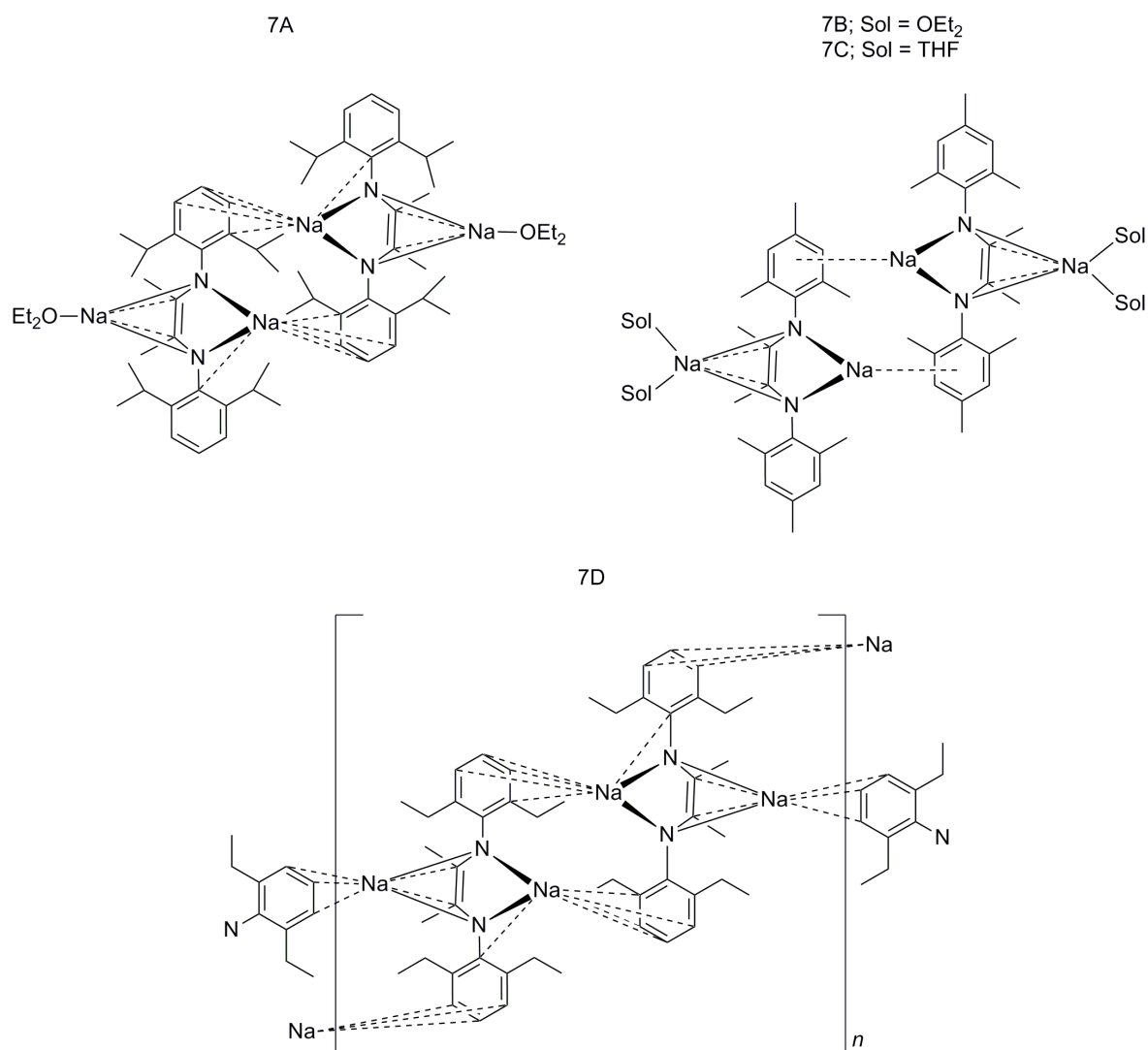
Fedushkin and co-workers reported the stepwise reduction of bis[N-(2,6-diisopropylphenyl)imino]acenaphthene ($\text{Bian}^{\text{Dipp}}$) with sodium in diethyl ether to mono-, di-, tri-, and tetraanionic species of the ligand. First the ligand was reduced to a tetraanion, and then it was converted to mono-, di-, and trianions by adding 3, 2 and 0.66 equivalents of free ligand, respectively. The monoanionic complex aggregated to the centrosymmetric dimer **6A** while the dianionic complex **6B** crystallized as a monomer as shown in Scheme 6. Single-crystal X-ray diffraction showed that the sodium atom in the anionic complex **6A** is η^6 -coordinated by the aryl π -system and is located essentially in the plane of the DAD backbone while the same showed that the sodium atoms in the dianionic complex **6B** were differently coordinated (one sodium atom is located substantially in the plane of the DAD backbone, while the other sits above the plane of the same and can be described as η^4 -coordinated by the DAD π -electronic system of the complex).^[7] The lithium complex **6C** with radical-monoanionic $\text{Bian}^{\text{Dipp}}$ ligand was prepared by treating the ligand in a 1:1 molar ratio with lithium in TMEDA. The TMEDA adduct of the lithium DAD complex **6C** is also shown in Scheme 6.^[8]



Scheme 6. Acenaphthene-based DAD complexes of sodium^[7] and lithium.^[8]

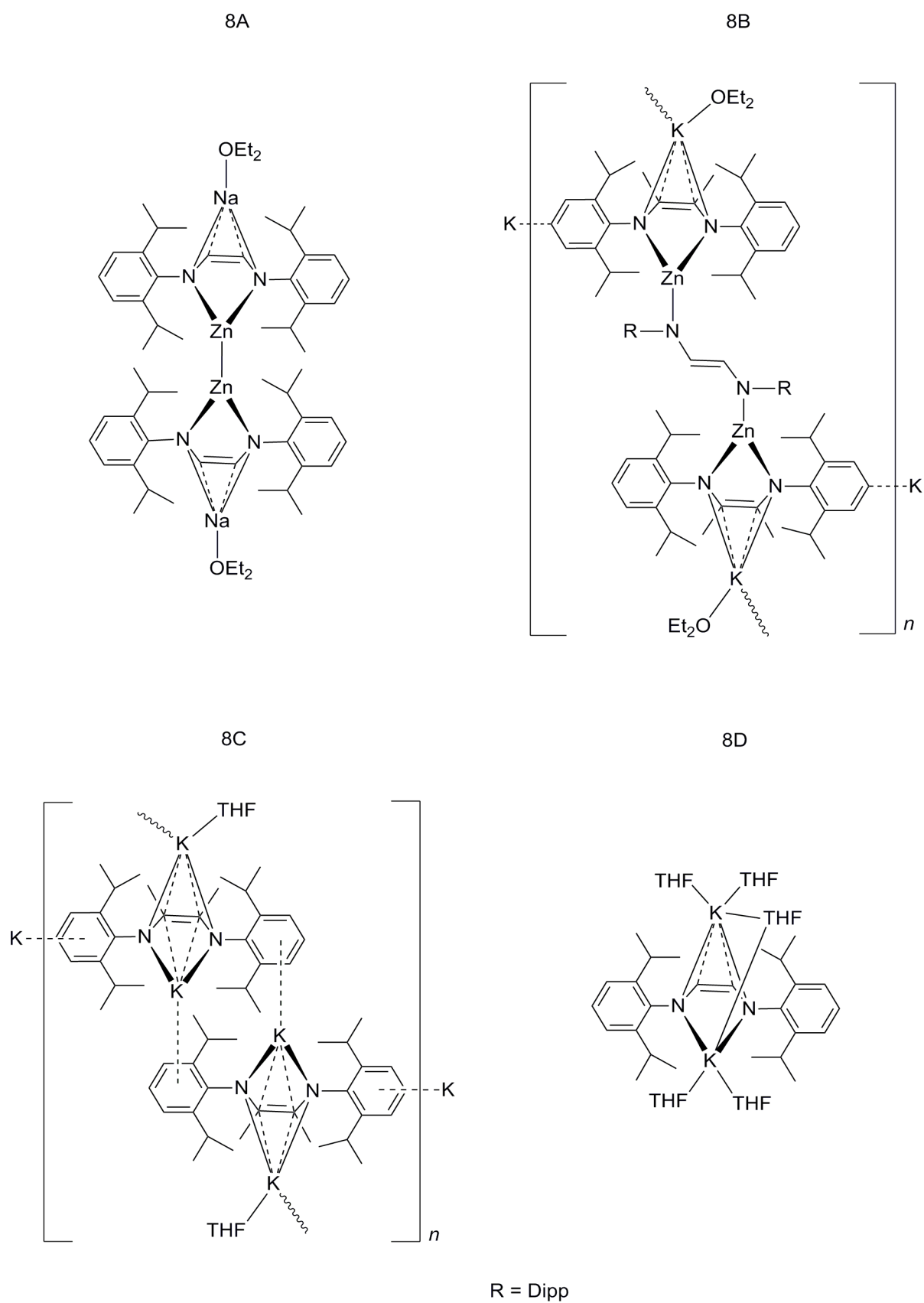
Wu and co-workers reported a series of sodium complexes with $\text{Me}_2\text{DAD}^{\text{Dipp}}$ and $\text{Me}_2\text{DAD}^{\text{Mes}}$ ligands by the reduction of the ligands with sodium.^[9] Similar to the reports of Fedushkin and co-workers,^[7] there are two different metal centers in all the sodium complexes reported by Wu and co-workers (Scheme 7, page 6). The $\text{Me}_2\text{DAD}^{\text{Dipp}}$ ligand was reduced by sodium (2

equiv.) in Et₂O to give dianionic centrosymmetric dimer 7A. The reduction of Me₂DAD^{Mes} ligand by sodium (2 equiv.) in Et₂O and THF yielded centrosymmetric dimers 7B and 7C, respectively, while the same of diethylphenyl substituted DAD ligand by sodium (2 equiv.) in toluene yielded 7D. The dimeric structure of 7A, 7B, and 7C is formed by short metal-carbon contacts between the unsolvated sodium atoms and the aromatic rings of the adjacent molecules. 7D is a three-dimensional coordination polymer in which all the sodium atoms involve in short metal-carbon contacts with the aromatic ring of the adjacent complex. Moreover, short Na-C_{ipso} contacts were observed in 7A and 7D.^[9]



Scheme 7. Influence of substituents at the N atoms of the DAD moiety on the molecular structures of sodium DAD complexes.^[9]

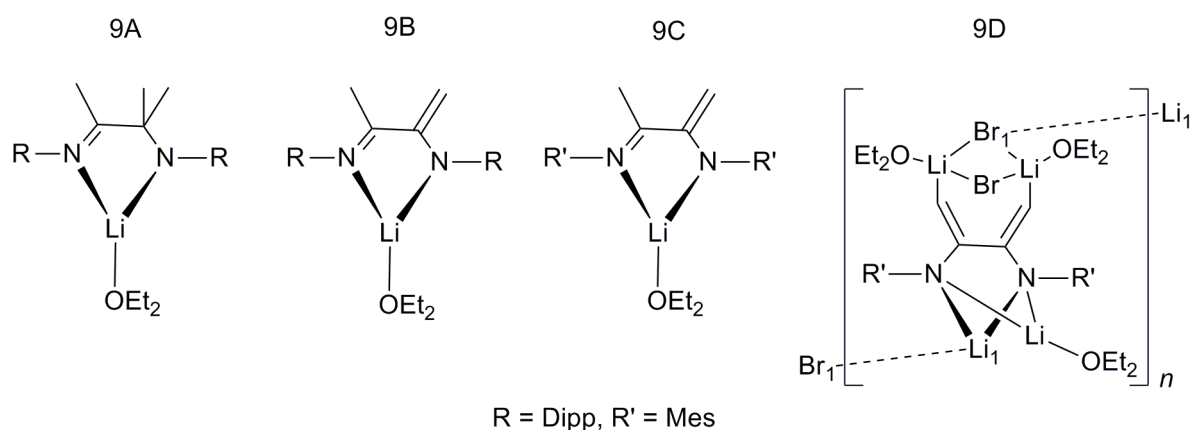
Wu and co-workers reported a series of mono- and dinuclear Zn complexes (Scheme 8).^[10]



Scheme 8. Bimetallic (Zn/Na and Zn/K)^[10] and potassium^[10,11] DAD complexes.

The precursor Zn complex $[\text{Zn}(\text{H}^2\text{DAD}^{\text{Dipp}})\text{Cl}_2]$ containing neutral $\text{H}^2\text{DAD}^{\text{Dipp}}$ ligand was prepared by treating $\text{H}^2\text{DAD}^{\text{Dipp}}$ ligand with ZnCl_2 (Scheme 8, page 7). The reduction of the precursor complex with sodium in Et_2O yielded the centrosymmetric dimer 8A in which the neutral ligand is doubly reduced to the dianion while the formal divalent Zn^{2+} ion reduced to monovalent Zn^+ . There is a metal-metal bond between the two Zn atoms, and each sodium atom is η^4 -coordinated by the DAD π -electronic system. The reduction of $[\text{Zn}(\text{H}^2\text{DAD}^{\text{Dipp}})\text{Cl}_2]$ with potassium in Et_2O yielded a mixture of coordination polymeric complexes 8B and 8C. In complex 8B, all the ligands are doubly reduced and the Zn centers remain in +2 oxidation state. The non-chelating DAD ligand, with the *trans* conformation, bridges the zinc atoms. The dipotassium complex 8C was crystallized in THF. All the potassium atoms in 8C are η^4 -coordinated by the C_2N_2 moiety and η^6 -coordinated by the aromatic ring of another DAD ligand, forming the linear polymeric chain.^[10] Mashima and co-workers prepared the dipotassium salt 8D by treating two equivalent of potassium with the $\text{H}^2\text{DAD}^{\text{Dipp}}$ ligand and used it as precursor to synthesize group 3 metal complexes with DAD ligands by salt metathesis reactions (Scheme 8, page 7).^[11]

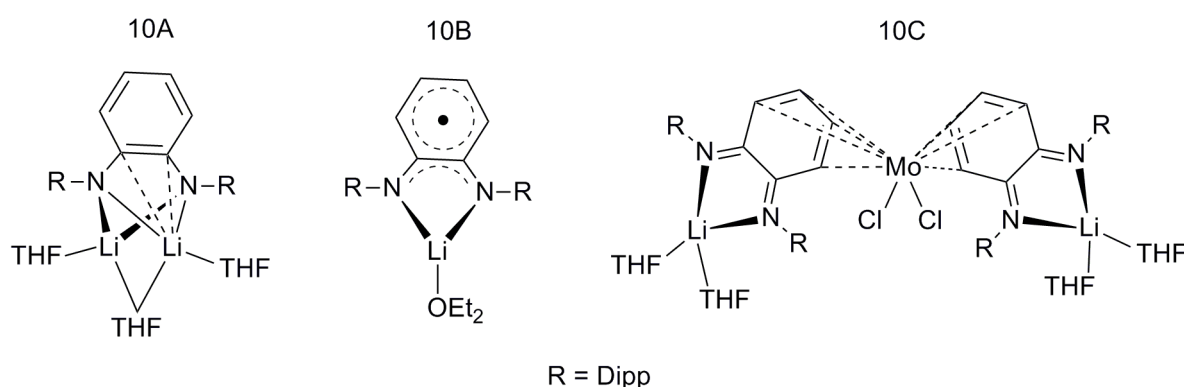
Clentsmith and co-workers demonstrated the carbon-carbon bond formation and selective reduction of one of the imine arms of $\text{Me}^2\text{DAD}^{\text{Dipp}}$ ligand by treating the ligand with 1 equiv. of MeLi in Et_2O to yield the *N*-lithiated salt $[\text{Li}(\text{DippN}=\text{C}(\text{CH}_3)\text{C}(\text{CH}_3)_2\text{N}^{\text{Dipp}})(\text{Et}_2\text{O})]$ (9A) (Scheme 9). In the *N*-lithiated salt 9A, the lithium atom is coordinated by amido and imino donors and oxygen.



Scheme 9. Reduction of DAD ligands by MeLi and LiN^iPr_2 .^[12]

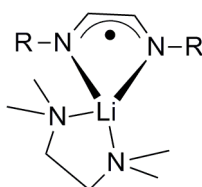
However, the treatment of $\text{Me}_2\text{DAD}^{\text{Dipp}}$ ligand with the sterically more hindered base Li^iPr_2 yielded the *N*-lithiated imine anion $[\text{Li}(\text{DippN}=\text{C}(\text{CH}_3)\text{C}(\text{=CH}_2)\text{N}^{\text{Dipp}})(\text{Et}_2\text{O})]$ (9B) by proton abstraction. On the other hand, treatment of $\text{Me}_2\text{DAD}^{\text{Mes}}$ with 1 equiv. of MeLi yielded the *N*-lithiated imine anion $[\text{Li}(\text{MesN}=\text{C}(\text{CH}_3)\text{C}(\text{=CH}_2)\text{N}^{\text{Mes}})(\text{Et}_2\text{O})]$ (9C) by proton abstraction, while that with excess MeLi · LiBr yielded the doubly *N*-lithiated salt of the diene/diamide $[\text{Li}(\text{MesNC}(\text{=CH}_2)\text{C}(\text{=CH}_2)\text{N}^{\text{Mes}})(\text{Et}_2\text{O})] \cdot 2 \text{LiBr}$ (9D) in which the Li1 atom is weakly bonded to the Br1 atom of an adjacent complex, forming the coordination polymeric chain (Scheme 9, page 8).^[12]

Song and co-workers reported the synthesis and structural characterization of dilithium complex 10A with DAD ligand (Scheme 10). The dilithium complex 10A was prepared by double deprotonation of *N,N'*-bis(2,6-diisopropylphenyl)-*o*-phenylenediamine with *n*-BuLi in THF. The treatment of complex 10A with $[\text{Mo}(\text{THF})_2\text{Cl}_4]$ (0.5 equiv.) yielded complex 10C in which the phenylene backbone of the ligand is dearomatized and the lithium atoms are coordinated by neutral DAD ligands (*KN*, *KN'*-chelation). The lithium complex 10B, the radical species, was prepared by one-electron oxidation of complex 10A with $\text{EuCl}_3(\text{DME})_2$ and characterized by X-ray crystallography and EPR spectroscopy.^[13]



Scheme 10. *Ortho*-phenylene-based DAD complexes of lithium and molybdenum.^[13]

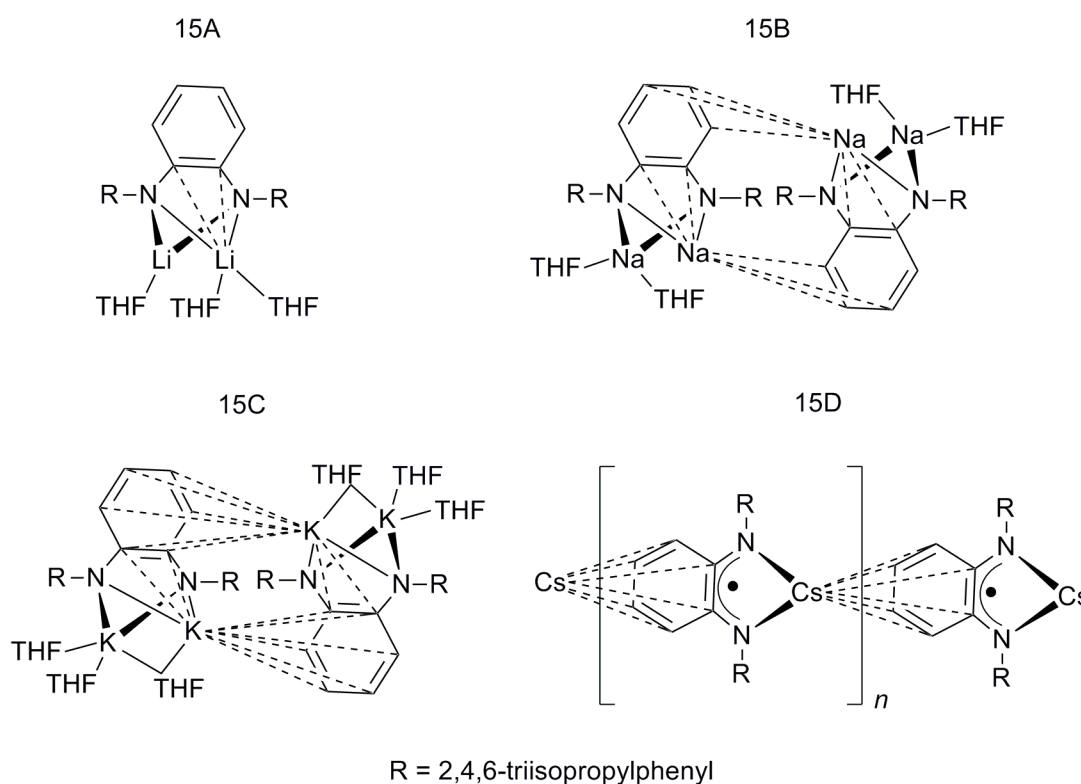
Trifonov and co-workers reported the TMEDA adduct of lithium $[\text{Li}(\text{H}_2\text{DAD}^{\text{Dipp}})(\text{TMEDA})]$ with radical-monoanionic $\text{H}_2\text{DAD}^{\text{Dipp}}$ ligand (Scheme 11, page 10). The yttrium complex $[\text{Y}(\text{H}_2\text{DAD}^{\text{Dipp}})(\text{THF})_2\text{Cl}_2]$ with radical-monoanionic $\text{H}_2\text{DAD}^{\text{Dipp}}$ ligand was treated with 4 equiv. of MeLi in the presence of TMEDA to yield a mixture of complexes $[\text{Li}(\text{H}_2\text{DAD}^{\text{Dipp}})(\text{TMEDA})]$ and $[\text{Li}(\text{TMEDA})_3][\text{YMe}_3]$.^[14]



R = Dipp

Scheme 11. TMEDA adduct of lithium with radical-monoanionic $\text{H}_2\text{DAD}^{\text{Dipp}}$ ligand.^[14]

Liddle and co-workers reported a series of alkali metal complexes with *ortho*-phenylene-based DAD ligand (Scheme 12, page 11).^[15] *N,N'*-Bis(2,4,6-triisopropylphenyl)-*o*-phenylenediamine (PDAH₂) was treated with 2 equiv. of *n*-BuLi, NaCH₂C₆H₅, and KCH₂C₆H₅ to yield dilithium (15A), disodium (15B), and dipotassium (15C) complexes, respectively. All these dianionic DAD complexes have two different metal centers, one is substantially in plane of the PDA backbone and chelated by the nitrogen atoms of the ligand, while the other sits over the PDA backbone and η^4 -coordinated to the C₂N₂ moiety of the ligand. The dilithium complex 15A is a monomer with three solvated THF molecules. The disodium complex 15B has four terminal THF molecules, while the dipotassium complex 15C has four terminal and two bridging THF molecules. In both 15B and 15C, the metal atom which sits above the C₂N₂ moiety forms metal-carbon contacts (three in 15B and six in 15C) to the phenylene ring of the PDA backbone of the adjacent complex, forming the dimer. Treatment of PDAH₂ with 2 equiv. of CsCH₂C₆H₅ yielded only the radical-monoanionic DAD complex of cesium (15D) in which the cesium atom forms six metal-carbon contacts to the phenylene ring of the PDA backbone of the adjacent complex, forming a linear coordination polymeric chain.^[15]



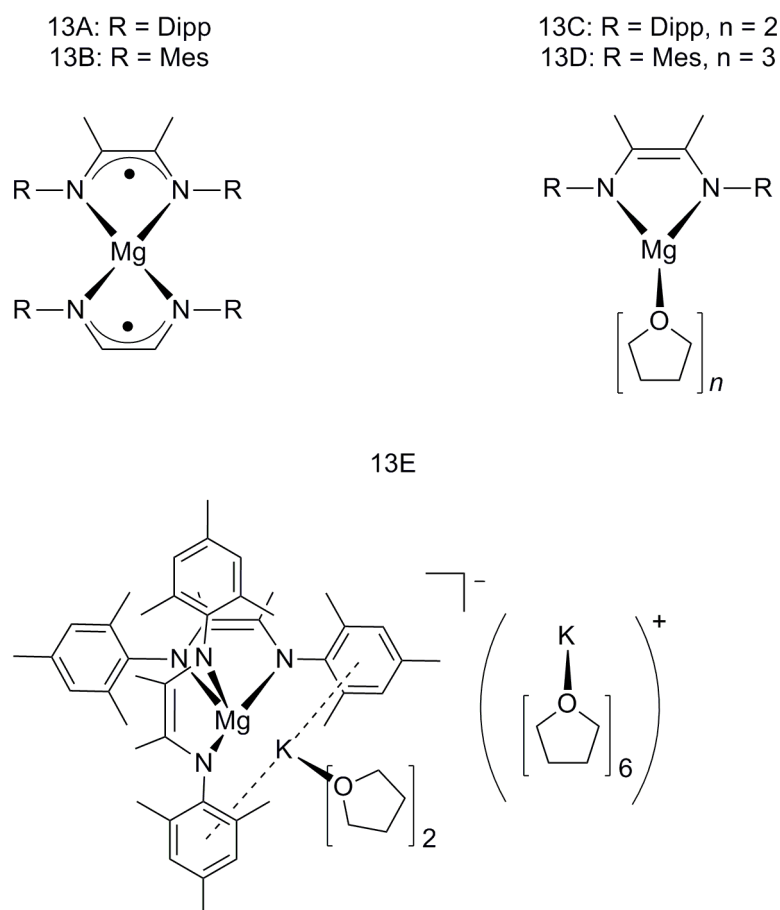
Scheme 12. A series of alkali metal complexes with *Ortho*-phenylene-based DAD ligand.^[15]

1.3. The chemistry of alkaline earth metal complexes with DAD ligands

Organometallic chemists are fascinated to homoleptic and heteroleptic alkaline earth metal complexes because their structural and chemical behaviors reflect the oxophilic and electropositive nature of alkaline earth metals in relation to those of early d-transition metals.^[16-17] The catalytic activity and selectivity of the alkaline earth metal complexes can be controlled by the well-defined nitrogen-based ligand architecture. Thus, various nitrogen-based ancillary ligands, such as tris(pyrazolyl)borates,^[18-21] aminotroponimines,^[22-23] β -diketiminates,^[24-30] and bis(imino)pyrroles,^[31] have been employed for the preparation of alkaline earth-metal complexes. Being an important class of bidentate ligand, DAD ligands have also been extensively utilized to synthesize alkaline earth metal complexes^[32-45,56] (especially magnesium and calcium^[32-41,56]). Among the possible coordination modes of the DAD ligands (Scheme 3, page 2), the radical anion and the enediamide dianions are the most common with alkaline earth metals.^[32-45,56] Most of the research in this area comprises group 2 metal complexes of rigid acenaphthene-based DAD ligands.^[37-41] DAD complexes of

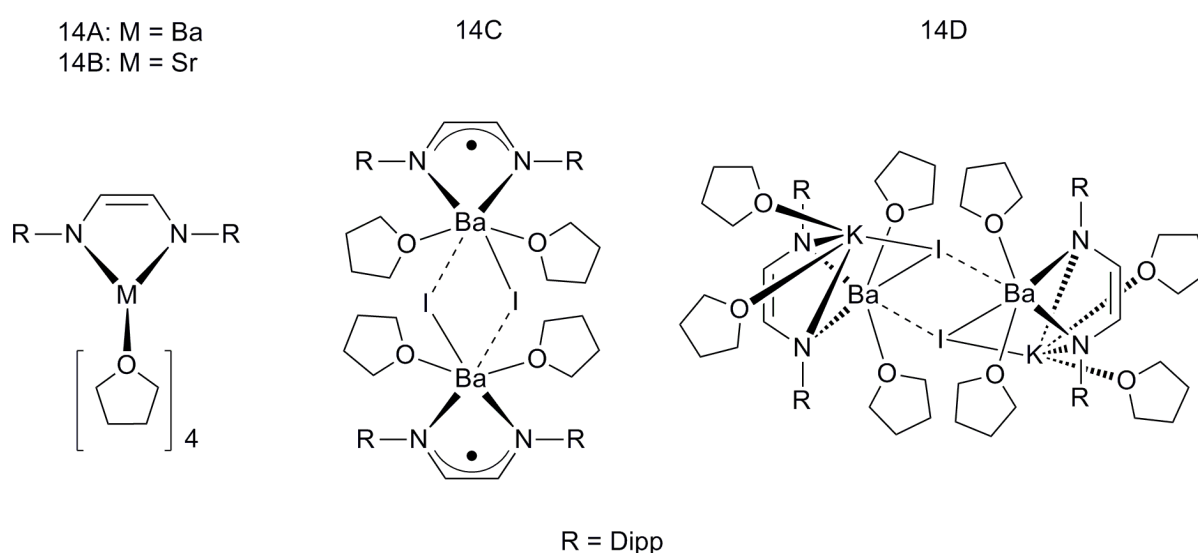
alkaline earth metals have been predominantly synthesized by salt metathesis reactions between alkali metal DAD precursors and alkaline earth metal halides.

Yang and co-workers reported series of magnesium complexes with DAD ligands prepared by salt metathesis (Scheme 13). The radical-monoanionic complex $[\text{Mg}(\text{Me}_2\text{DAD}^{\text{Dipp}})_2]$ (13A) or $[\text{Mg}(\text{Me}_2\text{DAD}^{\text{Mes}})_2]$ (13B) was prepared by reducing $\text{Me}_2\text{DAD}^{\text{Dipp}}$ or $\text{Me}_2\text{DAD}^{\text{Mes}}$ ligand with 1 equiv. of potassium (1 equiv.) followed by treating with anhydrous MgCl_2 (0.5 equiv.). Similarly, the dianionic complex $[\text{Mg}(\text{Me}_2\text{DAD}^{\text{Dipp}})(\text{THF})_2]$ (13C) or $[\text{Mg}(\text{Me}_2\text{DAD}^{\text{Mes}})(\text{THF})_3]$ (13D) was prepared by reducing $\text{Me}_2\text{DAD}^{\text{Dipp}}$ or $\text{Me}_2\text{DAD}^{\text{Mes}}$ ligand with potassium (2 equiv.) followed by treating with anhydrous MgCl_2 (1 equiv.). Treatment of $\text{Me}_2\text{DAD}^{\text{Mes}}$ ligand with 3 equiv. of potassium followed by 1 equiv. of anhydrous MgCl_2 yielded the complex $[\text{Mg}(\text{Me}_2\text{DAD}^{\text{Mes}})_2\text{K}(\text{THF})_2][\text{K}(\text{THF})_6]$ (13E). The DAD ligands in the anionic unit $[\text{Mg}(\text{Me}_2\text{DAD}^{\text{Mes}})_2\text{K}(\text{THF})_2]$ are in -2 valence, and the potassium atom in the same is η^6 -coordinated by two arene groups.^[36]



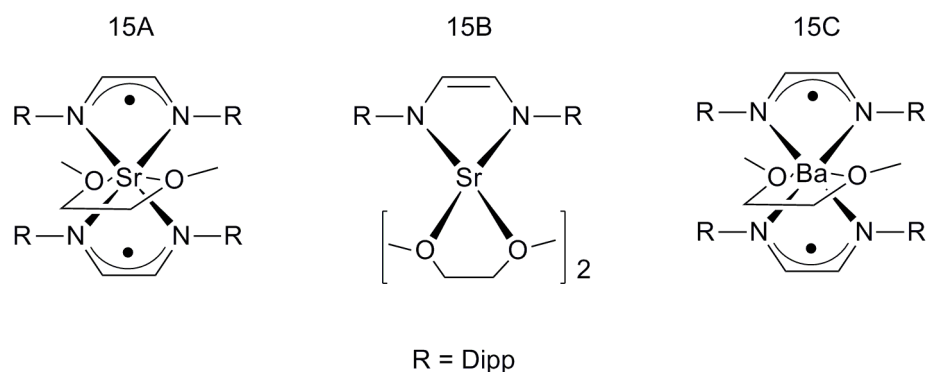
Scheme 13. Magnesium complexes with $\text{Me}_2\text{DAD}^{\text{Dipp}}$ and $\text{Me}_2\text{DAD}^{\text{Mes}}$ ligands.^[36]

Similar to alkali metal DAD complexes, alkaline earth metal complexes with DAD ligands can also be synthesized by direct metallation. Mashima et al. reported either direct metallation of $\text{H}^2\text{DAD}^{\text{Dipp}}$ ligand in the presence of iodine (1 mol %) by Ca and Sr or salt metathesis reaction of dipotassium salt of $\text{H}^2\text{DAD}^{\text{Dipp}}$ with CaI_2 and SrI_2 to yield enediamide type DAD complexes $[(\text{H}^2\text{DAD}^{\text{Dipp}})\text{Ca}(\text{THF})_4]$ (14A) and $[(\text{H}^2\text{DAD}^{\text{Dipp}})\text{Sr}(\text{THF})_4]$ (14B), respectively (Scheme 14).^[42] The iodide-bridged binuclear complex $[\text{K}(\text{THF})_2(\text{H}^2\text{DAD}^{\text{Dipp}})\text{Ba}(\mu\text{-I})(\text{THF})_2]_2$ (14C) was synthesized by the treatment of a dipotassium salt of $\text{H}^2\text{DAD}^{\text{Dipp}}$ with BaI_2 while $[(\text{H}^2\text{DAD}^{\text{Dipp}})\text{Ba}(\mu\text{-I})(\text{THF})_2]_2$ (14D) was synthesized by the treatment of the $\text{H}^2\text{DAD}^{\text{Dipp}}$ with 0.5 equiv. of Ba and BaI_2 or with Ba metal powder in the presence of iodine (10 mol%).



Scheme 14. Strontium and barium DAD complexes synthesized in the presence of iodine.^[42]

Recently, Edelmann et al. reported direct metallation of $\text{H}^2\text{DAD}^{\text{Dipp}}$ ligand by strontium or barium in the absence of iodine (Scheme 15, page 14).^[43] The treatment of $\text{H}^2\text{DAD}^{\text{Dipp}}$ ligand with strontium yielded strontium complexes with two radical-monoanionic $\text{H}^2\text{DAD}^{\text{Dipp}}$ ligands, $[(\text{H}^2\text{DAD}^{\text{Dipp}})_2\text{Sr}(\text{DME})]$ (15A), and dianionic $\text{H}^2\text{DAD}^{\text{Dipp}}$ ligand, $[(\text{H}^2\text{DAD}^{\text{Dipp}})\text{Sr}(\text{DME})_2]$ (15B), whereas the treatment of $\text{H}^2\text{DAD}^{\text{Dipp}}$ ligand with barium yielded only the barium complex with two radical-monoanionic $\text{H}^2\text{DAD}^{\text{Dipp}}$ ligands, $[(\text{H}^2\text{DAD}^{\text{Dipp}})_2\text{Ba}(\text{DME})]$ (15C). Moreover, the barium was successfully employed to transfer the monoanionic DAD ligand to holmium.

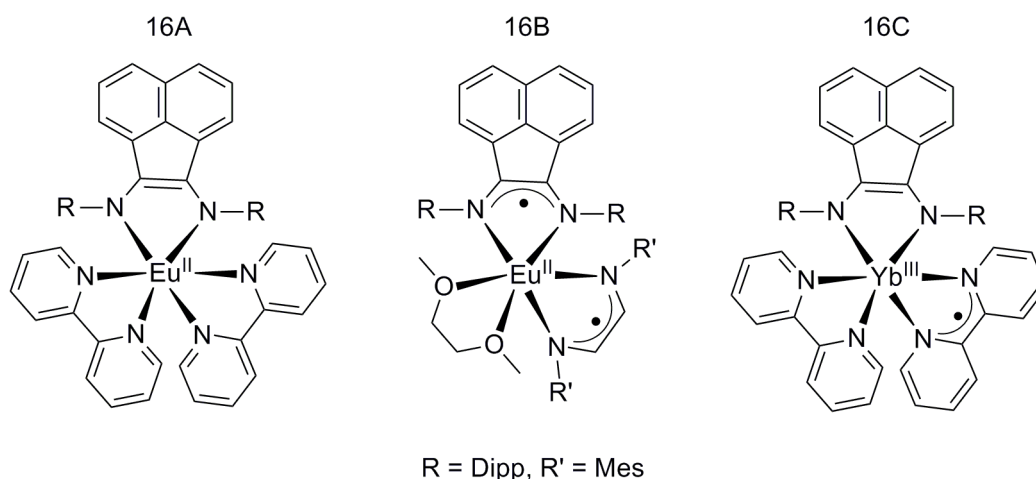


Scheme 15. Strontium and barium DAD complexes synthesized in the absence of iodine.^[43]

1.4. The chemistry of lanthanide complexes with DAD ligands

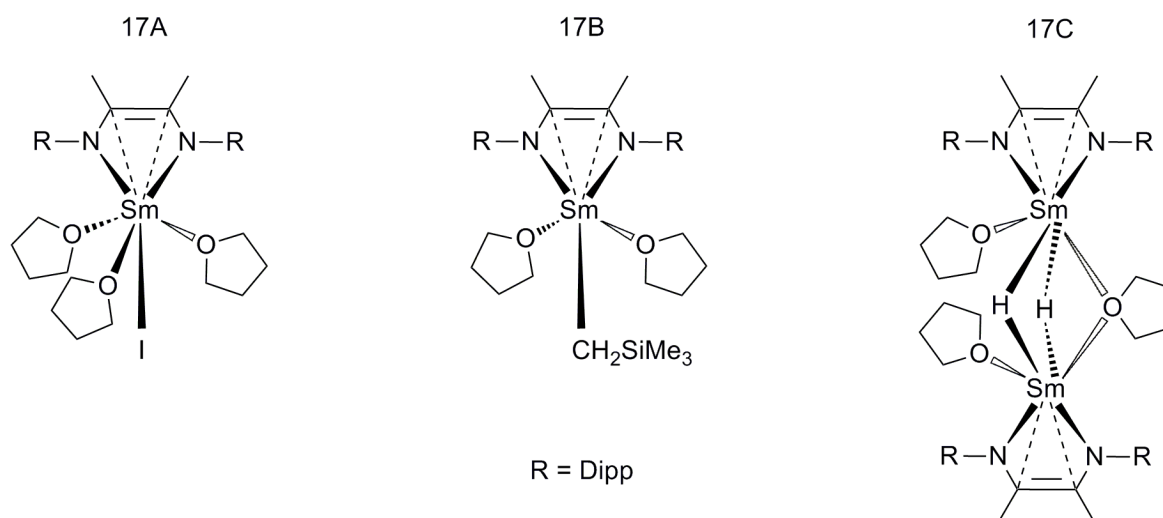
Modern organo-rare-earth metal chemistry is focused on the design of new ligand systems suitable for coordination to rare-earth metals and the investigation of the structure-reactivity relationships.^[100-103] The development of new fields of research has been stimulated by the use of DAD ligands in lanthanide chemistry during past three decades.^[104-126] Rare-earth complexes are used as catalysts (e.g. the ring opening polymerization of racemic lactide and β -butyrolactone^[118] and hydrosilylation of alkenes^[127-141,149]).

Among the possible coordination modes of DAD ligands, radical-monoanions and enediamide dianions are the most common coordination modes with lanthanides. Fedushkin and co-workers reported synthesis and characterization of europium and ytterbium complexes containing simultaneously two different redox-active ligands ($\text{Bian}^{\text{Dipp}}$ = bis[*N*-(2,6-diisopropylphenyl)imino]acenaphthene and Bipy = bipyridine) (Scheme 16, page 15). The complexes $[(\text{Bian}^{\text{Dipp}})\text{Eu}^{\text{II}}(\text{Bipy})_2]$ (16A) and $[(\text{Bian}^{\text{Dipp}})\text{Yb}^{\text{III}}(\text{Bipy})_2]$ (16C) were prepared by the addition of two molar equivalents of 2,2'-bipyridine (Bipy) to the europium complex $[(\text{Bian}^{\text{Dipp}})\text{Eu}^{\text{II}}(\text{DME})_2]$ in toluene and to the ytterbium complex $[(\text{Bian}^{\text{Dipp}})\text{Yb}^{\text{II}}(\text{DME})_2]$ in DME, respectively. The complex $[(\text{Bian}^{\text{Dipp}})\text{Eu}^{\text{I}}(\text{H}^2\text{DAD}^{\text{Mes}})(\text{DME})_2]$ (16B) was prepared by the addition of one equiv. of $\text{H}^2\text{DAD}^{\text{Mes}}$ to $[(\text{Bian}^{\text{Dipp}})\text{Eu}^{\text{II}}(\text{DME})_2]$ in toluene. Coordination environment of metal atoms in both complexes 16A and 16C is almost similar: the six nitrogen atoms form an irregular octahedron (which tends toward trigonal prismatic geometry) while the same in complex 16B is a distorted octahedral arrangement with three nitrogen and two oxygen atoms occupying equatorial position.^[126]



Scheme 16. Acenaphthene-based DAD complexes of europium and ytterbium.^[126]

Recently, Cui and co-workers reported synthesis and characterization of the ene-diamido samarium alkyl (17B) and hydride (17C) (Scheme 17). These complexes enabled highly regioselective hydrosilylation of a range of aryl-substituted internal alkenes, even in the presence of bulky groups.^[129] The monomeric samarium iodide complex 17A was prepared by treating $\text{Me}_2\text{DAD}^{\text{Dipp}}$ ligand with samarium (1 equiv.) and iodine (0.5 equiv.) in THF. The samarium atom is coordinated by the C_2N_2 moiety (η^4), three THF molecules, and an iodide ligand.



Scheme 17. Samarium iodide, alkyl, and hydride complexes with $\text{Me}_2\text{DAD}^{\text{Dipp}}$ ligand.^[149]

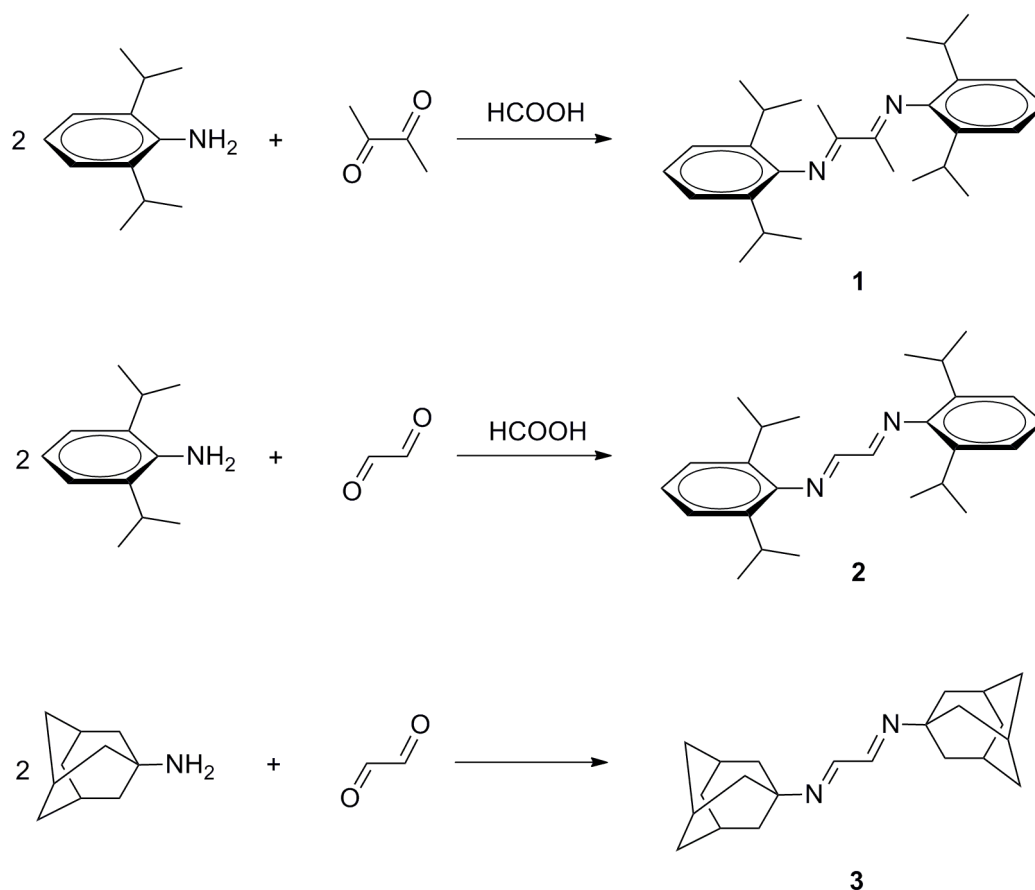
The samarium alkyl complex 17B was prepared by the reaction of 17A with $\text{KCH}_2\text{SiMe}_3$. The reaction of 17A with $n\text{-C}_6\text{H}_{13}\text{SiH}_3$ in *n*-hexane yielded the dimeric samarium hydride complex 17C in which the two samarium atoms are bridged by two hydrides and one THF molecule and are coordinated by two terminal THF molecules. In all these complexes, the samarium is η^4 -coordinated by the C_2N_2 moiety of the DAD ligand (Scheme 17, page 15).^[149]

Based on literature survey, the structural studies of alkali metal DAD complexes are mostly limited to lithium, sodium, and potassium.^[5-15] Moreover, most of these structural studies investigate mainly the influence of solvents or the influence of substituents at the C and N atoms of the DAD moiety on the molecular structures of these complexes. In order to study the influence of different alkali metals on the molecular structure of DAD complexes, it is necessary to use the same ligand and same donor solvent. Liddle and co-workers attempted to synthesize different alkali metal complexes with same DAD ligand and donor solvent.^[15] However, they were not successful to synthesize dirubidium and dicesium complexes. In this Ph.D work, such an attempt was made not only for dianionic DAD complexes but also for radical-monoanionic DAD complexes. For that purpose, the whole series of alkali metal complexes with both dianionic $\text{Me}_2\text{DAD}^{\text{Dipp}}$ and monoanionic DAD^{Dipp} ligands have been successfully synthesized and characterized. The molecular structure of most of these complexes, especially of monopotassium, mono- and dirubidium, and dicesium DAD complexes (for the first time), were successfully determined by X-ray crystallography and discussed in detail. For the first time, a series of heterobimetallic alkali metal DAD complexes were also synthesized, and X-ray structures of bimetallic (K/Li, Rb/Li, and Na/K) DAD complexes were successfully determined. In order to understand the reactivity of DAD complexes, Li, Na, and K complexes with radical-monoanionic $\text{Me}_2\text{DAD}^{\text{Dipp}}$ ligands were treated with carbodiimides to yield a series of new heterocyclic compounds. The research work was further extended to an alkaline earth metal (Ca) as well as lanthanides (Yb, Sm, and Eu).

2. Results and Discussion

2.1. Synthesis of DAD ligands (1-3)

Ligands $\text{Me}_2\text{DAD}^{\text{Dipp}}$ (**1**),^[66] $\text{H}_2\text{DAD}^{\text{Dipp}}$ (**2**),^[67] and $\text{H}_2\text{DAD}^{\text{Ad}}$ (**3**)^[68] were synthesized according to the published procedures (Scheme 18). A condensation reaction between 2,6-diisopropylaniline and butanedione was carried out in ethanol in a 2:1 molar ratio in the presence of a few drops of formic acid (catalyst) to yield ligand **1** as yellow precipitate. Similarly, ligand **2** was also prepared as yellow precipitate by reacting 2,6-diisopropylaniline with glyoxal in the presence of a few drops of formic acid. However, ligand **3** was prepared as white precipitate by reaction of 1-adamantylamine with glyoxal in the absence of formic acid.^[66-68]



Scheme 18. Synthesis of DAD ligands $\text{Me}_2\text{DAD}^{\text{Dipp}}$ (**1**),^[66] $\text{H}_2\text{DAD}^{\text{Dipp}}$ (**2**),^[67] and $\text{H}_2\text{DAD}^{\text{Ad}}$ (**3**).^[68]

2.2. Spectroscopic analysis of DAD ligands (1-3)

The ligands **1-3** were characterized by NMR and IR spectroscopy for the comparison study with the synthesized complexes. The NMR spectra were recorded in *d*8-THF, and all the protons and carbons were observed. The ¹H NMR and ¹³C NMR chemical shifts of ligands **1** and **2** are summarized in Table 1. In the ¹H NMR spectrum, the CH₃ protons of the isopropyl groups in **1** were observed as doublet at 1.14 ppm and 1.19 ppm, whereas those in **2** were observed as doublet only at 1.19 ppm. Similarly, in the ¹³C NMR spectrum, the CH₃ carbons of the isopropyl groups in **1** were observed at 22.8 ppm and 23.3 ppm, whereas those in **2** were observed only at 23.6 ppm. This reveals that the isopropyl groups in **1** are chemically non-equal. The CH₃ (of **1**) and CH (of **2**) protons at the DAD backbone were observed as singlet at 2.06 ppm and 8.1 ppm, respectively. The CH₃ (of **1**) carbons at the DAD backbone were observed at 16.5 ppm while the CCH₃ (of **1**) and CH (of **2**) carbons at the same were observed at 168.9 ppm and 164.3 ppm, respectively. The chemical shifts of all the other protons and carbons were almost similar for both **1** and **2**. ¹H NMR and ¹³C NMR chemical shifts of ligand **3** are summarized in Table 2 (page 19). The chemical shifts of the protons and carbons at the DAD backbone of **3** were closer to that of **2**.

Table 1. ¹H NMR and ¹³C NMR chemical shifts of ligands **1** and **2**.

¹ H NMR δ	1	2	¹³ C NMR δ	1	2
CH(CH ₃) ₂	1.14	-	NCCH ₃	16.5	-
CH(CH ₃) ₂	1.19	1.19	CH(CH ₃) ₂	22.8	-
NCCH ₃	2.06	-	CH(CH ₃) ₂	23.3	23.6
CH(CH ₃) ₂	2.74	2.96	CH(CH ₃) ₂	29.3	28.8
<i>para</i> -Ar	7.03	7.07	<i>meta</i> -Ar	123.6	123.7
<i>meta</i> -Ar	7.14	7.16	<i>para</i> -Ar	124.5	125.6
NCH	-	8.1	<i>ortho</i> -Ar	135.5	137.1
			<i>ipso</i> -Ar	147.1	149.4
			NCCH ₃	168.9	-
			NCH	-	164.3

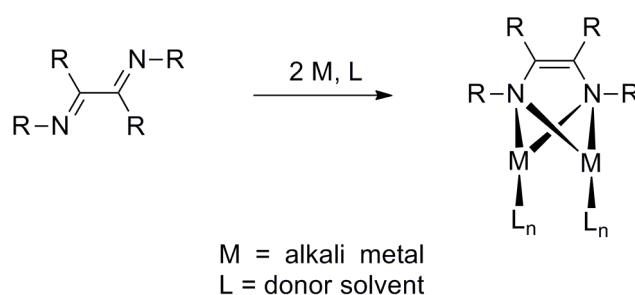
Table 2. ^1H NMR and ^{13}C NMR chemical shifts of ligand **3**.

^1H NMR δ	3	^{13}C NMR δ	3
CHCH₂	1.66 - 1.76	CHCH₂	30.5
CHCH₂	2.1	CHCH₂	37.3
CNCH	7.8	CHCH₂	43.6
		CNCH	58.6
		CNCH	157.9

For ligands **1**, **2**, and **3**, there is no literature reference for the IR frequency of the C=N bond. However, by comparing the IR spectra of the ligands **1-3**, the stretching vibrations corresponding to the C=N bond of the ligands **1**, **2**, and **3** were identified as strong band at 1630 cm^{-1} , strong band at 1625 cm^{-1} , and medium band at 1626 cm^{-1} , respectively. As there are not aromatic groups in **3**, it was possible to identify the absorption band of C=N bonds (1626 cm^{-1}). The absorption band of the aromatic groups in **1** and **2** was eliminated by comparing the IR spectrum of **1** and **2** with **3**. Consequently, the absorption band of C=N bonds in **1** (at 1630 cm^{-1}) and **2** (at 1635 cm^{-1}) were identified.

2.2. Alkali metal complexes with dianionic DAD ligands

Structural studies of alkali metal DAD complexes are mostly limited to lithium, sodium, and potassium.^[5-15] Liddle and co-workers attempted to synthesize the whole series of alkali metal complexes with same dianionic DAD ligand and donor solvent.^[15] However, they were not successful to synthesize rubidium and cesium complexes with dianionic DAD ligand. Such an attempt was made in this Ph.D work, and the whole series alkali metal complexes with dianionic DAD ligands were successfully synthesized and characterized. As shown in Scheme 19, alkali metal complexes with dianionic DAD ligands are generally synthesized in donor solvents by direct metallation.^[5-15]

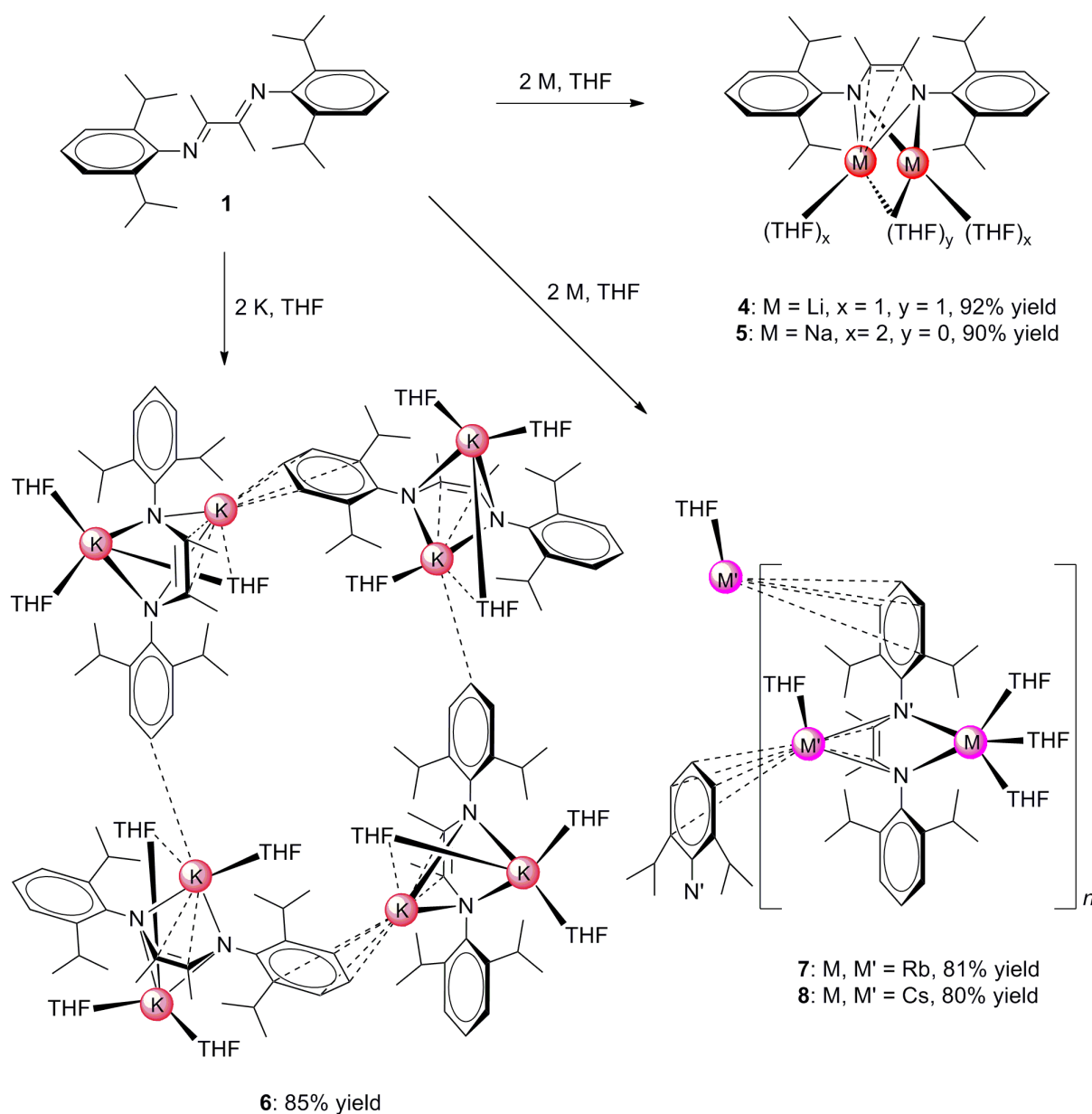


Scheme 19. General synthesis of alkali metal complexes with dianionic DAD ligands by direct metallation.

2.2.1. Synthesis of alkali metal complexes (4-8) with dianionic ^{Me2}DAD^{Dipp} ligands

In an attempt to investigate the structural relationship of new alkali metal complexes with dianionic DAD ligand, the whole series of alkali metal (except francium) complexes with ^{Me2}DAD^{Dipp} ligand (**1**) was prepared by direct metallation of **1** by alkali metals in a 1:2 molar ratio in THF, and the results are summarized in Scheme 20 (page 21). When a solution of **1** in THF was stirred with lithium metal at r.t., a deep red color developed after approximately 1 h. In order to ensure complete reaction, stirring was continued overnight, and the resulting orange-colored solution was concentrated before it was kept at 5 °C to yield [Li₂(^{Me2}DAD^{Dipp})(μ-THF)(THF)₂] (**4**) as orange blocks in excellent (92%) yield. In a similar way, complexes [Na₂(^{Me2}DAD^{Dipp})(THF)₄] (**5**) as red plates, {[K₂(^{Me2}DAD^{Dipp})(μ-THF)(THF)₂] · [K₂(^{Me2}DAD^{Dipp})(μ-THF)(THF)₃]}₂ (**6**) as red rods,

$\{[\text{Rb}_2(\text{Me}_2\text{DAD}^{\text{Dipp}})(\text{THF})_4]_2 \cdot \text{THF}\}_n$ (**7**) as red plates, and $\{[\text{Cs}_2(\text{Me}_2\text{DAD}^{\text{Dipp}})(\text{THF})_4] \cdot \text{THF}\}_n$ (**8**) as orange plates were also synthesized in 90%, 85%, 81%, and 80% yields, respectively. These highly air- and moisture-sensitive complexes were fully characterized by NMR and IR spectroscopy as well as MS and elemental analyses. Single-crystal structures of all the complexes were successfully determined by X-ray crystallography. Elemental analysis (values for C, H, and N of **4-8** were consistent with the proposed formulation of **4-8**, respectively) shows that complexes **7** and **8** keep the THF of crystallization (uncoordinated THF) upon drying.



Scheme 20: Synthesis of alkali metal complexes (**4-8**) with dianionic $\text{Me}_2\text{DAD}^{\text{Dipp}}$ ligand.

2.2.2. Spectroscopic analysis of the complexes (4-8)

The NMR spectra were recorded in d_8 -THF, and the ^1H NMR and ^{13}C NMR data of all the complexes together with the precursor ligand **1** are summarized in Tables 3 and 4, respectively. In the ^1H NMR spectra, compared to the neutral ligand **1**, the resonances corresponding to the CH_3 (DAD moiety), *meta*, and *para* protons of the complexes (**4-8**) were observed at higher field, whereas the resonances corresponding to the *tertiary* protons of the isopropyl group were observed at lower field. Moreover, the resonances corresponding to *tertiary* protons of the isopropyl group in **4**, as shown in the HSQC spectrum of **4** (Figure 1, page 23), were overlapped with the THF signal between 3.5 and 3.6 ppm while the same in **8** (Figure 2, page 24) were observed as broad signal at 3.76 ppm.

Table 3. ^1H NMR chemical shifts of alkali metal complexes (**4-8**) with dianionic $\text{Me}_2\text{DAD}^{\text{Dipp}}$ ligands.

δ in ppm	1	4	5	6	7	8
$\text{CH}(\text{CH}_3)_2$	1.14	1.02	1.02	1.02	1.02	1.03
$\text{CH}(\text{CH}_3)_2$	1.19	1.16	1.21	1.22	1.21	1.17
NCCH_3	2.06	1.54	1.65	1.65	1.62	1.56
$\text{CH}(\text{CH}_3)_2$	2.74	3.5 – 3.6	3.7	3.68	3.7	3.76
<i>para</i> -Ar	7.03	6.46	6.18	5.96	5.9	5.88
<i>meta</i> -Ar	7.14	6.79	6.69	6.63	6.61	6.61

Table 4. ^{13}C NMR chemical shifts of alkali metal complexes (**4-8**) with dianionic $\text{Me}_2\text{DAD}^{\text{Dipp}}$ ligands.

δ in ppm	1	4	5	6	7	8
NCCH_3	16.5	16.3	18.0	18.8	19.1	19.6
$\text{CH}(\text{CH}_3)_2$	22.8	24.3	24.2	24.2	24.5	24.8
$\text{CH}(\text{CH}_3)_2$	23.3	25.8	25.2	25.7	26.0	25.4
$\text{CH}(\text{CH}_3)_2$	29.3	27.6	27.4	27.5	27.4	27.2
<i>para</i> -Ar	124.5	117.1	112.3	109.1	108.2	108.1
NCCH_3	168.9	120.2	121.1	121.2	121.5	121.7
<i>meta</i> -Ar	123.6	122.5	122.6	122.9	123.0	123.6
<i>ortho</i> -Ar	135.5	142.5	139.4	137.2	136.4	136.0
<i>ipso</i> -Ar	147.1	154.4	156.6	155.6	155.0	154.0

In the ^{13}C NMR spectra, the resonances corresponding to the carbons of the DAD backbone – $\text{N}=\text{C}-\text{C}=\text{N}-$ of the neutral ligand **1** were observed at 168.9 ppm, whereas those of all the complexes (**4-8**) were observed at higher field between 120 and 122 ppm. These spectral data confirm the presence of olefinic carbons and the dianionic nature of the DAD moiety (corresponding to $-\text{N}-\text{C}(\text{Me})=\text{C}(\text{Me})-\text{N}-$).

The ^7Li NMR spectrum (155 MHz, d_8 -THF, 25 °C) of **4** displayed a single resonance at 2.62 ppm, suggesting the presence of equal lithium centres in solution and a pure product. Liddle and co-workers also observed a single resonance at 2.62 ppm for the dilithium complex of *N,N'*-bis(2,4,6-triisopropylphenyl)-*o*-phenylenediamide derivative.^[15]

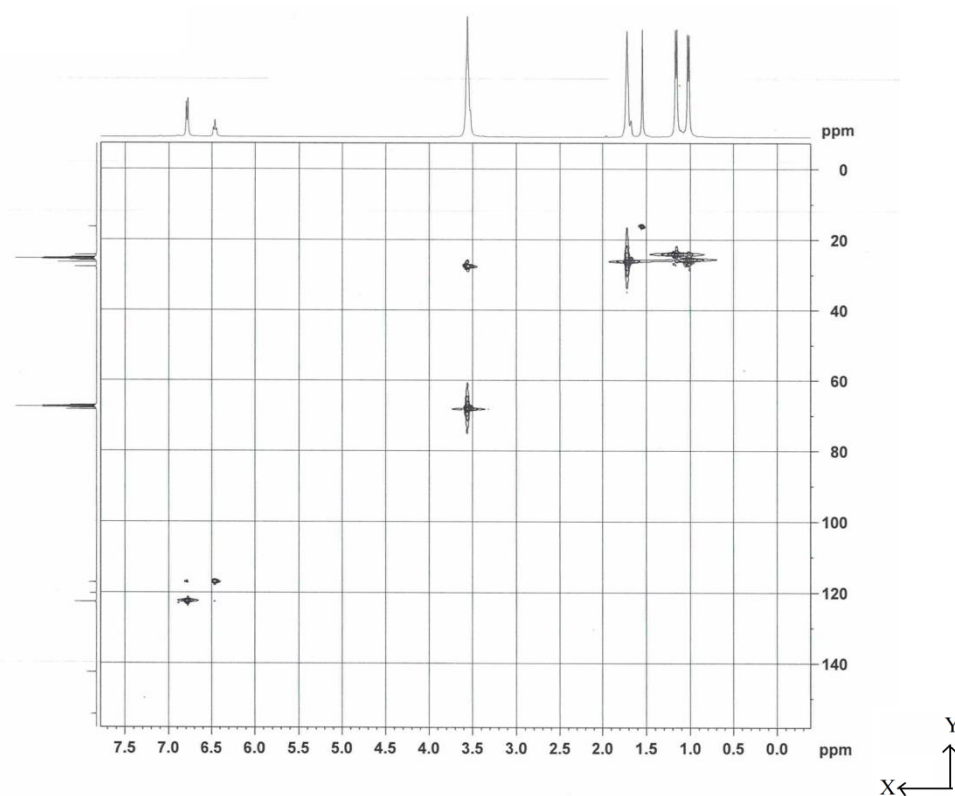


Figure 1. HSQC spectrum of **4** (X-axis: ^1H NMR chemical shifts (400 MHz), Y-axis: ^{13}C NMR chemical shifts (100 MHz), d_8 -THF, 23 °C).

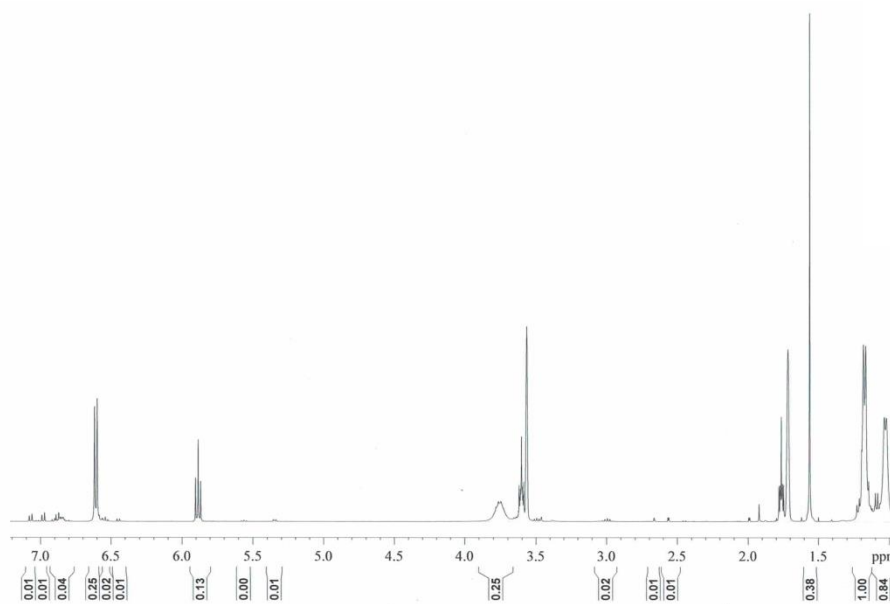


Figure 2. ^1H NMR spectrum of **8** (400 MHz, d_8 -THF, 23 °C).

The stretching vibrations of the C–N and C=C bonds of the DAD moiety in the complexes (**4-8**) could not be identified due to overlap of bands in their IR spectrum. However, the stretching vibrations of the C=N bond, manifested as a strong band at 1630 cm^{-1} in the IR spectrum of **1**, disappeared completely in the IR spectrum of all the complexes (**4-8**). The molecular ion peaks of the complexes were not observed in the EI mass spectrum of the complexes (**4-8**). However, the peaks at m/z 633 and 433 in the mass spectrum of **4** could be assigned to the fragments $[\text{M}^+ - \text{H}]$ and $[\text{M}^+ - (3\text{ C}_3\text{H}_7, \text{THF})]$, respectively, and the peak at m/z 651 in the mass spectrum of **5** could be assigned to the fragment $[\text{M}^+ - (\text{CH}_3, \text{THF})]$. The mass spectra of complexes (**6-8**) exhibited only the fragments of the monomeric species, and the peak at m/z 524 in the mass spectrum of **6** could be assigned to the fragment $[\text{K}_2(\text{Me}_2\text{DAD}^{\text{Dipp}})(\text{THF}) - 2\text{ CH}_3]$ while the same at m/z 420 in the mass spectrum of **7** and at m/z 898 in the mass spectrum of **8** could be assigned to the fragments $[\text{M}^+ - (4\text{ C}_3\text{H}_7, \text{C}_4\text{H}_6, 3\text{ THF})]$ and $[\text{M}^+ - 4\text{ CH}_3]$, respectively. Consequently, the complexes lose most readily THF ligands and $i\text{Pr}$ and Me groups in the mass spectrometer.

2.2.3. Molecular Structures of $[\text{Li}_2(\text{Me}_2\text{DAD}^{\text{Dipp}})(\mu\text{-THF})(\text{THF})_2]$ (4) and $[\text{Na}_2(\text{Me}_2\text{DAD}^{\text{Dipp}})(\text{THF})_4]$ (5)

The lithium complex **4** crystallizes from THF at 5 °C as a monomer in the monoclinic space group $P2_1$ and contains one molecule in the asymmetric unit. As shown in Figure 3, the lithium atom Li2 is coordinated by the chelating $\text{Me}_2\text{DAD}^{\text{Dipp}}$ ligand through its nitrogen atoms, forming a five-membered $\text{C}_2\text{N}_2\text{Li}$ ring, while the lithium atom Li1 is η^4 -coordinated by the DAD π -electronic system of the complex, forming a puckered four-membered ring Li_2N_2 with an angle of 78.6° between the planes LiN_2 . Additionally, each lithium atom is coordinated by a terminal THF molecule; a third THF molecule bridges the two lithium atoms resulting in coordination number 4 for Li2. The Li2 center is located substantially in the plane (N1-Li2-N2 plane deviates by 23.8° from $\text{Me}_2\text{C}_2\text{N}_2$ plane) of the DAD backbone, while the Li1 center sits above the plane (N1-Li1-N2 deviates by 77.6° from $\text{Me}_2\text{C}_2\text{N}_2$ plane) of the DAD backbone.

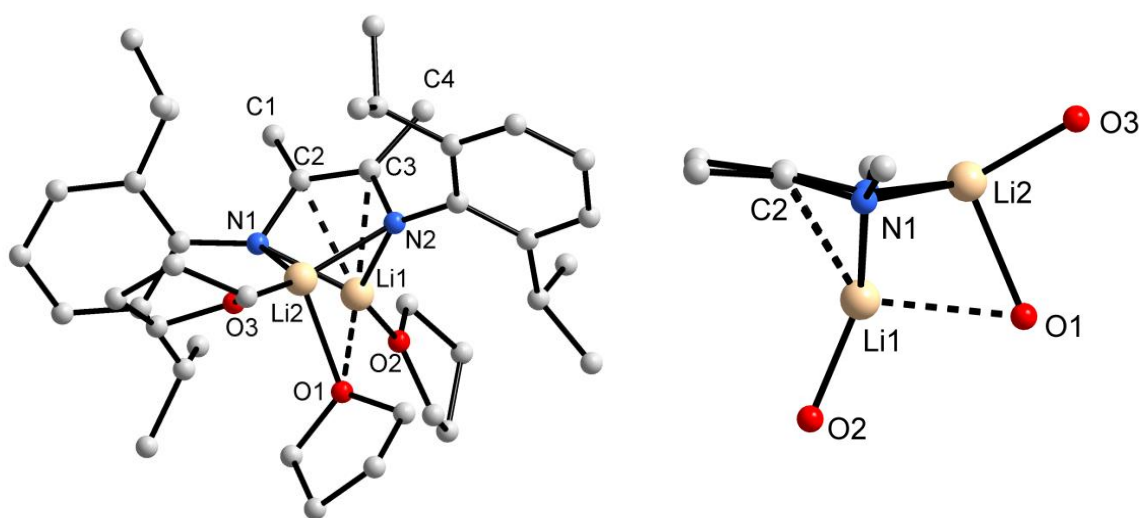


Figure 3. Molecular structure of **4** (left). Representation of the coordination sphere of the lithium atoms in **4** (right), viewed along the N1-N2 vector.

The coordination environment of Li1 and Li2 can be better described as a distorted trigonal pyramidal arrangement with two nitrogen atoms from the chelating ligand and an oxygen atom from the terminal THF ligand occupying the trigonal base and an oxygen atom from the bridging THF ligand occupying the apical position. The plane of the six-membered ring attached to N1 and N2 deviates from the plane of the DAD backbone by 66.6° and 76.9°,

respectively. In complex **4**, similar to the dimeric dilithium complex of *N,N'*-disilyl-*o*-phenylenediamide derivative with two bridged and two terminal THF ligands reported by Lappert and co-workers,^[6] the terminal THF bonds are shorter than the bridged one [Li–O bond lengths in **4**: Li1–O1 (2.244(6) Å), Li1–O2 (1.895(5) Å), Li2–O1 (2.166(5) Å), and Li2–O3 (1.946(4) Å)]. Moreover, the bridging THF is more strongly coordinated to the Li2 metal center than to the Li1. The Li–N bond lengths Li1–N1 (2.008(4) Å), Li1–N2 (2.030(6) Å), Li2–N1 (2.021(4) Å), and Li2–N2 (2.046(5) Å) in **4** are well within the range of those [Li–N: 2.077(4) Å/ 2.131(4) Å/ 1.942(4) Å/ 1.982(4) Å] in the monomeric dilithium complex of *N,N'*-bis(2,4,6-triisopropylphenyl)-*o*-phenylenediamide derivative reported by Liddle and co-workers.^[15] The distance (Li1–C3 2.260(6) Å and Li1–C2 2.260(5) Å, Li2...C2 2.798(4) Å, and Li2...C3 2.808(5) Å) between the metal centers and the carbon atoms of the DAD moiety confirms the π -interactions between the Li1 metal center and the olefinic carbons of the diazadiene moiety in **4**. The different bonding situation of the metal atoms (one σ -coordinated by the nitrogen atoms while the other is η^4 -coordinated by π -electronic system of the DAD moiety) was also reported by Liddle and co-workers. In fact, the Li1–C distances in **4** are shorter than those [Li–C: 2.492(4) Å/ 2.462(4) Å] in their report, reiterating the π -interactions between the Li1 metal center and diazadiene moiety.

The sodium complex **5** also crystallizes from THF at 5 °C as a monomer, however, in the monoclinic space group $P2_1/c$ with one molecule of the complex in the asymmetric unit. Similar to complex **4**, there are two differently coordinated metal atoms in complex **5** (for example, Na2 is σ^2 -coordinated to the nitrogen atoms while Na1 is η^4 -coordinated to the whole π -electronic system of the DAD moiety as shown in Figure 4, page 27). Additionally, each sodium atom is coordinated by two THF ligands resulting in coordination number 4 for each metal atom. Although, the coordination number of the metal atoms in complex **4** and **5** is the same, there are only three coordinated THF molecules (two terminal and one bridged) in complex **4** while there are four (all terminal) in complex **5**. The deviation of N1–Na2–N2 plane from Me₂C₂N₂ plane (38.2°) in **5** is significantly larger than N1–Li2–N2 plane from the same in **4** while the deviation of N1–Na1–N2 (76.6°) in **5** is similar to that of N1–Li1–N2 plane in **4**. The plane of the six-membered ring attached to N1 and N2 deviates from the plane of the DAD backbone by 45.7° and 68.1°, respectively. The angle between the NaN₂ planes of the four-membered puckered ring Na₂N₂ is 65.2°.

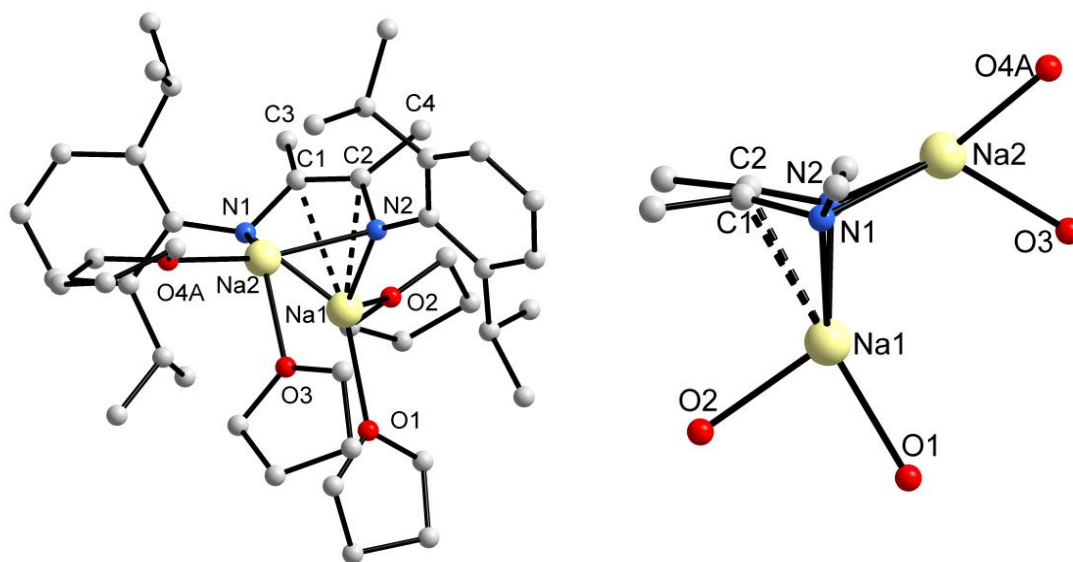


Figure 4. Molecular structure of **5** (left). Representation of the coordination sphere of the sodium atoms in **5** (right), viewed along the N1-N2 vector.

The structure of complex **5** is similar to the sodium complex with dianionic DAD $[\text{Na}_2(\text{Et}_2\text{O})_3(\text{DippNC})_2(\text{C}_{12}\text{H}_6)]$ reported by Fedushkin and co-workers.^[7] The Na–N bond lengths (in the range of 2.354(2) Å to 2.388(2) Å) and metal-carbon distances (Na1–C1 (2.608(3) Å), Na1–C2 (2.611(2) Å), Na2···C1 (3.059(3) Å), and Na2···C2 (3.048(3) Å) in complex **5** are similar to those [Na–N: in the range of 2.343(3) Å to 2.465(3) Å; Na–C: 2.596(3) Å/ 2.614(3) Å; Na···C: 3.053(3) Å/ 3.077(3) Å] in $[\text{Na}_2(\text{Et}_2\text{O})_3(\text{DippNC})_2(\text{C}_{12}\text{H}_6)]$, confirming the π -interactions between Na1 and DAD moiety. Notably, the Na–O bonds (in the range of 2.273(2) Å to 2.344(3) Å) in **5** are similar only to the Na–O bonds of the terminal Et_2O (2.289(3) Å/ 2.311(3) Å), not of the bridged Et_2O (2.456(3) Å/ 2.588(3) Å) in $[\text{Na}_2(\text{Et}_2\text{O})_3(\text{DippNC})_2(\text{C}_{12}\text{H}_6)]$. The η^4 -coordination between one of the metal centers and the π -electronic system of the DAD moiety in complex **5** is also consistent with the other reports of sodium complexes with dianionic DADs.^[9,15] Both Na1 and Na2 adopt distorted trigonal pyramidal geometry with two nitrogen atoms (N1 and N2) from the chelating ligand and an oxygen atom (O1 and O4, respectively) from the terminal THF ligand occupying the trigonal base and an oxygen atom (O2 and O3, respectively) from the terminal THF ligand occupying the apical position.

Compared to the neutral ligand **1**,^[66] the C–C bond length is shortened, whereas the C–N bond lengths are elongated in the DAD backbone of the complexes **4** and **5** (Table 5). A typical long-short-long sequence noticed in **4** and **5**, in the diazadiene backbone corresponding to a –NC(Me)=C(Me)N– bonding situation, is the most important feature for dianionic DAD ligands in enediamide coordination mode (Scheme 1, page 1). Thus, these structural data together with the spectroscopic results confirm the dianionic enediamide coordination (mode E in Scheme 3, page 2) of the ^{Me2}DAD^{Dipp} ligand in complex **4** and **5**.

Table 5. Selected bond lengths [Å] of **4** and **5**.

DAD moiety	1 ^[66]	4	5
C–N (average)	1.279(3)	1.419(3)	1.413(4)
C–C	1.498(3)	1.363(3)	1.372(4)

2.2.4. Molecular Structure of $\{[\text{K}_2(\text{Me}_2\text{DAD}^{\text{Dipp}})(\mu\text{-THF})(\text{THF})_2] \cdot [\text{K}_2(\text{Me}_2\text{DAD}^{\text{Dipp}})(\mu\text{-THF})(\text{THF})_3]\}_2$ (**6**)

The potassium complex **6** crystallizes from THF at 5 °C in the triclinic space group $P\bar{1}$ with two differently solvated molecules of the complex in the asymmetric unit. As shown in Figure 5 (page 29), the K2 and K4 atoms are coordinated by two nitrogen atoms of the ligand, and the coordination sphere of them are saturated by two terminal THF molecules and one bridged THF molecule, resulting in coordination number 5 for each. The K1 and K3 atoms are η^4 -coordinated by the π -electronic system of the DAD moiety of the ligand (similar to Li1 in **4** and Na1 in **5**) and a bridged THF molecule, and the K3 atom is additionally coordinated by a terminal THF molecule. However, the coordinatively unsaturated K1 atom forms three intermolecular K–C contacts to the phenyl-carbons (C59, C60, and C61) of the tetrakis(THF) solvated molecule while the same K2 forms an intermolecular K–C contact to the phenyl-*para*-carbon (C8) of the tris(THF) solvated molecule (Figure 6, page 30). The K1, K2, K3, and K4 metal centers deviate by 75.7°, 29.6°, 72.8°, and 30.5°, respectively, from the Me₂C₂N₂ plane, showing the same pattern noticed in the complexes **4** and **5** [One metal center

(K2 or K4) lies essentially in the plane defined by Me₂C₂N₂ while the other (K1 or K3) sits above the plane and η^4 -coordinated by the DAD π -electronic system of the DAD moiety].

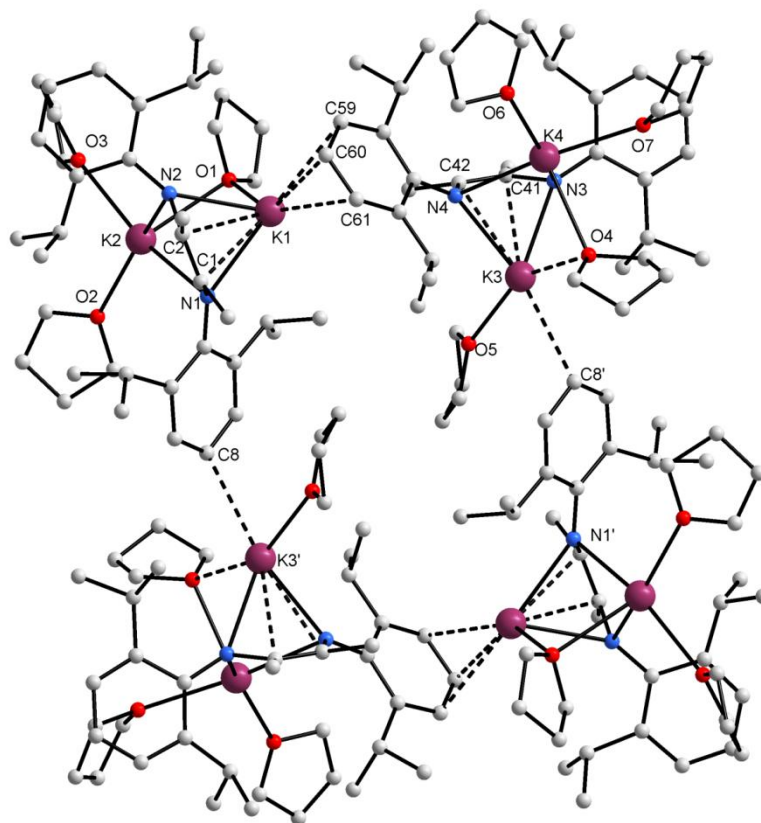


Figure 5. Molecular structure of **6**: Supramolecular aggregation of two tris(THF) solvated molecules and two tetrakis(THF) solvated molecules by intermolecular aryl π -coordination.

Interestingly, one μ -bridging THF coordinates almost equally to both metal centers (K1–O1 2.826(3) Å, K2–O1 2.879(2) Å) while the other coordinates more strongly to K4 metal center than K3 (K3–O4 (3.165(2) Å, K4–O4 (2.818(2) Å)). The K–N, K–O (terminal THF), and K–C (phenyl) bond lengths [in the range of 2.681(2) Å to 2.818(2) Å, 2.712(3) Å to 2.879(2) Å, and 2.965 (4) Å to 3.268 (4) Å, respectively] in complex **6** are comparable with their counterparts [in the range of 2.729(5) Å to 2.801(5) Å, 2.738(5) Å to 3.040(5) Å, and 2.982(6) Å to 3.314(6) Å, respectively] in the dimeric dipotassium complexes of *N,N'*-bis(2,4,6-triisopropylphenyl)-*o*-phenylenediamide derivative reported by Liddle and co-workers.^[15] The coordination geometry of K1 and K3 adopts a distorted trigonal pyramidal and trigonal bipyramidal geometry, respectively, while that of K2 and K4 adopts a distorted square pyramidal arrangement. Compared to complex **4** and **5**, the number of coordinated solvent molecules and the number of π -interactions in **6** are increased which is consistent with

the increase in ionic radius of K^+ (1.33 Å) compared to Li^+ (0.78 Å) and Na^+ (0.98 Å).^[15,62] It is also important to note that complex **6** is a centrosymmetric tetramer (aggregated by intermolecular aryl- π -coordination), whereas complex **4** and **5** are monomers. Thus, it is clear that the structure of complex **6** is impacted by the increased π -interactions (typical for heavier alkali metals).

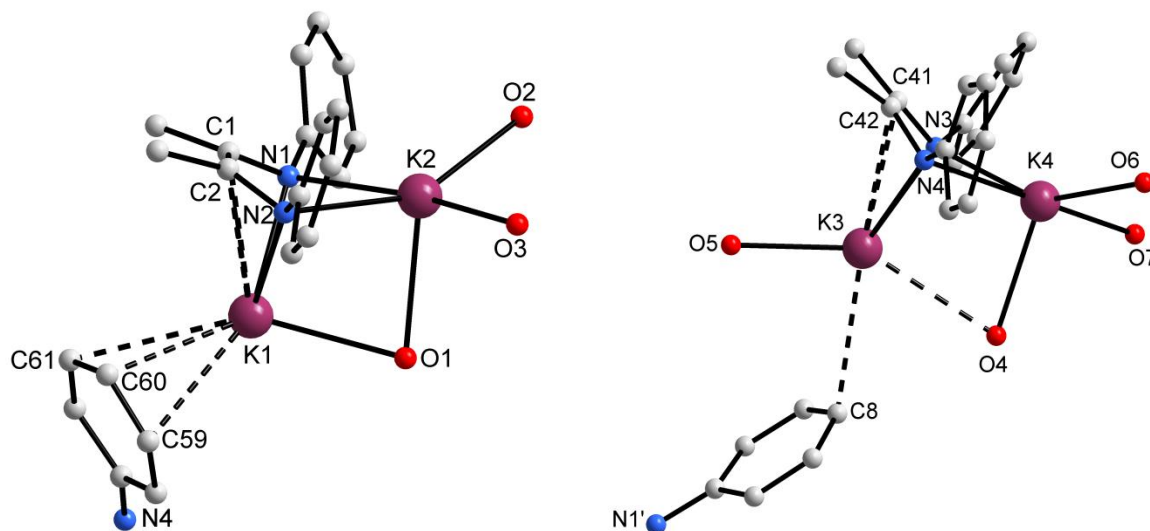


Figure 6. Representation of the coordination sphere of the potassium atoms (in complex **6**) in the tris(THF) solvated molecule (left), viewed along the N1-N2 vector and in the tetrakis(THF) solvated molecule (right), viewed along the N4-N3.

The plane of the six-membered ring attached to N1 and N2 deviates from the plane of the DAD backbone N1-C1-C2-N2 by 48.5° and 76.9°, respectively, while that attached to N3 and N4 deviates from the plane of the DAD backbone N3-C41-C42-N4 by 67.8° and 51.6°, respectively. The average C–C (shorter than in free ligand) and C–N (longer than in free ligand) bond lengths of the DAD moiety in **6** (Table 6, page 33) are similar to those in **4** and **5**, confirming the presence of olefinic carbons in the DAD backbone. The distances between K1 and K3 metal centers and carbons of the DAD backbone to which they are attached [K–C: in the range of 2.899(2) Å to 2.961(3) Å] in **6** are shorter than their counterparts [in the range of 3.170(6) Å to 3.188(6) Å] in the reports of Liddle and co-workers^[15], confirming the π -interactions between K1 and K3 metal centers and the olefinic carbons of the diazadiene moiety they are attached to. All these structural data in combination with spectral data confirm that the complex **6** contains characteristic dianionic DAD ligands.

2.2.5. Molecular Structures of $\{[\text{Rb}_2(\text{Me}_2\text{DAD}^{\text{Dipp}})(\text{THF})_4]_2 \cdot \text{THF}\}_n$ (**7**) and $\{[\text{Cs}_2(\text{Me}_2\text{DAD}^{\text{Dipp}})(\text{THF})_4] \cdot \text{THF}\}_n$ (**8**)

The rubidium complex **7** aggregates from THF at 5 °C as a coordination polymer in the monoclinic space group $P2_1/c$ with two symmetry independent molecules of the complex and an uncoordinated THF molecule in the asymmetric unit. The cesium complex **8** also aggregates from THF at 5 °C as a coordination polymer, however, in the monoclinic space group $C2/c$ with one molecule of the complex in the asymmetric unit. As shown in Figure 7, the molecular structures of complex **7** and complex **8** are similar. The Rb2 atom in **7** and the Cs1 atom in **8** are chelated by the ligand through its two nitrogen atoms while the Rb1 atom in **7** and the Cs2 atom in **8** are η^4 -coordinated by the π -electronic system of the DAD moiety of the ligand (similar to complexes **4-6**).

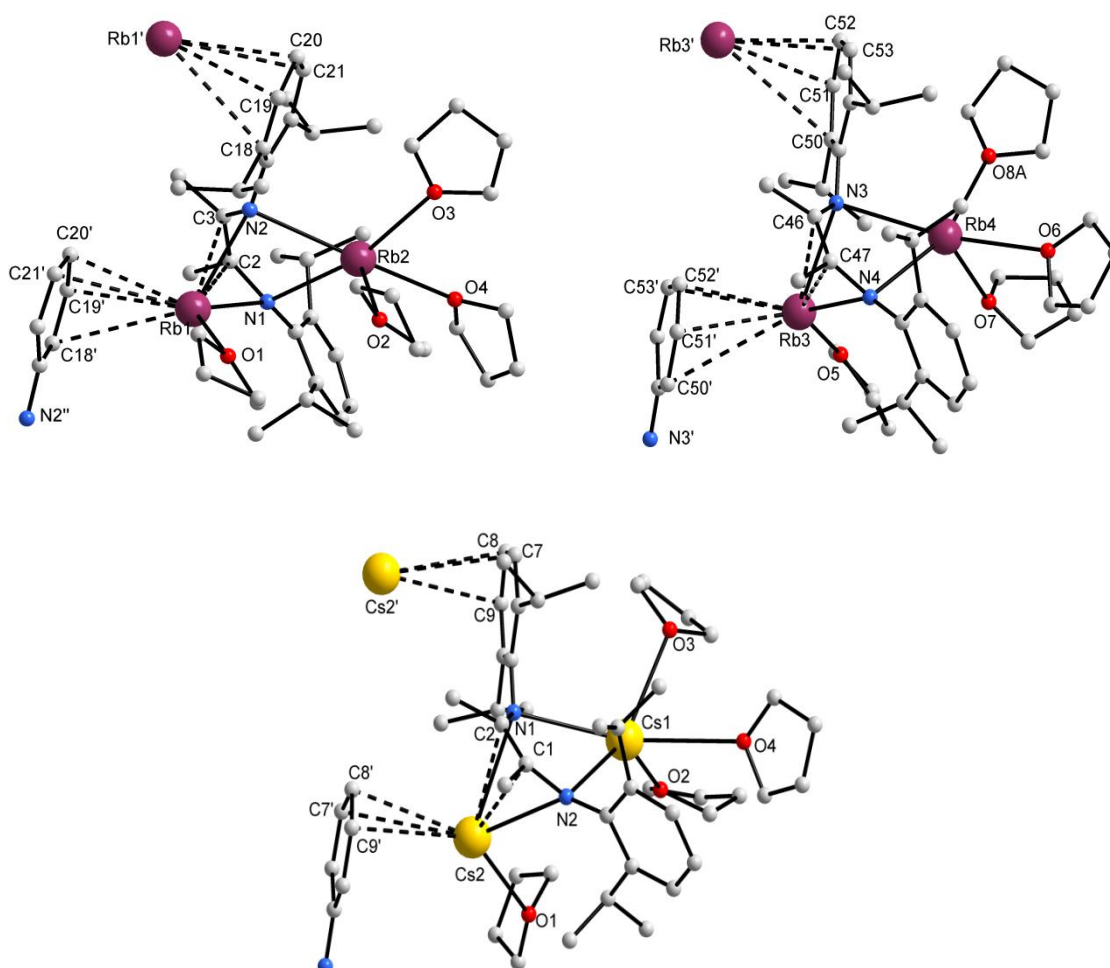


Figure 7. Molecular structure of **7** (molecule 1 (top-left) and 2 (top-right) in the asymmetric unit). Molecular structure of **8** (bottom).

The coordinative saturation of Rb2 and Cs1 is achieved by three THF molecules while that of Rb1 and Cs2 is achieved by a THF molecule and intermolecular metal-aryl contacts (four and three, respectively) to the aromatic ring of the adjacent molecule, forming a linear supramolecular coordination polymeric chain (Figure 8). Unlike complex **8**, complex **7** forms two symmetry independent linear supramolecular coordination polymeric chains as it contains two symmetry independent molecules with only minor differences in the bond lengths and angles.

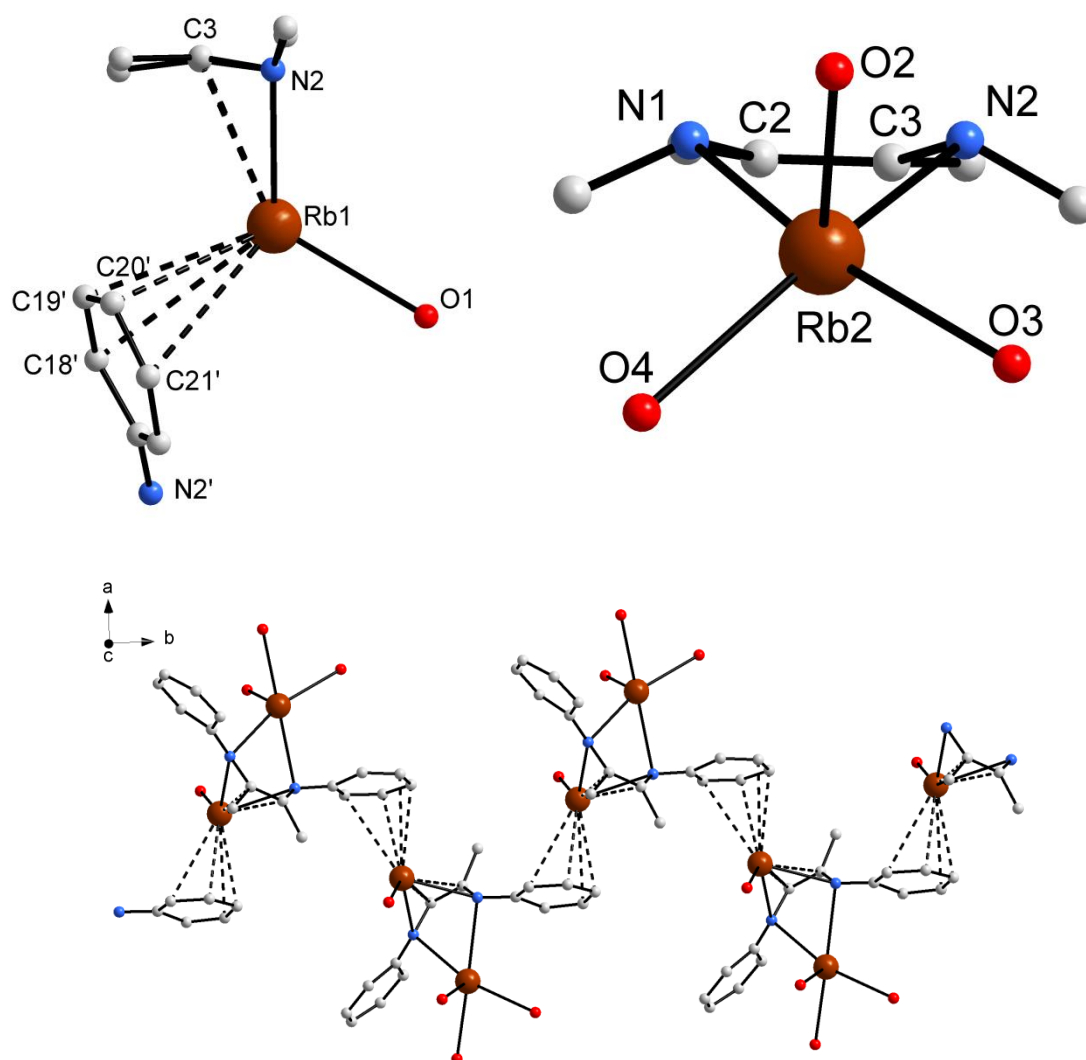


Figure 8. Representation of the coordination sphere of Rb1 (top-left) viewed along the N2-N1 vector and Rb2 (top-right) atoms in **7**. Representation of the intermolecular aryl π -coordination using the example of molecule 1 (isopropyl substituents omitted) and the coordination polymeric chain structure extends parallel to the crystallographic *b* axis (bottom).

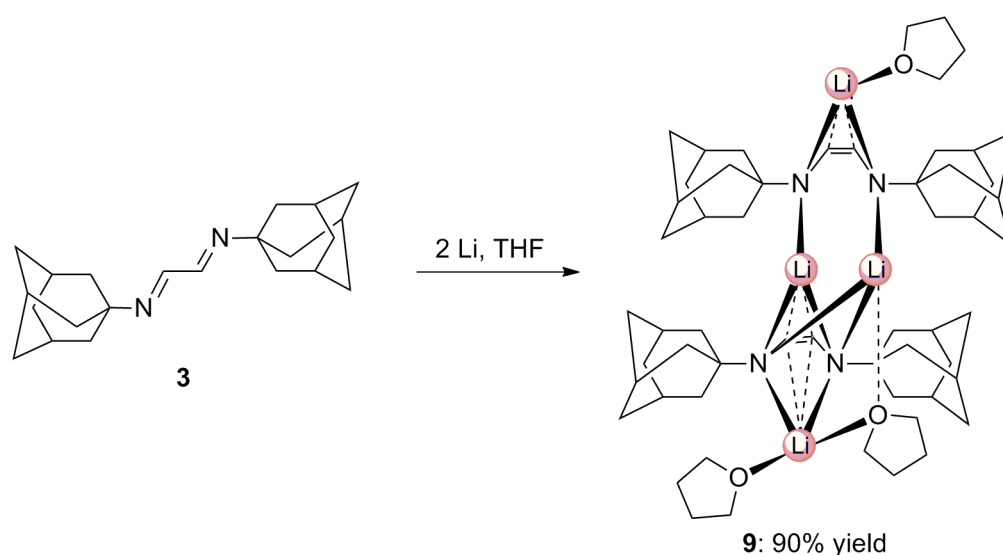
The plane of the six-membered ring attached to N1 and N2 in **7** deviates from the plane of the DAD backbone of the complex **7** by 44.7° and 62.9°, respectively, while the same in **8** deviates from the plane of the DAD backbone of the complex **8** by 53.9° and 54.0°, respectively. The Rb1, Rb2, Cs1, and Cs2 metal centers deviate from the Me₂C₂N₂ plane by 80.9°, 40.0°, 28.1°, and 88.1°, respectively. These findings indicate that one metal center (Rb2 in **7** or Cs1 in **8**) lies essentially in the plane of Me₂C₂N₂ while the other (Rb1 in **7** or Cs2 in **8**) sits above the plane of Me₂C₂N₂ and is η⁴-coordinated by the DAD π-electronic system of the complex as in the previous three complexes **4-6**. The Rb–N, Rb–O, and Rb–C bond lengths are in the range of 2.868(3) Å to 2.951(4) Å, 2.843(9) Å to 2.952(4) Å, and 3.028(4) Å to 3.057(4) Å, respectively, while the Cs–N, Cs–O, and Cs–C 2.992(4) Å to 3.125(5), Å, 3.003(6) Å to 3.217(9) Å, and 3.101(7) Å to 3.135(7) Å, respectively. The coordination geometry of Rb2 and Cs1 can be described as a distorted square-pyramidal arrangement with two nitrogen atoms (N1 and N2) from the chelating ligand and two oxygen atoms (O3 and O4) from the THF ligands occupying the basal position and an oxygen atom (O2) from the THF ligand occupying the apical position. The coordination geometry of Rb1 and Cs2 can be described as a distorted trigonal-pyramidal arrangement with two nitrogen atoms (N1 and N2) from the chelating ligand and an oxygen atom (O1) from the THF ligand occupying the trigonal base. The C–C (shorter than free ligand) and C–N (longer than free ligand) bond lengths of the DAD backbone are shown in the Table 6. All these structural parameters confirm the dianionic character of the Me₂DAD^{DiPP} ligand in complex **7** and **8**.

Table 6. Selected bond lengths [Å] of **6**, **7**, and **8**.

DAD moiety	6	7	8
C–N (average)	1.414(4)	1.413(4)	1.405(8)
C–C	1.362(3) (average)	1.367(6)	1.334(9)

2.2.6. Synthesis and molecular structure of lithium complex $\{Li_2(H^2DAD^{Ad})\}_2(\mu\text{-THF})(THF)_2$ (**9**) with dianionic H^2DAD^{Ad} ligand

In order to synthesize an alkali metal complex with the dianionic H^2DAD^{Ad} ligand (**3**), lithium metal was stirred with **3** in a 2:1 molar ratio in THF until all the lithium was consumed, and the resulting orange-colored solution was concentrated to afford the lithium complex $\{Li_2(H^2DAD^{Ad})\}_2(\mu\text{-THF})(THF)_2$ (**9**) as yellow powder in excellent yield (90%) (Scheme 21). Suitable crystals for X-ray diffraction analysis were grown from toluene at r.t. The stretching vibration corresponding to the C=N bond (observed as a medium band at 1626 cm^{-1} in the IR spectrum of the neutral ligand **3**) disappeared in the IR spectrum of **9**. The peak at m/z 513 in the EI mass spectrum of **9** could be assigned to the fragment $[M^+ - (2\text{ Li}, C_{10}H_{15}N, 3\text{ THF})]$. Compared to the ligand **3**, all the protons and carbons were observed at higher field in the 1H NMR and ^{13}C NMR spectra of **9** (Figure 9, page 35). However, the protons and carbons of the DAD moiety (NCHCHN) of **9** were observed at much higher field (5.37 and 111.3 ppm, respectively). This confirms the olefinic bond formation in the DAD backbone corresponding to -NCH=CHN- . The 7Li NMR spectrum (156 MHz, d_8 -Toluene, $22\text{ }^\circ\text{C}$) displayed a single resonance at 0.96 ppm, showing the presence of chemically equivalent lithium centers solution and a pure product.



Scheme 21. Synthesis of a lithium complex with the dianionic H^2DAD^{Ad} ligand (**3**).

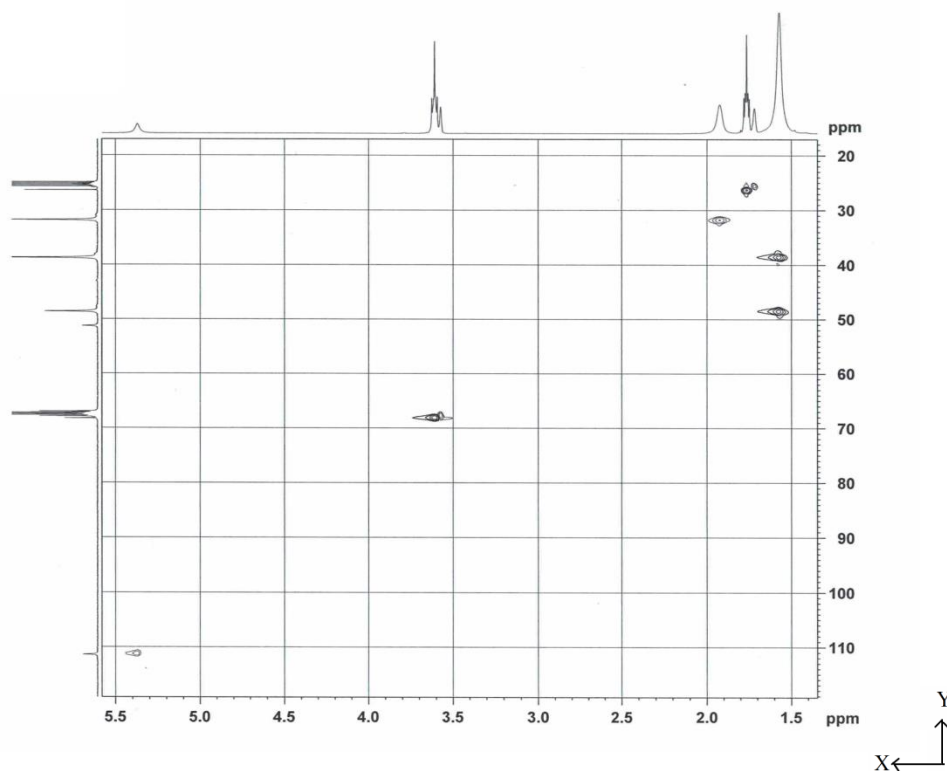


Figure 9. HSQC spectrum of **9** (X-axis: ^1H NMR chemical shifts (400 MHz), Y-axis: ^{13}C NMR chemical shifts (100 MHz), d_8 -THF, 20 °C).

The lithium complex (**9**) with $\text{H}_2\text{DAD}^{\text{Ad}}$ ligand aggregates from toluene at r.t. to a dimer in the triclinic space group $P\bar{1}$ with one molecule of the complex and one toluene molecule in the asymmetric unit. As shown in Figure 10 (page 36), the complex consists of four lithium atoms, two $\text{H}_2\text{DAD}^{\text{Ad}}$ ligands, and three THF molecules. The Li1 is chelated by the nitrogen atoms N1 and N2 the DAD moiety N1–C1–C2–N2 and is bridged to Li2 and Li3 by the nitrogen atoms N1 and N2, respectively. The Li2, Li3, and Li4 atoms are bridged by the chelating nitrogen atoms N3 and N4 of the DAD moiety N3–C23–C24–N4. The coordinative saturation of the Li2 is achieved by a μ -bridging THF molecule, while that of the Li4 atom is achieved by a terminal and a μ -bridging THF molecule. The coordinatively unsaturated Li1 atom is coordinated by only one terminal THF molecule. Thus, the coordination number of the Li1 and Li3 is 3, while that of Li2 and Li2 is 4. The plane N1–Li1–N2 deviates from the plane of the N1–C1–C2–N2 unit by 61.2° while the planes N3–Li2–N4, N3–Li3–N4, and N3–Li4–N4 deviate from the plane of the N3–C23–C24–N4 unit by 4.2° , 87.7° , and 89.6° ,

respectively. This situation can be described as one metal center (Li2) lies essentially in the plane of the $\text{H}_2\text{C}_2\text{N}_2$ unit while the others (Li1, Li3, and Li4) sit above the $\text{H}_2\text{C}_2\text{N}_2$ unit and are η^4 -coordinated by the DAD π -electronic system of the complex. The Li–N and Li–C bond lengths are in the range of 1.955(4) Å to 2.218(4) Å and 2.186(5) Å to 2.294(4) Å, respectively. Similar to complex $[\text{Li}_2(\text{Me}_2\text{DAD}^{\text{Dipp}})(\mu\text{-THF})(\text{THF})_2]$ (**4**), the Li–O bond lengths (Li1–O1 1.991(4) Å, Li2–O3 2.433(4) Å, Li4–O2 1.970(2) Å, and Li4–O3 2.097(4) Å) in **9** reveal that the bridged THF is more strongly coordinated to one metal center (Li4) than the other (Li2).

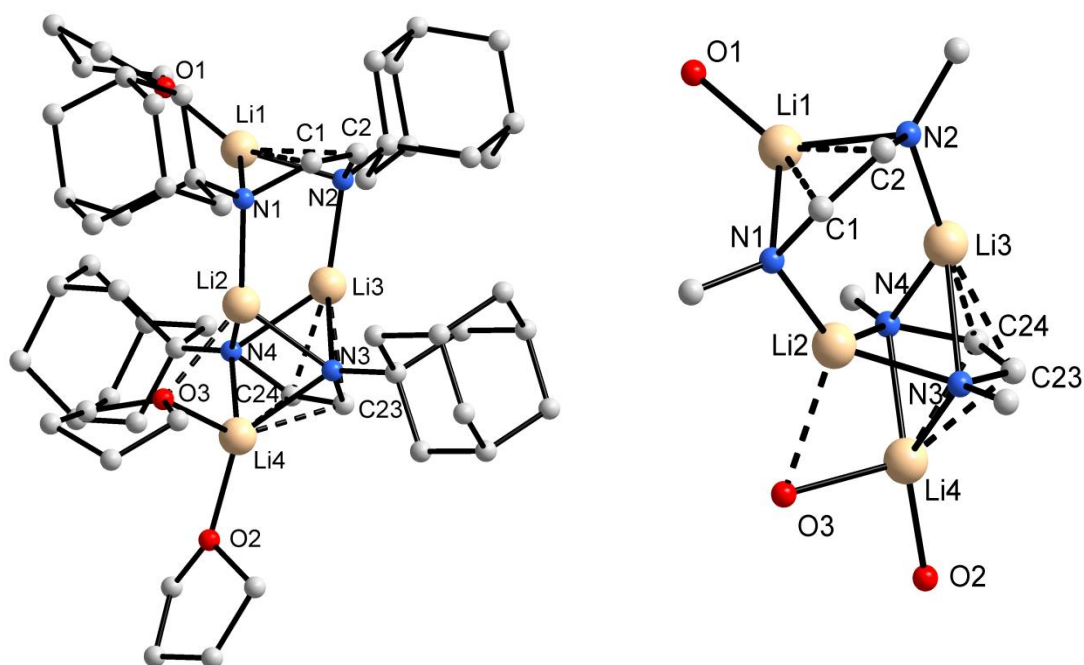


Figure 10. Molecular structure of **9** (left). Representation of the coordination sphere of the lithium atoms in complex **9**.

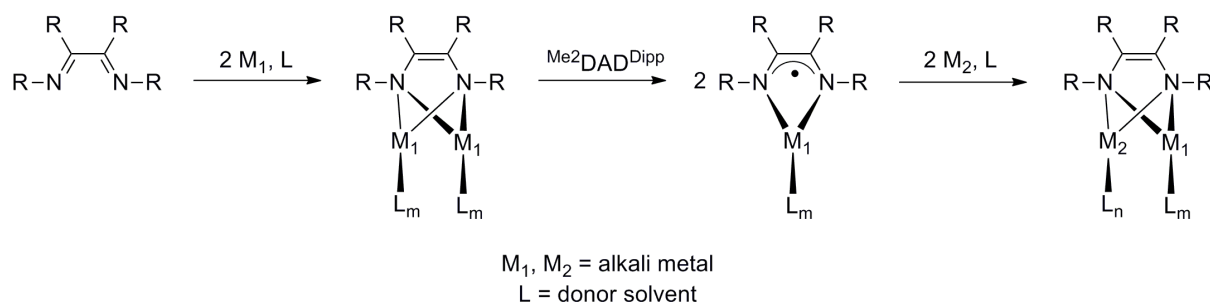
The sum of angles of the rectangular ring –Li3–N3–Li4–N4– is 360° , and its plane is almost perpendicular to the plane of N3–Li2–N4 (86.8°). The coordination geometry of Li1 adopts a distorted trigonal planar arrangement (sum of the angles being 359.8°) with atoms (N1, N2, and O1) occupying the corner of the triangle. The coordination geometry of Li2, Li3, and Li4 adopts a distorted trigonal pyramidal arrangement. Around Li2, atoms N1, N3, and N4 occupy the trigonal base and atom O3 occupies the apical position. Around Li3, atoms N2, N3, and N4 occupy the trigonal base and an unoccupied apical position. Around Li4, atoms N3, N4, and O2 occupy the trigonal base and atom O3 occupies the apical position. The geometrical parameters of the DAD backbone show elongated C–N [C1–N1 (1.406(3) Å),

C2–N2 (1.406(3) Å), C23–N3 (1.399(3) Å), and C24–N4 (1.405(3) Å) and shortened C–C [C1–C2 (1.355(3) Å), C23–C24 (1.351(3) Å)] bond lengths. The values for the free ligand (**3**) are reported as 1.255(3) Å (average) for C–N and 1.457(3) Å for C–C.^[68] These structural data in combination with the spectral data confirm the presence of olefinic carbons in the DAD backbone and the dianionic nature of the $\text{H}_2\text{DAD}^{\text{Ad}}$ ligand in complex **9**. It is important to note that the lithium complex **9** aggregates as a dimer not only from toluene but also from THF, whereas the lithium complex **4** crystallizes as a monomer from THF. This could be attributed to the substituents at the DAD moiety of the ligands.

2.3. Heterobimetallic alkali metal complexes with dianionic DAD ligands

In the homobimetallic complexes **4-8**, two different coordination sites were observed: one in the plane of the DAD moiety and the other above the plane of the same. In order to understand the preference of a particular alkali metal to a particular coordination site, it is necessary to provide two different alkali metals to a DAD ligand. It will offer the possibility for a specific metal ion to attach to a specific coordination site. For that purpose, heterobimetallic complexes containing exclusively alkali metals were synthesized by direct metallation. The heterobimetallic complexes reported so far in the literature are mainly the combination of alkali metals with alkaline earth or transition metals, and these complexes were prepared mostly by salt metathesis reactions between alkali metal precursor complexes and alkaline earth or transition metal halides.^[13,44]

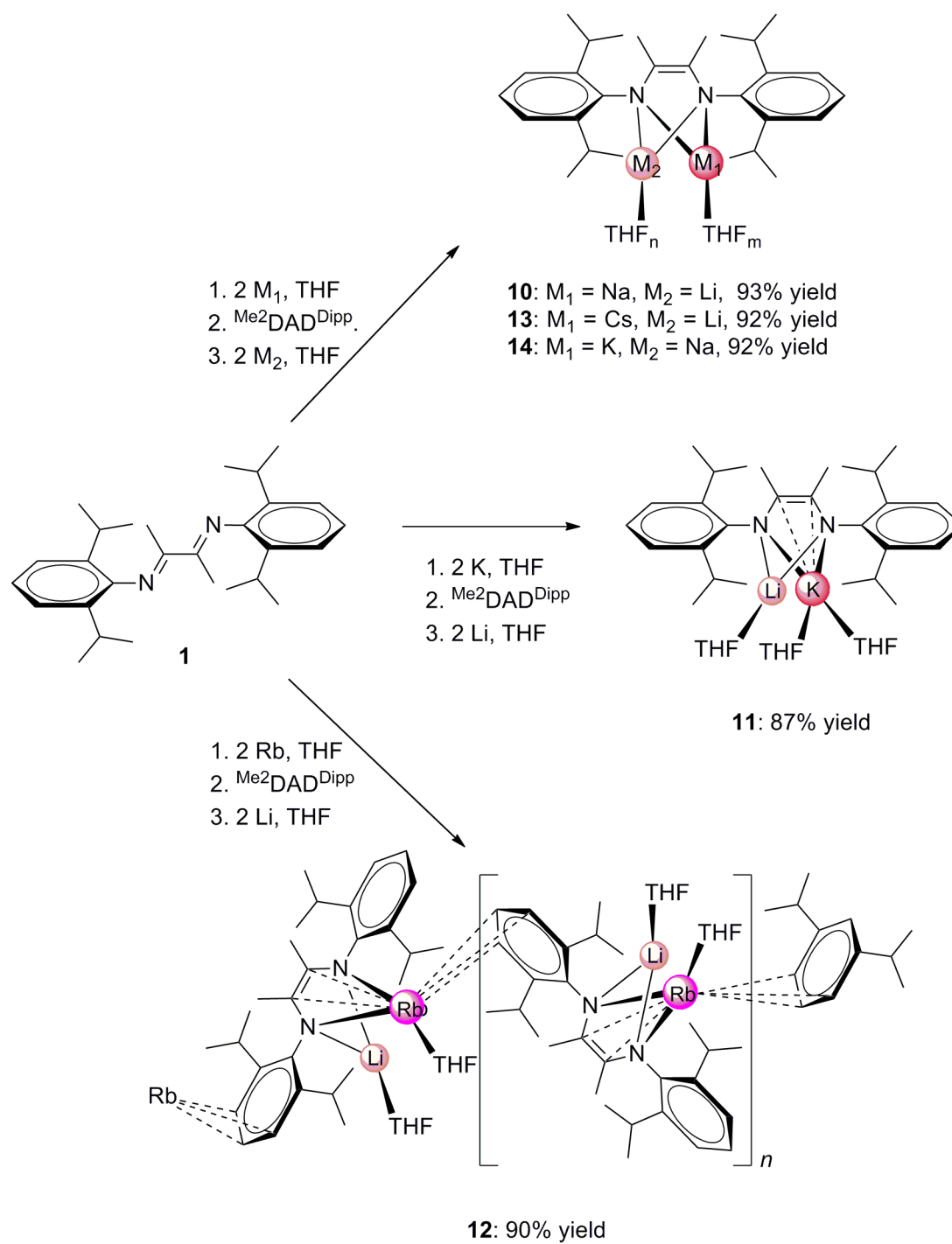
As shown in Scheme 22, to avoid insufficient or excessive reduction, alkali metal complex with dianionic DAD ligand was first synthesized and then treated with one equiv. of free DAD ligand. The resulting alkali metal complex with radical-monoanionic DAD ligand was further metallated with a different alkali metal (lighter).



Scheme 22. General synthesis of heterobimetallic alkali metal complexes with dianionic DAD ligands.

2.3.1. Synthesis of heterobimetallic alkali metal complexes (**10-14**) with dianionic $\text{Me}_2\text{DAD}^{\text{Dipp}}$ ligands

A series of heterobimetallic complexes with dianionic $\text{Me}_2\text{DAD}^{\text{Dipp}}$ (**1**) ligand were prepared by direct metallation and the results are summarized in Scheme 23 (page 40). Ligand **1** was first reduced in THF with excessive metal (more than 2 equiv. of Na) to a completely reduced dianionic ligand (color turned from yellow to bright red), and then it was filtered into a flask containing 1 equiv. of **1** (the intensity of the color increased immediately). The resulting radical-monoanionic $\text{Me}_2\text{DAD}^{\text{Dipp}}$ ligand was further reduced with 1 equiv. of lithium to yield the heterobimetallic complex $[\text{Na}(\text{THF})_m(\text{Me}_2\text{DAD}^{\text{Dipp}})\text{Li}(\text{THF})_n]$ (**10**) (color turned bright red again). Crystallization at 5 °C afforded **10** as red crystals in excellent 93% yield. Similarly, the heterobimetallic complexes $[\text{K}(\text{THF})_2(\text{Me}_2\text{DAD}^{\text{Dipp}})\text{Li}(\text{THF})]$ (**11**), $\{[\text{Rb}(\text{THF})(\text{Me}_2\text{DAD}^{\text{Dipp}})\text{Li}(\text{THF})] \cdot \text{THF}\}_n$ (**12**), and $[\text{Cs}(\text{THF})_m(\text{Me}_2\text{DAD}^{\text{Dipp}})\text{Li}(\text{THF})_n]$ (**13**) were prepared in good to excellent yields (87%, 90%, and 92%, respectively). The heterobimetallic complex $[\text{K}(\text{THF})_m(\text{Me}_2\text{DAD}^{\text{Dipp}})\text{Na}(\text{THF})_n]$ (**14**) was prepared similar to **11**. However, 1 equiv. of sodium was used instead of lithium in the final reduction step, and the yield of **14** was excellent (92%). All the heterobimetallic complexes were characterized by NMR and IR spectroscopy as well as MS analysis. A single-crystal X-ray diffraction analysis was successfully performed for the complexes **11**, **12**, and **14**. However, a fully refined structure model of **14** is not yet available. Elemental analysis (values for C, H, and N of **10-14** were consistent with the proposed formulation of **10-14**, respectively) showed that complex **12** keeps the THF of crystallization (uncoordinated THF) upon drying.



Scheme 23. Synthesis of heterobimetallic alkali metal complexes with dianionic $\text{Me}_2\text{DAD}^{\text{Dipp}}$ ligands.

2.3.2. Spectroscopic analysis of the complexes (10-14)

The NMR spectra of the heterobimetallic complexes were recorded in d_8 -THF, and all the proton and carbon signals were observed. The ^1H NMR and ^{13}C NMR data of the complexes (10-14) are summarized together with the precursor ligand **1** in Tables 7 and 8, respectively. Similar to the dianionic DAD complexes (4-8), the signals corresponding to the methyl protons of the DAD backbone (NCCH_3) and the *meta* and *para* protons of the aromatic ring in complexes (10-14) were observed at higher field, whereas the signals corresponding to the *tertiary* protons of the isopropyl groups was observed at lower field compared to the neutral ligand **1**. Moreover, the signal corresponding to the *tertiary* protons of the isopropyl groups in **10** overlapped with the THF signal between 3.57 and 3.64 ppm (Figure 11, page 42), and the *tertiary* protons of the isopropyl groups, *para* and *meta* protons of the aromatic ring in **14** were observed as broad signals (Figure 12, page 42).

Table 7. ^1H NMR chemical shifts of heterobimetallic complexes with dianionic $\text{Me}_2\text{DAD}^{\text{Dipp}}$ ligands (10-14).

δ in ppm	1	10	11	12	13	14
$\text{CH}(\text{CH}_3)_2$	1.14	1.03	1.01	1.01	1.01	1.03
$\text{CH}(\text{CH}_3)_2$	1.19	1.20	1.20	1.19	1.18	1.21
NCCH_3	2.06	1.58	1.57	1.53	1.47	1.65
$\text{CH}(\text{CH}_3)_2$	2.74	3.57 – 3.64	3.70	3.78	3.87	3.70
<i>para</i> -Ar	7.03	6.38	6.27	6.25	6.26	5.97
<i>meta</i> -Ar	7.14	6.78	6.74	6.73	6.72	6.66

Table 8. ^{13}C NMR chemical shifts of heterobimetallic complexes with dianionic $\text{Me}_2\text{DAD}^{\text{Dipp}}$ ligands (10-14).

δ in ppm	1	10	11	12	13	14
NCCH_3	16.5	16.8	16.9	17.0	17.2	18.2
$\text{CH}(\text{CH}_3)_2$	22.8	24.0	24.0	24.2	24.5	24.2
$\text{CH}(\text{CH}_3)_2$	23.3	25.4	25.5	25.5	25.5	25.2
$\text{CH}(\text{CH}_3)_2$	29.3	27.6	27.56	27.4	27.3	27.4
<i>para</i> -Ar	124.5	115.3	113.8	113.6	113.8	111.1
NCCH_3	168.9	122.3	121.3	121.2	121.4	121.1
<i>meta</i> -Ar	123.6	121.2	122.3	122.3	122.3	122.7
<i>ortho</i> -Ar	135.5	141.2	140.1	140.1	140.3	137.2
<i>ipso</i> -Ar	147.1	152.5	156.7	155.7	155.6	155.6

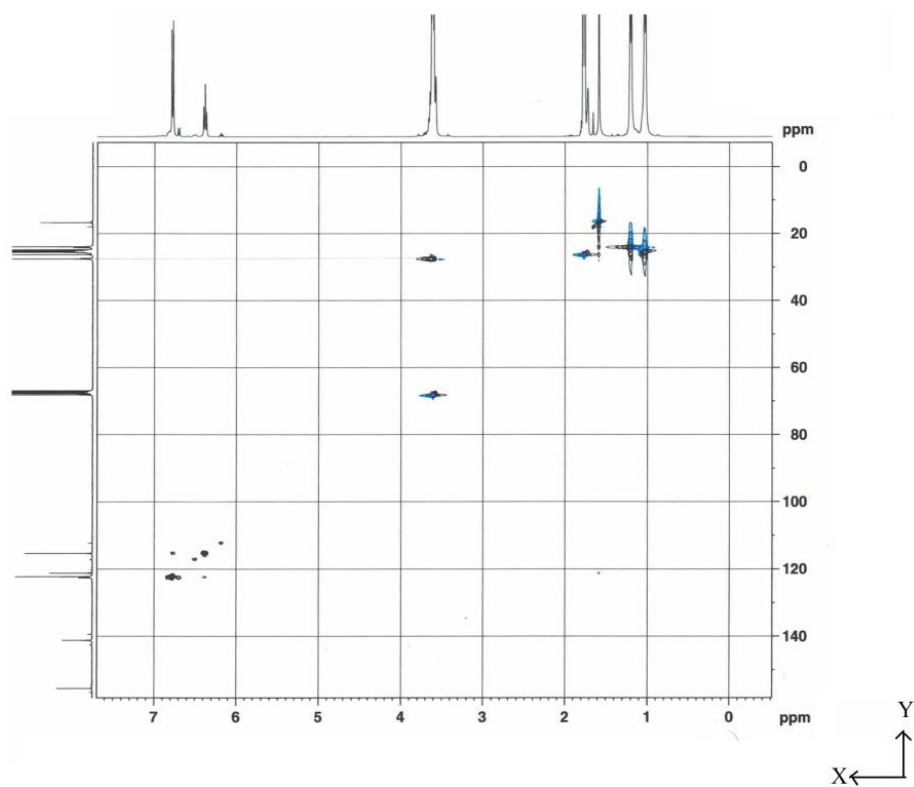


Figure 11. HSQC spectrum of **10** (X-axis: ^1H NMR chemical shifts (400 MHz), Y-axis: ^{13}C NMR chemical shifts (100 MHz), d_8 -THF, 24 °C).

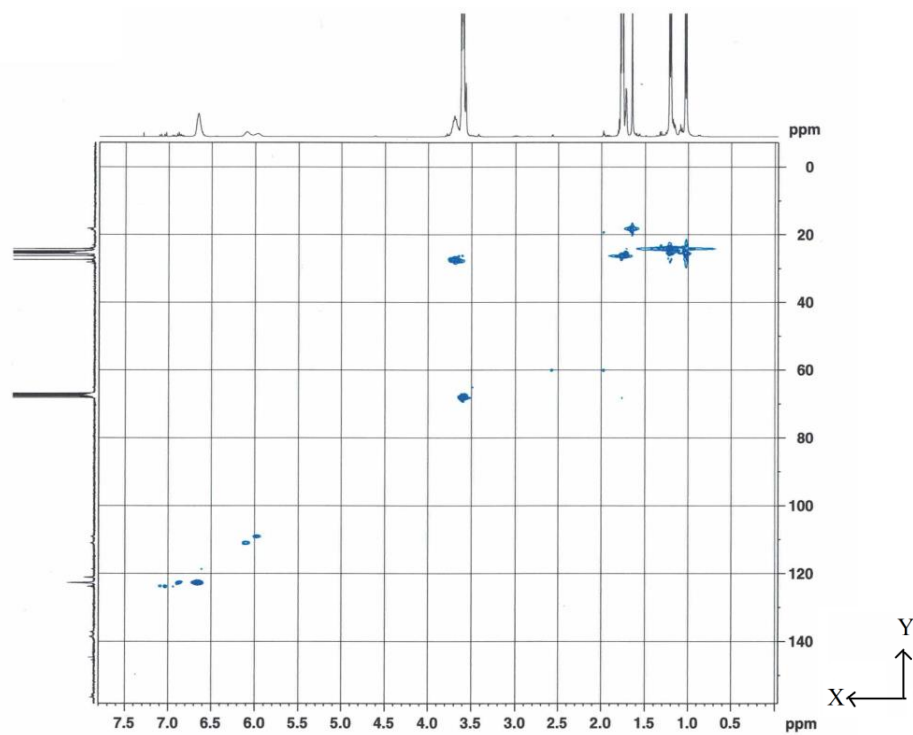


Figure 12. HSQC spectrum of **14** (X-axis: ^1H NMR chemical shifts (400 MHz), Y-axis: ^{13}C NMR chemical shifts (100 MHz), d_8 -THF, 21 °C).

The signals corresponding to the carbons of the DAD backbone ($-\text{N}=\text{C}-\text{C}=\text{N}-$) in the complexes (**10-14**) were observed between 121 and 123 ppm (higher field compared to the ligand **1**) in the ^{13}C NMR of the complexes, proving the olefinic carbons and the dianionic nature of the DAD moiety (corresponding to $-\text{N}-\text{C}(\text{Me})=\text{C}(\text{Me})-\text{N}-$). As shown in Table 9, only a single resonance was observed in the ^7Li NMR of the complexes (**10-13**) (156 MHz, d_8 -THF, 20-24 °C), suggesting the presence of chemically equivalent lithium centers solution and pure products.

Table 9. ^7Li NMR chemical shifts of heterobimetallic complexes with dianionic $^{\text{Me}_2}\text{DAD}^{\text{Dipp}}$ ligands (**10-13**).

Complexes	10	11	12	13
δ in ppm	0.43	0.31	2.36	2.29

Similar to the dianionic complexes (**4-8**), it was not possible to identify the bands corresponding to the stretching vibrations of the C–N and C=C bonds in the DAD moiety of the complexes (**10-14**) due to overlap of bands in their IR spectra. However, the strong band at 1630 cm^{-1} in the IR spectra of **1** corresponding to the stretching vibrations of the imine (C=N) bond completely disappeared in the IR spectra of all the complexes (**10-14**). The molecular ion peak was not observed in any of the EI mass spectra of the complexes. The peak at m/z 451 and 432 in the mass spectra of **10** could be assigned to the fragments $[\text{M}^+ - (2\text{ CH}_3, 2\text{ C}_3\text{H}_7, \text{C}_4\text{H}_6)]$ and $[\text{M}^+ - (4\text{ CH}_3, 2\text{ C}_3\text{H}_7)]$, respectively, while the peak at m/z 445 in the mass spectra of **11** could be assigned to the fragments $\text{M}^+ - (2\text{ H}, 5\text{ CH}_3, 2\text{ THF})$. In the case of complexes **12-14**, the peak at m/z 406 could be assigned to $[\text{Me}_2\text{DAD}^{\text{Dipp}} + 2\text{H}]$.

2.3.3. Molecular Structures of $[\text{K}(\text{THF})_2(\text{Me}_2\text{DAD}^{\text{Dipp}})\text{Li}(\text{THF})]$ (11) and $\{[\text{Rb}(\text{THF})(\text{Me}_2\text{DAD}^{\text{Dipp}})\text{Li}(\text{THF})] \cdot \text{THF}\}_n$ (12)

The heterobimetallic (K/Li) complex **11** crystallizes from THF at 5 °C as a monomer in the monoclinic space group $P2_1/c$ containing one molecule of the complex in the asymmetric unit. As expected, the lithium atom is chelated by the nitrogen donors of the $\text{Me}_2\text{DAD}^{\text{Dipp}}$ ligand, forming a five-membered $\text{C}_2\text{N}_2\text{Li}$ ring, while the potassium atom is η^4 -coordinated by the DAD π -electronic system of the complex, forming a puckered four-membered (LiN_2K) ring with the angle between planes LiN_2 and KN_2 is 70° (Figure 13). This proves once again the preference of π - over σ -coordination by heavier alkali metals. The lithium atom is coordinated by one THF molecule while the potassium atom by two THF molecules resulting in three-coordinate Li atom and four-coordinate K atom. The lithium metal center lies substantially in the plane (N1-Li1-N2 plane deviates by 22.8° from $\text{Me}_2\text{C}_2\text{N}_2$ plane) of the DAD backbone, whereas the potassium metal center is located above the plane (N1-K1-N2 deviates by 87.2° from $\text{Me}_2\text{C}_2\text{N}_2$ plane) and can be described as η^4 -coordinated by the DAD π -electronic system of the complex. This situation makes Li1 metal center in **11** similar to Li2 metal center in complex $[\text{Li}_2(\text{Me}_2\text{DAD}^{\text{Dipp}})(\mu\text{-THF})(\text{THF})_2]$ (**4**) while the K1 in **11** similar to K1 and K3 in complex $\{[\text{K}_2(\text{Me}_2\text{DAD}^{\text{Dipp}})(\mu\text{-THF})(\text{THF})_2] \cdot [\text{K}_2(\text{Me}_2\text{DAD}^{\text{Dipp}})(\mu\text{-THF})(\text{THF})_3]\}_2$ (**6**).

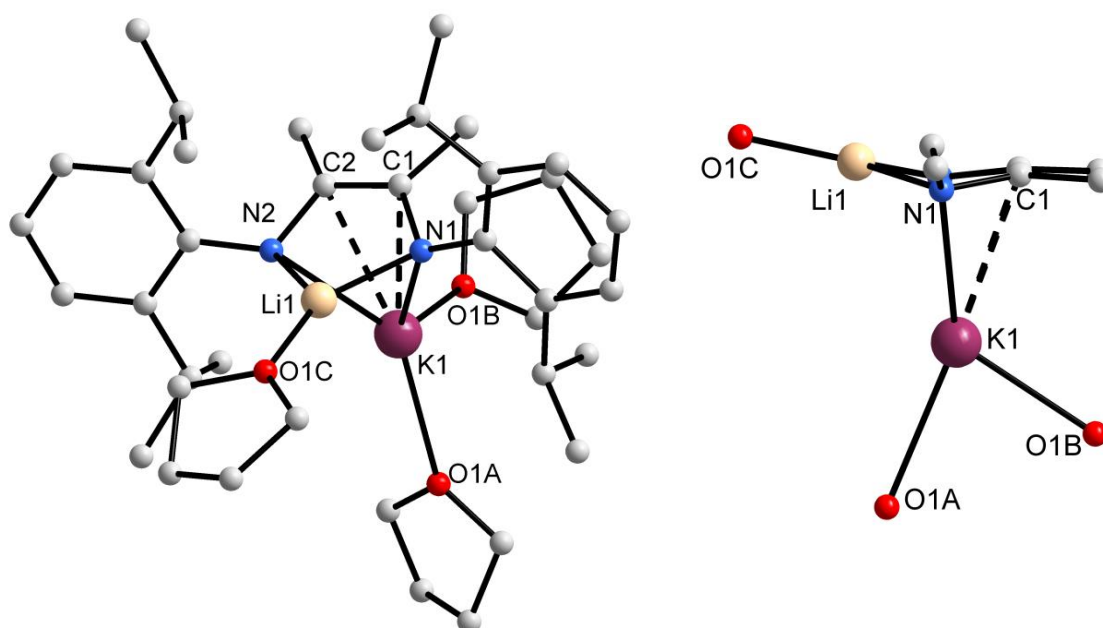


Figure 13. Molecular structure of **11** (left). Representation of the coordination sphere of the metal atoms Li and K in **11** (right), viewed along the N1-N2 vector.

The Li–O (1.874(1) Å) and Li–N (1.924(4)/1.928(4) Å) bond lengths in **11** are shorter than those in the lithium complexes **4** and **9** and in the heterobimetallic (Ca and Li) complex with $\text{Me}_2\text{DAD}^{\text{Dipp}}$ ligand **1** (1.934(8) Å for Li–O and 2.104(8) Å/ 2.095(8) Å for Li–N) reported by Yang and co-workers.^[44] The K–O (2.791(1) Å/ 2.695(5) Å) and K–C (2.920(2) Å/ 2.925(2) Å) bond lengths in **11** are comparable with those in **6**, while the K–N (2.838(2) Å/ 2.840(2) Å) are longer than those in **6**. The coordination environment of Li1 can be described as a trigonal planar geometry (the sum of angles being 360°) with two nitrogen atoms and an oxygen atom (O1C) occupying the corners of the triangle while that of K1 is best described as a distorted trigonal pyramidal arrangement with two nitrogen atoms and an oxygen atom (O1A) occupying the trigonal base and an oxygen atom (O1B) occupying the apical position. The plane of the six-membered ring attached to N1 and N2 deviates from the plane of the DAD backbone by 60.9° and 57.8°, respectively.

The heterobimetallic (Rb and Li) complex **12** aggregates from THF at 5 °C as a coordination polymer in the monoclinic space group $P2_1/c$ having two $\text{Me}_2\text{DAD}^{\text{Dipp}}$ ligands, two rubidium and lithium atoms, and two coordinated and uncoordinated THF molecules in the asymmetric unit. As shown in Figure 14 (page 46), two lithium atoms (Li1 and Li2) are coordinated by the chelating $\text{Me}_2\text{DAD}^{\text{Dipp}}$ ligand through its nitrogen atoms, forming two five-membered rings ($\text{C}_2\text{N}_2\text{Li1}$ and $\text{C}_2\text{N}_2\text{Li2}$) with the Li1 and Li2 metal centers located essentially in the plane of the DAD backbone (deviation between planes N1-C1-C2-N2 and N1-Li1-N2 being 17.1° while the same between planes N3-C29-C30-N4 and N3-Li1-N4 being 18.4°). Similarly, the rubidium atoms Rb1 and Rb2 are also chelated by a $\text{Me}_2\text{DAD}^{\text{Dipp}}$ ligand through its nitrogen atoms, forming two five-membered rings ($\text{C}_2\text{N}_2\text{Rb1}$ and $\text{C}_2\text{N}_2\text{Rb2}$). However, the Rb1 and Rb2 metal centers sit over the plane of the DAD backbone (deviation between planes N1-C1-C2-N2 and N1-Rb1-N2 being 88.2° while the same between planes N3-C29-C30-N4 and N3-Rb2-N4 being 89.6°) and can be described as η^4 -coordinated by the DAD π -electronic system of the complex. These deviation values of Li and Rb in **12** are similar to Li and K, respectively, in complex **11**. In the puckered four-membered rings $\text{Li1N}_2\text{Rb1}$ and $\text{Li2N}_2\text{Rb2}$, the angle between Li1N_2 and Rb1N_2 planes is 74.8° while the same between Li2N_2 and Rb2N_2 planes is 72.1°.

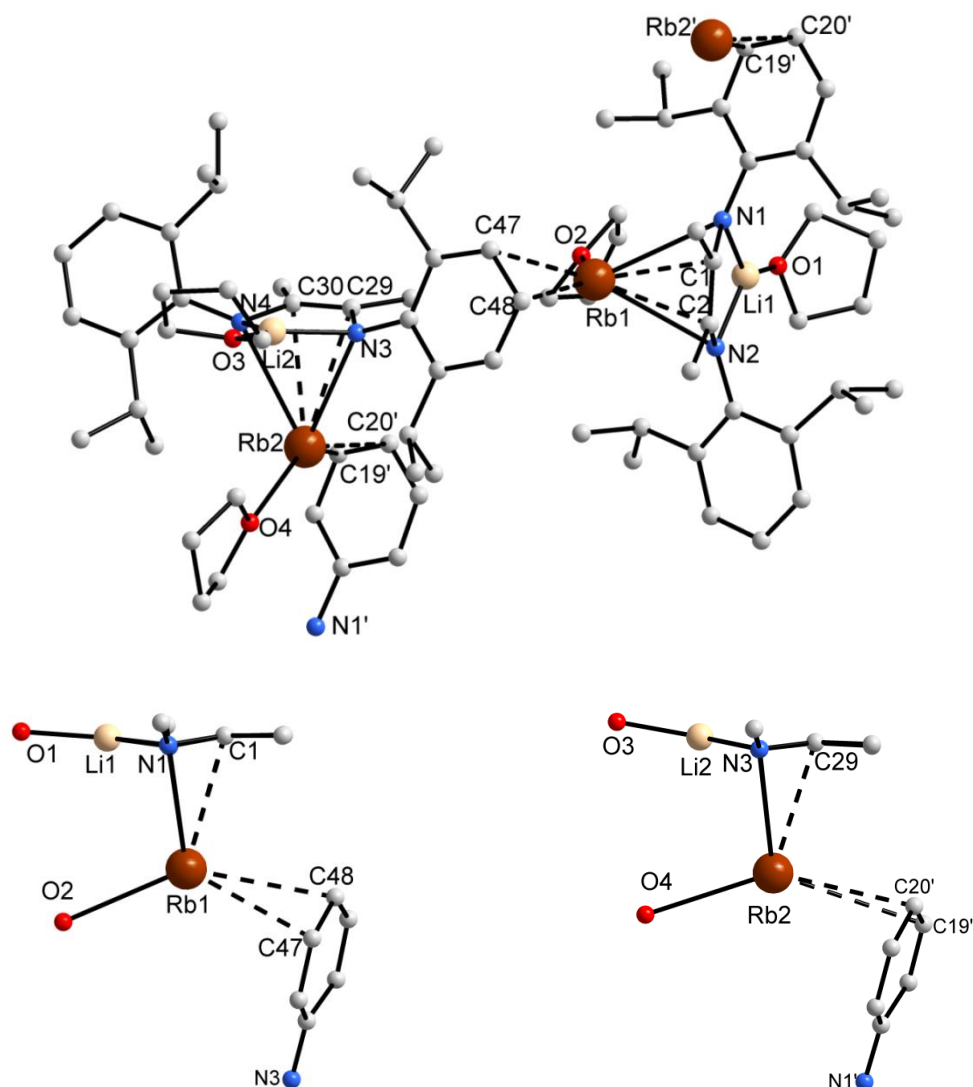


Figure 14. Molecular structure of **12** (top). Representation of the coordination sphere of the atoms Rb1 and Li1 viewed along the N1-N2 vector (bottom-left) and atoms Rb2 and Li2 viewed along the N3-N4 vector (bottom-right) in **12**.

Each lithium and rubidium atom is coordinated by a THF molecule. The Li–O [Li1–O1 (1.864(7) Å) and Li2–O3 (1.853(6) Å)] and Li–N [Li1–N1 (1.909(6) Å), Li1–N2 (1.909(6) Å), Li2–N4 (1.899(6) Å), Li2–N3 (1.910(6) Å)] bond lengths in **12** compare well with their counterparts in **11**. The Rb–O [Rb1–O2 (2.891(1) Å) and Rb2–O4 (2.950(3) Å)] and Rb–C [DAD backbone: Rb1–C2 (3.041(3) Å), Rb1–C1 (3.098(3) Å), Rb2–C30 (3.056(3) Å), and Rb2–C29 (3.106(3) Å); Aromatic ring: Rb1–C47 (3.238(4) Å) Rb1–C48 (3.278(4) Å)] bond lengths in **12** are similar to those in $\{[\text{Rb}_2(\text{Me}_2\text{DAD}^{\text{Dipp}})(\text{THF})_4]_2 \cdot \text{THF}\}_n$ (**7**) while the Rb–N [Rb1–N2 (2.953(3) Å), Rb1–N1 (3.075(3) Å), Rb2–N4 (3.009(3) Å), and Rb2–N3 (3.084(3)

Å)] bond lengths are longer than those in **7**. As noticed in complex **11**, the lighter metal atom (Li) in **12** prefers σ -coordination, whereas the heavier one (Rb) prefers π -coordination. However, the Rb atom in **12** is not only coordinated by the π -electronic system of the DAD backbone but also the aromatic ring of the adjacent molecule resulting in a coordination polymeric chain which is typical for Rb. The coordination environment of Li centers can be described as trigonal planar (the sum of angles being 360°) with two nitrogen atoms and an oxygen atom occupying the corners of the triangle, while that of the Rb centers can be described as a distorted trigonal pyramidal with two nitrogen atoms and an oxygen atom occupying the trigonal base. The plane of the six-membered ring attached to N1 and N2 deviates from the plane of the DAD backbone (N1-C1-C2-N2) by 64.9° and 60.4° , respectively, while the same attached to N3 and N4 deviates from the plane of the DAD backbone (N3-C29-C30-N4) by 59.9° and 59.7° .

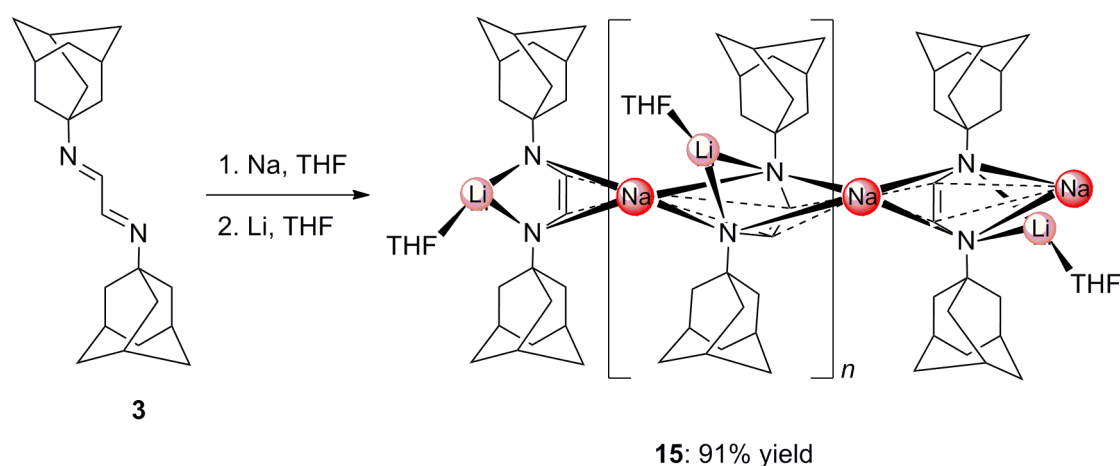
Compared to the precursor ligand **1**,^[66] the C–C bond length is shortened, whereas the C–N bond lengths are elongated in the DAD backbone of the complexes **11** and **12** (Table 10), similar to the dianionic $\text{Me}^2\text{DAD}^{\text{Dipp}}$ complexes **4-8**. This is corresponding to a $-\text{NC}(\text{Me})=\text{C}(\text{Me})\text{N}-$ bonding situation. The shorter distance between the metal center (K in **11** and Rb in **12**) and the olefinic carbons of the DAD moiety confirms the π -interactions between them. These structural data together with the spectral data confirm the dianionic character of the $\text{Me}^2\text{DAD}^{\text{Dipp}}$ ligand in complex **11** and **12**.

Table 10. Selected bond lengths [\AA] of **11** and **12**.

DAD moiety	1 ^[66]	11	12
C–N (average)	1.279(3)	1.414(2)	1.405(4)
C–C	1.498(3)	1.367(3)	1.372(4)

2.3.4. Synthesis and molecular structure of heterobimetallic complex $\{[\text{Na}(\text{H}^2\text{DAD}^{\text{Ad}})\text{Li}(\text{THF})]_4 \cdot \text{THF}\}_n$ (**15**) with dianionic $\text{H}^2\text{DAD}^{\text{Ad}}$ ligands

The heterobimetallic complex **15** was prepared by the treatment of $\text{H}^2\text{DAD}^{\text{Ad}}$ ligand (**3**) with 1 equiv. of sodium followed by 1 equiv. of lithium. When the solution of **3** (in THF/toluene) was stirred with sodium, the reaction mixture turned from colorless to red. The reaction mixture was further treated with lithium, and the resulting orange solution was stored at r.t. to afford **15** as orange crystals in excellent yield of 91% (Scheme 24). Elemental analysis values for C, H, and N of **15** were consistent with the proposed formulation, showing that complex **15** keeps the THF of crystallization (uncoordinated THF) upon drying.



Scheme 24. Synthesis of a heterobimetallic (Na/Li) complex with dianionic $\text{H}^2\text{DAD}^{\text{Ad}}$ ligands (**3**).

The ^1H NMR of **15** in *ds*-THF displayed a broad singlet at 1.56 and 1.93 ppm corresponding to the CH_2 protons. The singlets in the range of 7.05-7.19 ppm are assignable to protons of the DAD moiety (NCHCHN). In the ^{13}C NMR spectrum of the complex, the CH_2 carbon resonances were observed at 38.4 and 47.4 ppm, while the CH and quaternary carbon resonances were observed at 31.6 and 51.8 ppm, respectively. The carbon resonances of the DAD moiety were observed in the range of 126.0-129.6 ppm (NCHCHN), confirming the presence of olefinic carbons and the dianionic nature of the DAD moiety. The C=N bond stretching vibrations observed as a band at 1625 cm^{-1} in the IR spectra of the neutral ligand **3** completely disappeared in the IR spectrum of the complex. The mass spectrum of the

complex showed only fragments of the monomeric unit, and the peaks at $m/z = 433, 406, 383, 361, 340,$ and 326 could be assigned to the fragments $[M^+ - (2 \text{ H}, \text{CH}_2)], [M^+ - (\text{H}, 3 \text{ CH}_2)], [M^+ - (\text{H}, 3 \text{ CH}_2, \text{Na})], [M^+ - (3 \text{ CH}_2, 2 \text{ Na})], [M^+ - (\text{CH}_2, \text{Na}, \text{THF})],$ and $[M^+ - (2 \text{ CH}_2, \text{Na}, \text{THF})]$.

The heterobimetallic (Na and Li) complex **15** crystallizes from toluene at r.t. as a coordination polymer in the monoclinic space group $P2/n$ containing four $\text{H}^2\text{DAD}^{\text{Ad}}$ ligands, four Na and Li atoms, and four coordinated THF molecules of the complex and an uncoordinated THF molecule in the asymmetric unit. It is not meaningful to discuss the bond lengths and angles due to poor crystal data of **15**. As shown in Figure 15, the Li atom is chelated by two nitrogen atoms of the $\text{H}^2\text{DAD}^{\text{Ad}}$ ligand while the Na atom is sandwiched by two π -coordinated $\text{H}^2\text{DAD}^{\text{Ad}}$ ligands, forming the coordination polymeric chain (helical). Each Li atom is solvated by a THF molecule, resulting in coordination number 3, while the Na is unsolvated. The Li metal centers lie substantially in the plane of the DAD backbone, whereas the Na metal centers are located above the plane.

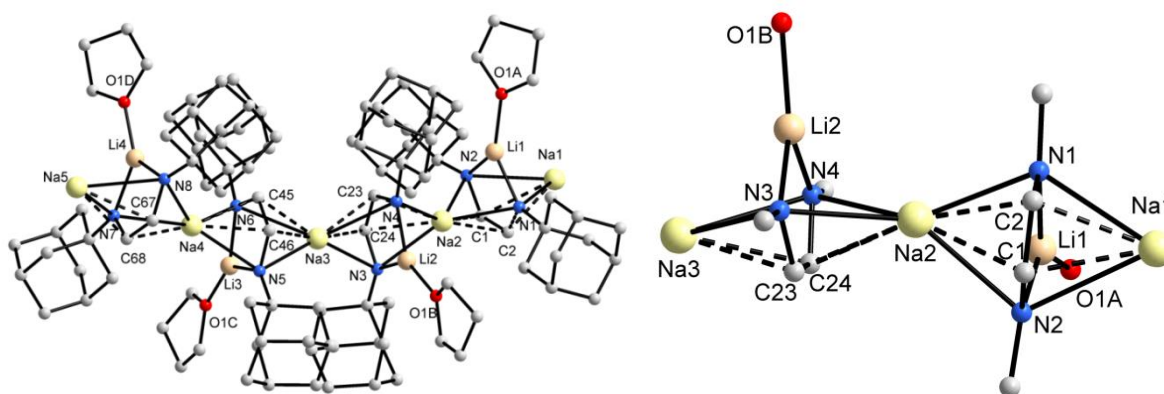


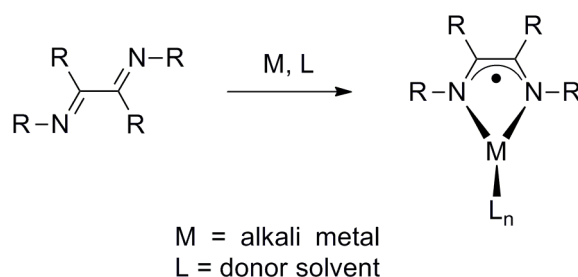
Figure 15. Molecular structure of **15** (left). Representation of the coordination sphere of the metal atoms Li and Na in **15** (right), viewed along the N3-N4 vector.

The sodium metal centers in **15** are comparable with the Na1 metal center in $[\text{Na}_2(\text{Me}^2\text{DAD}^{\text{Dipp}})(\text{THF})_4]$ (**5**). The Na1 metal center in **5** is coordinated by a DAD moiety (η^4 -coordination) and two THF molecules, while the Na metal centers in **15** are η^4 -coordinated by two adjacent DAD moieties. The η^4 -coordination of Na metal atom by DAD moiety was also observed in the heterobimetallic complexes $[\text{Zn}_2(\text{H}^2\text{DAD}^{\text{Dipp}})\text{Na}_2(\text{Et}_2\text{O})_2]$ and $[\text{Zn}_2(\text{Me}^2\text{DAD}^{\text{Mes}})\text{Na}_2(\text{THF})_2]$.^[10] In the latter, each sodium atoms are not only η^4 -coordinated

by the a DAD moiety but also coordinated by a THF ligand and aryl π -electronic system (η^2). The THF ligand and aryl π -coordination (η^2) are formally replaced by an additional η^4 -coordination in **15**. The coordination environment around the lithium centers can be described as trigonal planar with two nitrogen atoms and an oxygen atom occupying the corners of the triangle, while that around the sodium centers is best described as highly distorted tetrahedral with four nitrogen atoms occupying the corners of the tetrahedron.

2.4. Alkali metal complexes with radical-monoanionic DAD ligands

Alkali metal complexes with radical-monoanionic DAD ligands are generally synthesized by direct metallation of DAD ligands by alkali metals in a 1:1 molar ratio in donor solvents (Scheme 25).^[7,8,36] Structural studies of these complexes are exceedingly rare. Hence, a series of alkali metal complexes with radical-monoanionic $\text{Me}^2\text{DAD}^{\text{Dipp}}$ (**1**), $\text{H}^2\text{DAD}^{\text{Dipp}}$ (**2**) $\text{H}^2\text{DAD}^{\text{Ad}}$ (**3**) ligands were synthesized and characterized by electron paramagnetic resonance (EPR) spectroscopy. Paramagnetic metal complexes can be investigated in great detail by EPR spectroscopy. Molecular structures of most of these complexes were successfully determined by X-ray crystallography.

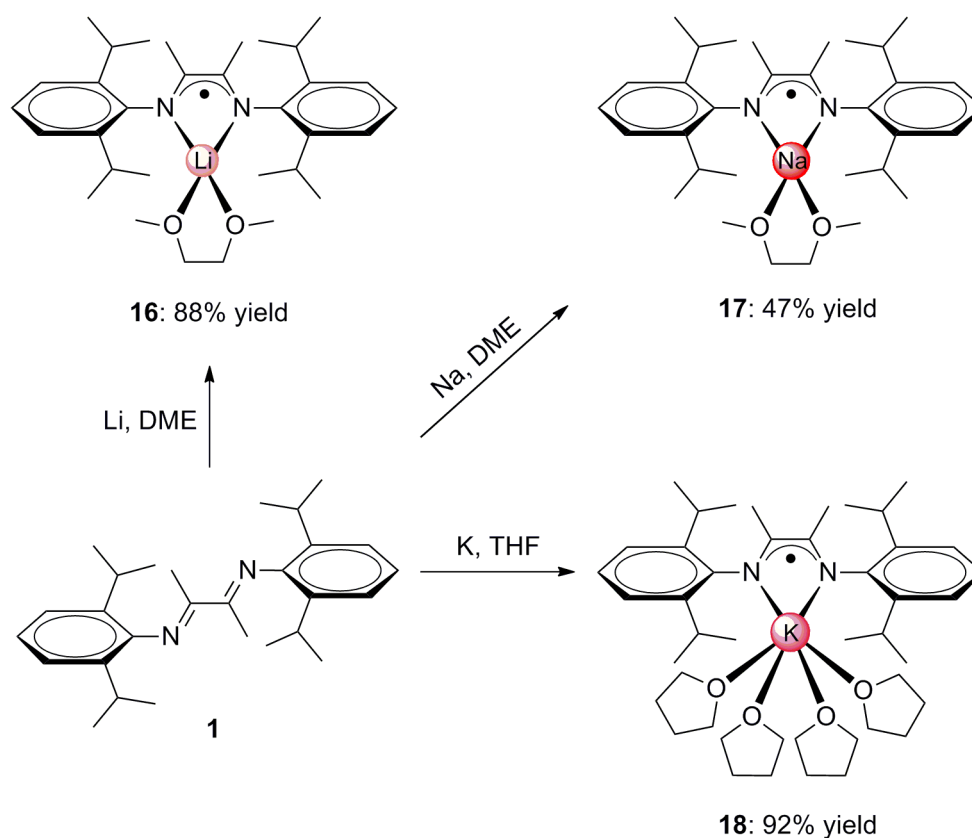


Scheme 25. General synthesis of alkali metal complexes with radical-monoanionic DAD ligands by direct metallation.

2.4.1. Synthesis of alkali metal complexes (16-18) with radical-monoanionic $\text{Me}^2\text{DAD}^{\text{Dipp}}$ ligands

A series of alkali metal complexes with radical-monoanionic $\text{Me}^2\text{DAD}^{\text{Dipp}}$ ligand (**1**) were synthesized by the treatment of $\text{Me}^2\text{DAD}^{\text{Dipp}}$ with alkali metals in a 1:1 molar ratio (in DME for Li and Na and in THF for K), and the results are summarized in Scheme 26 (page 52). THF was used for potassium because it was not possible to crystallize the complex when DME was used. When lithium metal was stirred with **1** in DME, the yellow color of the reaction mixture turned to red, however, stirring was continued until all the lithium was consumed. The final deep red solution was concentrated before it was kept at 5 °C to afford the monolithium complex $[\text{Li}(\text{Me}^2\text{DAD}^{\text{Dipp}})(\text{DME})]$ (**16**) as deep red blocks in good yield 88%. Similarly, the monosodium complex $[\text{Na}(\text{Me}^2\text{DAD}^{\text{Dipp}})(\text{DME})]$ (**17**) was synthesized in

47% yield in DME while the monopotassium complex $[\text{K}(\text{Me}_2\text{DAD}^{\text{Dipp}})(\text{THF})_4]$ (**18**) was synthesized in 92% yield in THF. All the complexes (**16-18**) were characterized by IR spectroscopy, MS, and elemental analysis. Additionally, the complexes **16** and **17** were investigated by EPR spectroscopy. Suitable single-crystals of **16** for X-ray diffraction analysis were successfully grown from DME. Elemental analysis values for C, H, and N of **16-18** were consistent with the proposed formulation of **10-14**, respectively.



Scheme 26. Synthesis of lithium, sodium, and potassium complexes with radical-monoanionic $\text{Me}_2\text{DAD}^{\text{Dipp}}$ ligands (**1**).

2.4.2. Spectroscopic analysis of the complexes (16-18)

The strong band at 1630 cm^{-1} corresponding to the stretching vibrations of the imine ($\text{C}=\text{N}$) bond in the IR spectra of **1** was not observed in the IR spectra of the complexes **16-18**. Although the molecular ion peak was not observed in any of the EI mass spectra of the complexes **16-18**, the peaks at m/z 458 and 415 in the mass spectra of **16** could be assigned to the fragments $[\text{M}^+ - \text{C}_3\text{H}_7]$ and $[\text{M}^+ - 2\text{C}_3\text{H}_7]$, respectively, while the peaks at m/z 487 and 416 in the mass spectra of **17** could be assigned to the fragments $[\text{M}^+ - 2\text{CH}_3]$ and $[\text{M}^+ - (\text{CH}_3, 2\text{C}_3\text{H}_7)]$, respectively. Similarly, the peaks at m/z 616, 576, and 500 in the MS of **18** could be assigned to the fragments $[\text{M}^+ - (\text{C}_3\text{H}_7, \text{THF})]$, $[\text{M}^+ - (\text{CH}_3, 2\text{C}_3\text{H}_7, \text{C}_4\text{H}_6)]$, and $[\text{M}^+ - (\text{CH}_3, 3\text{THF})]$, respectively.

The electronic structure of the complexes **16** and **17** was elucidated by continuous-wave (CW) EPR spectroscopy. As shown in Figure 16, the CW-EPR measurements of **16** in toluene at the Q-band frequencies showed a signal centered at about $g = 2.00$ mT. The spectral shape changed upon varying the temperature. However, the signal was preserved at all measured temperatures at the same field position. The calculated isotropic g value (2.003 mT) of the solvent-free complex $[\text{Li}(\text{Me}_2\text{DAD}^{\text{Dipp}})]$ is consistent with the experimental isotropic g -value of **16** ($g = 2.00$ mT). The nitrogen atoms of the ligand backbone were found to have slightly lower spin populations (approximately 25% each), while the lithium spin population is about 3%.

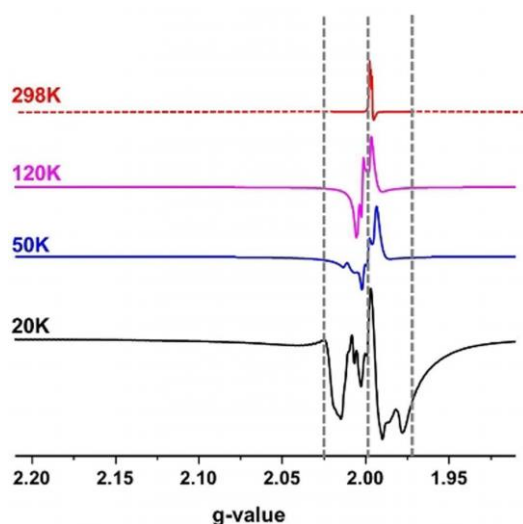


Figure 16. Q-band CW-EPR spectra of **16** in toluene recorded at different temperature.

These results show that the spin density is located mainly at the nitrogen atoms of the ligand and much less at lithium. These results are also in good agreement with the experimentally reported values for other Li-DAD complexes at room temperature.^[66] Measurement of complex **16** at the X-band and at room temperature was impossible due to the much stronger interaction of the lithium complex with the magnetic field within the X-band frequency range, which made it impossible to tune and set up the experiment properly.

Well-resolved CW-EPR spectra of **17** obtained at room temperature at both the X- and Q-band frequencies (9.4 and 34 GHz microwave frequency) are shown Figure 17. A slight non-equivalency of the methyl protons, a set of two protons with 0.57 mT and the remaining four with a splitting of 0.55 mT was revealed by simulation of the room-temperature spectrum at the X-band frequency. The $a_{\text{iso}}(^{14}\text{N})$ for two equivalent nitrogen atoms and $a_{\text{iso}}(^{23}\text{Na})$ were found to be 0.53 and 0.1 mT, respectively. The hyperfine coupling (although small) of the sodium is responsible for the spectral lineshapes. The Q-band spectrum was simulated by the same set of parameters at room temperature, and the experimental spectrum was recorded at 9.4 GHz.

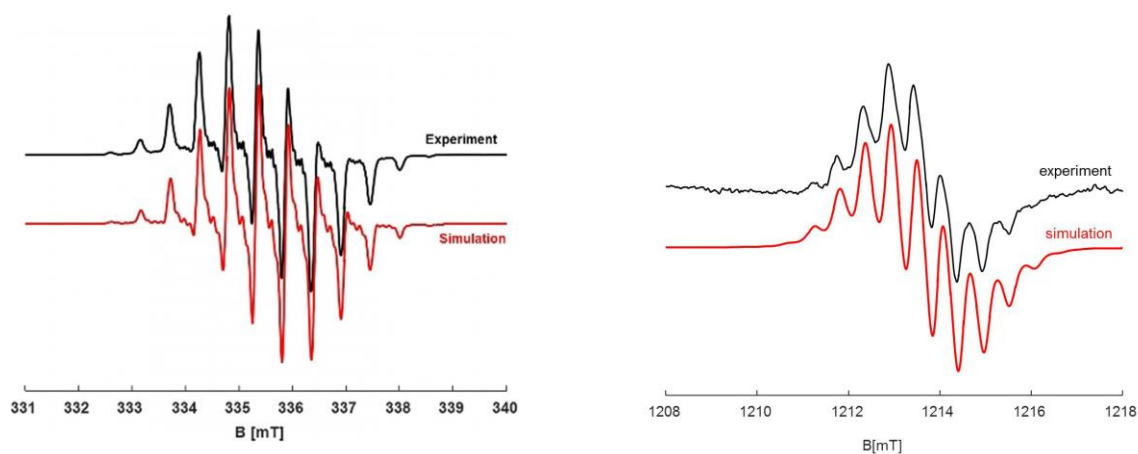


Figure 17. X-band CW-EPR spectrum of **17** in THF room-temperature (left): Experimental (black) and the simulated spectrum (red) at 9.4 GHz revealed $a_{\text{iso}}(^{14}\text{N}) = 0.53$ mT (#2), $a_{\text{iso}}(^1\text{H}) = 0.57, 0.55$ mT (#2, #4), and $a_{\text{iso}}(^{23}\text{Na}) = 0.1$ mT at $g_{\text{iso}} = 2.005$. Q-band CW-EPR spectrum of **17** in THF (right): Experimental (black) and the simulated spectrum (red) at 33.9 GHz revealed $a_{\text{iso}}(^{14}\text{N}) = 0.53$ mT (#2), $a_{\text{iso}}(^1\text{H}) = 0.57, 0.55$ mT (#2, #4) and $a_{\text{iso}}(^{23}\text{Na}) = 0.1$ mT at $g = [2.0078, 2.0061, 2.0023]$.

Calculation of the hyperfine couplings also substantiated the description of a delocalized spin distribution over the backbone of the ligand and to a lesser extent also on the metal site in **17**. However, the spin density observed at the metal center of the lithium complex **16** was larger than that of the sodium complex **17**. On the sodium p_z orbital, about 1.3% of the total spin population (calculated) was resided, and about 27.6% of the total spin population was carried by each nitrogen atom of the ligand backbone. Six methyl protons of the ligand backbone with an average value of 0.53 mT together with a 0.39 mT hyperfine coupling of the two equivalent nitrogen atoms were calculated. This is in good agreement with typical proton and nitrogen couplings reported for different metal complexes with DAD ligands^[43,157] and with the current experiment. A slightly larger coupling of 0.3 mT was obtained for sodium compared to the lithium complex **16**, but this value is still in the range of previously reported experimental findings. The calculated isotropic g -value (2.003 mT) is consistent with the experimental isotropic g -value (2.005 mT) at room temperature.

2.4.3. Molecular Structure of $[\text{Li}(\text{Me}_2\text{DAD}^{\text{Dipp}})(\text{DME})]$ (**16**)

The lithium complex **16** crystallizes from DME at 5 °C as a monomer in the tetragonal space group $P4_32_12$ containing half of the molecule in the asymmetric unit. As shown in Figure 18 (page 56), the lithium atom is chelated by the two nitrogen atoms of the DAD moiety, and the coordinative saturation of the metal is achieved by the DME ligand, thus resulting in coordination number 4. The five-membered metallacycle is almost planar (the deviation of the LiN_2 plane from the $\text{Me}_2\text{C}_2\text{N}_2$ plane is 0.2°). The coordination environment around the lithium atom can be described as distorted square planar instead of a more usual tetrahedral coordination, as the angle between LiO_2 and LiN_2 plane is $18\text{-}35^\circ$ (the range is from the disorder of DME ligand). This situation can be explained by the steric bulk of the isopropyl groups which force the DME molecule into the $\text{Me}_2\text{C}_2\text{N}_2$ plane. The planes of the six-membered aromatic rings attached to both N1 and N2 deviate from the $\text{Me}_2\text{C}_2\text{N}_2$ plane by 74.3° . The delocalization of the unpaired electron over the DAD π -system is well reflected by both the high geometric symmetry (two-fold rotational symmetry) and the electronic symmetry (confirmed by EPR-spectroscopy) of the complex. Compared to the neutral ligand **1**,^[66] the C–N bond lengths are elongated while C–C bond length is shortened (C–N: 1.329(3) Å and C–C': 1.448(3) Å) in the DAD backbone of **16**; however, not to the extent observed in the dilithium complex $[\text{Li}_2(\text{Me}_2\text{DAD}^{\text{Dipp}})(\mu\text{-THF})(\text{THF})_2]$ (**4**), proving the 1.5 bond order of the C–N bond in **16**. The Li–N bond lengths are equal (2.032(4) Å) and so are the Li–O

bonds (2.146(2) Å). The Li–N bond lengths in **16** are very similar to their counterparts (2.031(3) Å/ 2.043(3) Å) in the TMEDA adduct of lithium complex with radical anionic $\text{H}^2\text{DAD}^{\text{Dipp}}$ reported by Trifonov and co-workers.^[14] The radical anionic nature of the NCCN fragment is thus confirmed by all these structural data in combination with the spectral data. The sodium complex $[\text{Na}(\text{Me}^2\text{DAD}^{\text{Dipp}})(\text{DME})]$ (**17**) is isotopic with **16**, but the crystal quality did not allow for full refinement (Figure 18).

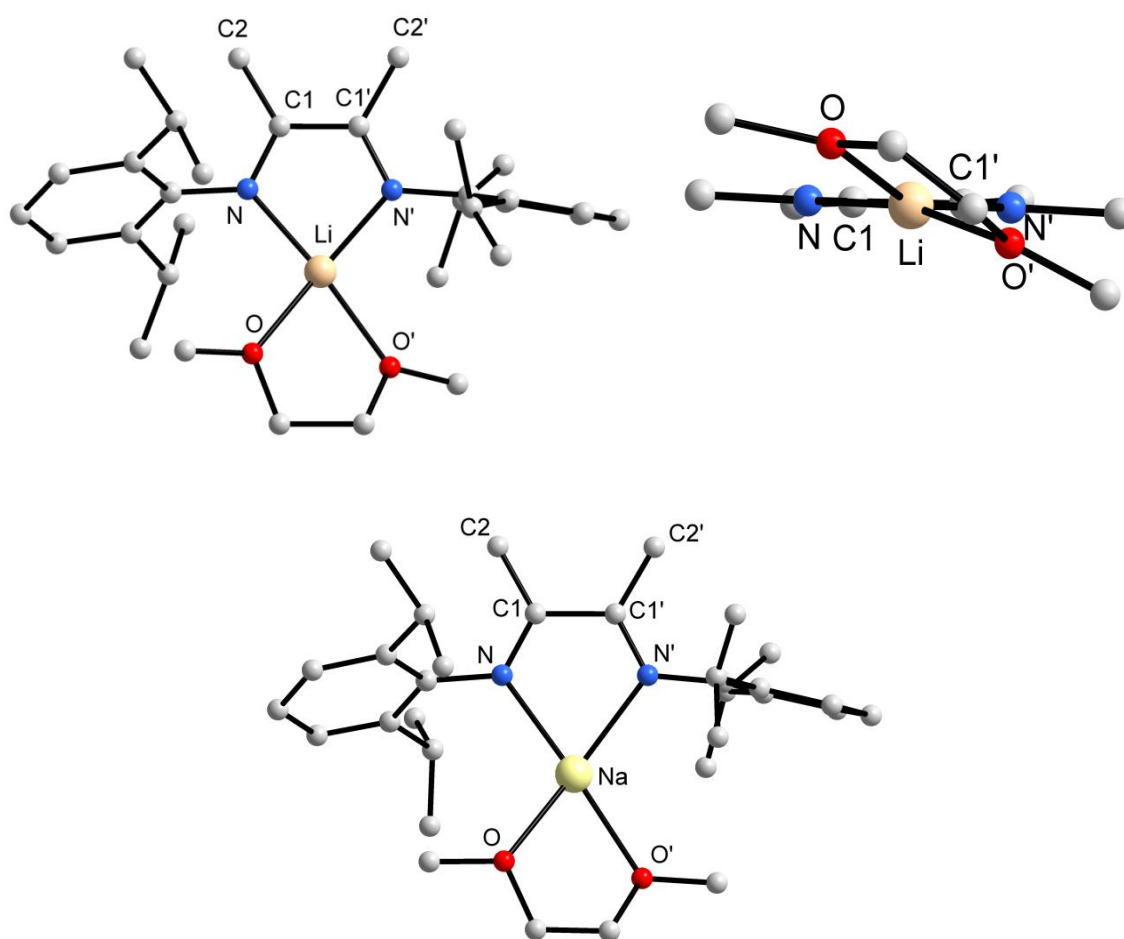
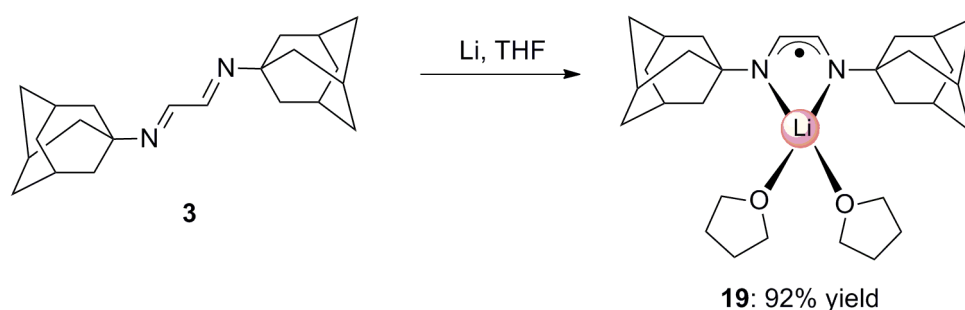


Figure 18. Molecular structure of **16** (top-left) and representation of the coordination sphere of the lithium atom in **16** (top-right). Molecular structure of **17** (bottom).

2.4.4. Synthesis of alkali metal complexes (**19-24**) with anionic $\text{H}^2\text{DAD}^{\text{Ad}}$ and $\text{H}^2\text{DAD}^{\text{Dipp}}$ ligands

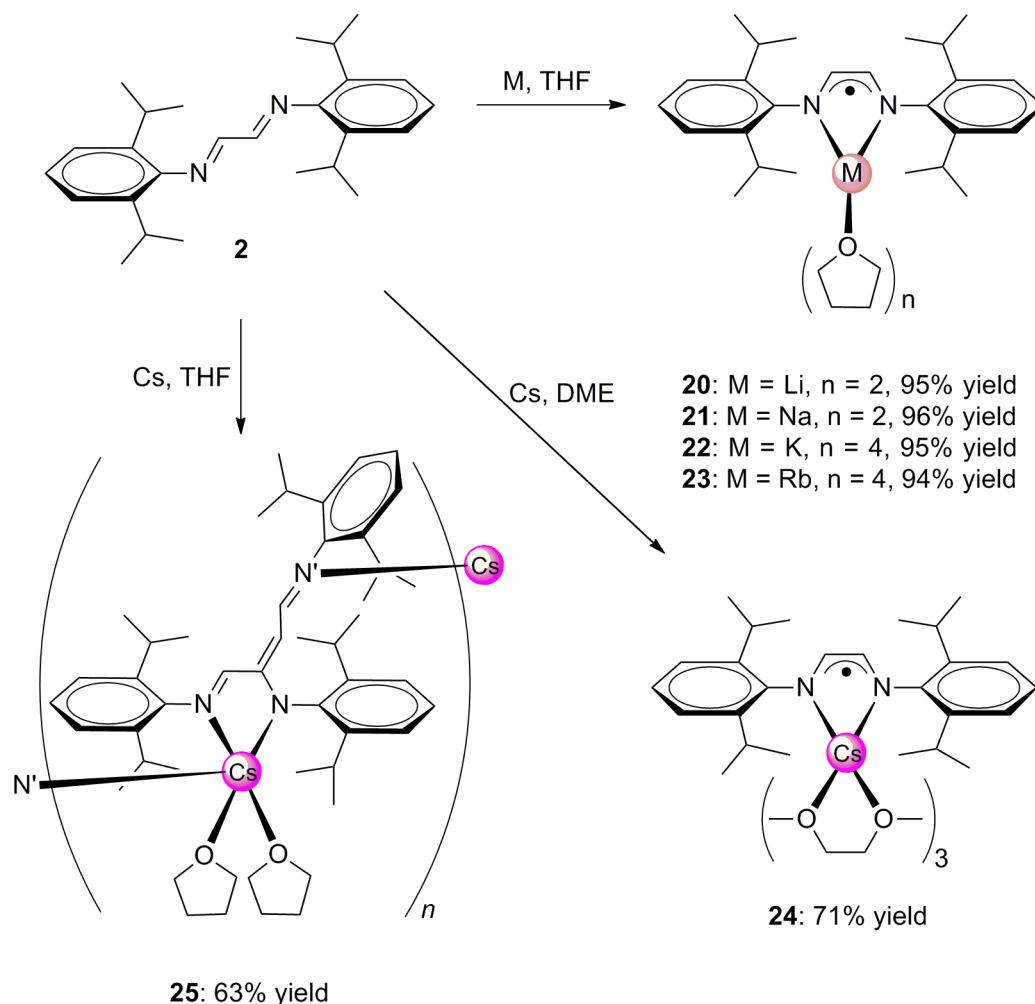
In an attempt to synthesize a lithium complex with a radical-monoanionic $\text{H}^2\text{DAD}^{\text{Ad}}$ ligand (**3**), lithium (1 equiv.) was stirred with **3** in THF until all the lithium was consumed, and the resulting red solution was concentrated before it was kept at 5 °C to yield the lithium complex $[\text{Li}(\text{H}^2\text{DAD}^{\text{Ad}})(\text{THF})_2]$ (**19**) in an excellent yield (92%) as orange crystals (Scheme 27). In a similar manner, the whole series of alkali metal complexes with radical-monoanionic $\text{H}^2\text{DAD}^{\text{Dipp}}$ ligand (**2**) were synthesized and the results are also summarized in Scheme 28 (page 58). The lithium complex $[\text{Li}(\text{H}^2\text{DAD}^{\text{Dipp}})(\text{THF})_2]$ (**20**), sodium complex $[\text{Na}(\text{H}^2\text{DAD}^{\text{Dipp}})(\text{THF})_2]$ (**21**), potassium complex $[\text{K}(\text{H}^2\text{DAD}^{\text{Dipp}})(\text{THF})_4]$ (**22**), and rubidium complex $[\text{Rb}(\text{H}^2\text{DAD}^{\text{Dipp}})(\text{THF})_4]$ (**23**) were prepared in THF in excellent yields (95%, 96%, 95%, and 94%, respectively). Suitable single-crystals of **19**, **20**, **22**, and **23** for X-ray diffraction analysis were successfully grown from THF. The cesium complex $[\text{Cs}(\text{H}^2\text{DAD}^{\text{Dipp}})(\text{DME})_3]$ (**24**) was prepared (in good yield 71%) in DME instead of THF and crystallized from *n*-pentane. All the complexes (**19-24**) were characterized by EPR and IR spectroscopy as well as MS and elemental analyses. Due to paramagnetic nature of the radical anionic DAD, it was not possible to obtain meaningful ^1H NMR and ^{13}C NMR spectra. Elemental analysis values for C, H, and N of **19-24** were consistent with the proposed formulation of **19-24**, respectively.



Scheme 27. Synthesis of a lithium complex with a radical-monoanionic $\text{H}^2\text{DAD}^{\text{Ad}}$ ligand (**3**).

The C=N bond stretching vibrations observed as a medium band at 1626 cm^{-1} in the IR spectra of the neutral ligand **3** disappeared in the IR spectra of **19**. Instead of the strong band

at 1625 cm^{-1} corresponding to the stretching vibrations of the imine ($\text{C}=\text{N}$) bond in the IR spectra of **2**, only a weak band was observed at 1626 cm^{-1} in the IR spectra of the complexes **20-24**. Although the molecular ion peak of **19** was not observed, the peaks at m/z 433, 361, and 326 in the MS of **19** could be assigned to the fragments $[\text{M}^+ - \text{C}_3\text{H}_5]$, $[\text{M}^+ - (\text{C}_3\text{H}_5, \text{THF})]$, and $[\text{M}^+ - \text{C}_{10}\text{H}_{15}\text{N}]$, respectively. Unfortunately, only fragments of ligand **2** were observed in the EI mass spectra of the complexes **20-24**.



Scheme 28. Synthesis of alkali metal complexes with radical-monoanionic $\text{H}_2\text{DAD}^{\text{Dipp}}$ ligands (**2**).

The cesium complex $[\text{Cs}(\text{DippNCHC}[\text{CHCHN}^{\text{Dipp}}]\text{N}^{\text{Dipp}})(\text{THF})_2]_n$ (**25**) was synthesized by treatment of **2** with cesium metal in THF and the resulting deep red mixture was concentrated in vacuum at $80\text{ }^\circ\text{C}$ for 2 h to afford a black oil. The black oil was mixed well with n -pentane and kept at room temperature to yield **25** in a moderate yield of 63%. The complex **25** were characterized by NMR and IR spectroscopy as well as MS and elemental analyses. In the IR

spectrum of **25**, the C=N bond stretching vibrations were observed as a medium band at 1627 cm^{-1} . The molecular ion peak was not observed in the EI mass spectrum of **25**. However, the peaks at m/z 709, 577, 562, and 534 could be assigned to the fragments $[\text{M}^+ - 2 \text{ THF}]$, $[\text{M}^+ - (\text{C}_3\text{H}_7, \text{Dipp}, \text{THF})]$, $[\text{M}^+ - (\text{CH}_3, \text{C}_3\text{H}_7, \text{Dipp}, \text{THF})]$, and $[\text{M}^+ - (2 \text{ C}_3\text{H}_7, \text{Dipp}, \text{THF})]$, respectively. In the ^1H NMR spectrum, resonances corresponding to the methyl protons were observed between 0.88 and 1.30 ppm as doublet (36H, $\text{CH}(\text{CH}_3)_2$); the secondary protons of the isopropyl groups were observed as multiplet at 2.88 ppm (6H, $\text{CH}(\text{CH}_3)_2$), and the protons of the aromatic rings were observed at 6.24 ppm as triplet (1H, *para*-Ar) and between 6.61 and 7.05 ppm as multiplet (8H, Ar). The other protons could not be identified due to delocalization of negative charge along the N-CH-C(=CHCHN)-N fragment. It was not possible to get any meaningful information from the ^{13}C NMR spectrum.

The investigation of complexes **20-24** in THF by EPR spectroscopy (Figure 19) revealed that the complexes are EPR-active at room temperature. The complexes **20** and **21** showed a broad signal which could be due to either unresolved hyperfine splitting or the contribution of metal centers. The complexes **22** and **24** showed the characteristics of a ligand centered radical. The complex **23** [with nuclear spin $I_{\text{Rb}} = 5/2$ (72%) and $I_{\text{Rb}} = 3/2$ (28%)] has a broad signal with slightly curved base line which could indicate the presence of spin density on the metal site, as well as on the ligand site. Further measurements at different conditions (temperature and frequency) would provide a precise picture.

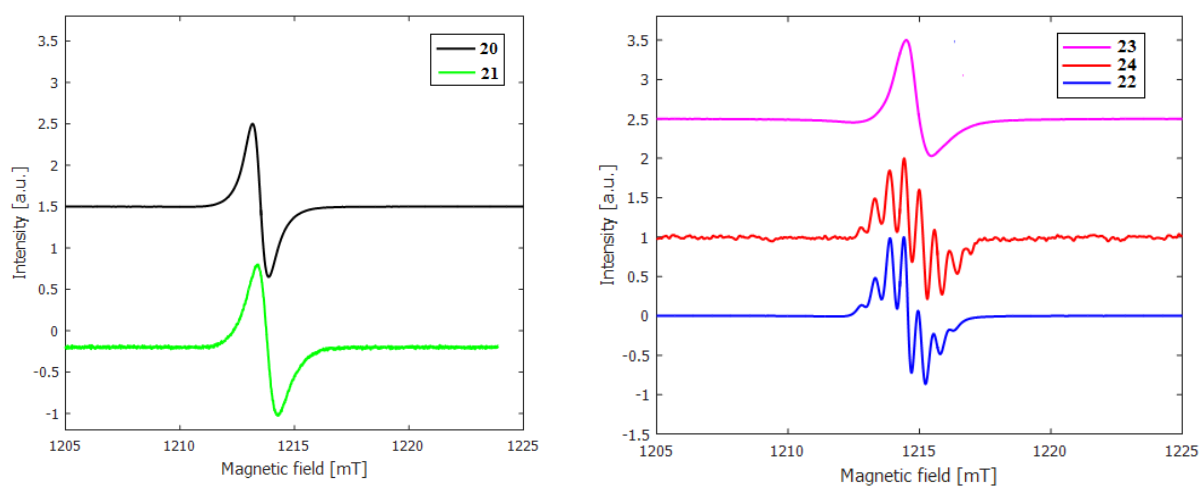


Figure 19. EPR spectrum of complexes **20-24** at room temperature.

2.4.5. Molecular Structures of $[\text{Li}(\text{H}^2\text{DAD}^{\text{Ad}})(\text{THF})_2]$ (**19**) and $[\text{Li}(\text{H}^2\text{DAD}^{\text{Dipp}})(\text{THF})_2]$ (**20**)

The lithium complex **19** with $\text{H}^2\text{DAD}^{\text{Ad}}$ crystallizes from THF at 5 °C as a monomer in the triclinic space group $P\bar{1}$ with one molecule of the complex in the asymmetric unit. The lithium complex **20** with $\text{H}^2\text{DAD}^{\text{Dipp}}$ also crystallizes from THF at 5 °C as a monomer; however, in the monoclinic space group $P2_1$. The molecular structure of **20** was determined from a 1:1 co-crystal with the free $\text{H}^2\text{DAD}^{\text{Dipp}}$ ligand. As shown in Figure 20, the lithium atom in both complexes is chelated by the two nitrogen atoms of the DAD moiety, and the coordinative saturation of the metal atoms is achieved by two THF ligands, resulting in coordination number 4. The lithium metal center in **19** and **20** lies essentially in the plane of $\text{H}_2\text{C}_2\text{N}_2$ fragment (Li atom in **19** and in **20** deviates by 3° and 6.8°, respectively).

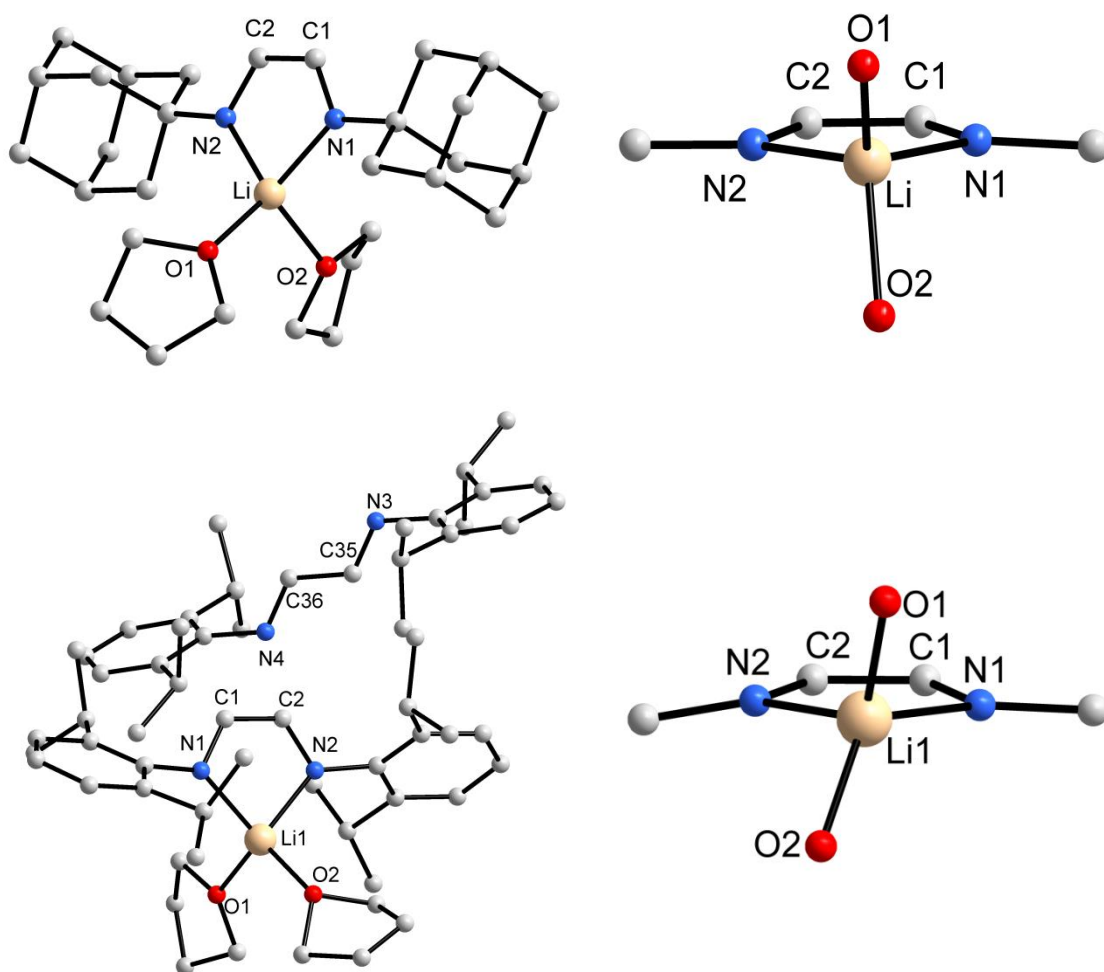


Figure 20. Molecular structure of **19** (top-left) and representation of the coordination sphere of the lithium atom in **19** (top-right). Molecular structure of **20** (bottom-left) and representation of the coordination sphere of the lithium atom in **20** (bottom-right).

The angle between LiO₂ and LiN₂ plane in **19** is 87.1° (almost perpendicular) while that in **20** is 76.7°. This could be because of packing effects in the crystal of **20**. It is important to note that the metal atoms in [Li(^{Me}₂DAD^{Dipp})(DME)] (**16**) and [Na(^{Me}₂DAD^{Dipp})(DME)] (**17**) were coordinatively saturated by a DME ligand while the same in [Li(^{H2}DAD^{Ad})(THF)₂] (**19**) and [Li(^{H2}DAD^{Dipp})(THF)₂] (**20**) were coordinated by two THF ligands. The coordination environment around the metal centers in both **19** and **20** can be described as distorted tetrahedral, which greatly differs from [Li(^{Me}₂DAD^{Dipp})(DME)] (**16**) where it was distorted square-planar. It is clearly the effect of the solvent molecules on the structures of these complexes (**16**, **19**, and **20**). In the complex **20**, the plane of the six-membered aromatic ring attached to N1 deviates from the plane of H₂C₂N₂ by 56.3°, while the same attached to N2 deviates by 65.4°. The Li–N bonds are almost same in both **19** (1.994(3) Å and 2.001(3) Å) and **20** (2.031(6) Å and 2.062(6) Å). Similarly, the Li–O bonds are also very similar in both **19** (1.953(2) Å and 2.002(3) Å) and **20** (1.963(2) Å and 1.977(6) Å). From these values, it is clear that the substituents at the N atoms have no influence on the M–N and M–O bond lengths in **19** and **20**. Moreover, the Li–N bond lengths in **19** and **20** are similar to those (2.032(4) Å) in **16**, whereas the Li–O bond lengths are shorter than those (2.146(2) Å) in **16**.

Table 11. Selected bond lengths [Å] of ligands (**3** and **2**) complexes (**19** and **20**).

DAD moiety	3 ^[68]	19	2 ^[67]	20
C–N (average)	1.255(3)	1.324(2)	1.234(3)	1.332(4)
C–C	1.457(3)	1.408(2)	1.445(3)	1.400(5)

Compared to their respective precursor ligands, the C–N bond lengths are elongated while the C–C bond length is shortened in the DAD moiety of both **19** and **20**; however, not to the extent of typical C–N single and C=C double bonds, respectively (Table 11). The Li–N bond lengths in both **19** and **20** and the C–N and C–C bond lengths of the DAD backbone in **20** are very similar to those [2.031(3) Å/ 2.043(3) Å for Li–N, 1.328(2) Å/ 1.329(2) Å for C–N and 1.403(2) Å for C–C] in the TMEDA adduct of lithium complex with radical-monoanionic ^{H2}DAD^{Dipp} reported by Trifonov and co-workers.^[14] All these structural data together with spectral data show that the NCCN fragment in both **19** and **20** is in radical-monoanionic state.

2.4.6. Molecular Structures of $[\text{K}(\text{H}^2\text{DAD}^{\text{Dipp}})(\text{THF})_4]$ (**22**) and $[\text{Rb}(\text{H}^2\text{DAD}^{\text{Dipp}})(\text{THF})_4]$ (**23**)

The potassium complex **22** and rubidium complex **23** are isotopic and crystallize from THF at 5 °C as monomers in the monoclinic space group $C2/c$ with one molecule of the complex in the asymmetric unit. As shown in Figure 21, both the potassium and rubidium atoms are chelated by the two nitrogen atoms of the $\text{H}^2\text{DAD}^{\text{Dipp}}$ ligand, forming a five-membered ring, and the coordinative saturation of the metals is achieved by four THF ligands, resulting in coordination number 6 for the metal atoms in both complexes.

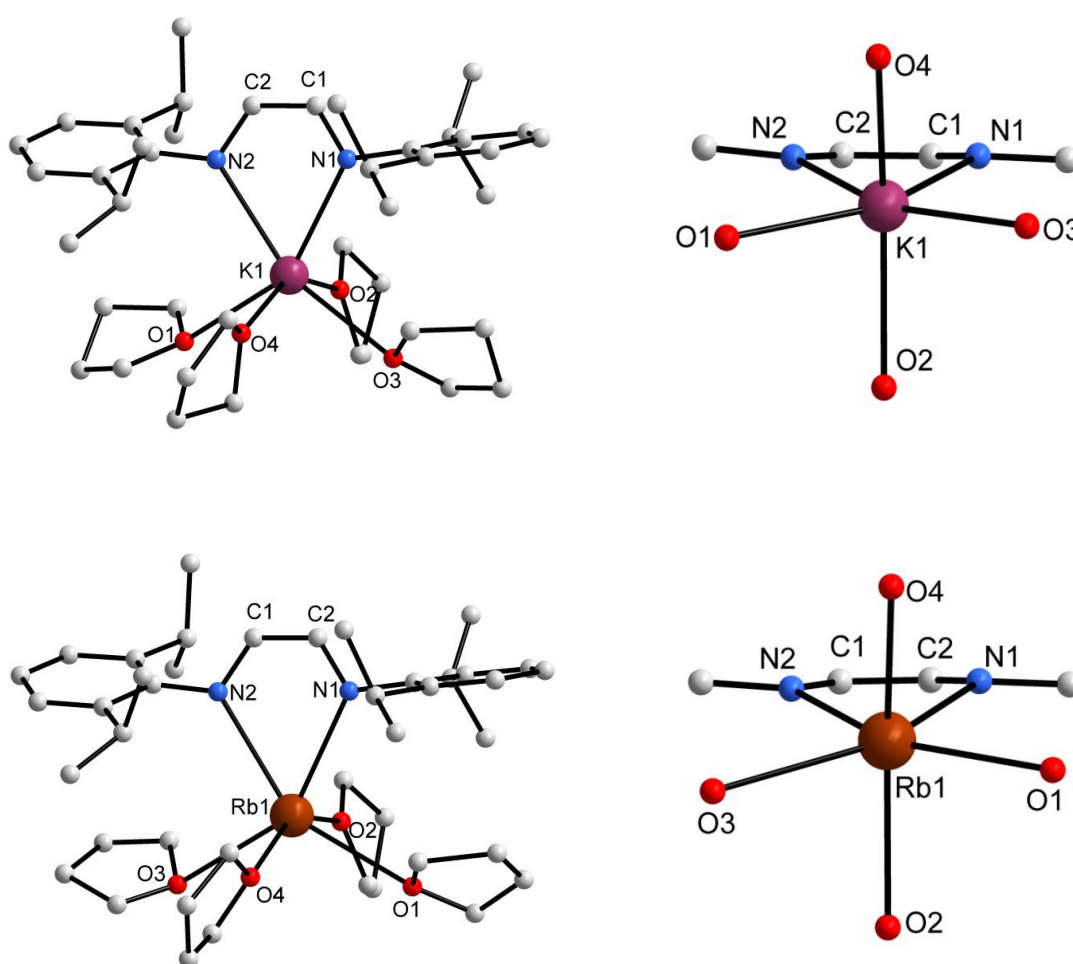


Figure 21. Molecular structure of **22** (top-left) and representation of the coordination sphere of the potassium atom in **22** (top-right). Molecular structure of **23** (bottom-left) and representation of the coordination sphere of the rubidium atom in **23** (bottom-right).

The K and Rb atoms are located slightly out of the plane of H₂C₂N₂ fragment (K and Rb deviate by 17.4° and 16.2°, respectively). The K–N and K–O bond lengths (Table 12) are similar to their counterparts in complex {[K₂(^{Me}₂DAD^{Dipp})(μ-THF)(THF)₂] · [K₂(^{Me}₂DAD^{Dipp})(μ-THF)(THF)₃]}₂ (**6**), while the Rb–N and Rb–O bond lengths are similar to those in {[Rb₂(^{Me}₂DAD^{Dipp})(THF)₄]₂ · THF}_n (**7**). In complex **22**, two oxygen atoms of the THF molecules are located almost parallel to the KN₂ plane with the angle 4.6° between O1–K–O3 and KN₂ planes (similar to the oxygen atoms of the DME in **16** and **17**) while the other two are almost perpendicular with an angle of 89.6° between the O2–K–O4 and KN₂ planes (similar **19** and **20**). Similarly in complex **23**, the angle between the O1–Rb–O3 and RbN₂ planes is 5.0° (almost parallel) while the same between O2–Rb–O4 and RbN₂ planes is 87.4° (almost perpendicular).

Table 12. Selected bond lengths [Å] of ligand **2** and complexes **22** and **23**.

	2 ^[67]	22	23
DAD moiety			
C–N (average)	1.234(3)	1.328(2)	1.325(3)
C–C	1.445(3)	1.403(2)	1.395(3)
M–N		{2.796(1)/ 2.785(1)}	{2.930(2)/ 2.927(2)}
M–O		{2.795(6)/ 2.727(2)/ 2.825(1)/ 2.704(8)}	{2.932(2)/ 2.866(2) 3.071(2)/ 2.890(1)}

Thus, the coordination environment of the K and Rb metal atoms adopts a highly distorted octahedral arrangement. It is surprising that the pronounced tendency for polymerization by multihapto π -coordination for the metal atoms K and Rb was not observed in **22** and **23**. The metal atom K in **22** is comparable with the metal atoms K2 and K4 in complex **6** and so is Rb in **23** with Rb2 and Rb4 in **7**. These metal centers, well protected by the bulky Dipp groups and saturated by the THF ligands, are not involved in aryl π -coordination, hence no aggregation. Moreover, they are located too far apart from the carbons of the DAD backbones to form any π -coordination between the metal centers and the DAD backbones. The plane of the six-membered aromatic ring attached to N1 and N2 deviates from the plane of the H₂C₂N₂ fragment by 73.5° and 58.3°, respectively, in complex **22** and by 77.1° and 60.3°, respectively, in complex **23**. As shown in Table 12 (page 63), compared to the free ligand **2**,^[67] the C–N bond lengths are elongated while the C–C bond lengths are shortened and the

values are similar to those in **20** and in the TMEDA adduct of lithium complex with radical anionic $\text{H}_2\text{DAD}^{\text{Dipp}}$ reported by Trifonov and co-workers.^[14] All these structural data together with the spectral data confirm the presence of radical-monoanionic $\text{H}_2\text{DAD}^{\text{Dipp}}$ ligands in complexes **22** and **23**.

2.4.7. Molecular Structure of $[\text{Cs}(\text{DippNCHC}(\text{=CHCHN}^{\text{Dipp}})\text{N}^{\text{Dipp}})(\text{THF})_2]_n$ (**25**)

The cesium complex **25** aggregates from *n*-pentane at r.t. as a coordination polymer in the monoclinic space group $P2_1/c$ containing a chelating $\text{DippNCHC}(\text{=CHCHN}^{\text{Dipp}})\text{N}^{\text{Dipp}}$ ligand, a cesium atom, and two THF ligands in the asymmetric unit. The molecular structure (Figure 22, page 65) shows that the cesium atom is coordinated by the imino/amido nitrogen donors (N1 and N2, respectively) of the chelating ligand (forming a five-membered ring) and an imino nitrogen atom (N3) from the adjacent monomeric unit (forming a coordination polymeric chain). The coordinative saturation of the Cs atom is achieved by two THF molecules, resulting in a five-coordinate Cs atom. The Cs atom is located slightly out of the plane of the central N-C-C-N fragment (deviation being 9.1°). The coordination environment of the Cs atom can be described as a highly distorted square pyramidal arrangement with two nitrogen atoms (N1 and N2) and two oxygen atoms (O1 and O2) occupying the base and a nitrogen atom (N3) occupying the apical positions. The plane of the six-membered aromatic ring attached to N1 deviates by 81.3° from the plane defined by N1-C1-C2-N2 while the same attached to N3 deviates by 76° from the plane defined by N2-C2-C27-C28-N3. Meanwhile, the plane of the six-membered aromatic ring attached to N2 deviates by 75.4° and 70.6° from the plan defined by N1-C1-C2-N2 and N2-C2-C27-C28-N3, respectively. The fragments N1-C1-C2-N2 and C27-C28-N3 are mostly in plane having a 20.8° deviation. The Cs–O bonds are not equal [Cs01–O2 (3.295(4) Å), Cs01–O1 (3.041(5) Å)] and so are the Cs–N bonds [Cs01–N1 (3.153(3) Å) bond is longer than the Cs01–N2 (2.994(3) Å) and Cs01–N3 (3.012(4) Å) bonds].

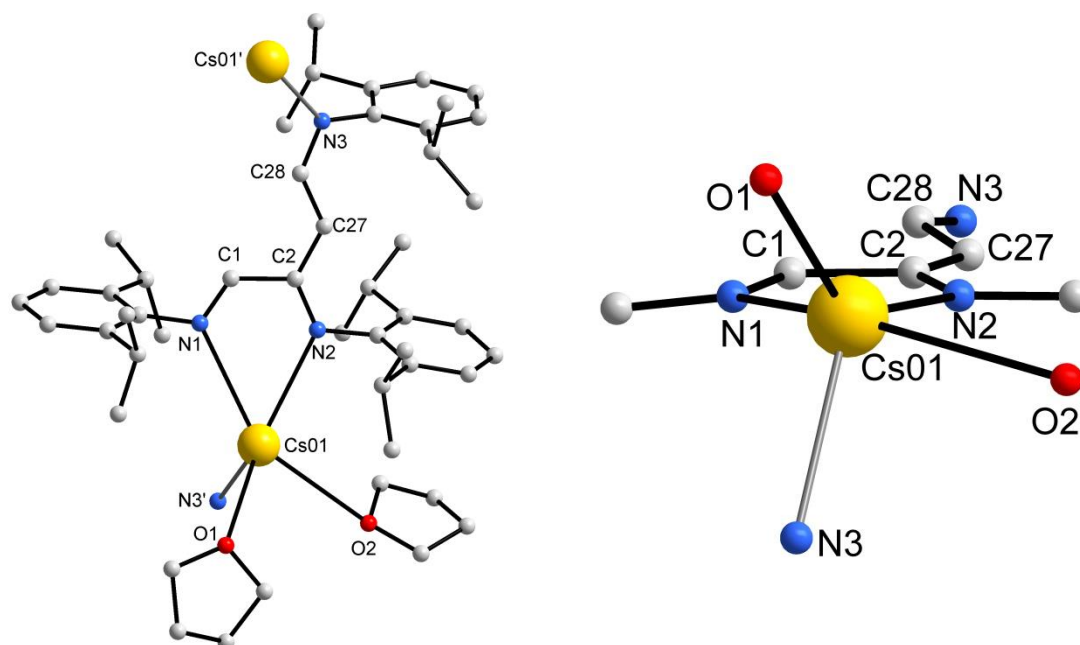


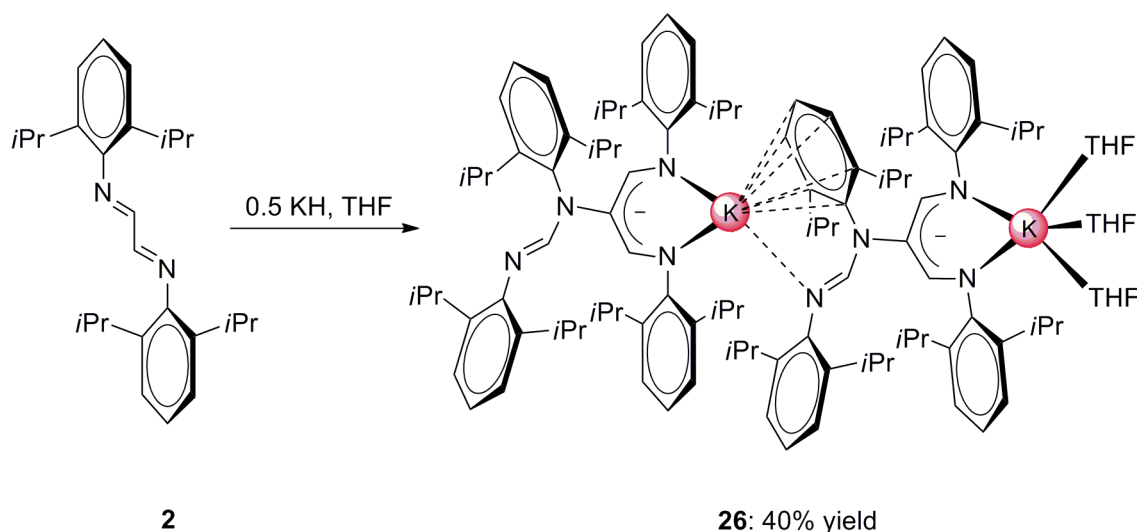
Figure 22. Molecular structure of **25** (left) and representation of the coordination sphere of the cesium atom in **25** (right).

The C1–C2 (1.499(6) Å) and C1–N1 (1.269(6) Å) bond lengths reflect a C–C single and an imine bond, respectively. Moreover, the C1–N1 bond length is only slightly longer than the C–N bond lengths (average: 1.234(3) Å) of the DAD backbone in the precursor ligand **2**.^[67] The C2–N2 (1.322(6) Å), C2–C27 (1.398(6) Å), C27–C28 (1.409(6) Å), and C28–N3 (1.317(6) Å) bond lengths as well as the almost equal Cs01–N2 and Cs01–N3 bond lengths reflect the delocalization of the negative charge along the N2–C2–C27–C28–N3 fragment. The Cs atoms in **25** are comparable with the Cs1 atoms in $\{[\text{Cs}_2(\text{Me}_2\text{DAD}^{\text{Dipp}})(\text{THF})_4] \cdot \text{THF}\}_n$ (**8**); one of the coordinated THF ligands in the latter is formally replaced by the N donor of the adjacent molecule. Moreover, the Cs atom in **25** is located too far from the carbons of both N1–C1–C2–N2 and N2–C2–C27–C28–N3 fragments; hence there is no π -coordination.

2.5. Reduction of $\text{H}_2\text{DAD}^{\text{Dipp}}$ ligand with KH

Clentsmith and co-workers demonstrated the carbon-carbon bond formation by treating the $\text{Me}_2\text{DAD}^{\text{Dipp}}$ ligand with MeLi. On the other hand, treatment of the $\text{Me}_2\text{DAD}^{\text{Dipp}}$ ligand with the more hindered base LiN^iPr_2 as well as treatment of the $\text{Me}_2\text{DAD}^{\text{Mes}}$ with MeLi resulted in proton abstraction. [12] These results prove that different DAD ligands react differently with various strong bases. Similarly, reduction of the $\text{H}_2\text{DAD}^{\text{Dipp}}$ (**2**) ligand with potassium hydride afforded an unprecedented potassium β -diketiminato complex $[\text{K}^{\text{DippNCHC}\{\text{DippNCHN}^{\text{Dipp}}\}\text{CHN}^{\text{Dipp}}\}(\text{THF})_{1.5}]$ (**26**) in a moderate yield of 40% (Scheme 29). Potassium hydride formally reduces a C=N bond of a DAD ligand, resulting in loss of H_2 . However, another DAD ligand reacts with the reduced DAD ligand to yield the bulky β -diketiminato complex **26**.

The ligand **2** was stirred overnight with KH (0.5 equiv.) in THF, and the resulting red solution was evaporated to dryness in vacuum. The residue was mixed well with *n*-pentane before it was kept at 5 °C to yield **26** as red crystals suitable for X-ray diffraction analysis. Elemental analysis values for C, H, and N of **26** were consistent with the proposed formulation of **26**. In the ^1H NMR of **26**, the resonances of the methyl protons were observed as doublets in the range of 0.91 to 1.26 ppm while those of the *tertiary* protons in the isopropyl groups were observed as multiplets between 3.0 and 3.5 ppm and at 4.1 ppm.



Scheme 29. Reduction of $\text{H}_2\text{DAD}^{\text{Dipp}}$ (**2**) ligand with potassium hydride.

The protons of the β -diketimate moiety and of the N=CH–N fragment were observed as singlet at 6.84 and 8.45 ppm, respectively. The *tertiary* and *quaternary* carbons of the β -diketimate moiety were observed at 156.7 and 112.8 ppm, respectively while the carbon of the N=CH–N fragment was observed at 159.0 ppm in the ^{13}C NMR of **26**. The C=N bond stretching vibrations were observed as a very strong band at 1632 cm^{-1} in the IR spectrum of **26**. The molecular ion peak of **26** was not observed in the EI mass spectra of **26**. However, the peaks at m/z 790, 751, 614, and 521 could be assigned to the fragments $[\text{M}^+ - 2\text{ THF}]$, $[\text{M}^+ - (\text{K}, 2\text{ THF})]$, $[\text{M}^+ - (\text{CH}_3, \text{Dipp}, 3\text{ THF})]$, and $[\text{M}^+ - (\text{C}_3\text{H}_7, \text{CHN}^{\text{Dipp}}, 3\text{ THF}, \text{K})]$, respectively.

2.5.1. Molecular Structure of $[\text{K}(\text{DippNCHC}\{\text{DippNCHN}^{\text{Dipp}}\}\text{CHN}^{\text{Dipp}})(\text{THF})_{1.5}]$ (**26**)

The potassium complex **26** aggregates from *n*-pentane at $5\text{ }^\circ\text{C}$ to a dimer in the orthorhombic space group $P2_12_12_1$ with one molecule of the complex in the asymmetric unit. The molecular structure (Figure 23, page 68) of the complex **26** shows that the K1 atom is chelated by the amido/imino nitrogen atoms N1 and N2 and is coordinated by an imino nitrogen atom N8 and the π -electronic system (symmetric η^6 -coordination) of the aromatic ring attached to N7, while the K2 atom is chelated by amido/imino nitrogen atoms N5 and N6 and coordinated by three THF molecules. The plane of the aromatic rings attached to N1 and N2 deviates from the plane of the central N2–C1–C2–C3–N1 fragment by 74.7° and 79.6° , respectively, while the same attached to N5 and N6 deviates from the plane of the central N5–C53–C54–C55–N6 fragment by 62° and 80.1° , respectively. Similarly, the plane of the aromatic rings attached to N3 and N4 deviate from the plane of the central N3–C28–N4 fragment by 75.5° and 72.6° while the same attached to N7 and N8 deviates from the plane of the central N7–C80–N8 fragment by 79.5° and 60.6° . The K1 atom deviates from the plane of the central N2–C1–C2–C3–N1 fragment by 20.9° , while the K2 atom deviates from the plane of the central N5–C53–C54–C55–N6 fragment by 31° . These values indicate that the metal atoms are located out of plane of the β -diketimate moiety, whereas the metal atoms are located in plane of the same in a similar β -diketimate potassium complex $[\text{K}(\text{DippNC}(\text{Me})\text{CHC}(\text{Me})\text{N}^{\text{Dipp}})]_n$.^[24]

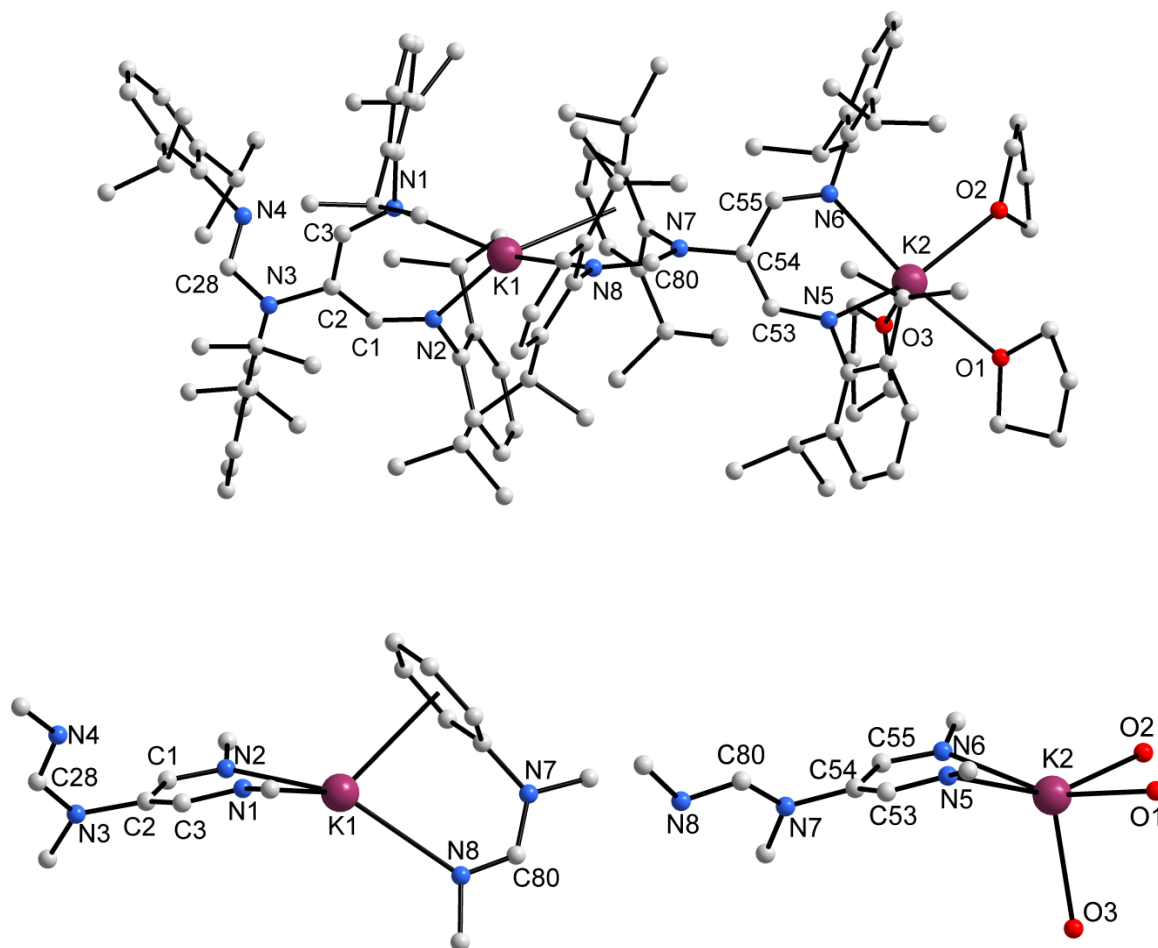


Figure 23. Molecular structure of **26** (top) and representation of the coordination sphere of the potassium atoms K1 (bottom-right) and K2 (bottom-right) in **26**.

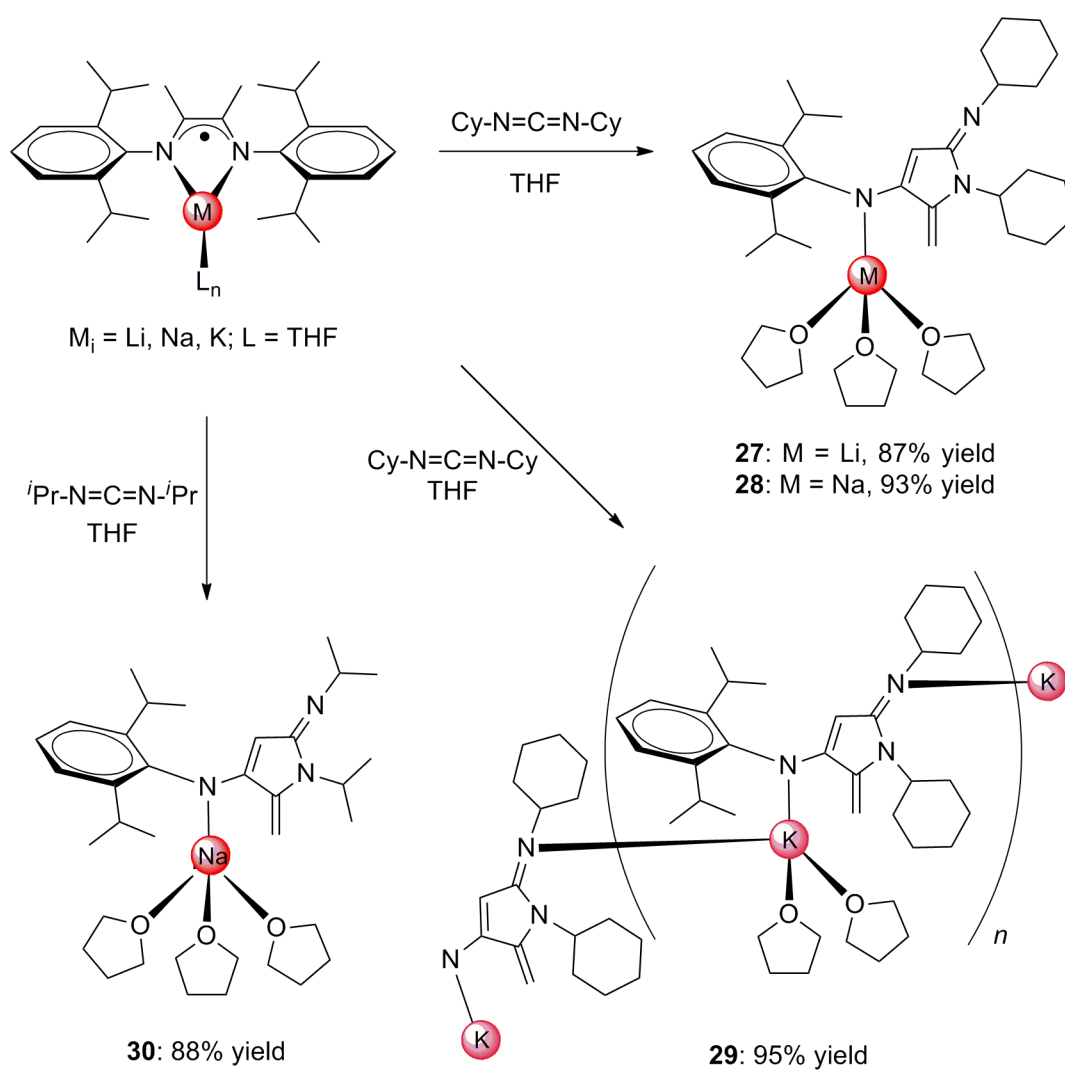
Interestingly, the potassium atom, known for its tendency to form multihapto π -interactions, prefers only the neutral aryl group over β -diketiminato group (to form π -interaction) in the case of K1 while it forms no π -interaction at all in the case of K2. The fragments N2-C1-C2-C3-N1 and N5-C53-C54-C55-N6 are not in plane with the fragments N3-C28-N4 and N7-C80-N8, respectively (torsion angle of C1-C2-N3-C28 is 118.6° and of C53-C54-N7-C80 is 48.5°). The coordination environment of the K1 atom adopts a distorted trigonal pyramid with three nitrogen atoms (N1 N2 and N8) occupying the trigonal base and an unoccupied apical position. However, the coordination around K2 atom adopts a highly distorted square pyramidal arrangement with two nitrogen (N5 and N6) and two oxygen (O1 and O2) atoms occupying the equatorial and an oxygen atom (O3) occupying the apical positions. The K1–N2, K2–N5, and K2–N6 [2.728(5) Å, 2.716(4) Å/ 2.720(5) Å, respectively] bond lengths are almost equal while the K1–N1 (2.664(4) Å) and K1–N8 (3.029(4) Å) are not. The C3–N1,

C1–N2, C53–N5, and C55–N6 [1.303(6) Å/ 1.317(6) Å/ 1.308(6) Å/ 1.289(6) Å, respectively] bond lengths are almost equal and so are the C1–C2, C2–C3, C53–C54, and C54–C55 [1.388(8) Å/ 1.396(7) Å/ 1.392(7) Å/ 1.403(7) Å, respectively] bond lengths. These values together with the sp²-hybridized carbon centers C2 and C54 (which are trigonal planar with the sum of angles being 360°) prove the well-delocalized negative charge on the β-diketimate moiety. The K–N bond lengths (except K1–N8 (3.029(4) Å) in **26** compare well with those in [K(DippNC(Me)CHC(Me)N^{Dipp})]_n while the average of the K–C (aryl) distances (3.256(6) Å) in **26** is shorter than that in the latter. The C2–N3, C28–N3, C28–N4, C54–N7, C80–N7, and C80–N8 [1.474(6) Å/ 1.333(8) Å/ 1.244(7) Å/ 1.455(6) Å/ 1.350(7) Å/ 1.293(6) Å, respectively] bond lengths also reflect the delocalization of negative charge along those bonds (as the values are formally neither C=N double nor C–N single bond). The K2–O1, K2–O2, and K2–O3 [2.634(1) Å/ 2.674(7) Å/ 2.778(1) Å, respectively] bond lengths are similar to the K–O bond lengths in the complex {[K₂(Me₂DAD^{Dipp})(μ-THF)(THF)₂] · [K₂(Me₂DAD^{Dipp})(μ-THF)(THF)₃]}₂ (**6**).

2.6. Reactions between alkali metal complexes with radical-monoanionic $\text{Me}_2\text{DAD}^{\text{Dipp}}$ ligands and carbodiimides

Scholz and co-workers have demonstrated that reactions between samarium complexes with dianionic DAD ligands and ketones yielded formal cycloaddition products.^[111] Cui and co-workers have showed that reactions between yttrium complexes with dianionic DAD ligands and isocyanate resulted in not only the same C–C coupling but also the C–N coupling of the C–C coupling product with another molecule of isocyanate.^[158] These studies indicate the unique reactivity of dianionic DAD ligands. In order to further explore the reactivity of radical-monoanionic DAD ligands, carbodiimides were treated with alkali metal complexes with radical-monoanionic $\text{Me}_2\text{DAD}^{\text{Dipp}}$ ligands to yield the interesting heterocyclic compounds **27-30** (Scheme 30, page 71). In this condensation reaction, the carbodiimide functional group attacks a C=N bond of the $\text{Me}_2\text{DAD}^{\text{Dipp}}$ ligand, resulting in formation of a heterocyclic compound (with the loss of a Dipp group, a N atom, and three H atoms from the $\text{Me}_2\text{DAD}^{\text{Dipp}}$ ligand).

The $\text{Me}_2\text{DAD}^{\text{Dipp}}$ ligand **1** (1 equiv.) was added to the dilithium complex **4** (1 equiv.) in THF to give the monolithium complex with radical-monoanionic $\text{Me}_2\text{DAD}^{\text{Dipp}}$ ligand. This monolithium complex in THF was treated with *N,N'*-dicyclohexylcarbodiimide (1 equiv.), and the resulting yellow solution was concentrated to an oily liquid before it was kept at -32 °C to yield $[\text{Li}(\text{DippN}^{\text{Cy-Pyr}})(\text{THF})_3]$ (**27**) in good yield (87%) as light yellow crystals suitable for X-ray diffraction analysis. Similarly, compounds $[\text{Na}(\text{DippN}^{\text{Cy-Pyr}})(\text{THF})_3]$ (**28**) and $\{[\text{K}(\text{DippN}^{\text{Cy-Pyr}})(\text{THF})_2]_4 \cdot \text{THF}\}_n$ (**29**) were synthesized in excellent yield (93% and 95%, respectively) by treating the monosodium and monopotassium complexes with *N,N'*-dicyclohexylcarbodiimide (1 equiv.), respectively. Treatment of the monosodium complex with *N,N'*-diisopropylcarbodiimide (1 equiv.) yielded the compound $[\text{Na}(\text{DippN}^{\text{iPr-Pyr}})(\text{THF})_3] \cdot \text{THF}$ (**30**) in 88% yield. Elemental analysis, values for C, H, and N of **29** and **30** were consistent with the proposed formulation, revealing that complexes **29** and **30** keep the THF of crystallization (uncoordinated THF) upon drying.



Scheme 30. Reactions between alkali metal complexes with radical-monoanionic $\text{Me}_2\text{DADipp}^{\cdot-}$ ligands and carbodiimides.

2.6.1. Spectroscopic analysis of the compounds (27-30)

The NMR spectra were recorded in d_8 -THF, and the ^1H NMR and ^{13}C NMR data of the compounds **28-30** are summarized in Tables 13 and 14 (page 73), respectively, and the numbering of the carbon atoms in the compounds is shown in Figure 24. The resonances corresponding to the methyl protons were observed as doublets in the range between 1.0 and 1.2 ppm in the ^1H NMR of **28** and **29**, and between 0.9 and 1.3 ppm in the ^1H NMR of **30**. The CH_2 protons of the cyclohexyl groups in **28** were in the range of 1.14 to 1.82 and 2.24 to 2.4 ppm, while for **29**, they were observed in the range of 1.10 to 1.78 and 2.27 to 2.40 ppm as broad multiplets. The CH_2 protons (1) of the pyrrole group were observed as two singlets for all the compounds **28-30**, showing that they are chemically non-equivalent [Table 13 (page 73), Figure 25 (page 74), Figure 26 (page 75)]. The CH protons (4) of the pyrrole groups were observed as singlets for all the compounds **28-30**. Compared to the *tertiary* protons (6, 7) of the cyclohexyl groups in **28** and **29**, the *tertiary* protons (6, 7) of the isopropyl groups in **30** were observed at lower field. The resonances corresponding to the *meta* and *para* protons (10, 11) as well as the *tertiary* protons (12) of the isopropyl groups in the aromatic ring were observed almost in the same range for all the compounds **28-30**.

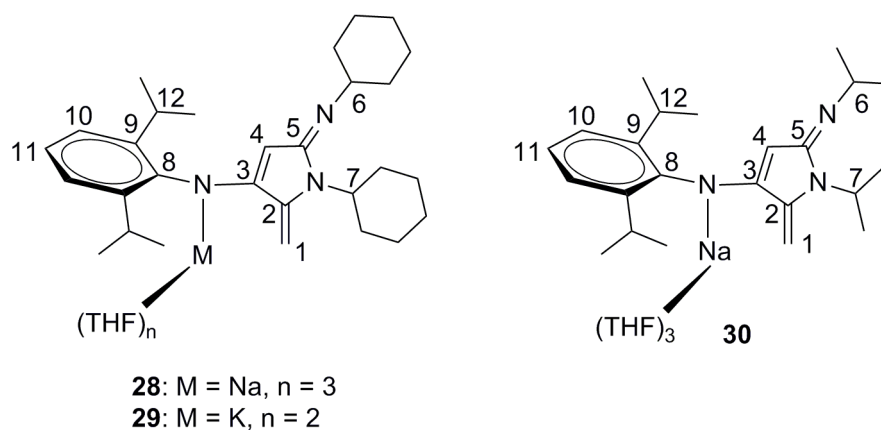


Figure 24. Numbering of the carbons in **28-30**.

Table 13. ^1H NMR chemical shifts of the compounds **28-30**.

δ in ppm	28	29	30
1	3.78, 4.06	3.74, 4.30	3.76, 4.07
4	3.73	3.67	3.69
6	2.89	2.87	3.19
7	4.23	4.20	4.81
10	6.95	6.89	6.95
11	6.78	6.70	6.79
12	3.35	3.27	3.35

Table 14. ^{13}C NMR chemical shifts of the compounds **28-30**.

δ in ppm	28	29	30
1	71.0	72.1	71.2
2	152.3	152.5	151.3
3	162.9	161.1	162.1
4	73.2	71.8	73.1
5	162.5	163.4	162.4
6	58.31	58.3	50.1
7	51.4	51.7	41.6
8	153.3	153.9	153.2
9	143.4	142.3	143.2
10	123.3	123.0	123.2
11	121.4	121.5	121.3
12	28.1	28.1	27.9

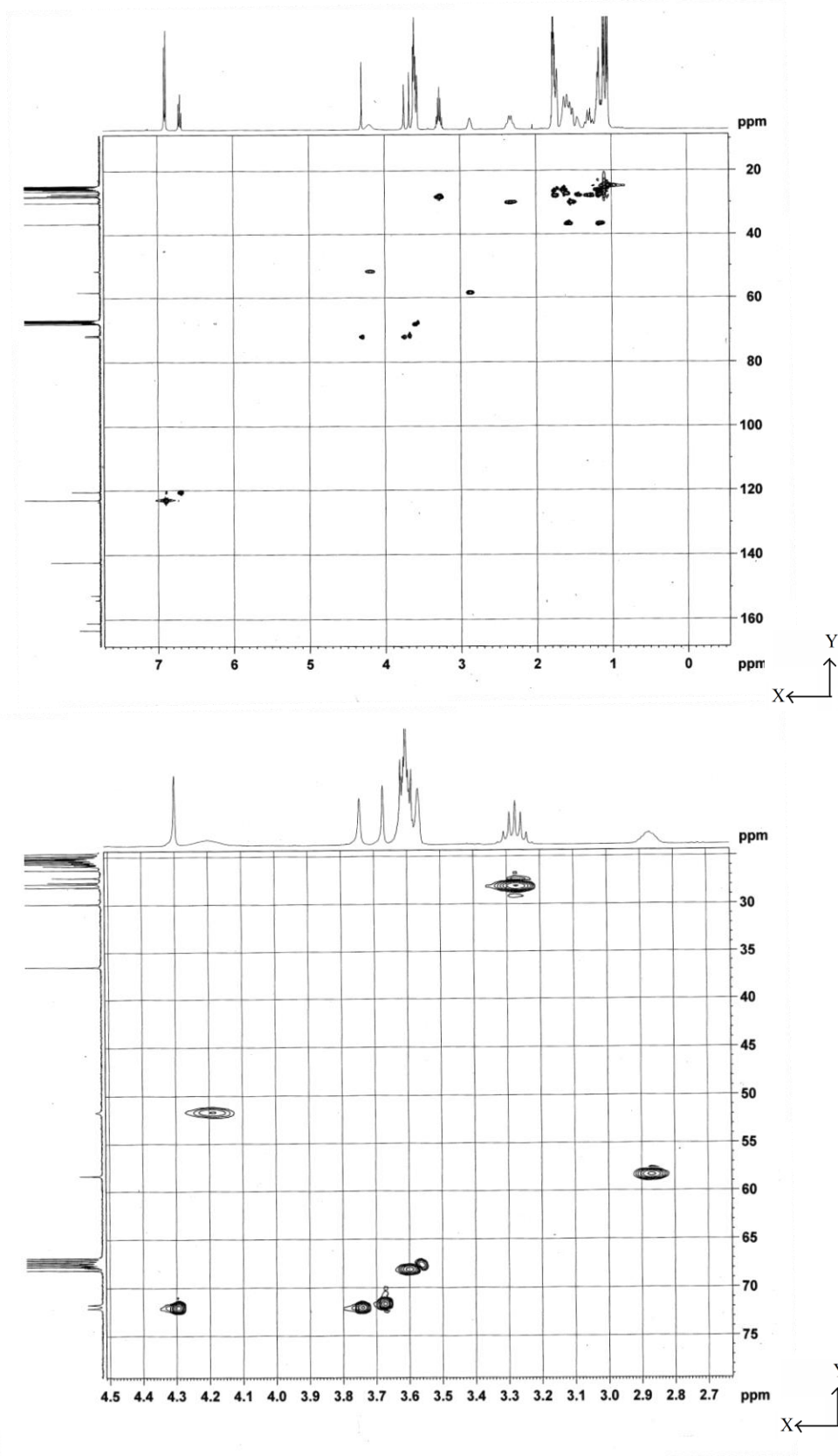


Figure 25. HSQC spectrum of **29** (*ds*-THF, 20 °C): full (top) and enlarged aliphatic region (bottom). X-axis: ^1H NMR chemical shifts (400 MHz), Y-axis: ^{13}C NMR chemical shifts (100 MHz).

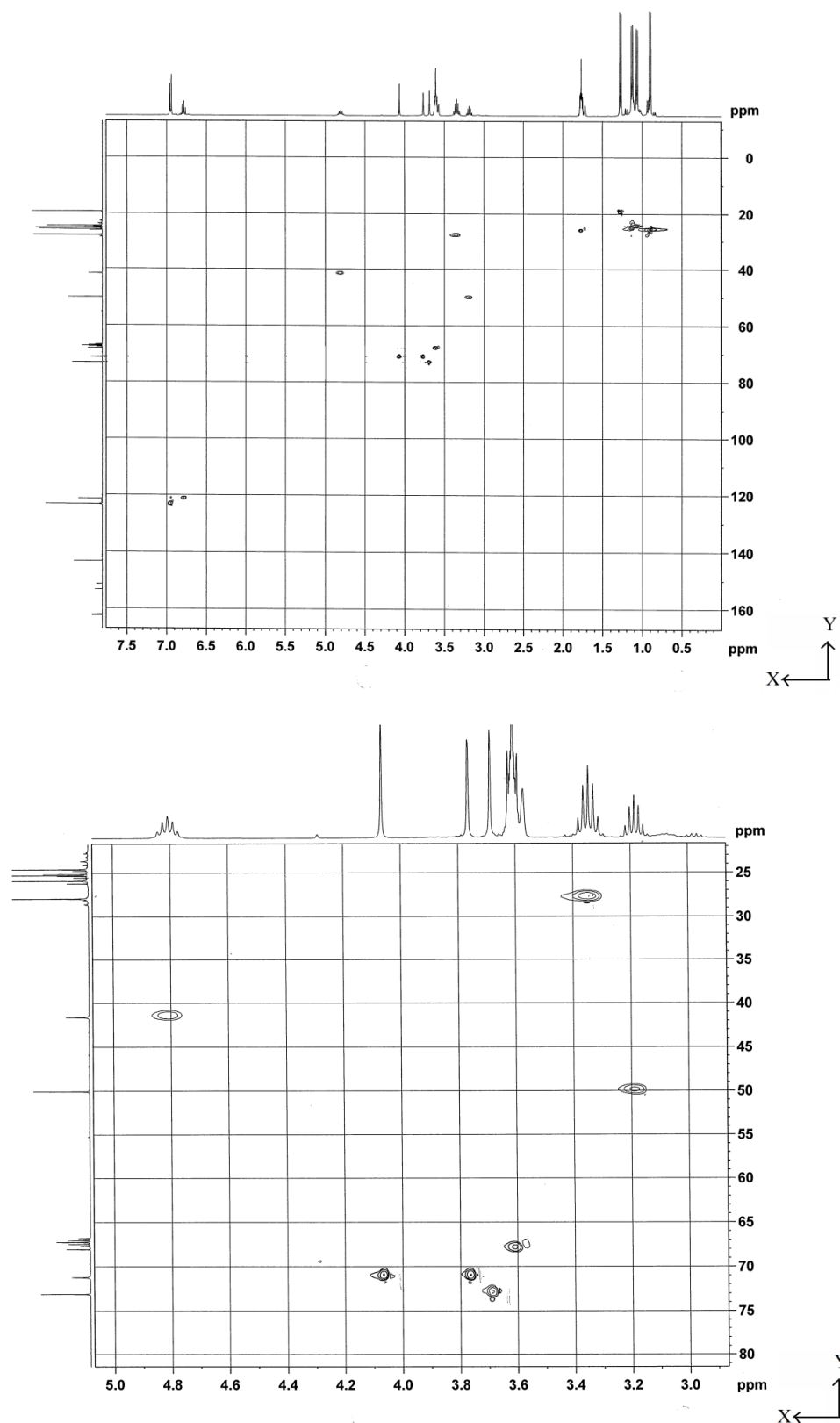


Figure 26. HSQC spectrum of **30** (400 MHz, d_8 -THF, 23 °C): full (top) and enlarged aliphatic region (bottom). X-axis: ^1H NMR chemical shifts (400 MHz), Y-axis: ^{13}C NMR chemical shifts (100 MHz).

The methyl carbons were observed in the range between 24 and 26 ppm in the ^{13}C NMR of **28** and **29**, and between 19 and 26 ppm in the ^{13}C NMR of **30**. The CH_2 carbons of the cyclohexyl groups in **28** were in the range of at 25.8, 27.1, 27.6, 27.8, 29.8, and 36.5, while for **29**, they were observed at 26.9, 27.1, 27.6, 27.8, 29.9, and 36.6 ppm (almost at same ppm). In the pyrrole group, the carbons C(2), C(3), and C(5) were observed at lower field than the carbons C(1) and C(4) for all the compounds (**28-30**). Compared to the *tertiary* carbons (6, 7) of the cyclohexyl groups in **28** and **29**, the *tertiary* carbons (6, 7) of the isopropyl groups in **30** were observed at higher field. The resonances corresponding to the carbons 8, 9, 10, 11 as well as the *tertiary* carbons (12) of the isopropyl groups at the aromatic ring were observed almost in the same range for all the compounds (**28-30**) [Figure 25 (page 74), Figure 26 (page 75)].

The IR spectra of all the compounds (except **30**) displayed the $\text{C}=\text{N}$ bond stretching vibrations as a strong band at 1637 cm^{-1} . The molecular ion peak was only observed in the EI mass spectrum of **27**. However, the base peak of **28** and **29** at m/z 433 could be assigned to the fragment $[\text{DippN}^{\text{Cy-Pyr}} + \text{H}]$ while and that of **30** at m/z 354 could be assigned to the fragment $[\text{DippN}^{\text{iPr-Pyr}} + \text{H}]$. The fragment $[\text{DippN}^{\text{Cy-Pyr}} + \text{H}]$ was also observed in the mass spectrum of **27** but not as base peak.

2.6.2. Molecular Structures of $[\text{Li}(\text{DippN}^{\text{Cy-Pyr}})(\text{THF})_3]$ (**27**), $[\text{Na}(\text{DippN}^{\text{Cy-Pyr}})(\text{THF})_3]$ (**28**), and $[\text{Na}(\text{DippN}^{\text{iPr-Pyr}})(\text{THF})_3] \cdot \text{THF}$ (**30**)

The lithium complex **27** and the sodium complex **28** crystallize from THF at $-32\text{ }^\circ\text{C}$ as monomers in the triclinic space group $P\bar{1}$ and contain one molecule of the complex in the asymmetric unit. The molecular structures of the complexes are shown in the Figure 27 (page 77). The metal atom in both **27** and **28** is coordinated by a nitrogen atom (N1) and three THF molecules, thus resulting in coordination number 4. The Li atom in **27** is located almost in the plane of the pyrrole unit (torsion angle of Li1-N1-C1-C4 being 178°), whereas the Na atom in **28** is located out of the plane (torsion angle of Na1-N1-C3-C4 being 153°). The coordination environment of the Li1 and Na1 metal atoms adopts a highly distorted tetrahedral geometry. The pyrrole unit in both **27** and **28** is mostly planar [torsion angles (N1-C1-C4-C3) -180° , (C2-N2-C3-N3) 174.4° , and (C4-C1-C2-C5) 178.1° in **27** and (N1-C3-C4-C5) -173.2° , (C2-

N2-C5-N3) 173° , and (C1-C2-C3-C4) 166° in **28**]. The nitrogen atom N1 in **27** and **28** is substituted with the 2,6-diisopropylphenyl group while the N2 and N3 are substituted with cyclohexyl groups. The plane of the phenyl ring deviates from the plane of the pyrrole unit by 88.0° (almost perpendicular) in the complex **27** and by 61.4° in the complex **28**.

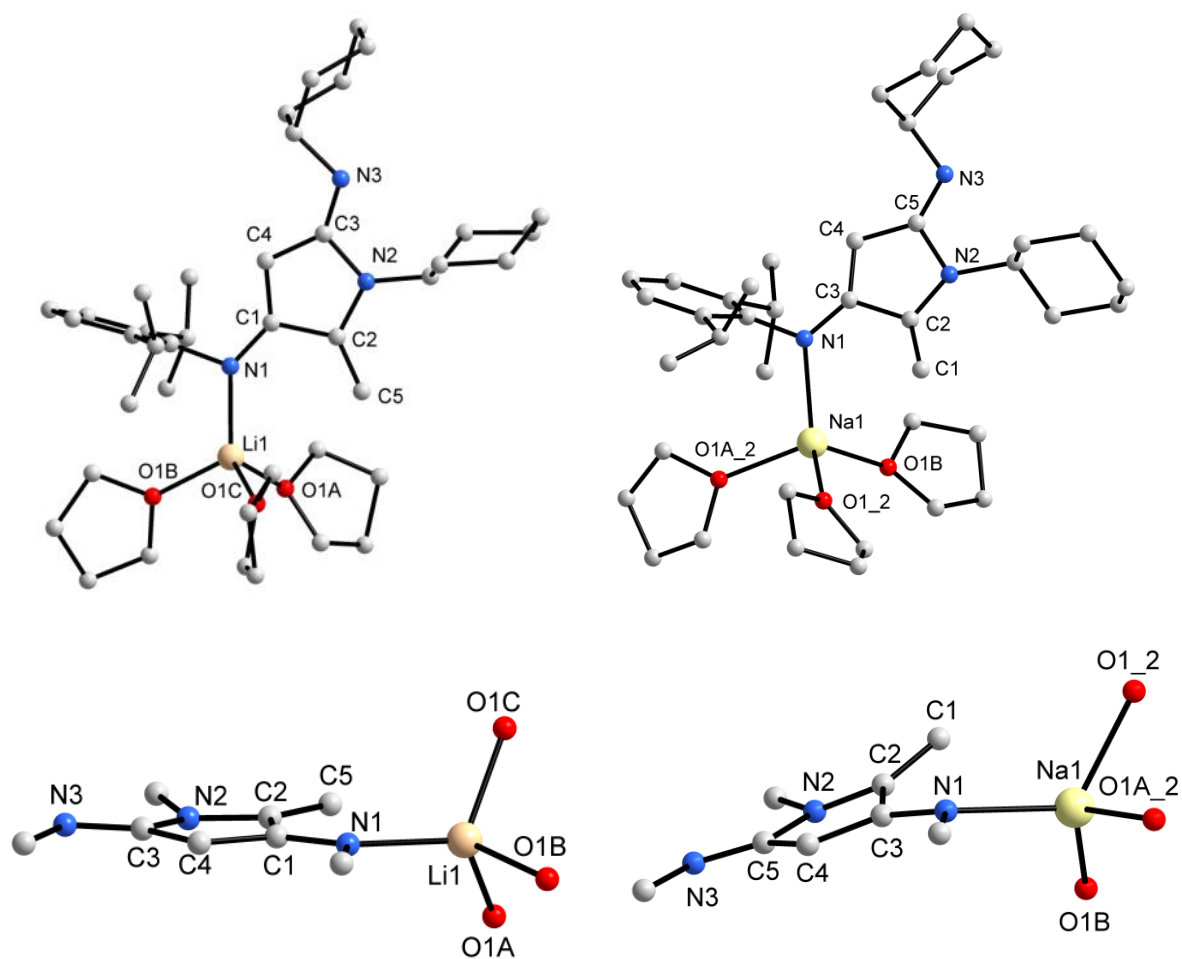


Figure 27. Molecular structures of **27** (top-left) and **28** (top-right). Representation of the coordination sphere of the lithium atom in **27** (bottom-left) and sodium atom in **28** (bottom-right).

In compound **27**, the C1–C4 (1.380(3) Å) and C2–C5 (1.326(3) Å) bond lengths formally reflect a C=C double bond while the C1–C2 (1.498(3) Å) and C4–C3 (1.436(2) Å) bond lengths represent a C–C single bond. Formally, the bond length C3–N3 (1.286(2) Å) in **27** reflects a C=N double bond while the C1–N1 (1.335(2) Å), C2–N2 (1.418(3) Å), and C3–N2 (1.417(3) Å) bonds represent C–N single bonds. The Li–N (2.014(3) Å) bond length compares well with the Li–N bond lengths [in the range of 2.006(3) Å to 2.077(4) Å] while

the Li–O bond lengths [2.006(7) Å/ 2.044(1) Å/ 2.071(2) Å] are slightly longer than the Li–O bond lengths [in the range of 1.931(3) Å to 1.987(3) Å] in similar lithium complexes {Li[C₅H₄–CH=NAr], Ar = Phenyl, 2,6-dimethylphenyl, or Dipp}.^[151] Similarly, in compound **28**, the C3–C4 (1.377(4) Å) and C2–C1 (1.335(4) Å) bond lengths formally reflect C=C double bonds while the C2–C3 (1.500(3) Å) and C4–C5 (1.437(4) Å) bond lengths formally represent C–C single bonds. The Na–N (2.334(2) Å) bond length is shorter than the Na–N bond lengths [in the range of 2.403(2) Å to 2.505(2) Å] while Na–O bond lengths [2.255(1) Å/ 2.307(3) Å/ 2.300(3) Å] similar to the Na–O bond lengths [in the range of 2.286(2) Å to 2.347(2) Å] in the sodium complexes [Na(ⁱPrNPh)(THF)₂]₂ and [Na(NPh₂)(THF)₂]₂.^[152]

The sodium complex **30** crystallizes from THF at -32 °C as a monomer in the monoclinic space group *P2/c* and contains one molecule of the complex and an uncoordinated THF molecule in the asymmetric unit. The molecular structure (Figure 28) of **30** shows that only minor differences in the bond lengths and angles between complexes **28** and **30** except the isopropyl groups at N2 and N3 in **30** (instead of the cyclohexyl groups in **28**) and the deviation of the plane of the aromatic ring from the plane of the pyrrole unit (80.9° in **30** instead of 61.4° in **28**).

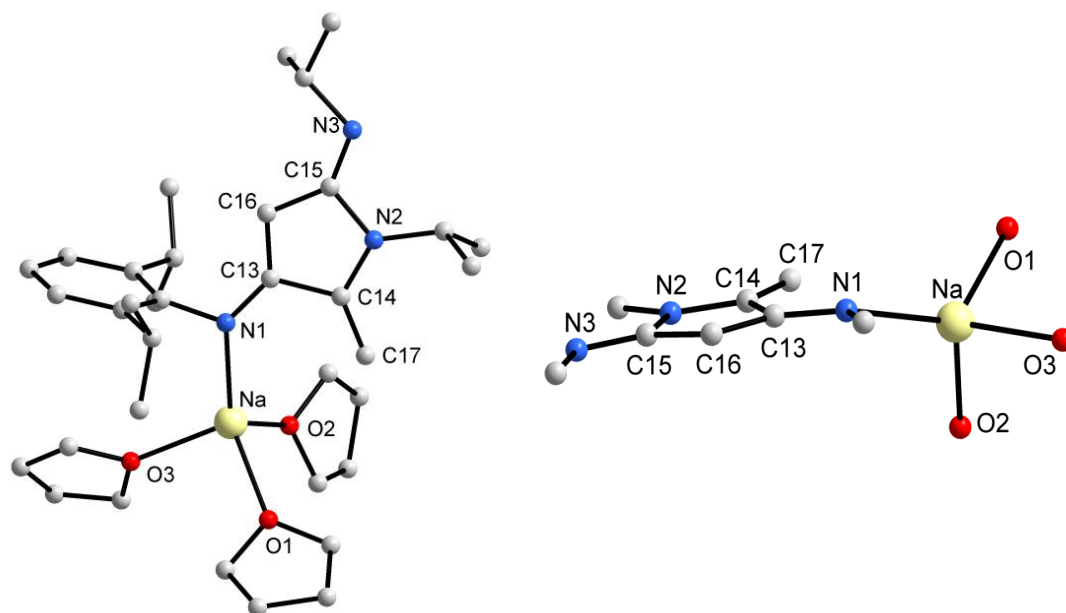


Figure 28. Molecular structure of **30** (left). Representation of the coordination sphere of the sodium atom in **30** (right).

2.6.3. Molecular Structure of $\{[K(\text{DippN}^{\text{Cy-Pyr}})(\text{THF})_2]_2 \cdot \text{THF}\}_n$ (**29**)

The potassium complex **29** crystallizes from THF at $-32\text{ }^\circ\text{C}$ as a coordination polymer in the triclinic space group $P\bar{1}$ containing two Dipp groups, two cyclohexyl-substituted pyrrole units, two potassium atoms, and four coordinated and one uncoordinated THF molecules in the asymmetric unit. As shown in the Figure 29, both of the pyrrole units in **29** are more planar (torsion angles 175.6° - 179.6°) than that in **27** and **28**.

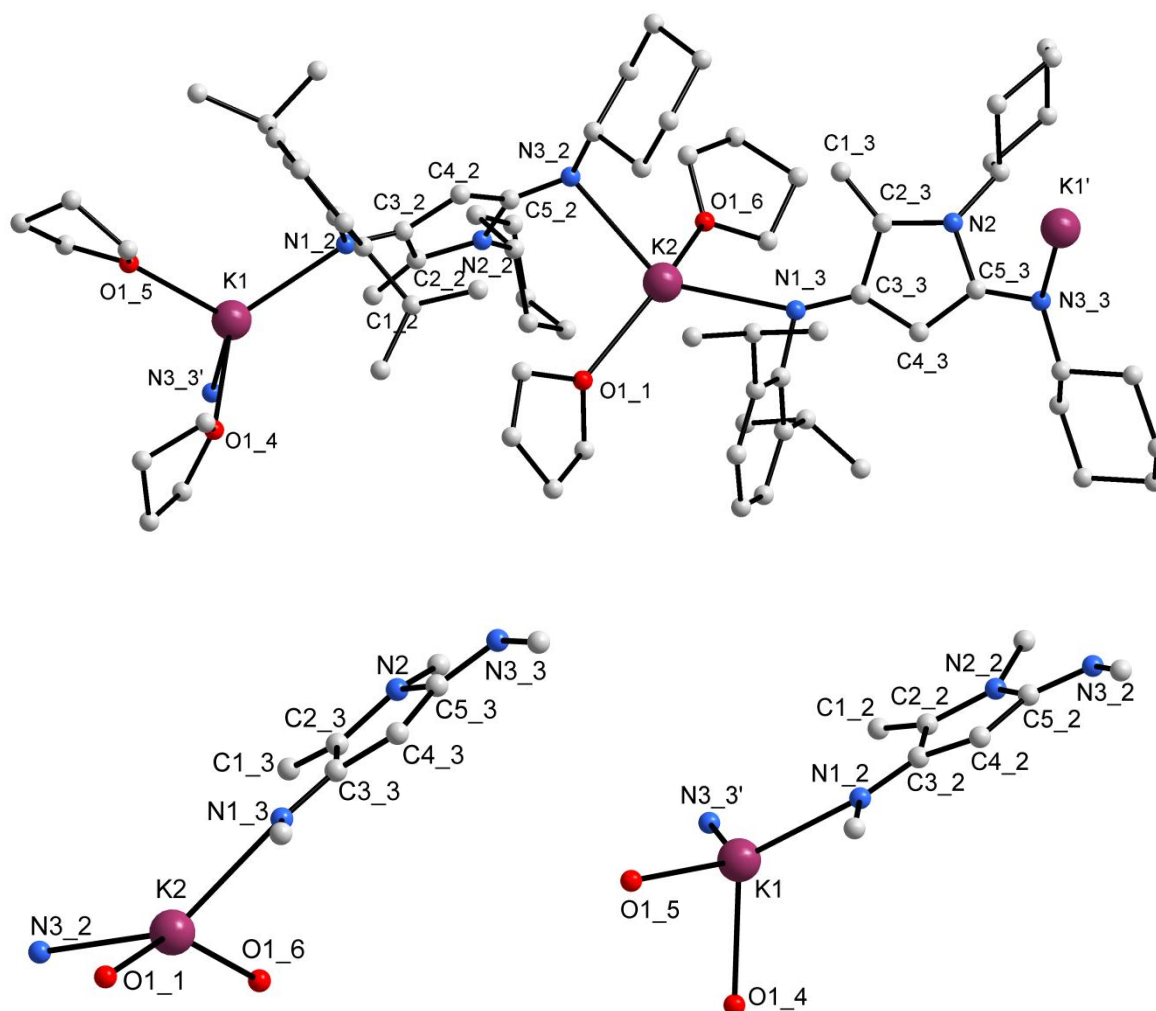


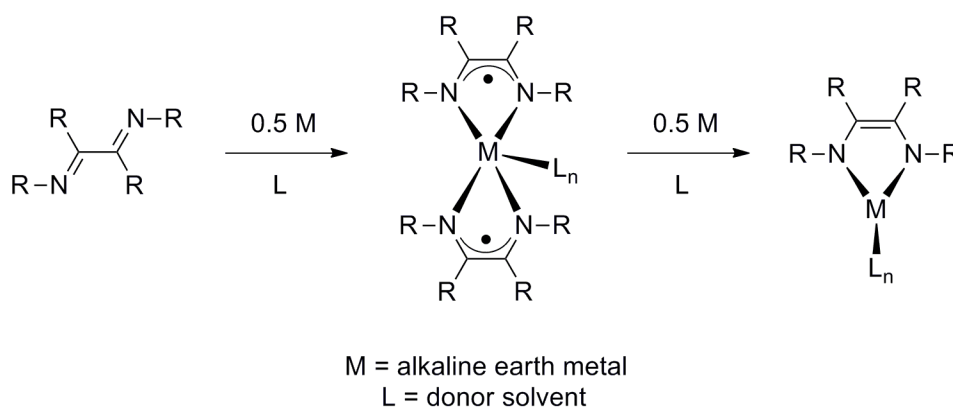
Figure 29. Molecular structure of **29** (left). Representation of the coordination sphere of the potassium atoms K1 (bottom-left) and K2 (bottom-right) in **29**.

The nitrogen atom N1 is substituted with 2,6-diisopropylphenyl group while the N2 and N3 are substituted with cyclohexyl group. The metal atoms are coordinated by two THF ligands, an amido nitrogen atom attached to the 2,6-diisopropylphenyl group, and an imino nitrogen

atom attached to the cyclohexyl group, forming the coordination polymeric chain. This is similar as in the lithium complex **29** and sodium complex **28**; one of the three THF ligands is formally replaced by the N donor group of an adjacent molecule. The four-coordinate potassium atom K2 is located out of plane of the pyrrole unit containing N2 while K1 is located more in the plane of the pyrrole unit containing N2_2 (torsion angle of K1-N1_2-C3_2-C4_2 being -172° and K2-N1_3-C3_3-C4_3 being -158.3°). The plane of the phenyl rings attached to N1_2 and N1_3 is almost perpendicular to the plane of the pyrrole units attached to the same (deviates by 76.7° and 75.3° , respectively). The K–N bond lengths [2.734(2) Å/ 2.851(2) Å/ 2.764(2) Å/ 2.814(2) Å] in **29** compare well with the K–N bond lengths [2.779(2) Å/ 2.754(2) Å/ 2.773(2) Å/ 2.752(2) Å] while the K–O bond lengths [2.682(6) Å/ 2.688(2) Å/ 2.677(2) Å/ 2.688(1) Å] in **29** are much shorter (probably because of the terminal THF molecules in **29**) than the K–O bond lengths [2.947(2) Å/ 2.868(2) Å] in the potassium complex $[\text{K}_2(\text{HNDipp})_2(\mu\text{-THF})]_\infty$.^[153] The coordination environment of the metal atoms adopts a similar arrangement (a highly distorted tetrahedral arrangement) as in complexes **27** and **28**; however, two corners of the tetrahedron are occupied by nitrogen atoms while the other two are occupied by oxygen atoms.

2.7. Alkaline earth metal complexes with radical-monoanionic and dianionic DAD ligands

Alkaline earth metal complexes with DAD ligands are mainly prepared by salt metathesis reactions between alkaline earth metal halides and alkali metal DAD complexes. However, direct metallations are also possible in which the DAD ligands are reduced by alkaline earth metals either in the presence^[42] or absence^[43] of iodine. The reduction of DAD ligands with 0.5 equiv. of alkaline earth metals yields complexes containing two radical-monoanionic DAD ligands while reactions with 1 equiv. of alkaline earth metals yield complexes containing dianionic DAD ligands as shown in Scheme 31. Compared to salt metathesis, direct metallation is more convenient as it is a simple one-step process. However, due to lower reactivity of alkaline earth metals as compared to alkali metals, salt metathesis is more feasible than direct metallation.

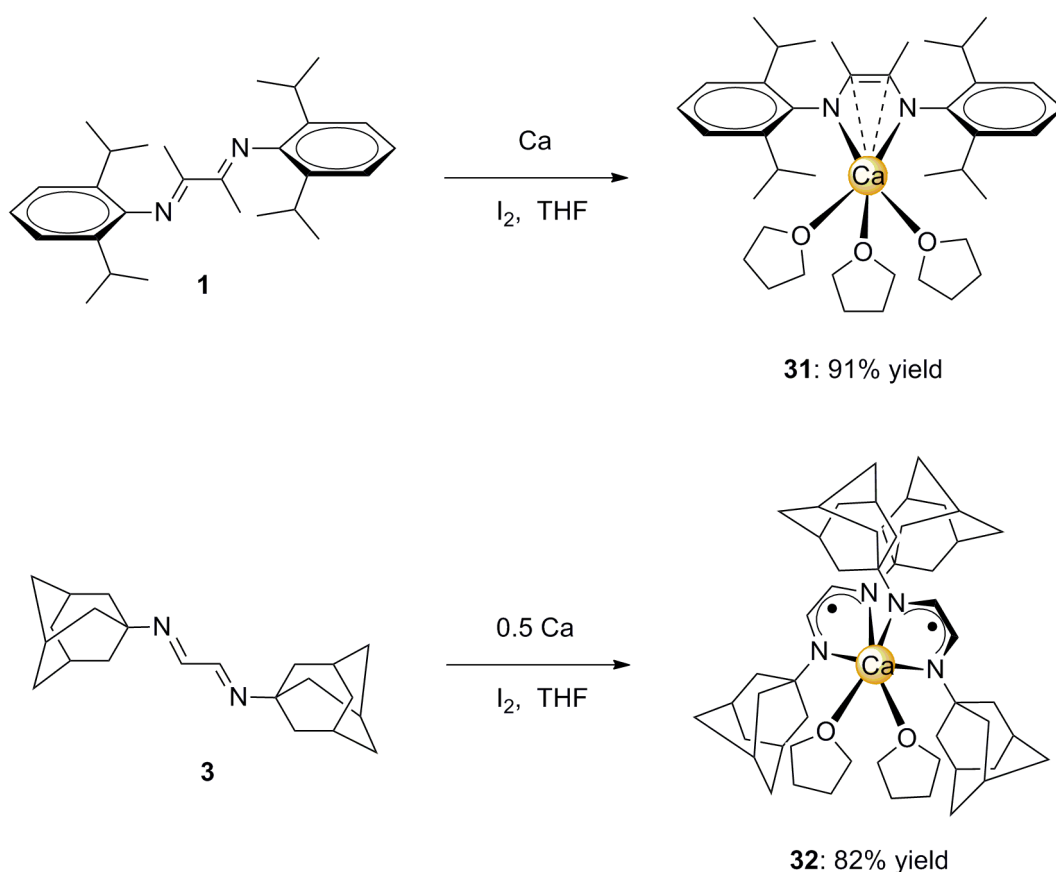


Scheme 31. Stepwise reduction of DAD ligands by alkaline earth metals.

2.7.1. Synthesis of a calcium complex (31) with dianionic $\text{Me}^2\text{DAD}^{\text{Dipp}}$ and (32) with radical-monoanionic $\text{H}^2\text{DAD}^{\text{Ad}}$ ligands

When the $\text{Me}^2\text{DAD}^{\text{Dipp}}$ ligand (**1**) (1.0 g, 2.5 mmol) was treated with 1 equiv. of calcium in THF in the presence of iodine (5 mg, 1.97×10^{-2} mmol), the color of the reaction mixture turned from yellow to red. To complete the reaction, the reaction mixture was stirred until all the calcium was consumed, and then it was concentrated and kept at 5 °C to afford the calcium complex $[\text{Ca}(\text{Me}^2\text{DAD}^{\text{Dipp}})(\text{THF})_3]$ (**31**) with dianionic $\text{Me}^2\text{DAD}^{\text{Dipp}}$ ligand in an

excellent yield of 91% (Scheme 32). Interestingly, when the $\text{H}^2\text{DAD}^{\text{Ad}}$ ligand (**3**) was treated with 0.5 equiv. of calcium in THF, the reaction mixture turned from colorless to deep green instead of the usual deep red. The deep green solution was concentrated and kept at 5 °C to yield the calcium complex $[\text{Ca}(\text{H}^2\text{DAD}^{\text{Ad}})_2(\text{THF})_2] \cdot \text{THF}$ (**32**) with radical-monoanionic $\text{H}^2\text{DAD}^{\text{Ad}}$ ligands in a good yield of 82%. In both cases, the reaction took place only if a small amount of iodine (5 mg, 1.97×10^{-2} mmol) was present. There was no reaction when magnesium was treated with both $\text{Me}^2\text{DAD}^{\text{Dipp}}$ and $\text{H}^2\text{DAD}^{\text{Ad}}$ in the presence or absence of iodine. However, in the presence of iodine, strontium and barium were reactive with the $\text{Me}^2\text{DAD}^{\text{Dipp}}$ ligand, and the respective complexes are currently being analyzed. Complexes **31** and **32** were characterized by NMR, EPR and IR spectroscopy as well as MS and elemental analyses. The single-crystal structures of **31** and **32** were successfully determined by X-ray crystallography. Elemental analysis, (values for C, H, and N of **31** and **32** were consistent with the proposed formulation of **31** and **32**, respectively) showing that complex **32** keeps the THF of crystallization (uncoordinated THF) upon drying.



Scheme 32. Synthesis of calcium DAD complexes by direct metallation in the presence of iodine.

2.7.2. Spectroscopic analysis of the complexes **31** and **32**

In the ^1H NMR of **31**, compared to the neutral ligand **1**, half of the methyl protons of the isopropyl groups were shifted upfield ($\delta = 1.07$) while the other half were shifted downfield ($\delta = 1.20$, respectively). The methyl protons attached to DAD moiety as well as *para* and *meta* protons of the aromatic ring were shifted upfield ($\delta = 1.57, 6.41, 6.78$, respectively) while the *tertiary* proton of the isopropyl groups was shifted downfield ($\delta = 3.74$). In the ^{13}C NMR of **31**, a remarkable high-field shift observed for the carbons ($\delta 118.6$) of DAD moiety (NCCN) (compared to the neutral ligand **1**) confirms the presence of olefinic carbons and the dianionic nature of the DAD moiety in **31**.

Due to the paramagnetic nature of the radical-monoanionic DAD ligands, it was not possible to obtain meaningful ^1H NMR and ^{13}C NMR of **32**. The investigation of the EPR spectrum of **32** (Figure 30) revealed that the calcium complex **32** is a ligand-centered radical at room temperature. However, further measurements at different conditions (temperature and frequency) would provide a more precise picture.

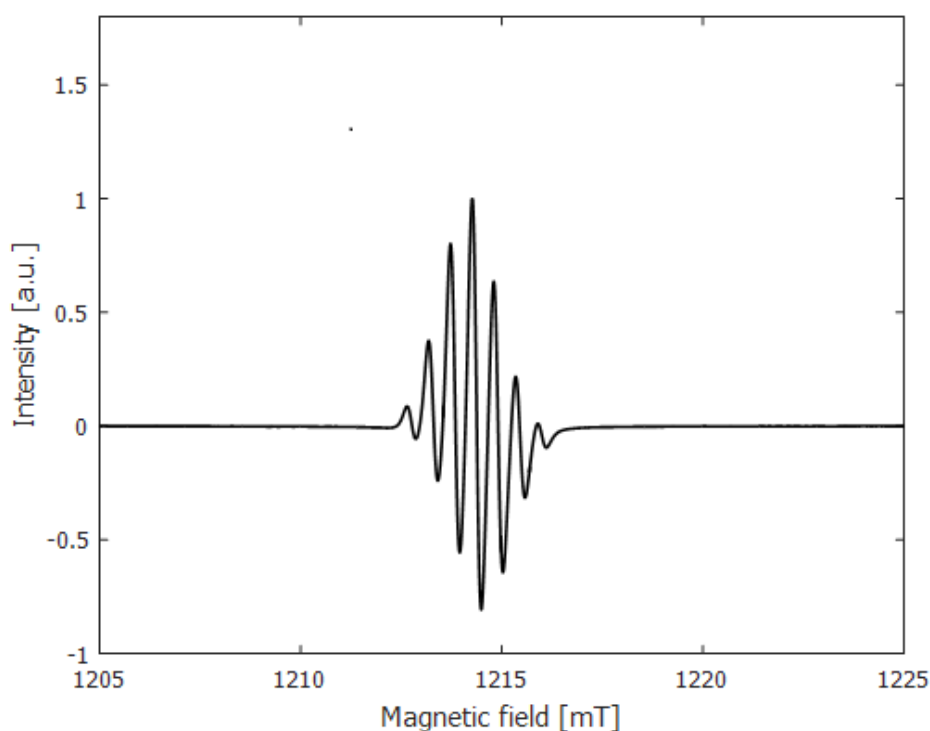


Figure 30. EPR spectrum of **32** at room temperature.

Although it was not possible to identify the bands corresponding to the stretching vibrations of the C–N and C=C bonds in the IR spectrum of **31** (due to overlap of bands), the strong band observed in the IR spectrum of **1** (corresponding to the stretching vibrations of the imine (C=N) bond at 1630 cm^{-1}) completely disappeared in the IR spectrum of **31**. A weak band at 1628 cm^{-1} corresponding to C=N stretching vibrations was observed in the IR spectrum of **32**. This could be because of some impurities (unreacted ligand **3**). In both complexes, the molecular ion peak was not observed in the EI mass spectrum. However, the peaks at m/z 522, 477, 433, and 184 in **31** could be assigned to fragments $[M^+ - (\text{CH}_3, \text{C}_2\text{H}_2, \text{C}_3\text{H}_7, \text{C}_4\text{H}_6)]$, $[M^+ - (3\text{ C}_3\text{H}_7, \text{C}_4\text{H}_6)]$, $[(M^+ - (\text{H}, 4\text{ C}_3\text{H}_7, \text{C}_4\text{H}_6))]$, and $[\text{Ca}(\text{THF})_2]$, respectively, and the peaks at m/z 733 and 697 in **32** could be assigned to fragments $[M^+ - (\text{C}_2\text{H}_3, \text{THF})]$ and $[M^+ - \text{C}_{10}\text{H}_{14}]$, respectively.

2.7.3. Molecular Structures of $[\text{Ca}(\text{Me}_2\text{DAD}^{\text{Dipp}})(\text{THF})_3]$ (**31**) and $[\text{Ca}(\text{H}^2\text{DAD}^{\text{Ad}})_2(\text{THF})_2 \cdot \text{THF}$ (**32**)

The calcium complex **31** crystallizes from THF at $5\text{ }^\circ\text{C}$ as a monomer in the orthorhombic space group *Pbca* with one molecule of the complex in the asymmetric unit. As shown in Figure 31 (page 85), the calcium atom is chelated by the two nitrogen atoms of the DAD moiety, forming a five-membered ring, and coordinative saturation of the Ca atom is achieved by the three THF ligands, thus resulting in coordination number 5. In the five-membered chelating ring, the Ca atom is located out of the plane defined by $\text{Me}_2\text{C}_2\text{N}_2$ with the angle between planes CaN_2 and $\text{Me}_2\text{C}_2\text{N}_2$ being 46.1° . The coordination environment around the calcium atom can be described as a distorted trigonal bipyramidal arrangement with the atoms N1, N2, and O2 occupying equatorial positions while the atoms O1 and O3 occupy apical positions. The Ca–N bonds are almost equal ($2.250(2)\text{ \AA}$ / $2.251(2)\text{ \AA}$) and so are the Ca–O bonds ($2.214(2)\text{ \AA}$ / $2.226(2)\text{ \AA}$ / $2.226(2)\text{ \AA}$). The Ca–N and Ca–O bond lengths in **31** are shorter than those in similar calcium complexes with the dianionic 1,2-bis[(2,6-diisopropylphenyl)imino]acenaphthene ligand [Ca–N: in the range of $2.345(2)\text{ \AA}$ to $2.396(2)\text{ \AA}$; Ca–O: in the range of $2.337(2)\text{ \AA}$ to $2.619(2)\text{ \AA}$] reported by Fedushkin and co-workers^[37] and the $\text{H}^2\text{DAD}^{\text{Dipp}}$ ligand [Ca–N: $2.361(2)\text{ \AA}$ / $2.335(2)\text{ \AA}$; Ca–O: in the range of $2.399(2)\text{ \AA}$ to $2.499(2)\text{ \AA}$] reported by Mashima and co-workers.^[42] The shorter distance between the Ca and the carbons of the DAD backbone (Ca–C: $(2.783(2)\text{ \AA}$ / $2.785(2)\text{ \AA}$) can be explained by minor π -coordination between the metal atom and the DAD moiety. Thus, the coordination

mode of the calcium atom towards the DAD ligand in **31** is similar to that of lighter alkali metals, i.e. primarily σ -coordination. The deviation between the central $\text{Me}_2\text{C}_2\text{N}_2$ moiety and the two terminal substituted aryl groups in complex **31** is significantly different (69.7° and 80.3° , respectively).

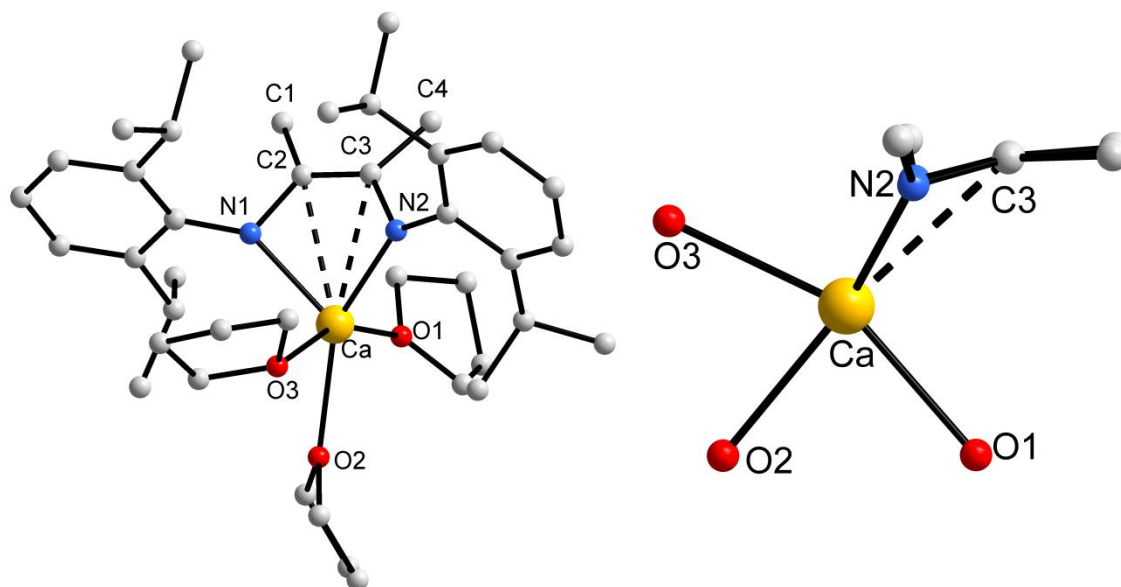


Figure 31. Molecular structure of **31** (left) and representation of the coordination sphere of the calcium atom in **31** viewed along the N2-N1 vector (right).

Compared to the neutral ligand **1**, the C–N bond lengths (C–N: $1.427(3)$ Å / $1.432(3)$ Å) of the DAD backbone in **31** are elongated, while the C–C bond length (C–C': $1.361(3)$ Å) is shortened. These values are similar to the alkali metal complexes $[\text{Li}_2(\text{Me}_2\text{DAD}^{\text{Dipp}})(\mu\text{-THF})(\text{THF})_2]$ (**4**), $[\text{Na}_2(\text{Me}_2\text{DAD}^{\text{Dipp}})(\text{THF})_4]$ (**5**), $\{[\text{K}_2(\text{Me}_2\text{DAD}^{\text{Dipp}})(\mu\text{-THF})(\text{THF})_2] \cdot [\text{K}_2(\text{Me}_2\text{DAD}^{\text{Dipp}})(\mu\text{-THF})(\text{THF})_3]\}_2$ (**6**), $\{[\text{Rb}_2(\text{Me}_2\text{DAD}^{\text{Dipp}})(\text{THF})_4]_2 \cdot \text{THF}\}_n$ (**7**), and $\{[\text{Cs}_2(\text{Me}_2\text{DAD}^{\text{Dipp}})(\text{THF})_4] \cdot \text{THF}\}_n$ (**8**) with dianionic $\text{Me}_2\text{DAD}^{\text{Dipp}}$ ligand. The values for the neutral ligand **1** are $1.279(3)$ Å / $1.280(3)$ Å for C–N and $1.498(3)$ Å for C–C'.^[66]

The calcium complex **32** crystallizes from THF at 5°C as a monomer in the monoclinic space group $P2_1/c$ with two molecules (enantiomers) of the complex and two uncoordinated THF molecules in the asymmetric unit. The molecular structure of the complex is shown in Figure 32 (page 86), having the calcium atom chelated by the four nitrogen atoms of two DAD moieties, to form two five-membered rings with the angle between planes N1-Ca-N2 and N3-

Ca-N4 is 82.8° (almost perpendicular). The coordinative saturation of the Ca atom is achieved by the two THF ligands, resulting in coordination number 6 for the Ca atom. The coordination environment around the calcium atom can be described as a distorted octahedral arrangement, and the sum of the angles N1–Ca–O1, O1–Ca–N3, N3–Ca–N4, and N4–Ca–N1 is 359.9° .

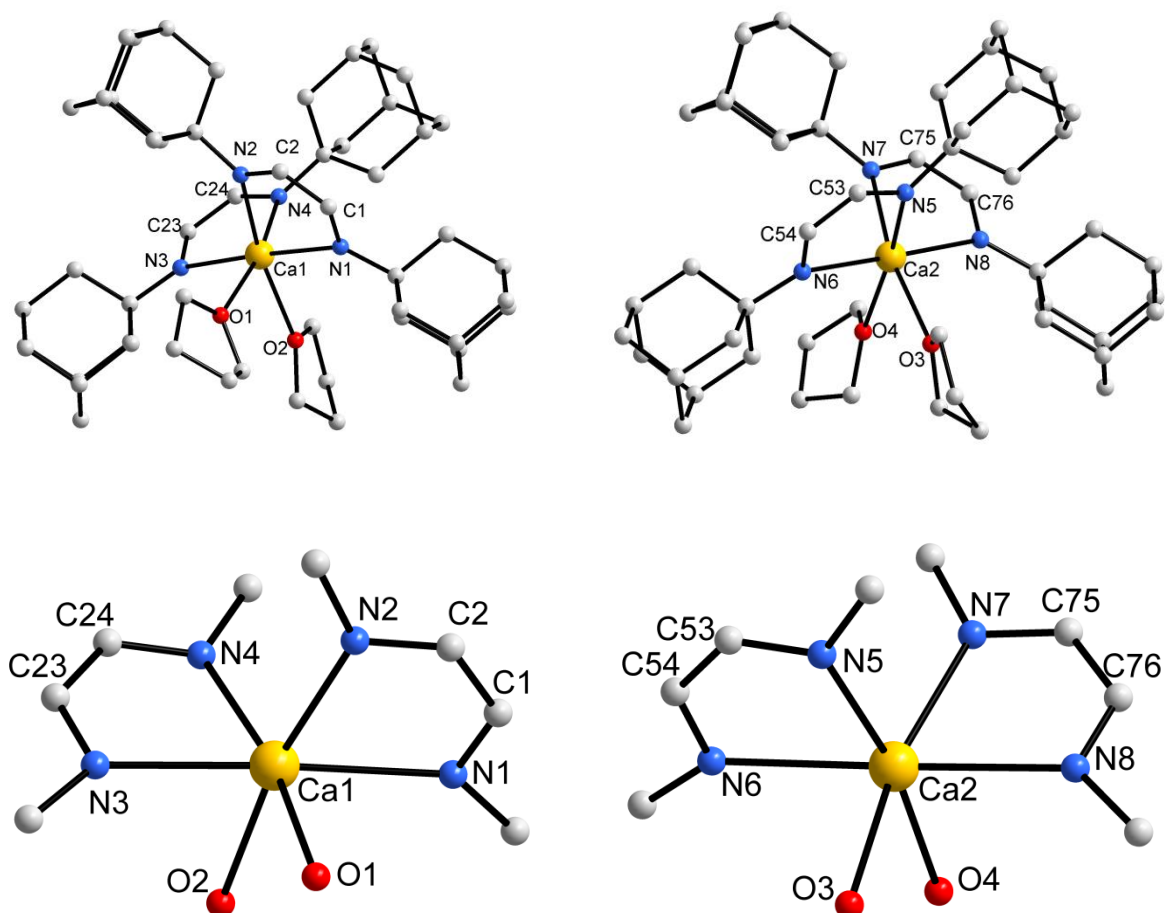


Figure 32. Molecular structure of **32**: Molecule 1 (top-left) and molecule 2 (top-right). Representation of the coordination sphere of the calcium atoms Ca1 (bottom-left) and Ca2 (bottom-right).

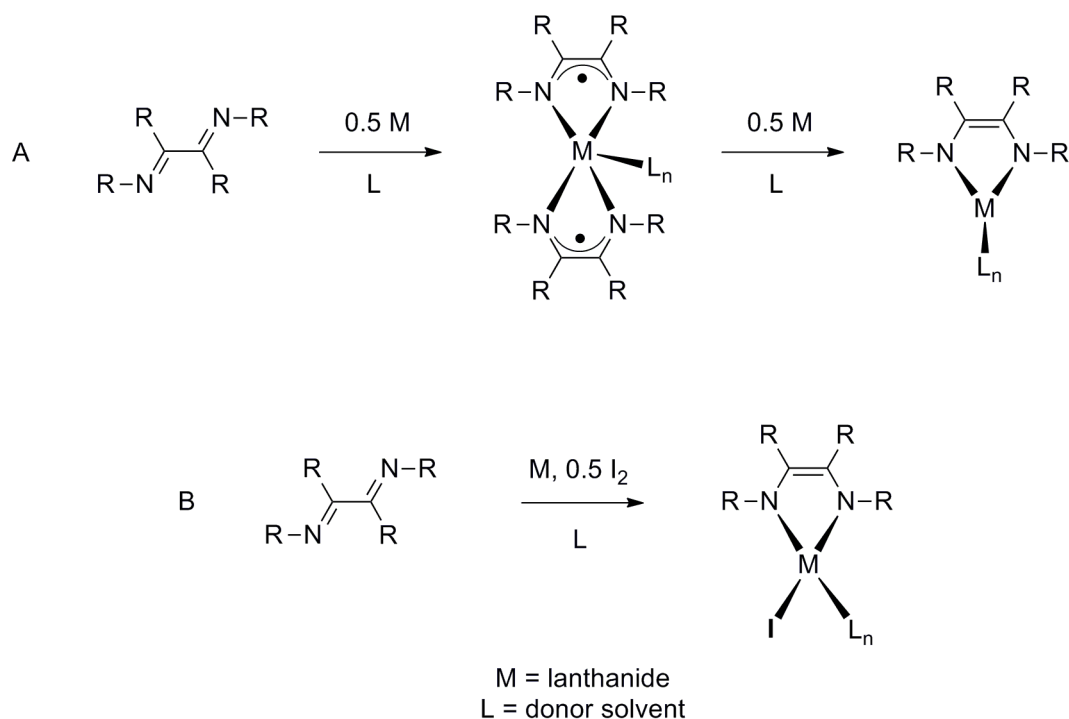
The calcium atom is located slightly out of the planes defined by N1–C1–C2–N2 (deviation 7.6°) and N3–C23–C24–N4 (deviation 6°). This shows that the coordination mode of calcium atom towards the DAD ligand in **32** is similar to that of lighter alkali metals, i.e. primarily σ -coordination. The Ca–N bonds are not equal [$2.502(2)$ Å/ $2.459(2)$ Å/ $2.500(2)$ Å/ $2.415(2)$ Å] and so are the Ca–O bonds [$2.556(2)$ Å/ $2.445(2)$ Å]. As expected, the Ca–N bond lengths in **32** are longer than those in **31**. However, the Ca–N bond lengths in **32** are longer than those [$2.371(2)$ Å/ $2.378(2)$ Å] in the calcium complex $[\text{Ca}(\text{Bian}^{\text{Dipp}})_2]$ ^[38] with two radical-

monoanionic 1,2-bis[(2,6-diisopropylphenyl)imino]acenaphthene ligands. This can most likely be traced back to the influence of the different substituents at both the N and C atoms of the DAD moiety and the solvation of Ca atom by THF ligands. The molecular structure of **32** differs greatly from the $[\text{Mg}(\text{Bian}^{\text{Dipp}})_2]$ and $[\text{Ca}(\text{Bian}^{\text{Dipp}})_2]$ complexes. In the latter, compared to $\text{H}^2\text{DAD}^{\text{Ad}}$ ligand, the sterically demanding $\text{Bian}^{\text{Dipp}}$ ligand inhibits the metal atoms from solvation. On the other hand, the molecular structure of **32** is comparable with the $[\text{Sr}(\text{H}^2\text{DAD}^{\text{Dipp}})_2(\text{DME})]$ and $[\text{Ba}(\text{H}^2\text{DAD}^{\text{Dipp}})_2(\text{DME})]$ complexes with two radical-monoanionic $\text{H}^2\text{DAD}^{\text{Dipp}}$ ligands. In the latter, a DME ligand is formally replaced by two THF ligands of **32**.

Compared to the neutral ligand **3**, the C–N bond lengths are elongated, while the C–C bond length is shortened [C1–N1 (1.331(3) Å)/ C2–N2 (1.326(3) Å)/ C23–N3 (1.326(3) Å)/ C24–N4 (1.327(3) Å)/ C1–C2 (1.406(3) Å)/ C23–C24 (1.396(3) Å)] in the DAD backbone of **32**; however, not to the extent noticed in lithium complex $[\{\text{Li}_2(\text{H}^2\text{DAD}^{\text{Ad}})\}_2(\mu\text{-THF})(\text{THF})_2]$ (**9**) with a dianionic $\text{H}^2\text{DAD}^{\text{Ad}}$ ligand. Moreover, these values are similar to those in $[\text{Li}(\text{H}^2\text{DAD}^{\text{Ad}})(\text{THF})_2]$ (**19**) with radical-monoanionic $\text{H}^2\text{DAD}^{\text{Ad}}$ ligand. The values for the neutral ligand **3** are 1.255(3) Å (average) for C–N and 1.457(3) for C–C.^[68] These structural data indicate the radical-monoanionic character among the several possible coordination modes of the DAD ligands (Scheme 3, page 2).

2.8. Lanthanide complexes with DAD ligands

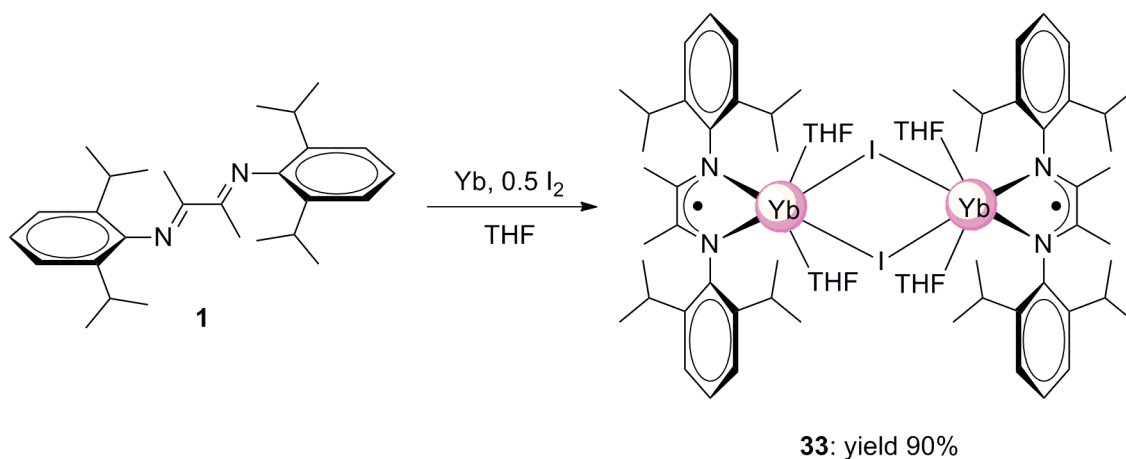
Lanthanide complexes with DAD ligands are mainly prepared by either direct metallation of DAD ligands with lanthanides or salt metathesis reactions between alkali metal precursors with lanthanide halides.^[104-126] Formation of alkali halide adducts by salt metathesis is very typical for lanthanides. Scheme 33 displays the general synthesis of the complexes by direct metallation. A is the stepwise reduction of the DAD ligands by lanthanides in the presence or absence of iodine: 0.5 equiv. of lanthanides yield complexes containing two radical-monoanionic DAD ligands while 1 equiv. of lanthanides yield complexes containing dianionic DAD ligands. B is the three-component reaction in which the DAD ligands are reduced by 1 equiv. of lanthanides together with 1 equiv. of iodine. Among the lanthanides, ytterbium, samarium, and europium are commonly used for direct metallation of DAD ligands. In this work as well, ytterbium was used for direct metallation of $^{\text{Me}_2}\text{DAD}^{\text{Dipp}}$ ligand (**1**) while samarium and europium were used for $^{\text{H}_2}\text{DAD}^{\text{Dipp}}$ ligand (**2**).



Scheme 33. A: Stepwise reduction of DAD ligands by lanthanides. B: Three-component reaction of DAD ligands, lanthanides, and iodine.

2.8.1. Synthesis and molecular structure of $[\text{Yb}_2(\mu\text{-I})_2(\text{Me}_2\text{DAD}^{\text{Dipp}})_2(\text{THF})_4] \cdot \text{THF}$ (33**)**

A three-component reaction of the $\text{Me}_2\text{DAD}^{\text{Dipp}}$ ligand (**1**), ytterbium, and iodine yielded an iodide-bridged dimeric ytterbium complex **33** with $\text{Me}_2\text{DAD}^{\text{Dipp}}$ ligand (Scheme 34). The three-component reaction was performed by treating **1** with ytterbium and iodine in THF, and the resulting dark red reaction mixture was dried in vacuum. By using *n*-pentane as solvent, the ytterbium complex **33** was separated from the residue and crystallized at 5 °C to afford (in excellent yield of 90%) as dark red crystals suitable for X-ray diffraction analysis. The ytterbium complex **33** was also characterized by MS and elemental analyses. The molecular ion peak was not observed in the EI mass spectrum of the complex. However, the peaks at m/z 637, 578, 559, and 524 could be assigned to the fragments $[\text{M}^+ - (2 \text{ C}_3\text{H}_7, \text{CH}_3\text{CCCH}_3, \text{THF})]$, $[\text{M}^+ - (2 \text{ THF}, \text{I})]$, $[\text{M}^+ - (8 \text{ CH}_3, \text{C}_3\text{H}_7, \text{I})]$, and $[\text{M}^+ - (\text{CH}_3\text{CCCH}_3, 2 \text{ THF}, \text{I})]$, respectively. Elemental analysis values for C, H, and N of **33** were consistent with the proposed formulation of **33**, suggesting that complex **33** keeps the THF of crystallization (uncoordinated THF) upon drying.



Scheme 34. Three-component reaction of $\text{Me}_2\text{DAD}^{\text{Dipp}}$ ligand (**1**), ytterbium, and iodine.

The ytterbium complex **33** crystallizes from *n*-pentane at 5 °C as a dimer in the monoclinic space group $P2_1/n$ containing half a molecule of the complex and half an uncoordinated THF molecule in the asymmetric unit. As shown in Figure 33, the ytterbium atom is coordinated by two nitrogen atoms N1 and N2, forming a five-membered ring with the angle between the planes of the fragments $\text{Me}_2\text{C}_2\text{N}_2$ and YbN_2 being 16.4° (slightly out of plane), and two μ -bridging iodine atoms which bridge the ytterbium atoms to form a rectangular four-membered Yb_2I_2 ring (sum of angles 360°). The ytterbium atom is coordinatively saturated by two THF ligands, resulting in six-coordinate Yb atom. There is a crystallographic inversion center in complex **33**, which is located at the center of the rectangular Yb_2I_2 ring. The coordination environment around the Yb atom can be described as an irregular hexacoordination. The plane of the two terminal substituted aryl groups deviates almost equally from the plane of the central $\text{Me}_2\text{C}_2\text{N}_2$ fragment (78.7° and 80.7° , respectively).

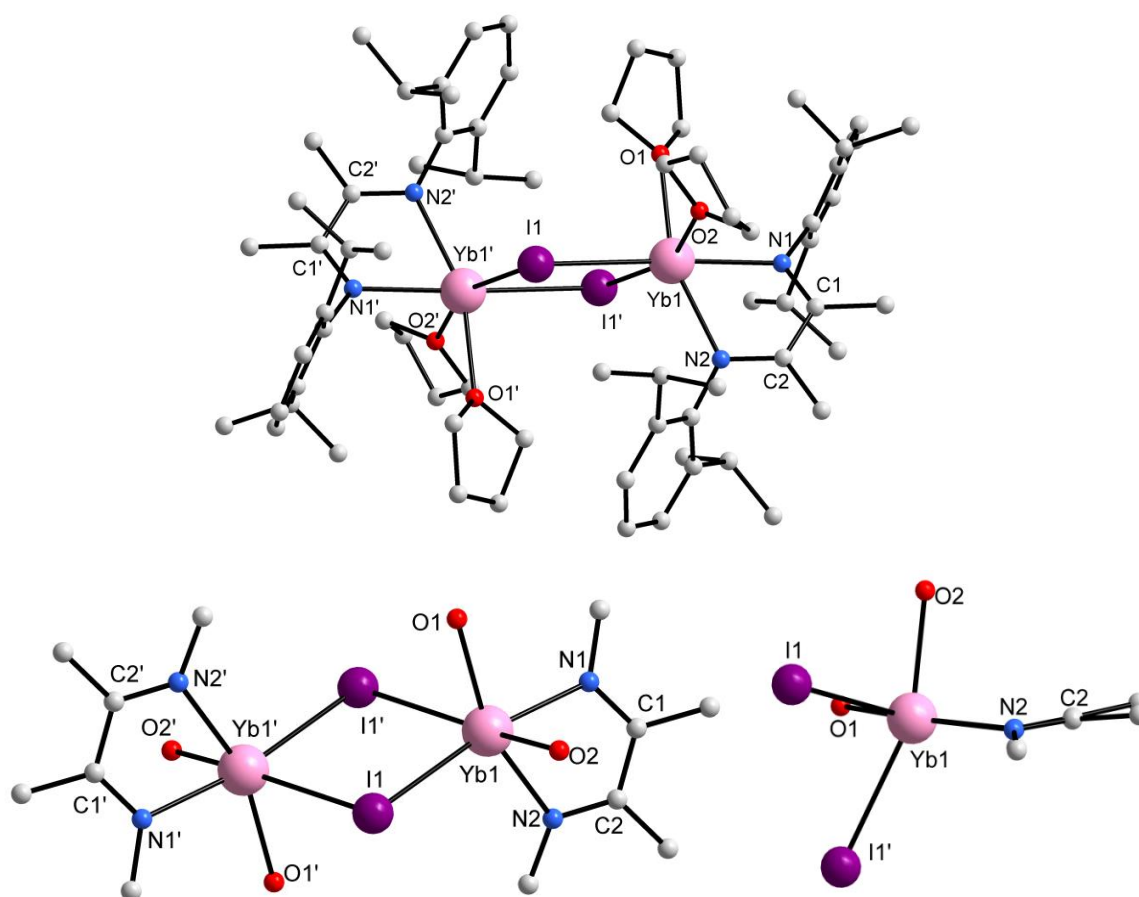
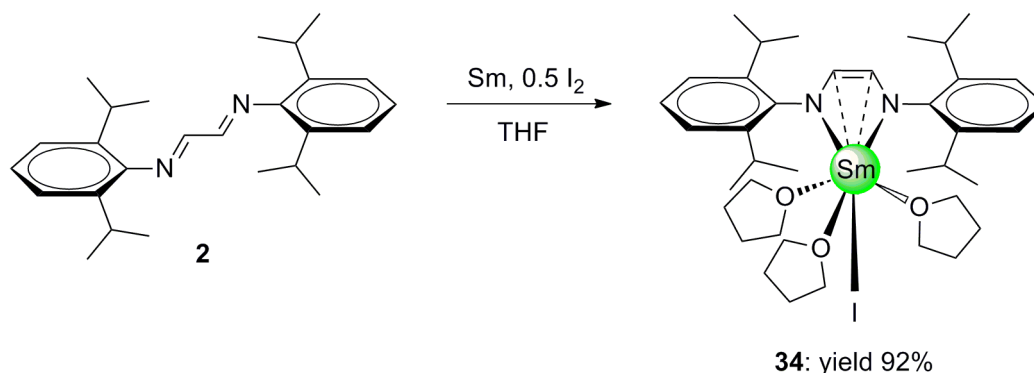


Figure 33. Molecular structure of **33** (top). Representation of the coordination sphere of the Yb atom.

The two Yb–N bonds are significantly non-equivalent, with Yb–N1 (2.462(3) Å) being longer than Yb–N2 (2.426(4) Å), whereas the Yb–O bond lengths are almost equal (2.467(3) and 2.468(3) Å). The Yb–N and the Yb–O bond lengths in **33** are longer than those (Yb–N: in the range of 2.136(3) Å to 2.148(3) Å; Yb–O: 2.305(3) Å, respectively) observed in the ytterbium(III) complexes $[\text{Yb}(\text{C}_5\text{Me}_4\text{H})(\text{H}^2\text{DAD}^{\text{Dipp}})(\text{THF})]$ and $[\text{Yb}(\text{C}_5\text{Me}_5)(\text{H}^2\text{DAD}^{\text{Dipp}})(\text{THF})]$ with dianionic $\text{H}^2\text{DAD}^{\text{Dipp}}$ ligand reported by Trifonov and co-workers. However, the Yb–N bond lengths are closer to those (2.358(1) Å/ 2.393(1) Å) in the ytterbium(III) complex $[\text{Yb}(\text{C}_5\text{MeH}_4)_2(\text{H}^2\text{DAD}^{\text{Dipp}})]$ with anionic $\text{H}^2\text{DAD}^{\text{Dipp}}$ ligand in their reports.^[114] Moreover, the Yb–N bond lengths in **33** are similar to those (Yb–N: 2.454(10) Å/ 2.439(9) Å) in Yb(II) complex $[\text{YbI}(\text{bipy})(\text{DME})_2]$ ^[110] containing radical-monoanionic bipy ligand. The Yb–O bond lengths in **33** are similar to those (Yb–O: 2.459(11) Å/ 2.498(9) Å) in the Yb(II) complex $[\{(\text{iPr})_2\text{ATI}\}\text{Yb}\{\text{N}-(\text{SiMe}_3)_2\}(\text{THF})_2]$ ^[23] and are longer than those (Yb–O: 2.368(14) Å) in the Ytterbium(III) complex $[\{\text{DippNC}(\text{=CH}_2)\text{C}(\text{=CH}_2)\text{N}^{\text{Dipp}}\}\text{Yb}(\text{THF})_2(\mu\text{-Cl})_2\text{Li}(\text{THF})_2]$.^[122] The Yb–I bond length (3.154(9) Å) in **33** is slightly longer than that (Yb–I: 3.120(1) Å) in the ytterbium(II) complexes in $[\text{YbI}(\text{bipy})(\text{DME})_2]$ ^[110] and 3.100(2) Å in $[\text{YbI}(\text{DIP}_2\text{pyr})(\text{THF})_3]$.^[154] This could be because the iodine atoms in **33** are μ -bridged, whereas they are terminally coordinated in the latter. The C–N bond lengths of the DAD moieties are elongated, while the C–C bond lengths are shortened [C1–N1 (1.345(5) Å), C2–N2 (1.340(7) Å), and (C1–C2 1.428(7) Å)] compared to the neutral ligand **1** (1.279(3) Å/ 1.280(3) Å for C–N and 1.498(3) Å for C–C).^[66] The C–N and C–C bond lengths of the DAD moiety are similar to those in the radical-monoanionic DAD complex $[\text{Li}(\text{Me}_2\text{DAD}^{\text{Dipp}})(\text{DME})]$ (**16**). Compared to the dianionic DAD complexes $[\text{Li}_2(\text{Me}_2\text{DAD}^{\text{Dipp}})(\mu\text{-THF})(\text{THF})_2]$ (**4**), $[\text{Na}_2(\text{Me}_2\text{DAD}^{\text{Dipp}})(\text{THF})_4]$ (**5**), $\{[\text{K}_2(\text{Me}_2\text{DAD}^{\text{Dipp}})(\mu\text{-THF})(\text{THF})_2] \cdot [\text{K}_2(\text{Me}_2\text{DAD}^{\text{Dipp}})(\mu\text{-THF})(\text{THF})_3]\}_2$ (**6**), $\{[\text{Rb}_2(\text{Me}_2\text{DAD}^{\text{Dipp}})(\text{THF})_4]_2 \cdot \text{THF}\}_n$ (**7**), and $\{[\text{Cs}_2(\text{Me}_2\text{DAD}^{\text{Dipp}})(\text{THF})_4] \cdot \text{THF}\}_n$ (**8**) and $[\text{Ca}(\text{Me}_2\text{DAD}^{\text{Dipp}})(\text{THF})_3]$ (**31**), the C–N bond lengths of the DAD moiety are shorter while the C–C bond length is longer. All these structural data indicate that the ligand has the negative valence of -1 and the metal atom is in the +2 oxidation state in complex **33**. However, EPR spectroscopy should be done to get a more precise picture.

2.8.3. Synthesis and molecular structure of $[\text{Sm}(\text{H}^2\text{DAD}^{\text{Dipp}})(\text{I})(\text{THF})_3]$ (**34**)

Unlike the ytterbium complex **33**, the three-component reaction of the $\text{H}^2\text{DAD}^{\text{Dipp}}$ ligand (**2**), samarium, and iodine yielded a monomeric samarium complex **34** with a dianionic DAD ligand instead of radical-monoanionic DAD (Scheme 35). The three-component reaction was carried out in THF by treating **2** with samarium and iodine, and the resulting dark blue reaction mixture was dried in vacuum. The samarium complex **34** was separated from the residue by using *n*-pentane as solvent and crystallized at 5 °C to afford dark blue crystals (in an excellent yield of 92%) suitable for X-ray diffraction analysis. The samarium complex **34** was characterized thoroughly by IR and NMR spectroscopy as well as MS analysis. Elemental analysis values for C, H, and N of **34** were consistent with the proposed formulation of **34**.



Scheme 35. Three-component reaction of $\text{H}^2\text{DAD}^{\text{Dipp}}$ ligand (**2**), samarium, and iodine.

Due to overlap of bands, it was not possible to identify the C–N and C=C stretching bands in the IR spectrum of **34**. Moreover, the appearance of a weak band at 1627 cm^{-1} , corresponding to the stretching vibrations of the imine (C=N) bond (observed as a strong band at 1625 cm^{-1} in the IR spectrum of **2**) in the IR spectrum of **34** could be because of some impurities (unreacted ligand). Although the molecular ion peak was not observed in the EI mass spectra of **34**, the peak at m/z 811 and the base peak at m/z 528 could be assigned to the fragments $[\text{M}^+ - 4\text{ CH}_3]$ and $[\text{M}^+ - (3\text{ THF}, \text{I})]$, respectively.

The paramagnetic effect of Sm^{3+} is well observed in the ^1H NMR spectrum of **34**. The ^1H NMR of **34**, as shown in Figure 34 (page 91), displayed a complete downfield shift (compared to the neutral ligand **2**) for all the protons. However, a remarkable downfield shift was observed for the *tertiary* proton of the isopropyl groups (a broad singlet at $\delta = 6.64$ ppm). The resonances of the CH_3 , *meta*, *para* protons as well as the protons of the DAD moiety (NCHCHN) were observed as a broad singlet at $\delta = 1.56$ ppm, a doublet at $\delta = 7.62$ ppm, a triplet at $\delta = 7.98$ ppm, and a singlet at $\delta = 8.55$ ppm, respectively.

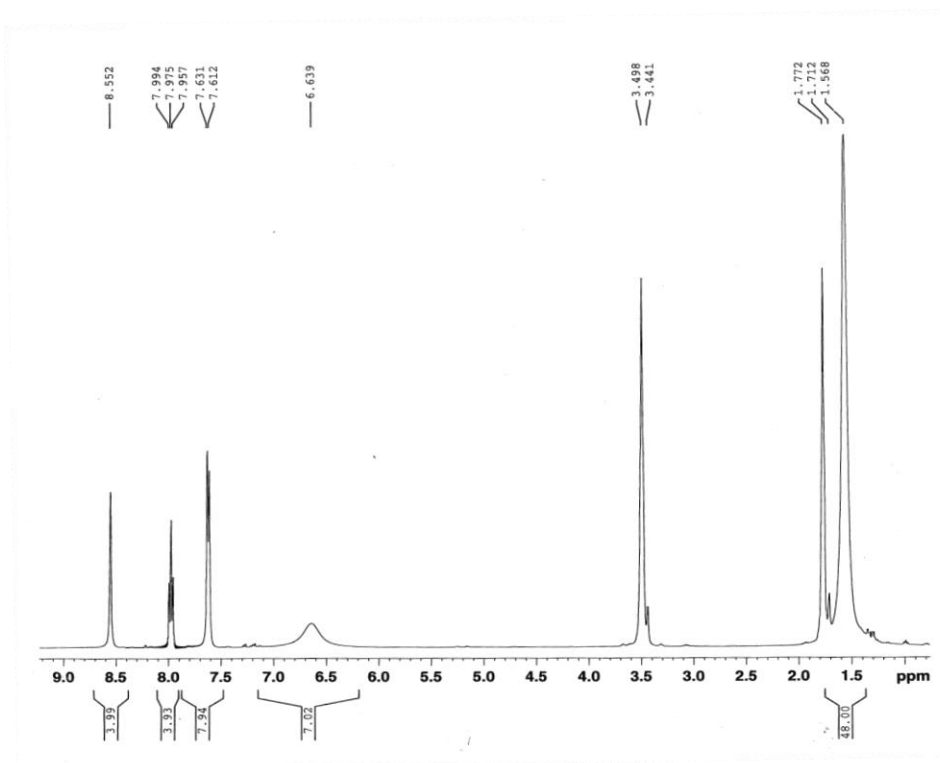


Figure 34. ^1H NMR spectrum of **34** (400 MHz, d_8 -THF, 22 °C).

In the ^{13}C NMR spectrum of **34**, compared to the free ligand **2**, the carbons in the DAD moiety (NCHCHN) shifted remarkably to upfield ($\delta = 130.6$ ppm for **34** and $\delta = 164.3$ ppm for **2**), and the values are typical for olefinic carbons, confirming the dianionic character of the $\text{H}_2\text{DAD}^{\text{Dipp}}$ ligand in **34** (Figure 35, page 94).

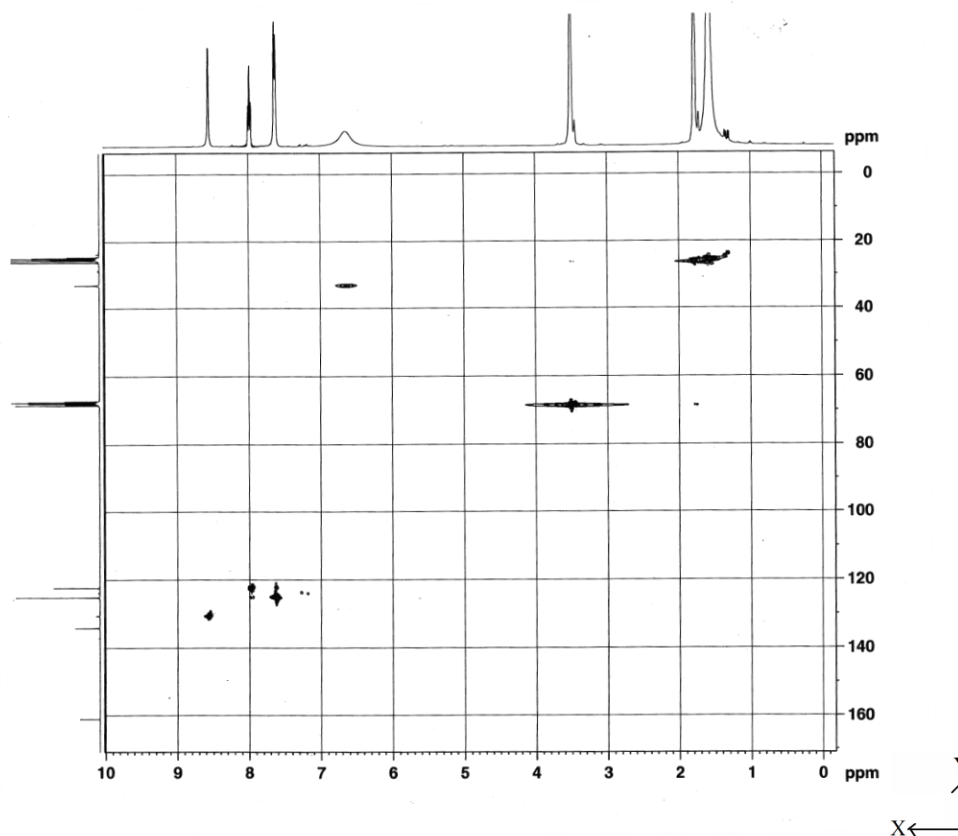


Figure 35. HSQC spectrum of **34** (400 MHz, d_8 -THF, 22 °C). X-axis: ^1H NMR chemical shifts (400 MHz), Y-axis: ^{13}C NMR chemical shifts (100 MHz).

The samarium complex **34** crystallizes from *n*-pentane at 5 °C as a monomer in the triclinic space group $P\bar{1}$ having one molecule of the complex in the asymmetric unit. The molecular structure of the complex reveals that the samarium atom is coordinated by the two nitrogen donors of the DAD ligand and an iodine atom (Figure 36, page 95). Unlike complex **33**, the iodine atom is terminally coordinated instead of bridged; hence the complex **34** exists as a monomer. The coordinative saturation of the samarium atom is achieved by three THF ligands, resulting in six-coordinate Sm atom. The samarium atom in the five-membered chelating ring is located out of the plane defined by $\text{H}_2\text{C}_2\text{N}_2$ (angle between planes SmN_2 and $\text{H}_2\text{C}_2\text{N}_2$ being 55.0°). The coordination environment of the samarium atom adopts an irregular hexa-coordination. The Sm–N bonds are almost equal (2.247(6) Å and 2.267(6) Å) while the Sm–O bonds (2.425(2) Å/ 2.457(5) Å/ 2.495(6) Å) are slightly non-equal. The Sm–N, Sm–O, and Sm–I (3.192(3) Å) bond lengths in **34** are almost similar to those [(2.236(2) Å/ 2.250(2)

Å) for Sm–N, (2.464(2) Å/ 2.494(2) Å/ 2.504(2) Å) for Sm–O, and (3.214(3) Å) for Sm–I] in the similar samarium(III) complex $[\text{Sm}(\text{Me}_2\text{DAD}^{\text{Dipp}})(\text{I})(\text{THF})_3]$.^[149,150] Moreover, the Sm–O bond lengths in **34** are shorter than those (Sm–O: 2.600(6) Å/ 2.596(6) Å/ 2.580(6) Å) while the Sm–I bond length in **34** is slightly shorter than that (Sm–I: 3.223(9) Å) in the samarium(II) complex $[\text{SmI}(\text{DIP}_2\text{pyr})(\text{THF})_3]$.^[154]

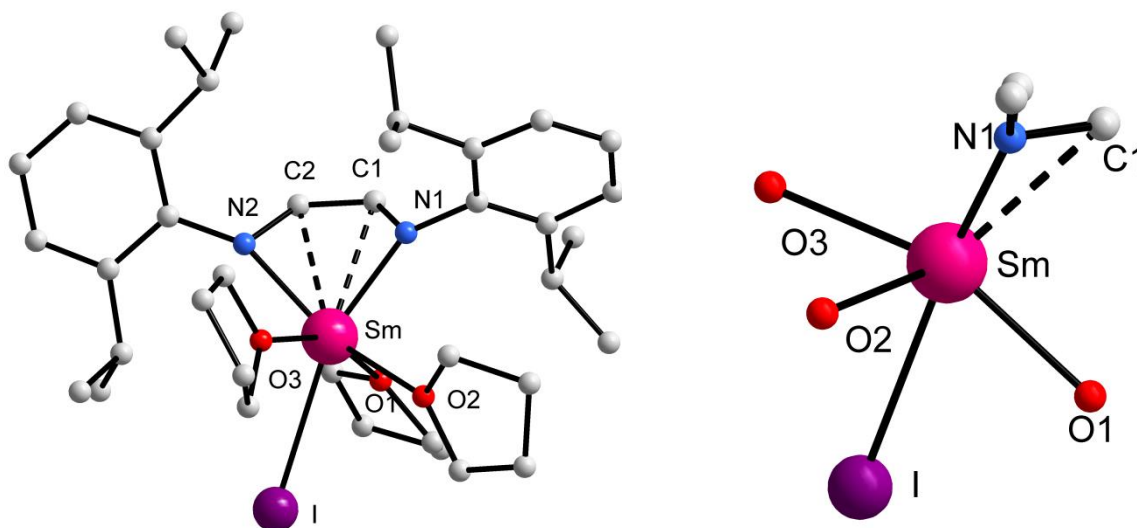
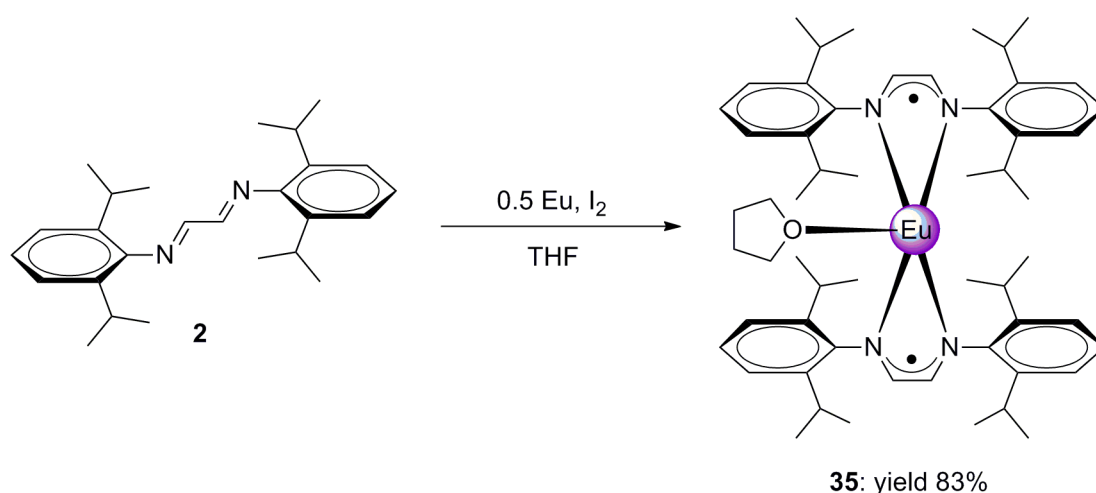


Figure 36. Molecular structure of **34** (left) and representation of the coordination sphere of the samarium atom in **34** viewed along the N1–N2 vector (right).

Similar to the calcium complex $[\text{Ca}(\text{Me}_2\text{DAD}^{\text{Dipp}})(\text{THF})_3]$ (**31**), the shorter distances between the Sm atom and the C atoms of the DAD moiety [Sm–C1 (2.655(6) Å) and Sm–C2 (2.662(7) Å)] indicate the minor π -coordination between the metal atom and the DAD moiety. The plane of the aromatic ring attached to N1 deviates by 71.0° from the plane of the central $\text{H}_2\text{C}_2\text{N}_2$ moiety while the same attached to N2 deviates by 63.7° . Compared to the neutral ligand **2**,^[67] the C–N bond lengths of the DAD backbone in **34** (1.378(8)/1.403(8) Å) are elongated, while the C–C bond length (1.365(1) Å) is shortened; however, to a larger extent than that noticed in the alkali metal complexes $[\text{Li}(\text{H}_2\text{DAD}^{\text{Dipp}})(\text{THF})_2]$ (**20**), $[\text{K}(\text{H}_2\text{DAD}^{\text{Dipp}})(\text{THF})_4]$ (**22**), and $[\text{Rb}(\text{H}_2\text{DAD}^{\text{Dipp}})(\text{THF})_4]$ (**23**) with monoanionic $\text{H}_2\text{DAD}^{\text{Dipp}}$ ligand. The values for the neutral ligand **2** are 1.234(3) Å (average) for C–N and 1.445(3) Å for C–C.^[67] The dianionic nature of the DAD moiety and +3 oxidation state of the Sm atom are thus confirmed by all these structural data together with the spectral data.

2.8.4. Synthesis and molecular structure of $[\text{Eu}(\text{H}^2\text{DAD}^{\text{Dipp}})_2(\text{THF})]$ (**35**)

The reduction of $\text{H}^2\text{DAD}^{\text{Dipp}}$ ligand (**2**) with europium metal (0.5 equiv.) in THF in the presence of iodine (5 mg, 1.97×10^{-2} mmol) resulted in a deep red solution which was concentrated in vacuum to a black oil. *n*-Pentane (20 mL) was added to the black oil before it was kept at 5 °C to yield the europium(II) complex **35** (in a good yield of 83%) as black crystals suitable for X-ray diffraction analysis (Scheme 36). The europium complex **35** with $\text{H}^2\text{DAD}^{\text{Dipp}}$ ligands was characterized by IR spectroscopy as well as MS and elemental analyses. Due to the strongly paramagnetic nature of the radical-monoanionic DAD and Eu^{3+} , it was not possible to obtain any meaningful information from ^1H NMR and ^{13}C NMR spectra.



Scheme 36. Synthesis of europium DAD complex by direct metallation in the presence of iodine.

Elemental analysis, values for C, H, and N of **35** were consistent with the proposed formulation of **35**, showing that complex **35** keeps the THF of crystallization (uncoordinated THF) upon drying. The EI mass spectra of the complex displayed no molecular ion peak, but the peaks at m/z 887, 729, 529, and 511 could be assigned to the fragments $[\text{M}^+ - 6 \text{CH}_3]$, $[\text{M}^+ - (\text{CH}_3, \text{Dipp}, \text{THF})]$, $[\text{M}^+ - (\text{H}^2\text{DAD}^{\text{Dipp}}, \text{THF})]$, and $[\text{M}^+ - (\text{CH}_3, 2 \text{Dipp}, 2 \text{C}_3\text{H}_7)]$, respectively.

The europium complex **35** crystallizes from *n*-pentane at 5 °C as a monomer in the monoclinic space group $P2_1/n$ containing one molecule of the complex in the asymmetric unit. The molecular structure of the complex is shown in Figure 37, having the Eu atom chelated by the four nitrogen atoms from two DAD moieties to form two five-membered rings with an angle between planes N1-Eu-N2 and N3-Eu-N4 of 68°. The Eu atom is coordinated by only one THF ligand, resulting in a coordinatively unsaturated five-coordinate Eu atom, although the complex is sterically saturated due to the bulky Dipp groups. The coordination environment around the Eu atom adopts an irregular five-coordination.

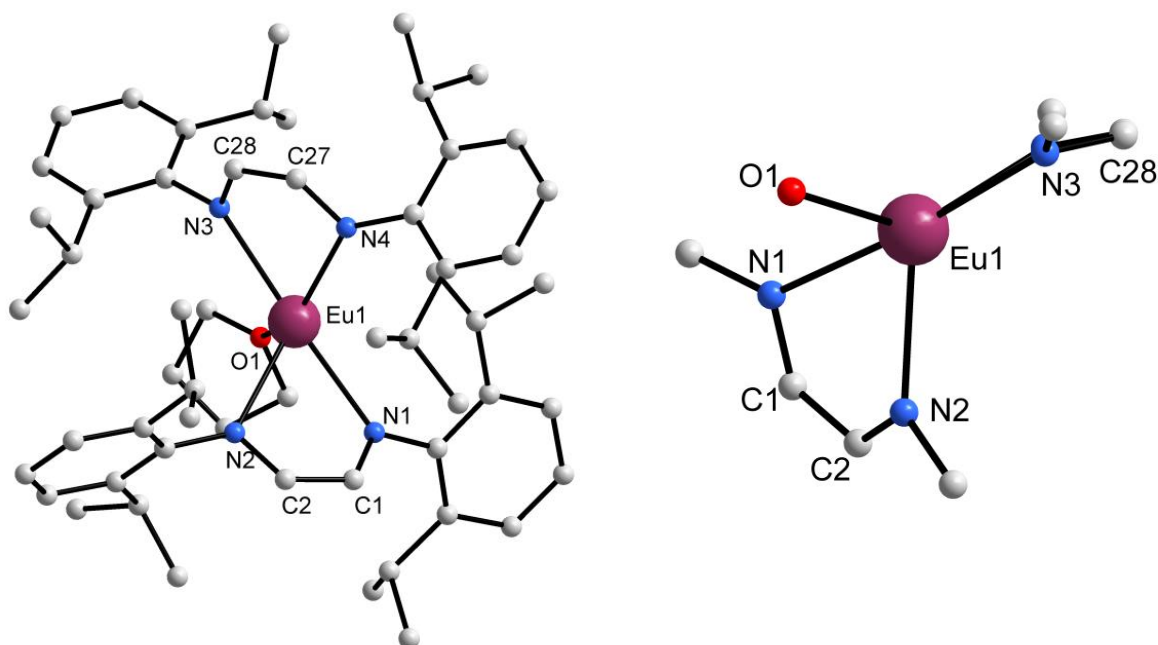


Figure 37. Molecular structure of **35** (left) and representation of the coordination sphere of the Eu atom in **35** viewed along the N3-N4 vector (right).

The Eu atom is located more in the plane defined by N3–C28–C27–N4 (deviation 19.7°) than the plane defined by N1–C1–C2–N2 (deviation 27.4°). The Eu–N bonds in **35** are slightly non-equal (2.573(2) Å, 2.536(2) Å, 2.552(2) Å, and 2.596(2) Å) and are longer than those (Eu–N: 2.475(3) Å and 2.445(3) Å) in the europium(II) complex [Eu(Bian^{Dipp})(DME)₂] with the dianionic 1,2-bis[(2,6-diisopropylphenyl)imino]acenaphthene ligand, while they are similar to those (Eu–N: in the range of 2.566(1) Å to 2.589(9) Å) in the europium(II) complexes [Eu₂(μ-I)₂(Bian^{Dipp})₂(DME)₂] and [Eu₂(μ-Br)₂(Bian^{Dipp})₂(DME)₂] with radical-monoanionic 1,2-bis[(2,6-diisopropylphenyl)imino]acenaphthene ligands.^[123] The Eu–O (2.557(1) Å) bond length in **35** is within the range (2.472(9) Å to 2.600(3) Å) of the Eu–O

bond lengths in the europium(II) complexes [$\{(i\text{Pr})_2\text{ATI}\}\text{Eu}\{\text{N}(\text{SiMe}_3)_2\}(\text{THF})_2$]^[23] and [$\text{SmI}(\text{DIP}_2\text{pyr})(\text{THF})_3$].^[154] Compared to the neutral ligand **2**,^[67] the C–N bond lengths (1.334(3) Å/ 1.332(3) Å/ 1.336(3) Å/ 1.330(3) Å) of the DAD backbone in **35** are elongated, while the C–C bond lengths (1.403(3) Å/ 1.402(3) Å) are shortened, similar to the extent noticed in the alkali metal complexes [$\text{Li}(\text{H}^2\text{DAD}^{\text{Dipp}})(\text{THF})_2$] (**20**), [$\text{K}(\text{H}^2\text{DAD}^{\text{Dipp}})(\text{THF})_4$] (**22**), and [$\text{Rb}(\text{H}^2\text{DAD}^{\text{Dipp}})(\text{THF})_4$] (**23**) with radical-monoanionic $\text{H}^2\text{DAD}^{\text{Dipp}}$ ligand. The values for the neutral ligand **2** are 1.234(3) Å (average) for C–N and 1.445(3) Å for C–C.^[67] These structural data indicate the radical-monoanionic character of the ligand among the several possible coordination modes of the DAD ligands (Scheme 3, page 2) and +2 oxidation state of the Eu metal atom in **35**. However, EPR spectroscopy should be done to get a more precise picture.

3. Summary

Synthesis and structural characterization of DAD alkali metal complexes was the main objective of this Ph.D. thesis. For that purpose, the three different DAD ligands $\text{Me}_2\text{DAD}^{\text{Dipp}}$ (**1**),^[66] $\text{H}_2\text{DAD}^{\text{Dipp}}$ (**2**),^[67] and $\text{H}_2\text{DAD}^{\text{Ad}}$ (**3**)^[68] were prepared according to the published procedures. In the beginning of the Ph.D work, the whole series of alkali metal complexes with dianionic $\text{Me}_2\text{DAD}^{\text{Dipp}}$ ligands were synthesized by direct metallation of **1** with alkali metals in THF. A variety of structural arrangements are observed as a consequence of the significant range of ionic radii exhibited by the alkali metals. The X-ray crystal structure of the dilithium complex $[\text{Li}_2(\text{Me}_2\text{DAD}^{\text{Dipp}})(\mu\text{-THF})(\text{THF})_2]$ (**4**) and disodium complex $[\text{Na}_2(\text{Me}_2\text{DAD}^{\text{Dipp}})(\text{THF})_4]$ (**5**) revealed that both of the complexes adopt monomeric structures as shown in Figure 38, whereas the same of the dipotassium complex $\{[\text{K}_2(\text{Me}_2\text{DAD}^{\text{Dipp}})(\mu\text{-THF})(\text{THF})_2] \cdot [\text{K}_2(\text{Me}_2\text{DAD}^{\text{Dipp}})(\mu\text{-THF})(\text{THF})_3]\}_2$ (**6**) showed that the complex adopts a supramolecular tetrameric structure as shown in Figure 39 (page 100).

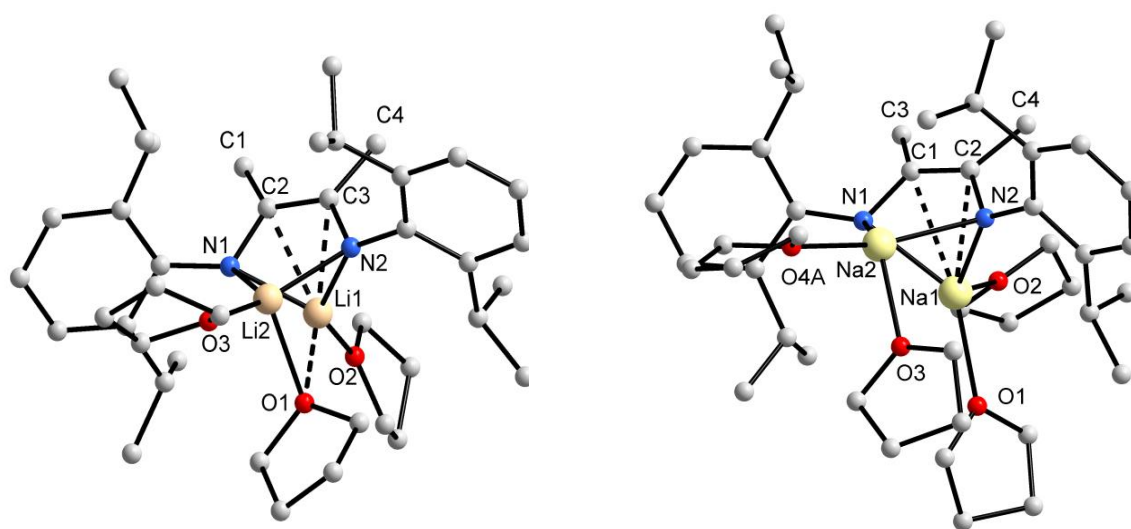


Figure 38. Molecular structures of $[\text{Li}_2(\text{Me}_2\text{DAD}^{\text{Dipp}})(\mu\text{-THF})(\text{THF})_2]$ (**4**) (left) and $[\text{Na}_2(\text{Me}_2\text{DAD}^{\text{Dipp}})(\text{THF})_4]$ (**5**) (right).

The dirubidium $\{[\text{Rb}_2(\text{Me}_2\text{DAD}^{\text{Dipp}})(\text{THF})_4]_2 \cdot \text{THF}\}_n$ (**7**) and dicesium $\{[\text{Cs}_2(\text{Me}_2\text{DAD}^{\text{Dipp}})(\text{THF})_4] \cdot \text{THF}\}_n$ (**8**) complexes with dianionic $\text{Me}_2\text{DAD}^{\text{Dipp}}$ ligands were the first of this kind,

and the single-crystal X-ray analysis of both complexes confirmed the coordination polymeric structures as shown in Figure 40. The tendency of the heavier alkali metals potassium, rubidium, and cesium to form multihapto π -interactions is well reflected in complexes **6-8**.

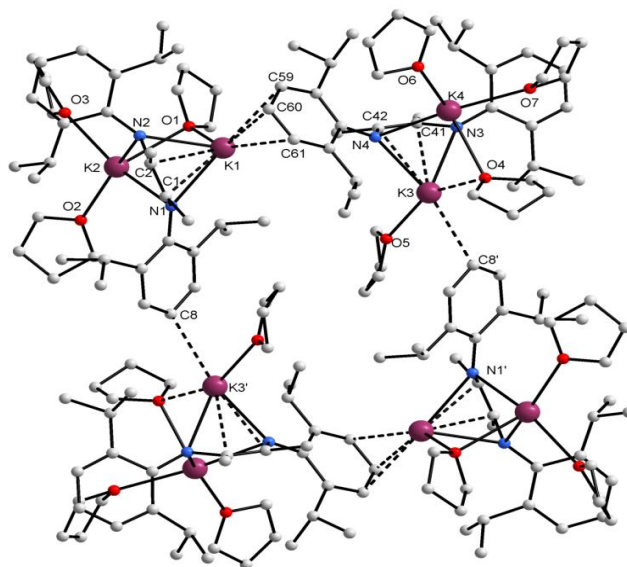


Figure 39. Molecular structure of $\{[K_2(\text{Me}_2\text{DAD}^{\text{Dipp}})(\mu\text{-THF})(\text{THF})_2] \cdot [K_2(\text{Me}_2\text{DAD}^{\text{Dipp}})(\mu\text{-THF})(\text{THF})_3]\}_2$ (**6**).

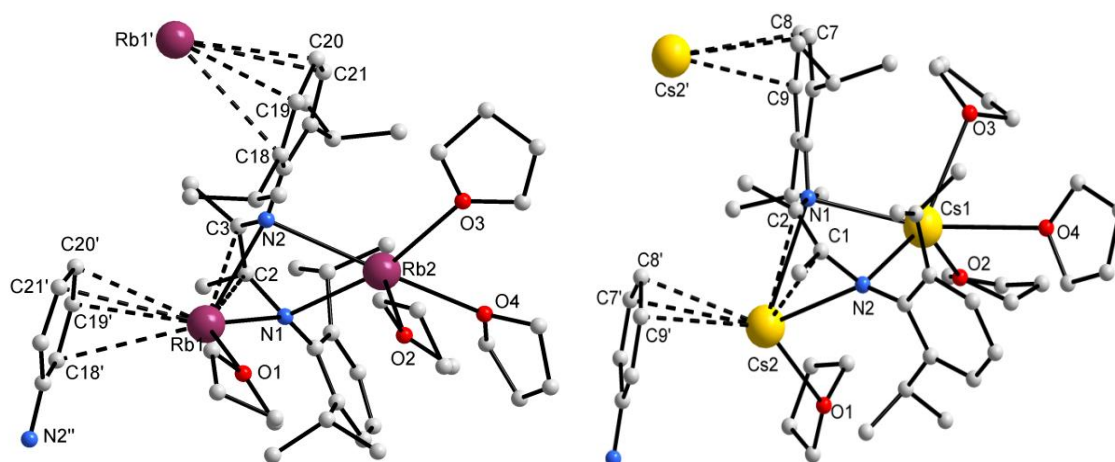


Figure 40. Molecular structures of $\{[\text{Rb}_2(\text{Me}_2\text{DAD}^{\text{Dipp}})(\text{THF})_4]_2 \cdot \text{THF}\}_n$ (**7**) (molecule 1: left) and $\{[\text{Cs}_2(\text{Me}_2\text{DAD}^{\text{Dipp}})(\text{THF})_4] \cdot \text{THF}\}_n$ (**8**) (right).

An attempt was made to synthesize alkali metal complex with dianionic $\text{H}^2\text{DAD}^{\text{Ad}}$ ligand (**3**) by treating **3** with 2 equiv. of lithium to yield the tetranuclear lithium complex $[\{\text{Li}_2(\text{H}^2\text{DAD}^{\text{Ad}})\}_2(\mu\text{-THF})(\text{THF})_2]$ (**9**). The dimeric structure of the complex (Figure 41) shows the influence of the substituents at the N atoms of the DAD moiety as the lithium complex with Dipp group $[\text{Li}_2(\text{Me}^2\text{DAD}^{\text{Dipp}})(\mu\text{-THF})(\text{THF})_2]$ (**4**) is a monomer.

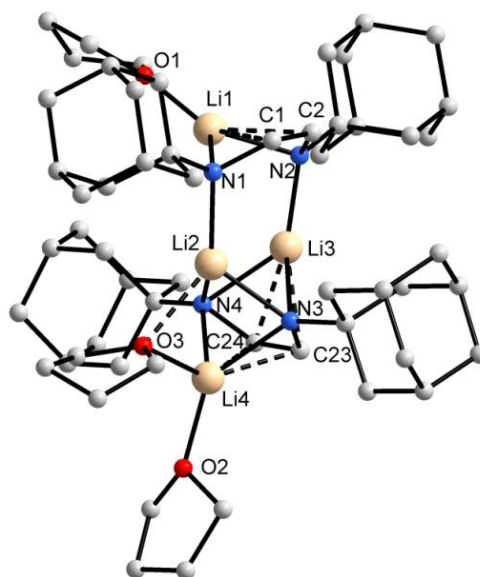


Figure 41. Molecular structure of $[\{\text{Li}_2(\text{H}^2\text{DAD}^{\text{Ad}})\}_2(\mu\text{-THF})(\text{THF})_2]$ (**9**).

In an attempt to synthesize heterobimetallic alkali metal complexes with dianionic DAD ligands, **1** was first treated with 1 equiv. sodium followed by 1 equiv. lithium in THF to yield the heterobimetallic complex $[\text{Na}(\text{THF})_m(\text{Me}^2\text{DAD}^{\text{Dipp}})\text{Li}(\text{THF})_n]$ (**10**), the first of that kind. Similarly, the heterobimetallic complexes $[\text{K}(\text{THF})_2(\text{Me}^2\text{DAD}^{\text{Dipp}})\text{Li}(\text{THF})]$ (**11**), $\{[\text{Rb}(\text{THF})(\text{Me}^2\text{DAD}^{\text{Dipp}})\text{Li}(\text{THF})] \cdot \text{THF}\}_n$ (**12**), and $[\text{Cs}(\text{THF})_m(\text{Me}^2\text{DAD}^{\text{Dipp}})\text{Li}(\text{THF})_n]$ (**13**) were prepared by treating **1** with potassium, rubidium, and cesium, respectively, followed by lithium, while the heterobimetallic complex $[\text{K}(\text{THF})_m(\text{Me}^2\text{DAD}^{\text{Dipp}})\text{Na}(\text{THF})_n]$ (**14**) was prepared by the treatment of **1** with potassium followed by sodium. X-ray diffraction analysis of **11** and **12** showed that **11** crystallizes as a monomer, while **12** aggregates as a coordination polymer (Figure 42, page 102). In a similar manner, the treatment of **3** with sodium followed by lithium yielded the heterobimetallic complex $\{[\text{Na}(\text{H}^2\text{DAD}^{\text{Ad}})\text{Li}(\text{THF})_4] \cdot \text{THF}\}_n$ (**15**) which is a coordination polymer (Figure 43, page 102). In **11**, **12**, and **15**, lithium atoms prefer

σ -coordination, whereas potassium, rubidium, and sodium, respectively, prefer π -coordination. Interestingly, potassium in **11** is not coordinated by aryl π -electronic system like rubidium in **12**.

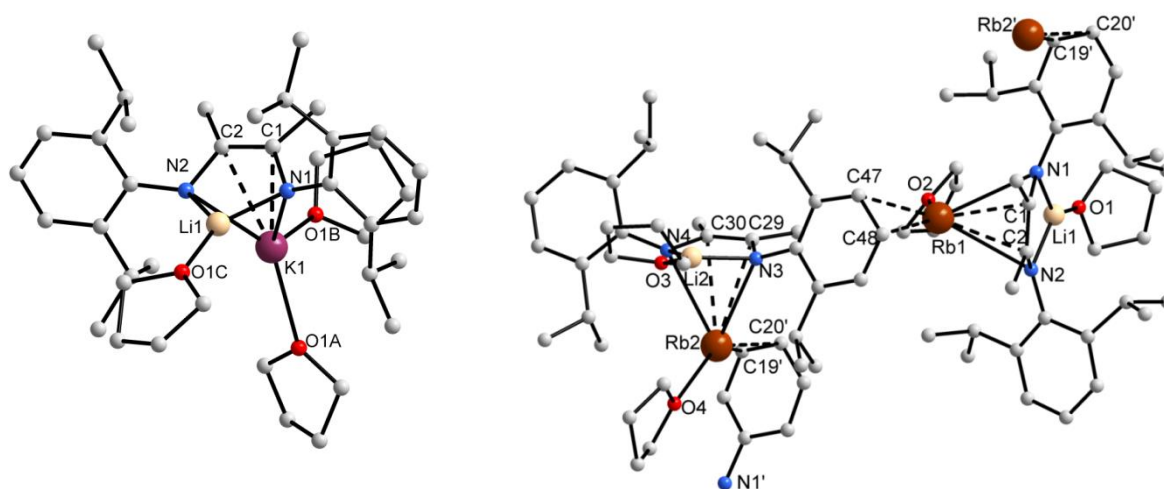


Figure 42. Molecular structure of [K(THF)₂(^{Me}2DAD^{Dipp})Li(THF)] (**11**) (left) and {[Rb(THF)(^{Me}2DAD^{Dipp})Li(THF)] · THF}_n (**12**) (right).

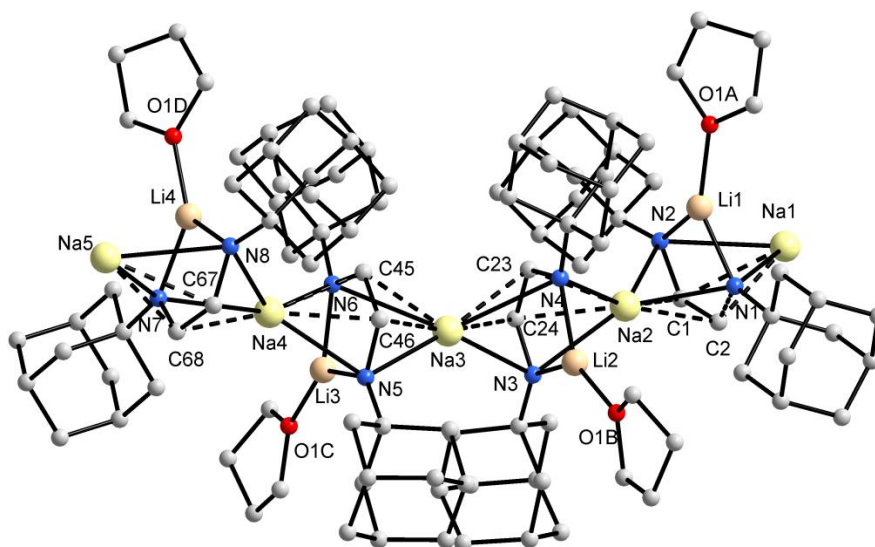


Figure 43. Molecular structure of {[Na(^{H2}DAD^{Ad})Li(THF)]₄ · THF}_n (**15**).

The radical-monoanionic $\text{Me}_2\text{DAD}^{\text{Dipp}}$ complexes $[\text{Li}(\text{Me}_2\text{DAD}^{\text{Dipp}})(\text{DME})]$ (**16**) and $[\text{Na}(\text{Me}_2\text{DAD}^{\text{Dipp}})(\text{DME})]$ (**17**) were prepared in DME by the treatment of **1** with lithium and sodium, respectively in a 1:1 molar ratio. Similarly, treatment of **1** with potassium in THF yielded the complex $[\text{K}(\text{Me}_2\text{DAD}^{\text{Dipp}})(\text{THF})_4]$ (**18**). The DME adduct **16** was successfully analyzed by X-ray crystallography, and the molecular structure of the complex is shown in Figure 44. The paramagnetic complexes **16** and **17** were also analyzed by EPR spectroscopy. Similarly, treatment of **3** with lithium yielded the complex $[\text{Li}(\text{H}_2\text{DAD}^{\text{Ad}})(\text{THF})_2]$ (**19**). The molecular structure of complex **19** showed that the complex is a monomeric THF adduct (Figure 44).

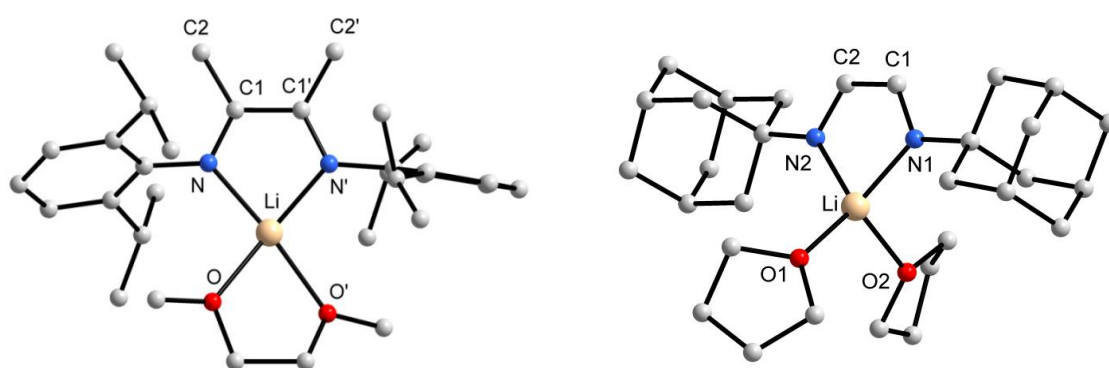


Figure 44. Molecular structures of $[\text{Li}(\text{Me}_2\text{DAD}^{\text{Dipp}})(\text{DME})]$ (**16**) (left) and $[\text{Li}(\text{H}_2\text{DAD}^{\text{Ad}})(\text{THF})_2]$ (**19**) (right).

In an attempt to synthesize the whole series of alkali metal complexes with monoanionic DAD ligands, direct metallation of **2** was carried out either in THF with lithium, sodium, potassium, and rubidium in a 1:1 molar ratio to yield the complexes $[\text{Li}(\text{H}_2\text{DAD}^{\text{Dipp}})(\text{THF})_2]$ (**20**), $[\text{Na}(\text{H}_2\text{DAD}^{\text{Dipp}})(\text{THF})_2]$ (**21**), $[\text{K}(\text{H}_2\text{DAD}^{\text{Dipp}})(\text{THF})_4]$ (**22**), and $[\text{Rb}(\text{H}_2\text{DAD}^{\text{Dipp}})(\text{THF})_4]$ (**23**), respectively, or in DME with cesium in a 1:1 molar ratio to yield the complex $[\text{Cs}(\text{H}_2\text{DAD}^{\text{Dipp}})(\text{DME})_3]$ (**24**). Similarly, treatment of **2** with cesium in THF followed by vacuum drying at 80 °C yielded an unexpected cesium complex $[\text{Cs}(\text{DippNCHC}[\text{CHCHN}^{\text{Dipp}}]\text{N}^{\text{Dipp}})(\text{THF})_2]_n$ (**25**). The molecular structures of **20**, **22**, **23**, and **25** were successfully determined by X-ray diffraction analyses (Figure 45, page 104).

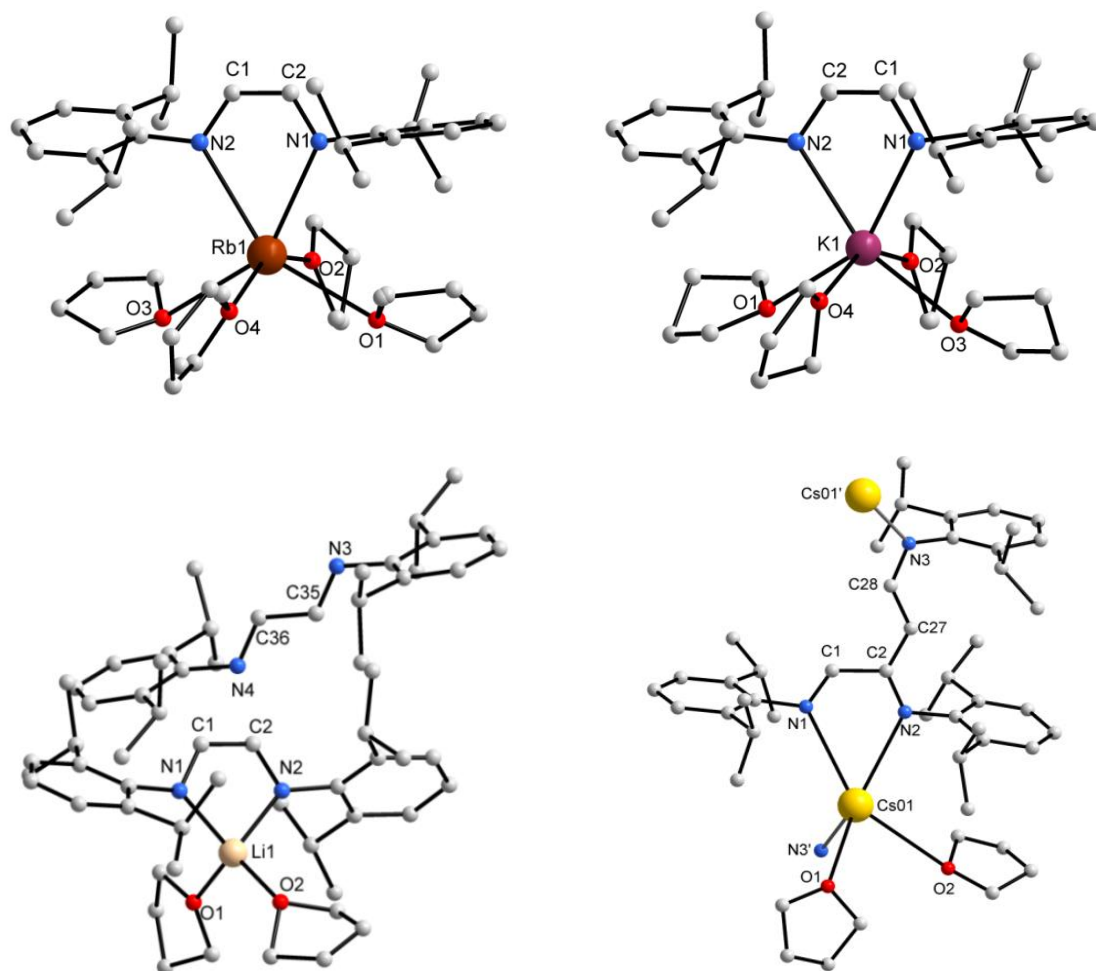


Figure 45. Molecular structures of $[\text{Li}(\text{H}^2\text{DAD}^{\text{Dipp}})(\text{THF})_2]$ (**20**) (bottom-left), $[\text{K}(\text{H}^2\text{DAD}^{\text{Dipp}})(\text{THF})_4]$ (**22**) (top-left), $[\text{Rb}(\text{H}^2\text{DAD}^{\text{Dipp}})(\text{THF})_4]$ (**23**) (top-right), and $[\text{Cs}(\text{DippNCHC}[\text{CHCHN}^{\text{Dipp}}]\text{N}^{\text{Dipp}})(\text{THF})_2]_n$ (**25**) (bottom-right).

The preliminary data of the EPR measurements of the complexes **20-24** confirmed the paramagnetic nature of the complexes. However, further measurements at different conditions are needed to get a clearer picture. The lithium, potassium, and rubidium complexes (**20**, **22**, and **23**, respectively) crystallize as monomers, whereas the cesium complex **25** aggregates as a coordination polymer. Notably, the potassium (**22**) and rubidium (**23**) complexes are isotopic. Surprisingly, the tendency of the heavier alkali metals potassium, rubidium, and cesium to form multihapto π -interactions is not observed in complexes **22**, **23**, and **25**.

The reduction of **2** with potassium hydride in a 2:1 molar ratio yielded an unprecedented potassium β -diketiminate complex $[\text{K}^{\text{DippNCHC}\{\text{DippNCHN}^{\text{Dipp}}\}\text{CHN}^{\text{Dipp}}(\text{THF})_{1.5}]$ (**26**). The molecular structure of the complex revealed that the complex aggregates as a dimer containing a tris(THF) solvated potassium atom and an unsolvated potassium atom which is coordinated to the π -electronic system (symmetric η^6 -coordination) of the aromatic ring and the imino nitrogen atom of the adjacent molecule, forming a dimeric structure (Figure 46).

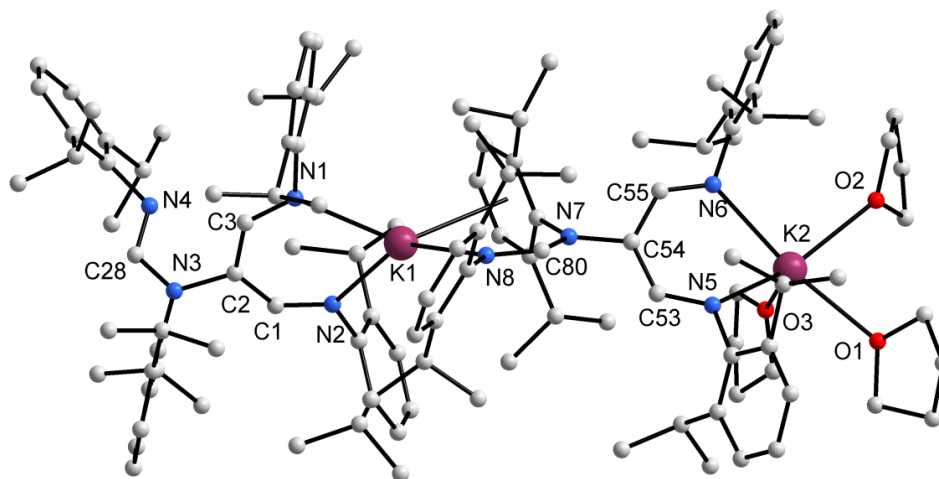


Figure 46. Molecular structure of $[\text{K}^{\text{DippNCHC}\{\text{DippNCHN}^{\text{Dipp}}\}\text{CHN}^{\text{Dipp}}(\text{THF})_{1.5}]$ (**26**).

Lithium, sodium and potassium complexes with the radical-monoanionic $\text{Me}_2\text{DAD}^{\text{Dipp}}$ ligand (**1**) were prepared in THF and treated with with *N,N'*-dicyclohexylcarbodiimide in a 1:1 molar ratio to yield the heterocyclic compounds $[\text{Li}^{\text{DippN}^{\text{Cy-Pyr}}(\text{THF})_3}]$ (**27**), $[\text{Na}^{\text{DippN}^{\text{Cy-Pyr}}(\text{THF})_3}]$ (**28**), and $\{[\text{K}^{\text{DippN}^{\text{Cy-Pyr}}(\text{THF})_2]_4 \cdot \text{THF}\}_n$ (**29**), respectively. In a similar way, a sodium complex with radical-monoanionic $\text{Me}_2\text{DAD}^{\text{Dipp}}$ ligand (**1**) was treated with *N,N'*-diisopropylcarbodiimide to yield the sodium compound $[\text{Na}^{\text{DippN}^{\text{iPr-Pyr}}(\text{THF})_3}] \cdot \text{THF}$ (**30**). Compounds **27**, **28**, and **30** crystallize as monomers (Figure 47, page 106), whereas compound **29** aggregates as a coordination polymer (Figure 48, page 106).

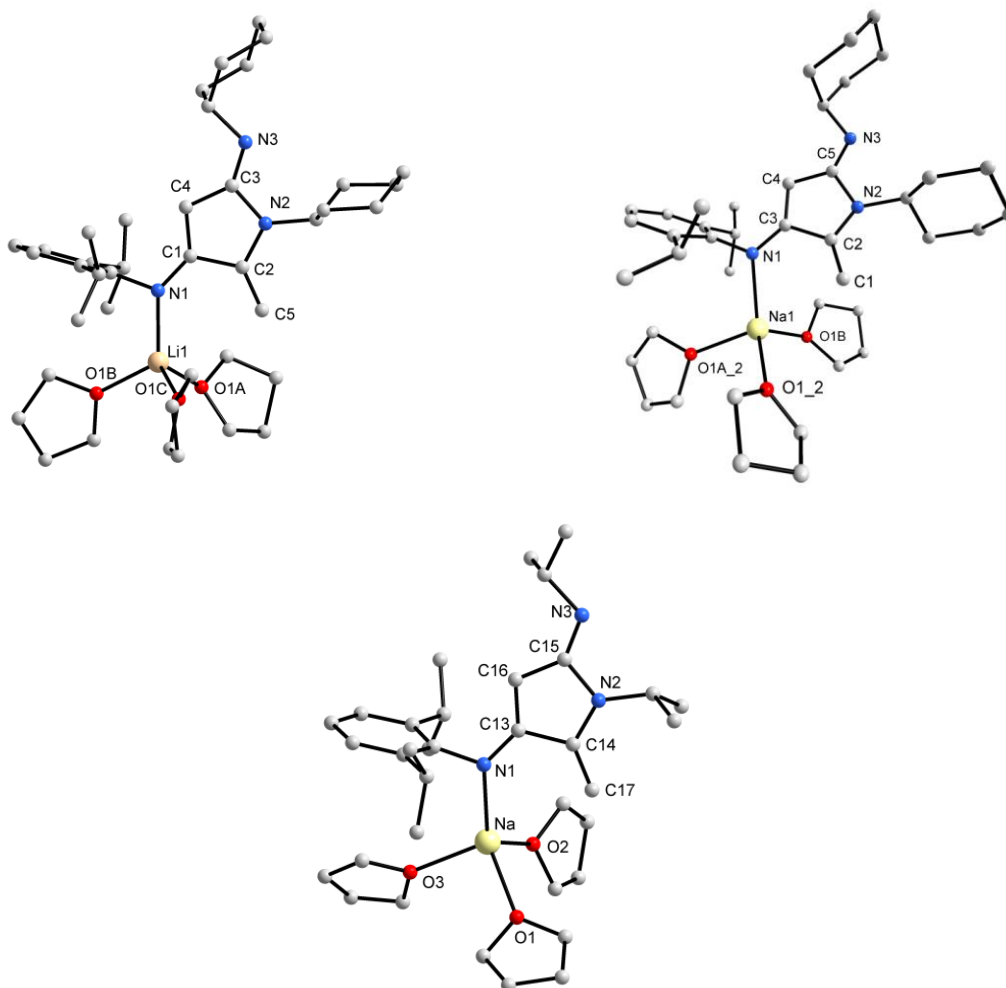


Figure 47. Molecular structures of $[\text{Li}(\text{DippN}^{\text{Cy-Pyr}})(\text{THF})_3]$ (**27**) (top-left), $[\text{Na}(\text{DippN}^{\text{Cy-Pyr}})(\text{THF})_3]$ (**28**) (top-right), and $[\text{Na}(\text{DippN}^{\text{iPr-Pyr}})(\text{THF})_3] \cdot \text{THF}$ (**30**) (bottom).

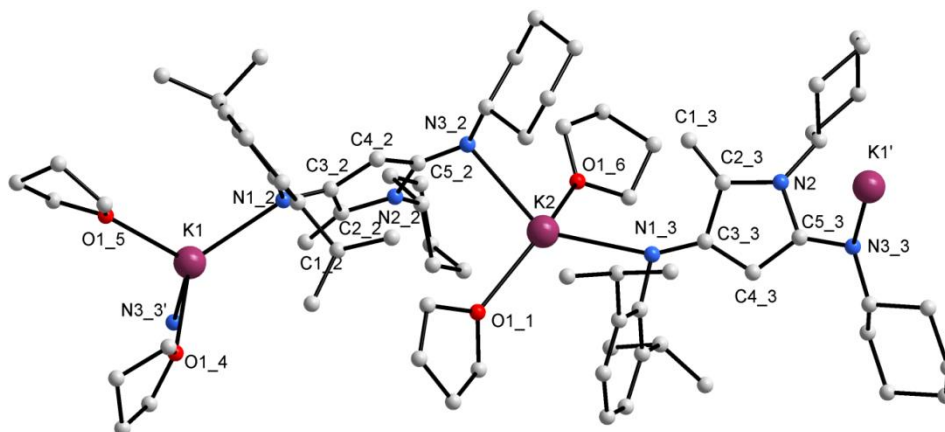


Figure 48. Molecular structure of $\{[\text{K}(\text{DippN}^{\text{Cy-Pyr}})(\text{THF})_2]_4 \cdot \text{THF}\}_n$ (**29**).

In the last part of this Ph.D. work, DAD complexes of alkaline earth metals and lanthanides have been synthesized. For that purpose, **1** was treated with calcium in a 1:1 molar ratio in the presence of iodine to yield the calcium complex $[\text{Ca}^{\text{Me}_2\text{DAD}^{\text{Dipp}}}(\text{THF})_3]$ (**31**) with dianionic $\text{Me}_2\text{DAD}^{\text{Dipp}}$ ligand. Similarly, the calcium complex $[\text{Ca}^{\text{H}_2\text{DAD}^{\text{Ad}}}_2(\text{THF})_2] \cdot \text{THF}$ (**32**) containing a radical-monoanionic $\text{H}_2\text{DAD}^{\text{Ad}}$ ligand was prepared by treating **3** with calcium in a 2:1 molar ratio. As shown in Figure 49, both of the complexes exist as monomers. However, the molecules of complex **32** are enantiomers. The calcium atom in **31** is coordinated by a dianionic DAD ligand and three THF molecules, whereas that in **32** is coordinated by two radical-monoanionic DAD ligands and two THF molecules. The calcium atom in **31** is partly coordinated by the π -electronic system of the DAD moiety.

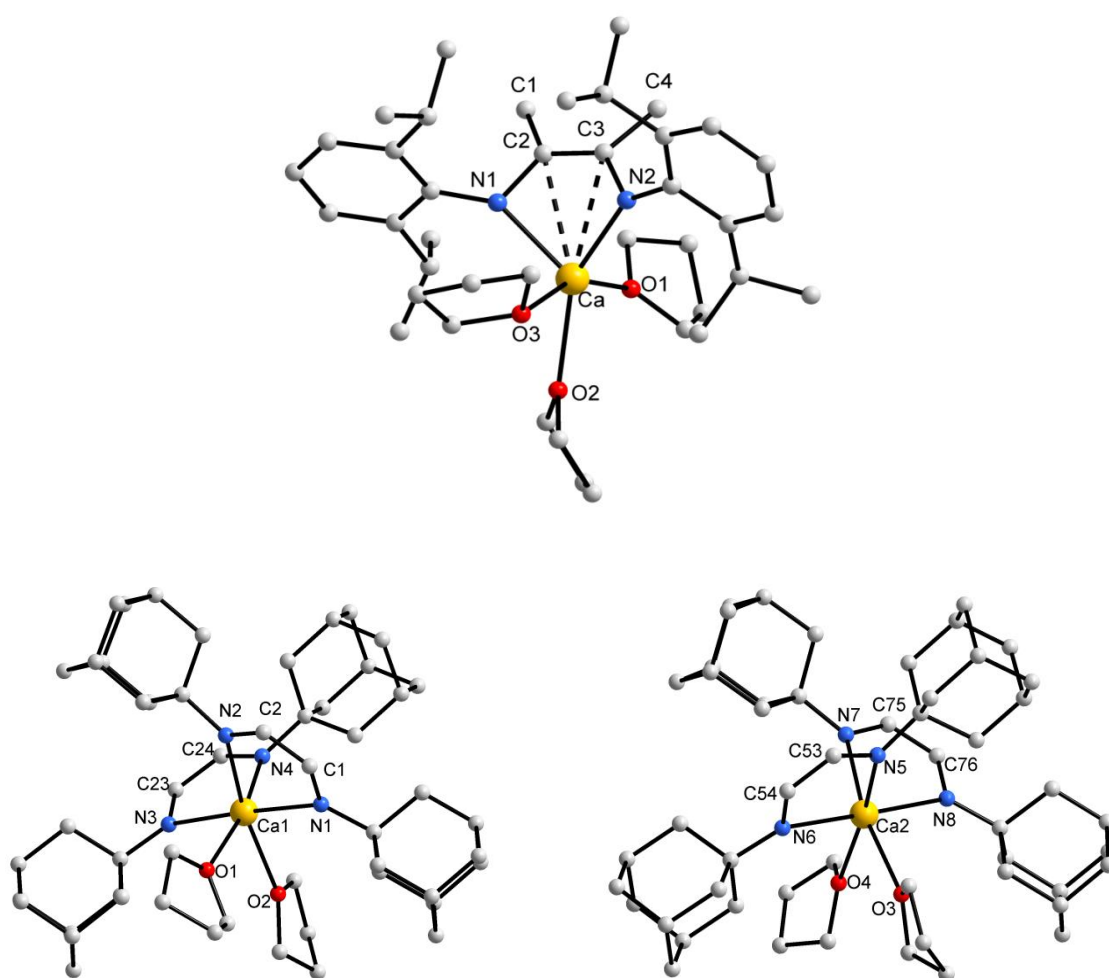


Figure 49. Molecular structures of $[\text{Ca}^{\text{Me}_2\text{DAD}^{\text{Dipp}}}(\text{THF})_3]$ (**31**) (top) and $[\text{Ca}^{\text{H}_2\text{DAD}^{\text{Ad}}}_2(\text{THF})_2] \cdot \text{THF}$ (**32**) (bottom).

The ytterbium(II) complex $[\text{Yb}_2(\mu\text{-I})_2(\text{Me}_2\text{DAD}^{\text{Dipp}})_2(\text{THF})_4] \cdot \text{THF}$ (**33**) with radical-monoanionic $\text{Me}_2\text{DAD}^{\text{Dipp}}$ ligand was prepared by the treatment of **1** with ytterbium and iodine in equivalent molar concentrations. A similar reaction between **2** and samarium yielded the samarium(III) complex $[\text{Sm}(\text{H}_2\text{DAD}^{\text{Dipp}})(\text{I})(\text{THF})_3]$ (**34**) with dianionic $\text{H}_2\text{DAD}^{\text{Dipp}}$ ligand. Treatment of **2** with europium in a 2:1 molar ratio in the presence of iodine yielded the europium(II) complex $[\text{Eu}(\text{H}_2\text{DAD}^{\text{Dipp}})_2(\text{THF})]$ (**35**) containing two radical-monoanionic $\text{H}_2\text{DAD}^{\text{Dipp}}$ ligands. The X-ray diffraction analysis of the complexes revealed that the ytterbium(II) complex **33** aggregates as a dimer, whereas the samarium(III) complex **34** and the europium(II) complex **35** crystallize as monomers (Figure 50). Notably, the samarium atom in **34** showed a minor π -coordination to the DAD moiety.

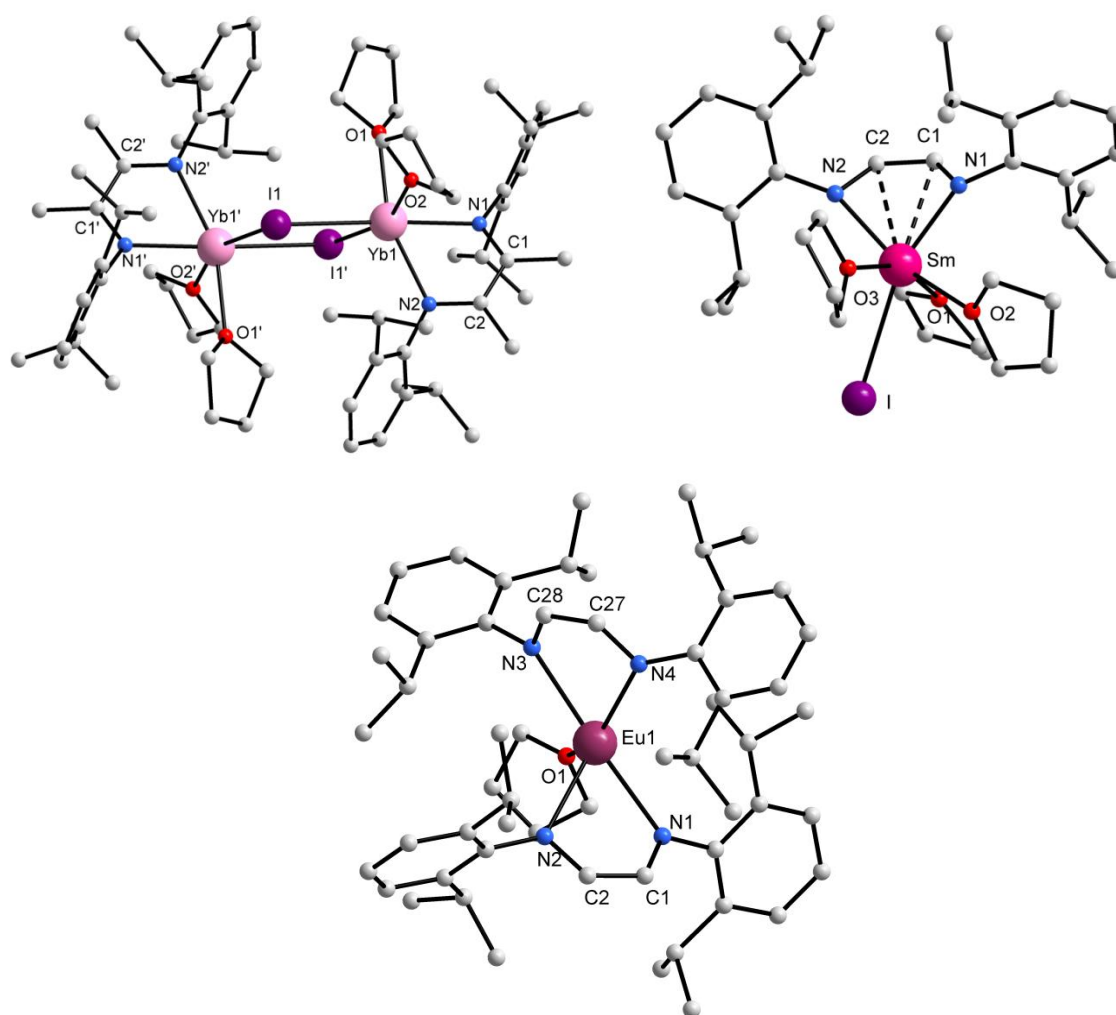


Figure 50. Molecular structures of $[\text{Yb}_2(\mu\text{-I})_2(\text{Me}_2\text{DAD}^{\text{Dipp}})_2(\text{THF})_4] \cdot \text{THF}$ (**33**) (top-left), $[\text{Sm}(\text{H}_2\text{DAD}^{\text{Dipp}})(\text{I})(\text{THF})_3]$ (**34**) (top-right), and $[\text{Eu}(\text{H}_2\text{DAD}^{\text{Dipp}})_2(\text{THF})]$ (**35**) (bottom).

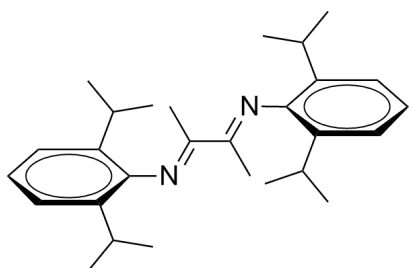
4. Experimental section

General

All operations were performed under an inert argon atmosphere by using standard dry box and Schlenk techniques. THF, DME, toluene, and *n*-pentane were dried according to common procedures and were distilled under an argon atmosphere prior to use. The starting materials $\text{Me}_2\text{DAD}^{\text{Dipp}}$ (**1**),^[66] $\text{H}_2\text{DAD}^{\text{Dipp}}$ (**2**),^[67] and $\text{H}_2\text{DAD}^{\text{Ad}}$ (**3**)^[68] were prepared according to published procedures. Metals and chemicals were obtained from commercial sources. Sodium, potassium, and potassium hydride were freed from paraffin oil by washing with *n*-pentane and were stored in a dry box. ^1H NMR (400 MHz), ^{13}C NMR (100 MHz), and ^7Li NMR (155 MHz) spectra were recorded in d_8 -THF solutions on a Bruker DPX 400 spectrometer. Chemical shifts were referenced to TMS for ^1H NMR (400 MHz) and ^{13}C NMR and to LiCl in D_2O (1 M) for ^7Li NMR. IR spectra were measured with an ATR IR spectrometer Bruker Vertex V70. Mass spectra (EI, 70 eV) were recorded with a MAT 95 apparatus. Microanalyses of the compounds were performed by using a Leco CHNS 932 apparatus. Q-band CW-EPR (33.9 GHz) measurements were conducted with a Bruker EMX-plusQ spectrometer by using an ER5106QT resonator. X-Band (9.43 GHz) room-temperature CW-EPR measurements were performed with a Magnettech MiniScope MS400 benchtop spectrometer. MATLAB 8.60 (The MathWorks, Inc., Natick, MA, USA) was used for baseline correction of the EPR spectra.

$\text{Me}_2\text{DAD}^{\text{Dipp}}$ (**1**)

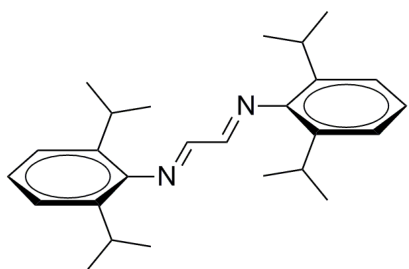
A few drops of formic acid were added as catalyst into a 500 mL flask containing ethanol (250 mL), 2,6-diisopropylaniline (50 g, 280 mmol), and butanedione (12 g, 140 mmol). After stirring the reaction mixture for few hours, $\text{Me}_2\text{DAD}^{\text{Dipp}}$ appeared as a yellow precipitate. Stirring was further continued for two days and the yellow precipitate was collected by filtration and washed with cold methanol to afford the analytically pure $\text{Me}_2\text{DAD}^{\text{Dipp}}$ ligand (**1**). ^1H NMR (400 MHz, d_8 -THF, 23 °C): δ = 1.14 (d, $^3J_{\text{HH}}$ = 6.8 Hz, 12H, $\text{CH}(\text{CH}_3)_2$), 1.19 (d, $^3J_{\text{HH}}$ = 6.8 Hz, 12H, $\text{CH}(\text{CH}_3)_2$), 2.06 (s, 6H, NCCH_3), 2.74 (sep, $^3J_{\text{HH}}$ = 6.8 Hz, 4H, $\text{CH}(\text{CH}_3)_2$), 7.03 (t, $^3J_{\text{HH}}$ = 7.6 Hz, 4H, *para*-Ar), 7.14 (d, 7.6 Hz, 2H, *meta*-Ar) ppm. ^{13}C NMR (100 MHz, d_8 -THF, 23 °C): δ = 16.5 (NCCH_3), 22.8 ($\text{CH}(\text{CH}_3)_2$), 23.3 ($\text{CH}(\text{CH}_3)_2$), 29.3 ($\text{CH}(\text{CH}_3)_2$), 123.6



(*meta*-Ar), 124.5 (*para*-Ar), 135.5 (*ortho*-Ar), 147.1 (*ipso*-Ar), 168.9 (NCCH₃) ppm. **IR** (ATR): $\nu = 3062$ w, 2956 s, 2926 m, 2867 m, 1661 w, 1630 s, 1590 w, 1464 m, 1437 m, 1381 w, 1363 s, 1322 m, 1254 w, 1243 w, 1181 m, 1121 s, 1101 m, 1057 w, 1042 w, 968 w, 933 m, 820 m, 807 w, 792 m, 762 vs, 687 m, 614 w, 526 w, 465 w, 428 m, 285 w, 257 w, 212 w, 182 w, 106 w, 92 w, 61 w cm⁻¹.

H²DAD^{Dipp} (2)

A few drops of formic acid were added as catalyst into a 250 mL flask containing ethanol (125 mL), 2,6-diisopropylaniline (25 g, 140 mmol), and glyoxal (7.8 mL, 70 mmol, 40% in water). After stirring the reaction mixture for a few hours,

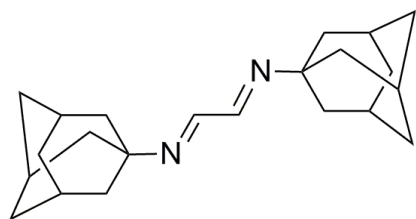


H²DAD^{Dipp} appeared as a yellow precipitate. Stirring was further continued for two days and the yellow precipitate was collected by filtration and washed with cold methanol to afford the analytically pure **H²DAD^{Dipp}** ligand (2). **¹H**

NMR (400 MHz, *d*₈-THF, 23 °C): $\delta = 1.19$ (d, ³J_{HH} = 6.8 Hz, 24H, CH(CH₃)₂), 2.96 (sep, ³J_{HH} = 6.8 Hz, 4H, CH(CH₃)₂), 7.07 (t, ³J_{HH} = 7.6 Hz, 4H, *para*-Ar), 7.16 (d, 7.6 Hz, 2H, *meta*-Ar), 8.11 (s, 2H, NCH) ppm. **¹³C NMR** (100 MHz, *d*₈-THF, 23 °C): $\delta = 23.6$ (CH(CH₃)₂), 28.8 (CH(CH₃)₂), 123.7 (*meta*-Ar), 125.6 (*para*-Ar), 137.1 (*ortho*-Ar), 149.4 (*ipso*-Ar), 164.3 (NCH) ppm. **IR** (ATR): $\nu = 3063$ w, 2961 s, 2926 m, 2867 w, 1625 s, 1588 w, 1464 m, 1435 m, 1382 w, 1360 w, 1329 w, 1289 w, 1255 w, 1240 w, 1175 m, 1108 w, 1097 w, 1060 w, 1046 w, 958 w, 924 m, 887 w, 820 m, 805 w, 789 s, 760 vs, 678 m, 612 w, 583 w, 514 w, 470 w, 430 w, 348 m, 273 m, 220 w, 180 w, 140 w, 123 w, 107 w, 81 w, 74 w, 65 w, 55 m cm⁻¹.

H²DAD^{Ad} (3)

1-Adamantylamine (12.89 g, 82.6 mmol) was dissolved in 500 mL of H₂O:EtOH (1:1) in a 1L flask. The flask was cooled with ice, and the mixture was stirred for 30 minutes. Glyoxal (6



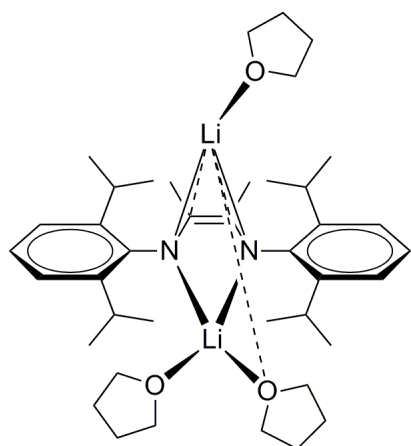
mL, wt. 40% in water, 41.4 mmol) was added dropwise and by the end of the addition, a colorless solid began to precipitate. Stirring was continued for 1h to complete the reaction, and the colorless solid product was filtered and washed with 50 mL of H₂O:EtOH (1:1) to afford the

analytically pure **H²DAD^{Ad}** ligand (3). **¹H NMR** (400 MHz, *d*₈-THF, 21 °C): $\delta = 1.66 - 1.76$ (m, 24 H, CHCH₂), 2.1 (s, 6H, CHCH₂), 7.8 (s, 2 H, CNCH) ppm. **¹³C NMR** (100 MHz, *d*₈-

THF, 22 °C): δ = 30.5 (CHCH₂), 37.3 (CHCH₂), 43.6 (CHCH₂), 58.6 (CNCH), 157.9 (CNCH) ppm. **IR** (ATR): ν = 2909 vs, 2897 vs, 2883 vs, 2847 vs, 1626 m, 1452 m, 1367 w, 1355 w, 1342 m, 1317 m, 1306 m, 1285 w, 1262 w, 1189 w, 1178 w, 1118 w, 1091 s, 1041 w, 984 w, 939 m, 910 m, 814 m, 776 w, 720 m, 646 m, 613 w, 468 vs, 450 w, 422 vs, 407 w, 363 w, 295 vs, 247 m, 173 s, 125 w, 105 w, 91 w, 70 w, 61 w cm⁻¹.

[Li₂(Me²DAD^{Dipp})(μ -THF)(THF)₂] (4)

Lithium (70 mg, 10 mmol, slightly in excess) was added to a solution of **1** (2.0 g, 4.9 mmol) in 100 mL of THF, and the resulting mixture was stirred overnight at r.t. with a glass-coated



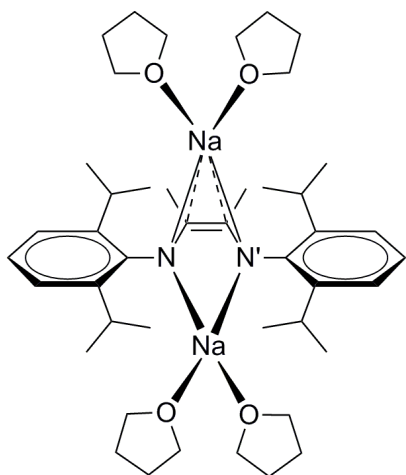
stirring bar. The reaction mixture (turned from yellow to orange) was filtered, and the filtrate was concentrated in vacuum to approximately 20 mL before it was kept at 5 °C to yield **4** (2.9 g, 92%) as orange blocks. Anal. Calcd for C₄₀H₆₄Li₂N₂O₃ (M_r = 634.83): C, 75.68; H, 10.16; N, 4.41. Found: C, 75.55; H, 10.29; N, 4.49. ¹H NMR (400 MHz, d₈-THF, 23 °C): δ = 1.02 (d, ³J_{HH} = 6.8 Hz, 12H, CH(CH₃)₂), 1.16 (d, ³J_{HH} = 6.8 Hz, 12H, CH(CH₃)₂), 1.54 (s, 6H, NCCH₃), 1.72 (s, THF), 3.56 (s, THF), 3.5 – 3.6

(4H, CH(CH₃)₂), 6.46 (t, ³J_{HH} = 7.2 Hz, 2H, *para*-Ar), 6.79 (d, ³J_{HH} = 7.6 Hz, 4H, *meta*-Ar) ppm. ¹³C NMR (100 MHz, d₈-THF, 24 °C): δ = 16.3 (NCCH₃), 24.3 (CH(CH₃)₂), 25.8 (CH(CH₃)₂), 26.3 (THF), 27.6 (CH(CH₃)₂), 68.2 (THF), 117.1 (*para*-Ar), 120.2 (NCCH₃), 122.5 (*meta*-Ar), 142.5 (*ortho*-Ar), 154.4 (*ipso*-Ar) ppm. ⁷Li NMR (155 MHz, d₈-THF, 25 °C): δ = 0.73 ppm. **MS** (EI): m/z = 633 (1%) [M⁺ – H], 433 (1%) [M⁺ – (3 C₃H₇, THF)], 406 (76%) [Me²DAD^{Dipp} + 2H], 361 (88%) [Me²DAD^{Dipp} – C₃H₇], 202 (100%) [Me²DAD^{Dipp} – (2 CH₃, 4 C₃H₇)], 606 (1%), 579 (1%), 500 (1%), 391 (1%), 274 (1%), 216 (3%), 188 (26%), 160 (48%). **IR** (ATR): ν = 3050 w, 2956 s, 2870 m, 1583 w, 1554 w, 1452 m, 1423 vs, 1316 s, 1252 vs, 1150 w, 1115 m, 1036 s, 978 w, 941 w, 887 m, 831 w, 771 s, 689 w, 590 m, 550 m, 440 w cm⁻¹. Mp: 125 °C.

[Na₂(Me²DAD^{Dipp})(THF)₄] (5)

Sodium (230 mg, 10 mmol, slightly in excess) was added to a solution of **1** (2.0 g, 4.9 mmol) in 100 mL of THF, and the resulting mixture was stirred overnight at r.t. with a glass-coated stirring bar. The reaction mixture (turned from yellow to bright red) was filtered, and the filtrate was concentrated in vacuum to approximately 20 mL before it was kept at 5 °C to

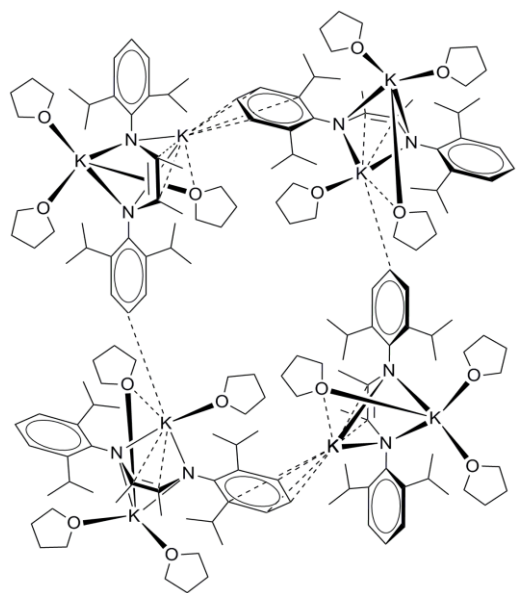
yield **5** (3.3 g, 90%) as red plates. Anal. Calcd for $C_{44}H_{72}N_2Na_2O_4$ ($M_r = 739.03$): C, 71.51; H, 9.82; N, 3.79. Found: C, 71.96; H, 9.74; N, 3.88. 1H NMR (400 MHz, d_8 -THF, 22 °C): $\delta =$



1.02 (d, $^3J_{HH} = 6.8$ Hz, 12H, $CH(CH_3)_2$), 1.21 (d, $^3J_{HH} = 6.8$ Hz, 12H, $CH(CH_3)_2$), 1.65 (s, 6H, $NCCH_3$), 1.76 (m, THF), 3.6 (m, THF), 3.7 (sep, $^3J_{HH} = 6.8$ Hz, 4H, $CH(CH_3)_2$), 6.18 (t, $^3J_{HH} = 7.2$ and 7.6 Hz, 2H, *para*-Ar), 6.69 (d, $^3J_{HH} = 7.2$ Hz, 4H, *meta*-Ar) ppm. ^{13}C NMR (100 MHz, d_8 -THF, 23 °C): $\delta = 18.0$ ($NCCH_3$), 24.2 ($CH(CH_3)_2$), 25.2 ($CH(CH_3)_2$), 26.3 (THF), 27.4 ($CH(CH_3)_2$), 68.2 (THF), 112.3 (*para*-Ar), 121.1 ($NCCH_3$), 122.6 (*meta*-Ar), 139.4 (*ortho*-Ar), 156.6 (*ipso*-Ar) ppm. MS (EI): $m/z = 651$ (2%) [$M^+ - (CH_3, THF)$], 604 (2%) [$M^+ - (H, 6 CH_3, C_3H_7)$], 566 (1%) [$M^+ - 4 C_3H_7$], 402 (35%) [$M^+ - (8 CH_3, 3 THF)$], 387 (65%) [$M^+ - (9 CH_3, 3 THF)$], 371 (20%) [$M^+ - (H, 10 CH_3, 3 THF)$], 361 (50%) [$^{Me_2}DAD^{Dipp} - C_3H_7$], 202 (100%) [$^{Me_2}DAD^{Dipp} - (2 CH_3, 4 C_3H_7)$], 732 (1%), 500 (8%), 457 (2%), 334 (20%), 284 (8%), 234 (4%), 227 (10%), 212 (50%), 188 (15%), 162 (95%). IR (ATR): $\nu = 3032$ w, 2954 s, 2865 s, 1664 w, 1580 m, 1536 w, 1458 m, 1406 vs, 1310 vs, 1249 vs, 1198 m, 1135 m, 1115 m, 1046 s, 1015 m, 944 w, 930 w, 898 m, 847 w, 747 s, 723 m, 693 w, 664 w, 635 w, 613 w, 570 m, 554 m, 519 w, 490 w, 451 m, 427 w, 383 w, 320 w, 286 m, 267 s, 228 m, 163 s, 79 m, 54 s cm^{-1} . Mp: 129 °C.

$\{[K_2(^{Me_2}DAD^{Dipp})(\mu-THF)(THF)_2] \cdot [K_2(^{Me_2}DAD^{Dipp})(\mu-THF)(THF)_3]\}_2$ (**6**)

Potassium (390 mg, 10 mmol, slightly in excess) was added to a solution of **1** (2.0 g, 4.9



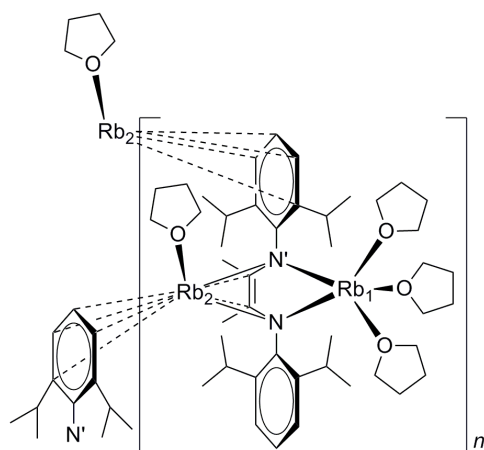
mmol) in 100 mL of THF, and the resulting mixture was stirred overnight at r.t. with a glass-coated stirring bar. The reaction mixture (turned from yellow to bright red) was filtered, and the filtrate was concentrated in vacuum to approximately 20 mL before it was kept at 5 °C to yield **6** (3.1 g, 85%) as red rods. Anal. Calcd for $C_{84}H_{136}K_4N_4O_7$ ($M_r = 1470.39$): C, 68.61; H, 9.32; N, 3.81. Found: C, 68.33; H, 9.29; N, 3.9. 1H NMR (400 MHz, d_8 -THF, 23 °C): $\delta = 1.02$ (d, $^3J_{HH} = 6.8$ Hz, 12H, $CH(CH_3)_2$), 1.22 (d, $^3J_{HH} = 6.8$ Hz, 12H, $CH(CH_3)_2$), 1.65 (s, 6H, $NCCH_3$), 1.76 (m, THF), 3.6 (m, THF), 3.68 (sep, $^3J_{HH} = 6.8$ Hz, 4H, $CH(CH_3)_2$),

1.65 (s, 6H, $NCCH_3$), 1.76 (m, THF), 3.6 (m, THF), 3.68 (sep, $^3J_{HH} = 6.8$ Hz, 4H, $CH(CH_3)_2$),

5.96 (t, $^3J_{\text{HH}} = 7.2$ Hz, 2H, *para*-Ar), 6.63 (d, $^3J_{\text{HH}} = 7.2$ Hz, 4H, *meta*-Ar) ppm. ^{13}C NMR (100 MHz, d_8 -THF, 24 °C): $\delta = 18.8$ (NCCH₃), 24.2 (CH(CH₃)₂), 25.7 (CH(CH₃)₂), 26.3 (THF), 27.5 (CH(CH₃)₂), 68.2 (THF), 109.1 (*para*-Ar), 121.2 (NCCH₃), 122.9 (*meta*-Ar), 137.2 (*ortho*-Ar), 155.6 (*ipso*-Ar) ppm. **MS** (EI): $m/z = 524$ (1%) [K₂(THF)(^{Me2}DAD^{Dipp}) – 2 CH₃], 480 (1%) [K₂(THF)(^{Me2}DAD^{Dipp}) – (H, 2 CH₃, C₃H₇)], 406 (95%) [^{Me2}DAD^{Dipp} + 2H], 361 (88%) [^{Me2}DAD^{Dipp} – C₃H₇], 202 (96%) [^{Me2}DAD^{Dipp} – (2 CH₃, 4 C₃H₇)], 806 (1%), 732 (1%), 666 (1%), 633 (1%), 480 (1%), 391 (2%), 231 (33%), 215 (22%), 204 (100%), 188 (84%), 175 (60%), 162 (83%). **IR** (ATR): $\nu = 3060$ w, 2953 m, 2861 m, 1577 m, 1553 w, 1513 w, 1458 m, 1404 vs, 1365 m, 1322 s, 1276 vs, 1249 s, 1195 m, 1133 m, 1096 m, 1051 m, 1015 m, 952 w, 846 w, 781 w, 758 s, 738 s, 727 m, 693 w, 640 w, 571 m, 544 w, 517 w, 492 w, 467 w, 444 m cm⁻¹. Mp: 105 °C.

{[Rb₂(^{Me2}DAD^{Dipp})(THF)₄]₂ · THF}_n (7)

A solution of **1** (2.0 g, 4.9 mmol) in 100 mL of THF was added into a flask containing rubidium (850 mg, 10 mmol, slightly in excess), and the resulting mixture was stirred



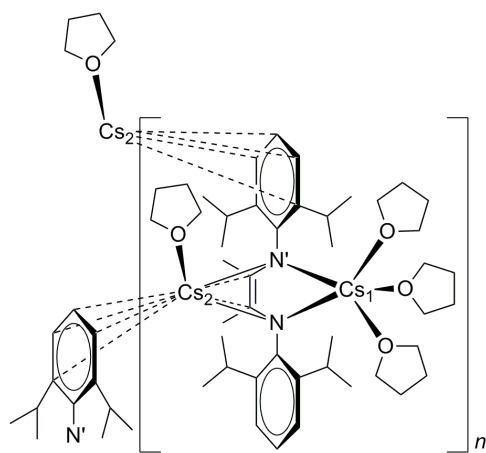
overnight at r.t. with a glass-coated stirring bar. The reaction mixture (turned from yellow to bright red) was filtered, and the filtrate was concentrated in vacuum to approximately 20 mL before it was kept at 5 °C to yield **7** (3.6 g, 81%) as red plates. Anal. Calcd for C₉₂H₁₅₂N₄O₉Rb₄ (M_r = 1800.08): C, 61.39; H, 8.51; N, 3.11. Found: C, 61.58; H, 8.55; N, 3.21. ^1H NMR (400 MHz, d_8 -THF, 24 °C): $\delta = 1.02$ (d, $^3J_{\text{HH}} = 7.2$ Hz, 12H, CH(CH₃)₂), 1.21 (d, $^3J_{\text{HH}} = 6.8$ Hz, 12H,

CH(CH₃)₂), 1.62 (s, 6H, NCCH₃), 1.76 (m, THF), 3.6 (m, THF), 3.7 (sep, $^3J_{\text{HH}} = 6.8$ Hz, 4H, CH(CH₃)₂), 5.9 (t, $^3J_{\text{HH}} = 7.6$ Hz, 2H, *para*-Ar), 6.61 (d, $^3J_{\text{HH}} = 7.6$ Hz, 4H, *meta*-Ar) ppm. ^{13}C NMR (100 MHz, d_8 -THF, 25 °C): $\delta = 19.1$ (NCCH₃), 24.5 (CH(CH₃)₂), 26.0 (CH(CH₃)₂), 26.3 (THF), 27.4 (CH(CH₃)₂), 68.2 (THF), 108.2 (*para*-Ar), 121.5 (NCCH₃), 123.0 (*meta*-Ar), 136.4 (*ortho*-Ar), 155.0 (*ipso*-Ar) ppm. **MS** (EI): m/z (rel. int.) = 633 (1%) [M⁺ – (H, 2 CH₃, C₄H₆, 2 THF)], 581 (1%) [M⁺ – (2 H, 9 CH₃, 2 THF)], 420 (1%) [M⁺ – (4 C₃H₇, C₄H₆, 3 THF)], 406 (89%) [^{Me2}DAD^{Dipp} + 2H], 361 (83%) [^{Me2}DAD^{Dipp} – C₃H₇], 202 (95%) [^{Me2}DAD^{Dipp} – (2 CH₃, 4 C₃H₇)], 806 (1%), 500 (1%), 391 (2%), 228 (5%), 214 (9%), 204 (100%), 188 (79%), 176 (73%), 173 (68%), 160 (90%). **IR** (ATR): $\nu = 3058$ w, 2951 m, 2863 m, 1575 m, 1525 w, , 1454 w, 1406 vs, 1328 vs, 1276 s, 1192 w, 1137 m, 1100 m, 1051 w,

1016 w, 942 w, 917 w, 834 w, 738 s, 691 w, 607 w, 569 m, 529 w, 498 w, 444 w cm^{-1} . Mp: 240 °C (dec).

$\{[\text{Cs}_2(\text{Me}_2\text{DAD}^{\text{Dipp}})(\text{THF})_4] \cdot \text{THF}\}_n$ (8)

A solution of **1** (2.0 g, 4.9 mmol) in 100 mL of THF was added into a flask containing cesium (1.33 g, 10 mmol, slightly in excess), and the resulting mixture was stirred overnight at r.t.



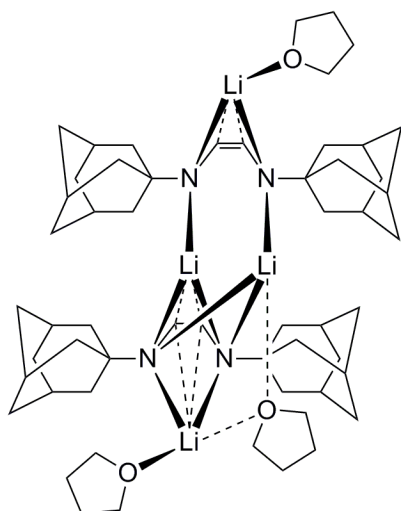
with a glass-coated stirring bar. The reaction mixture (turned from yellow to orange) was filtered, and the filtrate was concentrated in vacuum to approximately 20 mL before it was kept at 5 °C to yield **8** (4.06 g, 80%) as orange plates. Anal. Calcd for $\text{C}_{48}\text{H}_{80}\text{Cs}_2\text{N}_2\text{O}_5$ ($M_r = 1030.97$): C, 55.92; H, 7.82; N, 2.72. Found: C, 55.35; H, 7.44; N, 3.00. ^1H NMR (400 MHz, d_8 -THF, 22 °C): $\delta = 1.03$ (d, $^3J_{\text{HH}} = 6$ Hz, 12H, $\text{CH}(\text{CH}_3)_2$), 1.17 (d, $^3J_{\text{HH}} = 6.8$ Hz, 12H,

$\text{CH}(\text{CH}_3)_2$), 1.56 (s, 6H, CCH_3), 1.76 (m, THF), 3.6 (m, THF), 3.76 (sep, $^3J_{\text{HH}} = 6.8$ Hz, 4H, $\text{CH}(\text{CH}_3)_2$), 5.88 (t, $^3J_{\text{HH}} = 7.6$, 2H, *para*-Ar), 6.61 (d, $^3J_{\text{HH}} = 7.6$ Hz, 4H, *meta*-Ar) ppm. ^{13}C NMR (100 MHz, d_8 -THF, 23 °C): $\delta = 19.6$ (NCCH_3), 24.8 ($\text{CH}(\text{CH}_3)_2$), 25.4 ($\text{CH}(\text{CH}_3)_2$), 26.3 (THF), 27.2 ($\text{CH}(\text{CH}_3)_2$), 68.2 (THF), 108.1 (*para*-Ar), 121.7 (NCCH_3), 123.6 (*meta*-Ar), 136.0 (*ortho*-Ar), 154.0 (*ipso*-Ar) ppm. MS (EI): m/z (rel. int.) = 898 (1%) [$\text{M}^+ - 4 \text{CH}_3$], 806 (93%) [$\text{M}^+ - (\text{C}_6\text{H}_9, \text{THF})$], 761 (5%) [$\text{M}^+ - (2 \text{H}, \text{C}_6\text{H}_9, \text{C}_3\text{H}_7, \text{THF})$], 406 (72%) [$\text{Me}_2\text{DAD}^{\text{Dipp}} + 2\text{H}$], 361 (72%) [$\text{Me}_2\text{DAD}^{\text{Dipp}} - \text{C}_3\text{H}_7$], 202 (98%) [$\text{Me}_2\text{DAD}^{\text{Dipp}} - (2 \text{CH}_3, 4 \text{C}_3\text{H}_7)$], 1013 (1%), 848 (1%), 666 (1%), 604 (7%), 501 (15%), 417 (8%), 387 (8%), 335 (34%), 313 (6%), 285 (15%), 204 (100%), 188 (46%), 179 (54%), 160 (64%). IR (ATR): $\nu = 3061$ w, 3021 w, 2958 m, 2923 m, 2859 m, 2817 w, 1641 w, 1576 m, 1528 w, 1459 m, 1403 s, 1330 s, 1279 s, 1253 m, 1193 m, 1135 m, 1109 m, 1097 m, 1052 m, 1016 m, 986 m, 954 m, 927 m, 899 m, 881 w, 843 w, 817 w, 792 w, 760 m, 744 s, 721 m, 693 m, 642 m, 610 m, 590 m, 571 m, 559 m, 512 m, 491 m, 451 m, 441 m, 404 m, 376 m, 338 w, 309 m, 259 m, 223 m, 153 s, 145 s, 137 s, 80 vs, 65 vs cm^{-1} . Mp: 229 °C.

$\{[\text{Li}_2(\text{H}_2\text{DAD}^{\text{Ad}})]_2(\mu\text{-THF})(\text{THF})_2\}$ (9)

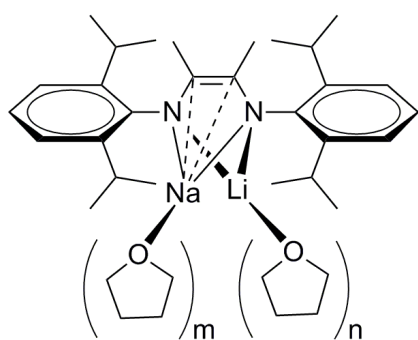
Lithium (43 mg, 6.2 mmol) was added to a solution of **3** (1.0 g, 3.1 mmol) in 100 mL of THF, and the resulting mixture was stirred at r.t. with a glass-coated stirring bar until all the lithium was consumed. The reaction mixture (turned from colorless to reddish yellow) was filtered,

and the filtrate was then evaporated to dryness in vacuum to yield **9** (1.25 g, 90%) as a yellow powder. Crystallization of **9** from toluene at r.t. yielded $[\{\text{Li}_2(\text{H}^2\text{DAD}^{\text{Ad}})\}_2(\mu\text{-THF})(\text{THF})_2] \cdot \text{C}_7\text{H}_8$ as yellow crystals. Anal. Calcd for $\text{C}_{56}\text{H}_{88}\text{Li}_4\text{N}_4\text{O}_3$ ($M_r = 893.09$): C, 75.31; H, 9.93; N, 6.27. Found: C, 75.19; H, 10.00; N, 6.25. $^1\text{H NMR}$ (400 MHz, d_8 -THF, 20 °C): $\delta = 1.57$ (s, 24 H, CHCH_2), 1.92 (s, 6H, CHCH_2), 5.37 (s, 2 H, CHNC) ppm. $^{13}\text{C NMR}$ (100 MHz, d_8 -THF, 21 °C): $\delta = 31.8$ (CHCH_2), 38.7 (CHCH_2), 48.6 (CHCH_2), 51.2 (CHNC), 111.3 (CHNC) ppm. $^7\text{Li NMR}$ (156 MHz, d_8 -Toluene, 22 °C): $\delta = 0.96$ ppm. **MS** (EI): m/z (rel. int.) = 513 (4%) [$\text{M}^+ - (2 \text{ Li}, \text{C}_{10}\text{H}_{15}\text{N}, 3 \text{ THF})$], 499 (15%) [$\text{M}^+ - (\text{H}, 2 \text{ Li}, \text{C}_{11}\text{H}_{16}\text{N}, 3 \text{ THF})$], 487 (6%) [$\text{M}^+ - (2 \text{ Li}, \text{C}_{12}\text{H}_{17}\text{N}, 3 \text{ THF})$], 361 (7%) [$\{\text{Li}(\text{H}^2\text{DAD}^{\text{Ad}})(\text{THF})\} - 3 \text{ CH}_2$], 326 (50%) [$\{\text{Li}(\text{H}^2\text{DAD}^{\text{Ad}})(\text{THF})_2\} - \text{C}_{10}\text{H}_{15}\text{N}$], 297 (93%) [$\text{H}^2\text{DAD}^{\text{Ad}} - \text{C}_2\text{H}_3$], 169 (4%) [$\{\text{Li}(\text{H}^2\text{DAD}^{\text{Ad}})\} - \text{C}_{11}\text{H}_{16}\text{N}$], 151 (65%) [$\text{Li}(\text{THF})_2$], 135 (100%) [$\text{C}_{10}\text{H}_{15}$], 79 (54%) [$\text{Li}(\text{THF})$], 577 (1%), 541 (1%), 525 (3%), 474 (1%), 406 (3%), 390 (3%), 364 (15%), 351 (8%), 340 (9%), 313 (12%), 256 (2%), 231 (5%), 217 (4%), 202 (17%), 191 (10%), 178 (31%), 164 (70%), 122 (12%), 108 (25%), 94 (98%), 91 (19%). **IR** (ATR): $\nu = 2975$ w, 2894 vs, 2841 s, 2673 w, 2653 w, 1665 w, 1546 w, 1517 w, 1446 m, 1389 m, 1377 m, 1343 w, 1301 m, 1279 w, 1262 w, 1244 w, 1209 w, 1182 w, 1150 vs, 1129 vs, 1095 s, 1062 vs, 1040 vs, 988 w, 975 w, 955 w, 931 w, 910 m, 831 w, 813 w, 777 w, 705 m, 677 w, 638 w, 620 w, 561 m, 522 m, 487 m, 442 m, 423 w, 411 w, 396 w, 307 m, 233 m, 182 w, 164 w, 138 w, 101 w, 91 w, 78 w, 57 m cm^{-1} . Mp: 232 °C.



[Na(THF) $_m$ ($\text{Me}_2\text{DAD}^{\text{Dipp}}$)Li(THF) $_n$] (10)

A solution of **1** (1.0 g, 2.5 mmol) in 100 mL of THF was added to sodium (138 mg, 6 mmol, in excess), and the resulting mixture was stirred overnight at r.t. with a glass-coated stirring bar. The reaction mixture (turned from yellow to orange) was filtered into a flask containing **1** (1.0 g, 2.5 mmol). The intensity of the color increased immediately, and the reaction mixture was further stirred overnight. Lithium (50 mg, 7.2 mmol, in excess) was added to the reaction mixture before it was stirred for 2 d. The reaction mixture was then filtered, and the filtrate was concentrated in vacuum to approximately 20 mL before it was kept at 5 °C to yield **10** (2.7 g, 93%) as red crystals. Anal.



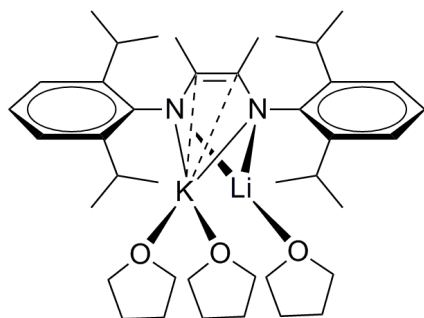
bar. The reaction mixture (turned from yellow to orange) was filtered into a flask containing **1** (1.0 g, 2.5 mmol). The intensity of the color increased immediately, and the reaction mixture was further stirred overnight. Lithium (50 mg, 7.2 mmol, in excess) was added to the reaction mixture before it was stirred for 2 d. The reaction mixture was then filtered, and the filtrate was concentrated in vacuum to

approximately 20 mL before it was kept at 5 °C to yield **10** (2.7 g, 93%) as red crystals. Anal.

Calcd for $C_{36}H_{56}LiN_2NaO_2$ ($M_r = 578.77$): C, 74.71; H, 9.75; N, 4.84. Found: C, 74.60; H, 9.67; N, 4.87. 1H NMR (400 MHz, d_8 -THF, 24 °C): $\delta = 1.03$ (d, $^3J_{HH} = 6.8$ Hz, 12H, $CH(CH_3)_2$), 1.20 (d, $^3J_{HH} = 6.8$ Hz, 12H, $CH(CH_3)_2$), 1.58 (s, 6H, $NCCH_3$), 1.76 (m, THF), 3.6 (m, THF), 3.57 – 3.64 (4H, $CH(CH_3)_2$), 6.38 (t, $^3J_{HH} = 7.6$ Hz, 2H, *para*-Ar), 6.78 (d, $^3J_{HH} = 7.6$ Hz, 4H, *meta*-Ar) ppm. ^{13}C NMR (100 MHz, d_8 -THF, 23 °C): $\delta = 16.8$ ($NCCH_3$), 24.0 ($CH(CH_3)_2$), 25.4 ($CH(CH_3)_2$), 26.3 (THF), 27.6 ($CH(CH_3)_2$), 68.2 (THF), 115.3 (*para*-Ar), 122.3 ($NCCH_3$), 121.2 (*meta*-Ar), 141.2 (*ortho*-Ar), 155.5 (*ipso*-Ar) ppm. 7Li NMR (156 MHz, d_8 -THF, 23 °C): $\delta = 0.43$ ppm. MS (EI): m/z (rel. int.) = 451 (2%) [$M^+ - (2 CH_3, 2 C_3H_7, C_4H_6)$], 432 (6%) [$M^+ - (4 CH_3, 2 C_3H_7)$], 406 (96%) [$^{Me_2}DAD^{Dipp} + 2H$], 361 (98%) [$^{Me_2}DAD^{Dipp} - C_3H_7$], 202 (100%) [$^{Me_2}DAD^{Dipp} - (2 CH_3, 4 C_3H_7)$], 489 (1%), 478 (4%), 334 (55%), 312 (10%), 284 (27%), 216 (18%), 188 (65%), 160 (85%). IR (ATR): $\nu = 3037$ w, 2955 s, 2865 m, 1663 w, 1581 m, 1459 m, 1414 vs, 1378 m, 1356 m, 1307 s, 1241 vs, 1149 m, 1139 m, 1112 m, 1045 s, 980 w, 937 m, 891 s, 854 m, 823 w, 767 s, 721 w, 668 w, 618 w, 597 m, 574 m, 558 s, 521 m, 499 m, 450 m, 424 m, 375 w, 310 m, 272 s, 199 s, 174 s, 139 s, 106 m, 65 s cm^{-1} . Mp: 110 °C.

[K(THF) $_2$ ($^{Me_2}DAD^{Dipp}$)Li(THF)] (11)

A solution of **1** (1.0 g, 2.5 mmol) in 100 mL of THF was added to potassium (235 mg, 6 mmol, in excess), and the resulting mixture was stirred overnight at r.t. with a glass-coated



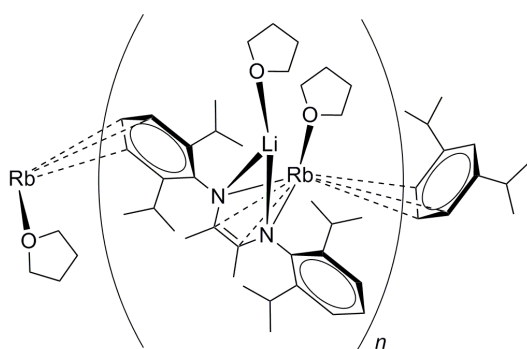
stirring bar. The reaction mixture (turned from yellow to bright red) was filtered into a flask containing **1** (1.0 g, 2.5 mmol). The intensity of the color increased immediately, and the reaction mixture was further stirred overnight. Lithium (50 mg, 7.2 mmol, in excess) was added to the reaction mixture before it was stirred for 2 d. The reaction

mixture was then filtered, and the filtrate was concentrated in vacuum to approximately 20 mL before it was kept at 5 °C to yield **11** (2.9 g, 87%) as orange blocks. Anal. Calcd for $C_{40}H_{64}KLiN_2O_3$ ($M_r = 666.99$): C, 72.03; H, 9.67; N, 4.20. Found: C, 72.62; H, 9.42; N, 4.68. 1H NMR (400 MHz, d_8 -THF, 20 °C): $\delta = 1.01$ (d, $^3J_{HH} = 7.2$ Hz, 12H, $CH(CH_3)_2$), 1.20 (d, $^3J_{HH} = 6.8$ Hz, 12H, $CH(CH_3)_2$), 1.57 (s, 6H, $NCCH_3$), 1.76 (m, THF), 3.6 (m, THF), 3.70 (sep, $^3J_{HH} = 6.8$ Hz, 4H, $CH(CH_3)_2$), 6.27 (t, $^3J_{HH} = 7.6$ Hz, 2H, *para*-Ar), 6.74 (d, $^3J_{HH} = 7.2$ Hz, 4H, *meta*-Ar) ppm. ^{13}C NMR (100 MHz, d_8 -THF, 21 °C): $\delta = 16.9$ ($NCCH_3$), 24.0 ($CH(CH_3)_2$), 25.5 ($CH(CH_3)_2$), 26.3 (THF), 27.6 ($CH(CH_3)_2$), 68.2 (THF), 113.8 (*para*-Ar), 121.2 ($NCCH_3$), 122.3 (*meta*-Ar), 140.1 (*ortho*-Ar), 155.7 (*ipso*-Ar) ppm. 7Li NMR (156

MHz, d_8 -THF, 20 °C): δ = 0.31 ppm. **MS** (EI): m/z (rel. int.) = 445 (1%) [$M^+ - (2 \text{ H}, 5 \text{ CH}_3, 2 \text{ THF})$], 406 (70%) [$^{\text{Me}_2\text{DAD}^{\text{Dipp}}} + 2\text{H}$], 361 (22%) [$^{\text{Me}_2\text{DAD}^{\text{Dipp}}} - \text{C}_3\text{H}_7$], 202 (100%) [$^{\text{Me}_2\text{DAD}^{\text{Dipp}}} - (2 \text{ CH}_3, 4 \text{ C}_3\text{H}_7)$], 478 (1%), 334 (10%), 312 (3%), 284 (5%), 216 (4%), 188 (35%), 160 (43%). **IR** (ATR): ν = 3042 w, 2956 m, 2931 m, 2864 m, 2698 w, 1642 w, 1578 m, 1538 w, 1459 m, 1410 vs, 1377 m, 1352 m, 1309 s, 1249 vs, 1152 m, 1136 m, 1112 s, 1044 s, 984 w, 946 m, 895 s, 853 m, 838 m, 822 m, 760 vs, 725 m, 697 m, 668 m, 615 m, 591 s, 577 s, 559 s, 502 s, 439 s, 423 s, 315 m, 263 s, 230 s, 106 vs, 80 vs, 61 vs cm^{-1} . Mp: 76 °C.

{[Rb(THF)($^{\text{Me}_2\text{DAD}^{\text{Dipp}}})\text{Li(THF)]} \cdot \text{THF}$] $_n$ (12**)**

A solution of **1** (1.0 g, 2.5 mmol) in 100 mL of THF was added to rubidium (513 mg, 6 mmol, in excess), and the resulting mixture was stirred overnight at r.t. with a glass-coated stirring



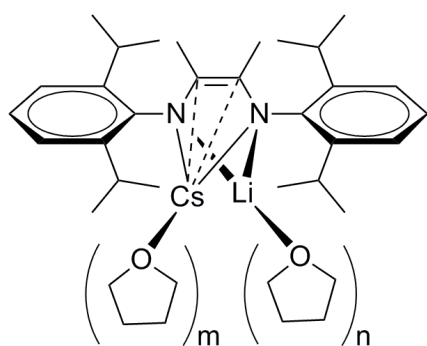
bar. The reaction mixture (turned from yellow to bright red) was filtered into a flask containing **1** (1.0 g, 2.5 mmol). The intensity of the color increased immediately, and the reaction mixture was further stirred overnight. Lithium (50 mg, 7.2 mmol, in excess) was added to the reaction mixture before it was stirred for 2 d. The reaction

mixture was then filtered, and the filtrate was concentrated in vacuum to approximately 20 mL before it was kept at -32 °C to yield **12** (3.2 g, 90%) as red crystals. Anal. Calcd for $\text{C}_{40}\text{H}_{64}\text{LiN}_2\text{O}_3\text{Rb}$ ($M_r = 713.36$): C, 67.35; H, 9.04; N, 3.93. Found: C, 67.27; H, 9.23; N, 3.94. **^1H NMR** (400 MHz, d_8 -THF, 23 °C): δ = 1.01 (d, $^3J_{\text{HH}} = 6.8$ Hz, 12H, $\text{CH}(\text{CH}_3)_2$), 1.19 (d, $^3J_{\text{HH}} = 6.8$ Hz, 12H, $\text{CH}(\text{CH}_3)_2$), 1.53 (s, 6H, CCH_3), 1.76 (m, THF), 3.6 (m, THF), 3.78 (sep, $^3J_{\text{HH}} = 6.8$ Hz, 4H, $\text{CH}(\text{CH}_3)_2$), 6.25 (t, $^3J_{\text{HH}} = 7.6$, 2H, *para*-Ar), 6.73 (d, $^3J_{\text{HH}} = 7.6$ Hz, 4H, *meta*-Ar) ppm. **^{13}C NMR** (100 MHz, d_8 -THF, 24 °C): δ = 17.0 (NCCH_3), 24.2 ($\text{CH}(\text{CH}_3)_2$), 25.5 ($\text{CH}(\text{CH}_3)_2$), 26.3 (THF), 27.4 ($\text{CH}(\text{CH}_3)_2$), 68.2 (THF), 113.6 (*para*-Ar), 121.2 (NCCH_3), 122.3 (*meta*-Ar), 140.1 (*ortho*-Ar), 155.7 (*ipso*-Ar) ppm. **^7Li NMR** (156 MHz, d_8 -THF, 24 °C): δ = 2.36 ppm. **MS** (EI): m/z (rel. int.) = 406 (88%) [$^{\text{Me}_2\text{DAD}^{\text{Dipp}}} + 2\text{H}$], 361 (98%) [$^{\text{Me}_2\text{DAD}^{\text{Dipp}}} - \text{C}_3\text{H}_7$], 202 (100%) [$^{\text{Me}_2\text{DAD}^{\text{Dipp}}} - (2 \text{ CH}_3, 4 \text{ C}_3\text{H}_7)$], 732 (1%), 671 (1%), 633 (4%), 606 (3%), 534 (3%), 500 (2%), 417 (3%), 334 (3%), 268 (1%), 228 (4%), 214 (7%), 188 (83%), 160 (90%). **IR** (ATR): ν = 3060 w, 2958 vs, 2865 s, 1659 w, 1640 w, 1580 m, 1539 m, 1516 m, 1460 s, 1408 vs, 1382 s, 1357 s, 1318 vs, 1254 vs, 1185 m, 1154 m, 1137 m, 1116 m, 1014 m, 1003 w, 950 w, 934 w, 885 m, 864 m, 819 w, 785 s, 761 s, 740 s,

665 m, 637 m, 615 m, 596 m, 578 m, 556 m, 502 m, 438 s, 372 w, 331 m, 268 m, 175 w, 161 w, 144 m, 105 m, 78 s, 64 m cm⁻¹. Mp: 172 °C.

[Cs(THF)_m(Me²DAD^{Dipp})Li(THF)_n] (13)

A solution of **1** (1.0 g, 2.5 mmol) in 100 mL of THF was added to cesium (797 mg, 6 mmol, in excess), and the resulting mixture was stirred overnight at r.t. with a glass-coated stirring



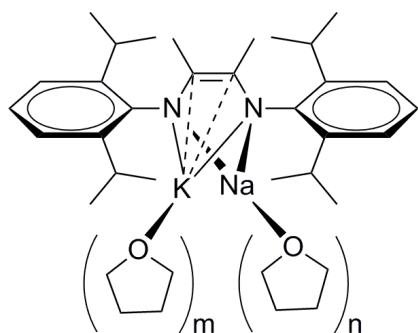
bar. The reaction mixture (turned from yellow to orange) was filtered into a flask containing **1** (1.0 g, 2.5 mmol). The intensity of the color increased immediately, and the reaction mixture was further stirred overnight. Lithium (50 mg, 7.2 mmol, in excess) was added to the reaction mixture before it was stirred for 2 d. The reaction mixture was then filtered, and the filtrate was concentrated in

vacuum to approximately 20 mL before it was kept at -32 °C to yield **13** (2.5 g, 92%) as red crystals. Anal. Calcd for C₂₈H₄₀CsLiN₂ (M_r = 544.48): C, 61.77; H, 7.40; N, 5.15. Found: C, 61.74; H, 7.50; N, 5.14. ¹H NMR (400 MHz, d₈-THF, 22 °C): δ = 1.01 (d, ³J_{HH} = 6.8 Hz, 12H, CH(CH₃)₂), 1.18 (d, ³J_{HH} = 6.8 Hz, 12H, CH(CH₃)₂), 1.47 (s, 6H, NCCH₃), 1.72 (s, THF), 3.56 (s, THF), 3.87 (sep, ³J_{HH} = 6.8 Hz, 4H, CH(CH₃)₂), 6.26 (t, ³J_{HH} = 7.6 Hz, 2H, *para*-Ar), 6.72 (d, ³J_{HH} = 7.2 Hz, 4H, *meta*-Ar) ppm. ¹³C NMR (100 MHz, d₈-THF, 23 °C): δ = 17.2 (NCCH₃), 24.5 (CH(CH₃)₂), 25.4 (CH(CH₃)₂), 26.3 (THF), 27.3 (CH(CH₃)₂), 68.2 (THF), 113.8 (*para*-Ar), 121.4 (NCCH₃), 122.3 (*meta*-Ar), 140.3 (*ortho*-Ar), 155.6 (*ipso*-Ar) ppm. ⁷Li NMR (156 MHz, d₈-THF, 20 °C): δ = 2.29 ppm. MS (EI): m/z (rel. int.) = 406 (66%) [Me²DAD^{Dipp} + 2H], 361 (95%) [Me²DAD^{Dipp} - C₃H₇], 202 (100%) [Me²DAD^{Dipp} - (2 CH₃, 4 C₃H₇)], 579 (1%), 534 (2%), 500 (10%), 478 (1%), 430 (1%), 416 (6%), 347 (35%), 334 (13%), 312 (4%), 284 (10%), 231 (6%), 219 (14%), 188 (63%), 177 (77%), 162 (88%). IR (ATR): ν = 3058 w, 2957 s, 2864 m, 1663 w, 1579 m, 1532 m, 1460 s, 1406 vs, 1381 s, 1355 s, 1319 vs, 1252 vs, 1191 m, 1136 m, 1109 s, 1055 s, 1017 m, 950 m, 933 m, 885 m, 836 m, 782 s, 760 s, 740 s, 659 m, 634 m, 615 s, 595 s, 575 s, 557 s, 502 vs, 439 vs, 316 w, 266 m, 226 m, 207 m, 145 s, 103 vs, 84 vs, 59 s cm⁻¹. Mp: 211 °C.

[K(THF)_m(Me²DAD^{Dipp})Na(THF)_n] (14)

A solution of **1** (1.0 g, 2.5 mmol) in 100 mL of THF was added to potassium (235 mg, 6 mmol, in excess), and the resulting mixture was stirred overnight at r.t. with a glass-coated stirring bar. The reaction mixture (turned from yellow to bright red) was filtered into a flask

containing **1** (1.0 g, 2.5 mmol). The intensity of the color increased immediately, and the reaction mixture was further stirred overnight. Sodium (166 mg, 7.2 mmol, in excess) was



added to the reaction mixture before it was stirred for 2 d.

The reaction mixture was then filtered, and the filtrate was concentrated in vacuum to approximately 20 mL before it was kept at 5 °C to yield **14** (3.8 g, 92%) as red crystals.

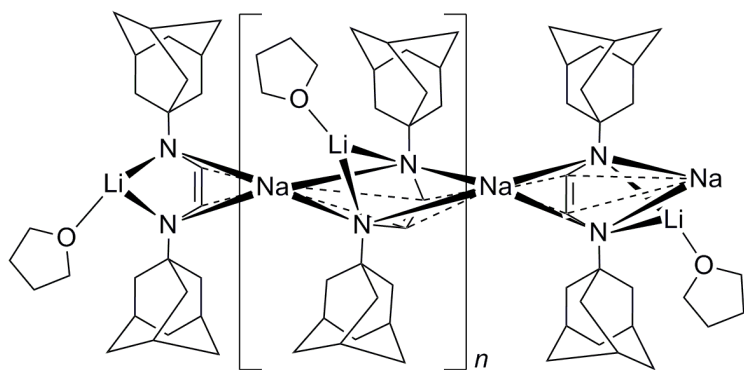
Anal. Calcd for $C_{48}H_{80}KN_2NaO_5$ ($M_r = 827.25$): C, 69.69; H, 9.75; N, 3.39. Found: C, 68.92; H, 9.57; N, 3.33. 1H NMR (400 MHz, d_8 -THF, 21 °C): $\delta = 1.03$ (d, $^3J_{HH} = 6.8$

Hz, 12H, $CH(CH_3)_2$), 1.21 (d, $^3J_{HH} = 6.8$ Hz, 12H, $CH(CH_3)_2$), 1.65 (s, 6H, $NCCH_3$), 1.76 (m, THF), 3.6 (m, THF), 3.7 (m, br, 4H, $CH(CH_3)_2$), 5.97 and 6.10 (br, 2H, *para*-Ar), 6.66 (br, 4H, *meta*-Ar) ppm. ^{13}C NMR (100 MHz, d_8 -THF, 23 °C): $\delta = 18.2$ (br) ($NCCH_3$), 24.2 ($CH(CH_3)_2$), 25.2 ($CH(CH_3)_2$), 26.3 (THF), 27.4 ($CH(CH_3)_2$), 68.2 (THF), 109.1 and 111.0 (br) (*para*-Ar), 121.1 ($NCCH_3$), 122.7 (*meta*-Ar), 137.2 and 138.6 (br) (*ortho*-Ar), 156.4 and 155.6 (br) (*ipso*-Ar) ppm. MS (EI): m/z (rel. int.) = 406 (30%) [$Me_2DAD^{Dipp} + 2H$], 361 (65%) [$Me_2DAD^{Dipp} - C_3H_7$], 202 (100%) [$Me_2DAD^{Dipp} - (2 CH_3, 4 C_3H_7)$], 478 (2%), 417 (1%), 347 (4%), 334 (22%), 312 (6%), 284 (10%), 235 (4%), 217 (5%), 188 (20%), 168 (45%), 160 (34%). IR (ATR): $\nu = 3034$ w, 2957 m, 2865 m, 1659 w, 1642 w, 1577 m, 1532 w, 1459 m, 1402 vs, 1379 m, 1318 vs, 1267 vs, 1251 vs, 1197 m, 1133 m, 1111 m, 1098 m, 1050 s, 1012 m, 947 m, 916 m, 895 m, 844 m, 818 m, 792 m, 750 s, 724 m, 692 m, 662 m, 638 m, 615 m, 568 s, 517 m, 491 m, 450 m, 383 m, 319 m, 306 m, 263 s, 241 s, 158 s, 135 vs, 120 vs, 83 vs, 68 s, 59 s cm^{-1} . Mp: 248 °C (dec).

$\{[Na(^{H^2}DAD^{Ad})Li(THF)]_4 \cdot THF\}_n$ (**15**)

A solution of **3** [1.0 g (3.1 mmol) in 100 mL of toluene and 2 mL of THF] was added to sodium (71 mg, 3.1 mmol), and the resulting mixture was stirred at r.t. with a glass-coated stirring bar until all the sodium was consumed. The reaction mixture turned from colorless to red. Lithium (28 mg, 4 mmol, in excess) was added to the reaction mixture, and it was further stirred for 2 d. The reaction mixture (turned from red to orange) was filtered, and the filtrate was concentrated in vacuum to approximately 20 mL before it was kept at 5 °C to yield **15** (1.25 g, 91%) as orange crystals. Anal. Calcd for $C_{108}H_{168}Li_4N_8Na_4O_5$ ($M_r = 1778.21$): C, 72.95; H, 9.52; N, 6.30. Found: C, 73.05; H, 9.53; N, 6.40. 1H NMR (400 MHz, d_8 -THF, 21 °C): $\delta = 1.56$ (s, br, 24 H, $CHCH_2$), 1.93 (s, br, 6H, $CHCH_2$), 7.05, 7.07, 7.09, 7.10, 7.12, 7.16, 7.17, 7.19 (s, 2 H, $CHNC$) ppm. ^{13}C NMR (100 MHz, d_8 -THF, 21 °C): $\delta = 31.6$ (br,

CHCH₂), 38.4 (br, CHCH₂), 47.4 (br, CHCH₂), 51.8 (br, CHNC), 126.0, 128.1, 128.7, 128.8, 129.6 (CHNC) ppm. **MS** (EI): m/z (rel. int.) = 433 (3%) [$M^+ - (2 \text{ H, CH}_2)$], 406 (12%) [$M^+ -$

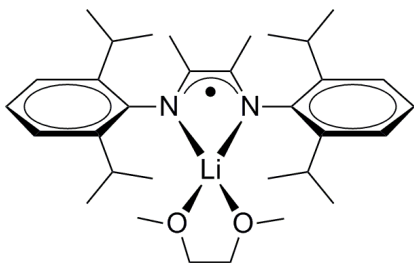


(H, 3 CH₂), 383 (9%) [$M^+ - (\text{H, 3 CH}_2, \text{Na})$], 361 (65%) [$M^+ - (3 \text{ CH}_2, 2 \text{ Na})$], 340 (10%) [$M^+ - (\text{CH}_2, \text{Na, THF})$], 326 (7%) [$M^+ - (2 \text{ CH}_2, \text{Na, THF})$], 297 (28%) [$^{H_2}\text{DAD}^{\text{Ad}} - \text{C}_2\text{H}_3$], 285 (7%) [$^{H_2}\text{DAD}^{\text{Ad}} - (\text{CH, 2 CH}_2)$], 258

(10%) [$^{H_2}\text{DAD}^{\text{Ad}} - (2 \text{ CH, 3 CH}_2)$], 202 (100%) [$^{H_2}\text{DAD}^{\text{Ad}} - (5 \text{ CH}_2, 4 \text{ CH})$], 188 (11%) [$^{H_2}\text{DAD}^{\text{Ad}} - (\text{H, C}_{10}\text{H}_{15}\text{N})$], 160 (21%) [$^{H_2}\text{DAD}^{\text{Ad}} - (\text{H, C}_{11}\text{H}_{16}\text{N})$], 135 (59%) [$\text{C}_{10}\text{H}_{15}\text{N}$], 79 (6%) [Li (THF)], 392 (2%), 378 (3%), 343 (2%), 176 (7%), 164 (6%), 151 (21%), 122 (3%), 108 (5%), 107 (3%), 94 (64%), 91 (9%). **IR** (ATR): $\nu = 2899$ vs, 2845 s, 2656 w, 2114 w, 1880 w, 1665 w, 1530 w, 1450 m, 1382 w, 1355 w, 1342 w, 1308 w, 1286 w, 1244 w, 1224 w, 1152 m, 1096 m, 1063 w, 1041 w, 995 w, 976 w, 932 w, 905 w, 887 w, 813 w, 768 w, 733 w, 702 w, 634 w, 607 w, 582 m, 526 w, 420 vs, 345 w, 273 m, 236 w, 190 m, 157 w, 118 m, 102 w, 82 m, 65 w cm^{-1} . Mp: 187 °C.

[Li(^{Me}₂DAD^{Dipp})(DME)] (16)

Lithium (35 mg, 5 mmol, slightly in excess) was added to a solution of **1** (2.0 g, 4.9 mmol) in DME (100 mL). The mixture was stirred at r.t. with a glass-coated stirring bar until all the lithium was consumed and then the mixture was filtered.

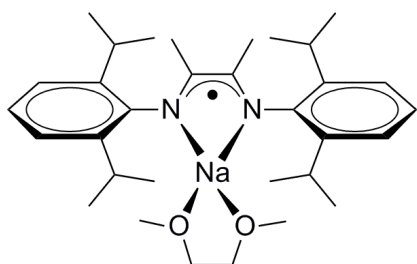


The deep red filtrate was concentrated in vacuum to approximately 30 mL. Crystallization at 5 °C yielded **16** (2.2 g, 88%) as deep red blocks. Anal. Calcd for C₃₂H₅₀LiN₂O₂ (501.69): C, 76.61; H, 10.05; N, 5.58.

Found: C, 76.58; H, 10.22; N, 5.64. **MS** (EI): m/z (rel. int.) = 458 (2%) [$M^+ - \text{C}_3\text{H}_7$], 415 (2%) [$M^+ - 2 \text{ C}_3\text{H}_7$], 406 (42%) [$^{\text{Me}_2}\text{DAD}^{\text{Dipp}} + 2\text{H}$], 361 (95%) [$^{\text{Me}_2}\text{DAD}^{\text{Dipp}} - \text{C}_3\text{H}_7$], 202 (100%) [$^{\text{Me}_2}\text{DAD}^{\text{Dipp}} - (2 \text{ CH}_3, 4 \text{ C}_3\text{H}_7)$], 589 (1%), 524 (1%), 487 (1%), 389 (1%), 345 (1%), 319 (1%), 247 (2%), 214 (2%), 188 (20%), 172 (18%), 160 (67%), 144 (22%), 133 (11%). **IR** (ATR): $\nu = 3050$ w, 2957 s, 2868 m, 1655 w, 1594 m, 1547 w, 1511 w, 1452 s, 1428 s, 1393 vs, 1316 s, 1244 vs, 1205 m, 1151 m, 1117 m, 1065 s, 1029 m, 1016 m, 978 m, 933 w, 862 m, 811 w, 779 s, 750 m, 733 m, 666 w, 627 w, 583 w, 541 w, 438 m cm^{-1} . Mp: 135 °C.

[Na^{(Me₂DAD^{Dipp})(DME)] (17)}

Sodium (115 mg, 5 mmol, slightly in excess) was added to a solution of **1** (2.0 g, 4.9 mmol) in DME (100 mL). The mixture was stirred at r.t. with a glass-coated stirring bar until all the



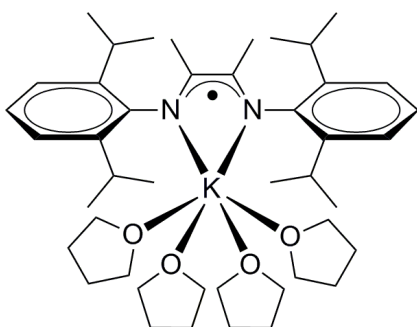
sodium was consumed and the mixture was then filtered.

The deep red filtrate was concentrated in vacuum to a black oil. *n*-Pentane (20 mL) was added to the dark oil, and the solution was mixed well before it was kept at 5 °C to yield **17** (1.2 g, 47%) as deep red crystals. Anal. Calcd for

C₃₂H₅₀N₂NaO₂ (517.74): C, 74.23; H, 9.73; N, 5.41. Found: C, 74.69; H, 9.26; N, 5.48. **MS** (EI): *m/z* (rel. int.) = 487 (1%) [M⁺ - 2 CH₃], 416 (1%) [M⁺ - (CH₃, 2 C₃H₇)], 406 (18%) [Me₂DAD^{Dipp} + 2H], 361 (100%) [Me₂DAD^{Dipp} - C₃H₇], 319 (3%) [M⁺ - (CH₃, 3 C₃H₇, C₄H₆)], 202 (99%) [Me₂DAD^{Dipp} - (2 CH₃, 4 C₃H₇)], 522 (1%), 389 (2%), 272 (1%), 214 (5%), 186 (40%), 172 (44%), 160 (84%), 144 (50%), 133 (26%). **IR** (ATR): ν = 3062 w, 2957 s, 2927 m, 2867 m, 1662 s, 1631 w, 1590 m, 1522 s, 1464 m, 1438 s, 1382 m, 1363 s, 1321 m, 1253 m, 1206 m, 1182 m, 1121 s, 1102 m, 1057 m, 1042 m, 984 m, 933 m, 904 s, 882 s, 860 s, 820 m, 792 vs, 781 m, 762 m, 738 m, 716 m, 688 m, 622 m, 526 m, 465 m, 428 m, 412 m cm⁻¹. Mp: 130 °C.

[K^{(Me₂DAD^{Dipp})(THF)₄] (18)}

Potassium (193 mg, 5 mmol, slightly in excess) was added to a solution of **1** (2.0 g, 4.9 mmol) in THF (100 mL). The mixture was stirred at r.t. with a glass-coated stirring bar until all the



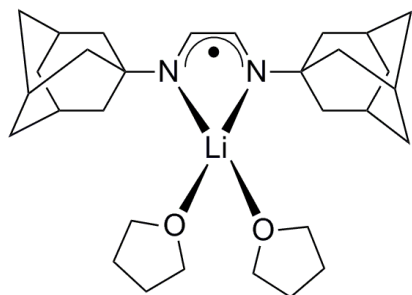
potassium was consumed and the mixture was then filtered. The deep red filtrate was concentrated in vacuum to a black oil. *n*-Pentane (20 mL) was added to the dark oil, and the solution was mixed well before it was kept at 5 °C to yield **18** (3.3 g, 92%) as deep red crystals. Anal. Calcd for C₄₄H₇₂KN₂O₄ (732.15): C, 72.18; H, 9.91; N, 3.83.

Found: C, 72.41; H, 9.12; N, 3.72. **MS** (EI): *m/z* (rel. int.) = 616 (1%) [M⁺ - (C₃H₇, THF)], 576 (2%) [M⁺ - (CH₃, 2 C₃H₇, C₄H₆)], 500 (6%) [M⁺ - (CH₃, 3 THF)], 406 (42%) [Me₂DAD^{Dipp} + 2 H], 361 (95%) [Me₂DAD^{Dipp} - C₃H₇], 202 (100%) [Me₂DAD^{Dipp} - (2 CH₃, 4 C₃H₇)], 66 (1%), 534 (1%), 478 (1%), 450 (1%), 334 (12%), 316 (7%), 284 (6%), 234 (2%), 186 (58%), 172 (61%), 160 (83%), 144 (67%), 133 (51%). **IR** (ATR): ν = 3063 w, 2957 s, 2927 m, 2867 m, 1659 w, 1630 w, 1590 m, 1523 m, 1459 s, 1435 s, 1420 m, 1402 m, 1380 m, 1362 s, 1313 m, 1254 m, 1242 m, 1203 m, 1184 m, 1142 m, 1123 s, 1105 m, 1057 m, 1042 m,

999 w, 967 w, 934 m, 882 w, 851 w, 832 w, 820 m, 785 s, 762 vs, 737 m, 722 m, 699 m, 689 m, 668 w, 638 w, 604 m, 580 w, 530 w, 511 w, 466 w, 431 m, 412 m, 354 m, 252 s, 164 vs, 109 s, 80 vs, 65 vs cm^{-1} . Mp: 110 °C.

$[\text{Li}(\text{H}^2\text{DAD}^{\text{Ad}})(\text{THF})_2]$ (**19**)

Lithium (21 mg, 3.1 mmol) was added to a solution of **3** (1.0 g, 3.1 mmol) in 100 mL of THF, and the resulting mixture was stirred at r.t. with a glass-coated stirring bar until all the lithium



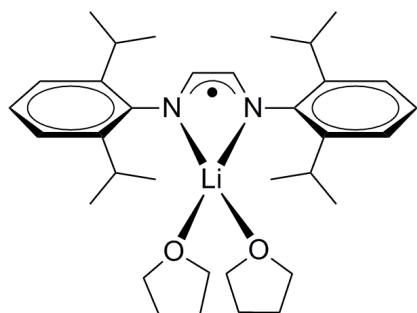
was consumed. The reaction mixture (turned from colorless to red) was filtered, and the filtrate was concentrated in vacuum to approximately 20 mL before it was kept at 5 °C to yield **19** (1.36 g, 92%) as orange crystals. Anal. Calcd for $\text{C}_{30}\text{H}_{48}\text{LiN}_2\text{O}_2$ ($M_r = 475.66$): C, 75.75; H, 10.17; N, 5.89. Found: C, 75.47; H, 10.02; N, 5.80. $^1\text{H NMR}$ (400

MHz, d_8 -THF, 25 °C), $^{13}\text{C NMR}$ (100 MHz, d_8 -THF, 22 °C), and $^7\text{Li NMR}$ (156 MHz, d_8 -THF, 25 °C): because of the paramagnetic properties of the radical anionic DAD, it was not possible to obtain any meaningful $^1\text{H NMR}$, $^{13}\text{C NMR}$, and $^7\text{Li NMR}$. **MS** (EI): m/z (rel. int.) = 433 (4%) [$\text{M}^+ - \text{C}_3\text{H}_5$], 361 (2%) [$\text{M}^+ - (\text{C}_3\text{H}_5, \text{THF})$], 326 (48%) [$\text{M}^+ - \text{C}_{10}\text{H}_{15}\text{N}$], 297 (93%) [$\text{H}^2\text{DAD}^{\text{Ad}} - \text{C}_2\text{H}_3$], 254 (10%) [$\text{M}^+ - (\text{C}_{11}\text{H}_{16}\text{N}, \text{THF},)$], 189 (18%) [$\text{H}^2\text{DAD}^{\text{Ad}} - \text{C}_{10}\text{H}_{15}$], 169 (10%) [$\text{M}^+ - (\text{C}_{11}\text{H}_{16}\text{N}, 2 \text{ THF})$], 162 (28%) [$\text{H}^2\text{DAD}^{\text{Ad}} - \text{C}_{11}\text{H}_{16}\text{N}$], 135 (100%) [$(\text{C}_{10}\text{H}_{15})$], 79 (53%) [$\text{Li} (\text{THF})$], 72 (25%) [THF], 350 (3%), 334 (3%), 267 (87%), 240 (6%), 202 (6%), 191 (22%), 164 (73%), 107 (21%), 98 (36%), 94 (76%). **IR** (ATR): $\nu = 2972$ w, 2899 s, 2845 m, 2656 w, 1664 w, 1629 w, 1538 w, 1473 m, 1449 m, 1365 w, 1342 w, 1302 m, 1263 w, 1228 s, 1179 m, 1127 m, 1093 m, 1047 s, 981 w, 953 w, 937 w, 906 m, 812 m, 761 m, 720 w, 669 w, 623 m, 602 m, 485 s, 470 s, 457 s, 433 s, 410 s, 359 s, 312 m, 278 m, 250 w, 212 w, 199 w, 165 m, 147 m, 129 m, 106 m, 88 s, 75 s, 64 s cm^{-1} . Mp: 219 °C.

$[\text{Li}(\text{H}^2\text{DAD}^{\text{Dipp}})(\text{THF})_2]$ (**20**)

Lithium (19 mg, 2.7 mmol) was added to a solution of **2** (1 g, 2.7 mmol) in 50 mL of THF, and the resulting mixture was stirred at r.t. with a glass-coated stirring bar until all the lithium was consumed. The reaction mixture (turned from yellow to deep red) was filtered, and the filtrate was then concentrated in vacuum to a black oil. The black oil was dried in vacuum at -196 °C to yield **20** (1.35 g, 95%) as dark red powder. Anal. Calcd for $\text{C}_{34}\text{H}_{52}\text{LiN}_2\text{O}_2$ ($M_r = 527.73$): C, 77.38; H, 9.93; N, 5.31. Found: C, 77.41; H, 9.88; N, 5.40. $^1\text{H NMR}$ (400 MHz, d_8 -THF, 20 °C) and $^{13}\text{C NMR}$ (100 MHz, d_8 -THF, 23 °C): Because of the strongly

paramagnetic nature of the radical anionic DAD, it was not possible to obtain any meaningful ^1H NMR and ^{13}C NMR. ^7Li NMR (155 MHz, d_8 -THF, 20 °C): $\delta = 1.24$ ppm. MS (EI): m/z

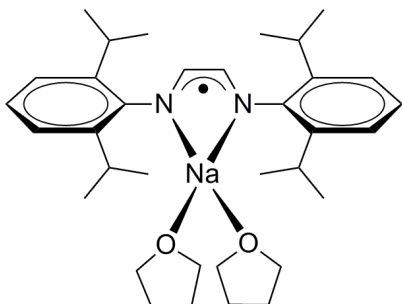


(rel. Int.) = 378 (95%) [$\text{H}^2\text{DAD}^{\text{Dipp}}$], 361 (8%) [$\text{H}^2\text{DAD}^{\text{Dipp}} - \text{CH}_3$], 333 (100%) [$\text{H}^2\text{DAD}^{\text{Dipp}} - \text{C}_3\text{H}_7$], 202 (15%) [$\text{H}^2\text{DAD}^{\text{Dipp}} - (2 \text{ H}, 4 \text{ C}_3\text{H}_7)$], 534 (1%), 500 (1%), 449 (1%), 393 (1%), 319 (1%), 297 (1%), 275 (1%), 229 (2%), 188 (80%), 162 (72%). IR (ATR): $\nu = 3063$ w, 2958 s, 2927 m, 2866 m, 1660 w, 1626 w, 1588 w, 1543 w, 1457 vs, 1432 vs, 1381 w, 1361 w, 1317 s, 1265 vs, 1176 w,

1158 w, 1098 m, 1050 s, 962 w, 925 m, 893 m, 842 w, 794 s, 755 vs, 671 w, 609 w, 594 w, 528 w, 438 s, 420 s, 379 w, 342 m, 272 w, 240 w, 161 w, 129 w, 114 w, 87 w, 68 m, 56 m cm^{-1} . Mp: 91 °C.

[Na($\text{H}^2\text{DAD}^{\text{Dipp}}$)(THF) $_2$] (**21**)

Sodium (62 mg, 2.7 mmol) was added to a solution of **2** (1 g, 2.7 mmol) in 50 mL of THF, and the resulting mixture was stirred at r.t. with a glass-coated stirring bar until all the sodium

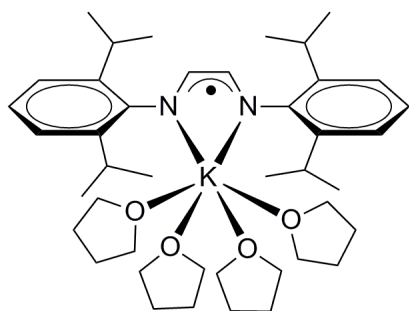


was consumed. The reaction mixture (turned from yellow to deep red) was filtered, and the filtrate was then concentrated in vacuum to a black oil. The black oil was dried in vacuum at -196 °C to yield **21** (1.4 g, 96%) as dark red powder. Anal. Calcd for $\text{C}_{34}\text{H}_{50}\text{N}_2\text{NaO}_2$ ($M_r = 543.78$): C, 75.10; H, 9.64; N, 5.15. Found: C, 75.08; H, 9.54; N, 5.20. ^1H NMR

(400 MHz, d_8 -THF, 22 °C) and ^{13}C NMR (100 MHz, d_8 -THF, 21 °C): because of the strongly paramagnetic nature of the radical anionic DAD, it was not possible to obtain any meaningful ^1H NMR and ^{13}C NMR. MS (EI): m/z (rel. Int.) = 378 (75%) [$\text{H}^2\text{DAD}^{\text{Dipp}}$], 361 (7%) [$\text{H}^2\text{DAD}^{\text{Dipp}} - \text{CH}_3$], 333 (100%) [$\text{H}^2\text{DAD}^{\text{Dipp}} - \text{C}_3\text{H}_7$], 202 (8%) [$\text{H}^2\text{DAD}^{\text{Dipp}} - (2 \text{ H}, 4 \text{ C}_3\text{H}_7)$], 534 (1%), 500 (1%), 460 (1%), 433 (1%), 389 (1%), 297 (20%), 258 (1%), 230 (1%), 188 (78%), 162 (73%). IR (ATR): $\nu = 3062$ w, 3010 w, 2958 vs, 2925 m, 2865 m, 2708 w, 1626 w, 1585 w, 1536 w, 1460 vs, 1426 vs, 1380 w, 1360 m, 1316 s, 1271 vs, 1177 w, 1159 w, 1142 w, 1096 m, 1049 s, 953 w, 921 m, 893 m, 839 w, 822 w, 791 s, 760 vs, 753 vs, 679 w, 666 w, 617 w, 595 w, 564 w, 516 w, 471 w, 442 w, 427 w, 352 w, 336 w, 257 m, 221 w, 196 m, 154 w, 103 w, 80 w, 69 w, 57 m cm^{-1} . Mp: 95 °C.

[K(^{H2}DAD^{Dipp})(THF)₄] (22)

Potassium (106 mg, 2.7 mmol) was added to a solution of **2** (1.0 g, 2.7 mmol) in 50 mL of THF, and the resulting mixture was stirred at r.t. with a glass-coated stirring bar until all the

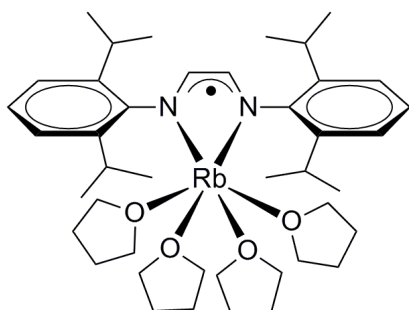


potassium was consumed. The reaction mixture (turned from yellow to deep red) was filtered, and the filtrate was then concentrated in vacuum to approximately 20 mL before it was kept at 5 °C to yield **22** (1.8 g, 95%) as dark red crystals. Anal. Calcd for C₄₂H₆₈KN₂O₄ (M_r = 704.10): C, 71.64; H, 9.73; N, 3.98. Found: C, 71.86; H, 9.46; N,

3.81. ¹H NMR (400 MHz, *d*₈-THF, 22 °C) and ¹³C NMR (100 MHz, *d*₈-THF, 23 °C): because of the strongly paramagnetic nature of the radical anionic DAD, it was not possible to obtain any meaningful ¹H NMR and ¹³C NMR. MS (EI): *m/z* (rel. Int.) = 378 (40%) [^{H2}DAD^{Dipp}], 361 (17%) [^{H2}DAD^{Dipp} – CH₃], 333 (87%) [^{H2}DAD^{Dipp} – C₃H₇], 202 (30%) [^{H2}DAD^{Dipp} – (2 H, 4 C₃H₇)], 162 (100%) [Dipp + H], 707 (1%), 649 (1%), 577 (3%), 534 (2%), 433 (1%), 389 (1%), 297 (1%), 188 (50%). IR (ATR): ν = 3062 w, 2957 s, 2866 m, 1661 w, 1626 w, 1587 w, 1534 vs, 1458 s, 1433 vs, 1408 s, 1370 s, 1338 m, 1317 m, 1279 m, 1255 m, 1239 m, 1215 m, 1181 m, 1142 w, 1096 m, 1056 s, 959 m, 931 m, 886 m, 873 m, 833 m, 821 m, 791 s, 748 vs, 674 m, 659 m, 636 m, 618 w, 586 m, 530 w, 506 w, 426 m, 389 w, 266 m, 155 vs, 114 m, 89 s, 79 s, 69 s, 63 s, 55 s cm⁻¹. Mp: 123 °C.

[Rb(^{H2}DAD^{Dipp})(THF)₄] (23)

A solution of **2** (1.0 g, 2.7 mmol) in 100 mL of THF was added to rubidium (231 mg, 2.7 mmol), and the resulting mixture was stirred at r.t. with a glass-coated stirring bar until all the



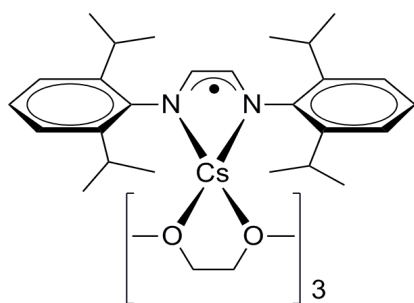
rubidium was consumed. The reaction mixture (turned from yellow to deep red) was filtered, and the filtrate was then concentrated in vacuum to approximately 20 mL before it was kept at 5 °C to yield **23** (1.9 g, 94%) as dark red crystals. Anal. Calcd for C₄₂H₆₈N₂O₄Rb (M_r = 750.47): C, 67.22; H, 9.13; N, 3.73. Found: C, 67.11; H, 9.19; N, 3.70.

¹H NMR (400 MHz, *d*₈-THF, 21 °C) and ¹³C NMR (100 MHz, *d*₈-THF, 23 °C): because of the strongly paramagnetic nature of the radical anionic DAD, it was not possible to obtain any meaningful ¹H NMR and ¹³C NMR. MS (EI): *m/z* (rel. Int.) = 378 (83%) [^{H2}DAD^{Dipp}], 361 (12%) [^{H2}DAD^{Dipp} – CH₃], 333 (100%) [^{H2}DAD^{Dipp} – C₃H₇], 202 (43%) [^{H2}DAD^{Dipp} – (2 H, 4 C₃H₇)], 780 (1%), 752 (25%), 709 (7%), 639 (1%), 591 (1%), 562 (38%), 576 (85%), 534

(61%), 521 (7%), 500 (3%), 423 (18%), 401 (40%), 389 (58%), 278 (15%), 214 (13%), 188 (85%), 162 (81%). **IR** (ATR): $\nu = 3054$ w, 3012 w, 2953 s, 2864 s, 2714 w, 1626 w, 1585 m, 1545 m, 1462 vs, 1426 vs, 1376 m, 1357 m, 1317 vs, 1273 vs, 1219 m, 1175 m, 1158 m, 1096 m, 1057 vs, 956 m, 914 s, 899 s, 832 m, 788 s, 748 vs, 658 m, 586 w, 524 w, 440 m, 412 m, 332 w, 265 m, 171 m, 134 vs, 83 vs, 63 vs cm^{-1} . Mp: 129 °C.

[Cs(^{H2}DAD^{Dipp})(DME)₃] (24)

A solution of **2** (1.0 g, 2.7 mmol) in 100 mL of DME was added to cesium (359 mg, 2.7 mmol), and the resulting mixture was stirred at r.t. with a glass-coated stirring bar until all the cesium was consumed. The reaction mixture (turned from yellow to deep red) was filtered, and the filtrate was concentrated under vacuum to a black liquid. *n*-Pentane (50 mL) was added to the black liquid, and the solution was mixed well before it was kept at 5 °C to yield **24** (1.5 g, 71%) as dark red crystals. Anal. Calcd for C₃₈H₆₆CsN₂O₆

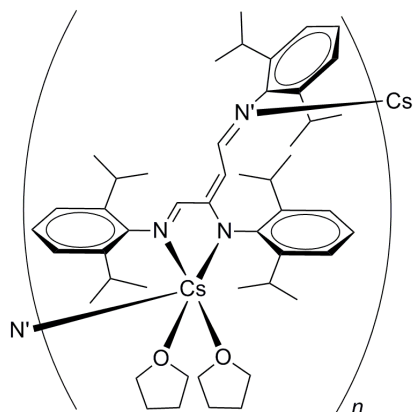


($M_r = 779.85$): C, 58.53; H, 8.53; N, 3.59. Found: C, 58.30; H, 8.57; N, 3.55. **¹H NMR** (400 MHz, *d*₈-THF, 24 °C) and **¹³C NMR** (100 MHz, *d*₈-THF, 25 °C): because of the strongly paramagnetic nature of the radical anionic DAD, it was not possible to obtain any meaningful **¹H NMR** and **¹³C NMR**. **MS** (EI): m/z (rel. Int.) = 378 (12%) [^{H2}DAD^{Dipp}], 361 (10%) [^{H2}DAD^{Dipp} – CH₃], 333 (78%) [^{H2}DAD^{Dipp} – C₃H₇], 202 (63%) [^{H2}DAD^{Dipp} – (2 H, 4 C₃H₇)], 162 (100%) [Dipp + H], 577 (38%), 562 (35%), 534 (75%), 500 (12%), 478 (2%), 401 (37%), 389 (62%), 312 (5%), 284 (12%), 214 (8%), 188 (58%), 177 (84%). **IR** (ATR): $\nu = 3047$ w, 3010 w, 2956 m, 2893 m, 2864 m, 2826 w, 2707 w, 1626 w, 1581 w, 1539 w, 1465 vs, 1421 vs, 1377 m, 1357 m, 1341 m, 1316 vs, 1275 vs, 1219 m, 1193 m, 1170 w, 1128 m, 1097 m, 1080 vs, 1058 m, 1031 m, 955 w, 937 w, 911 m, 852 m, 831 w, 817 m, 791 s, 754 vs, 680 w, 620 w, 600 w, 565 w, 525 w, 437 w, 409 w, 363 w, 333 w, 255 m, 192 w, 120 m, 92 s cm^{-1} . Mp: 95.8 °C.

[Cs(^{Dipp}NCHC[CHCHN^{Dipp}]N^{Dipp})(THF)₂]_n (25)

A solution of **2** (0.5 g, 1.3 mmol) in 100 mL of THF was added to cesium (345 mg, 2.6 mmol), and the resulting mixture was stirred at r.t. with a glass-coated stirring bar until all the cesium was consumed. The reaction mixture (turned from yellow to orange) was further stirred overnight after adding ^{H2}DAD^{Dipp} (0.5 g, 1.3 mmol). The deep red reaction mixture was filtered, and the filtrate was then concentrated at 80 °C in vacuum for 2 h to a black oil.

n-Pentane (20 mL) was added to the black oil and the solution was mixed well before it was kept at 5 °C to yield **25** (0.7 g, 63%) as red crystals. Anal. Calcd for C₄₈H₇₀CsN₃O₂ (M_r =

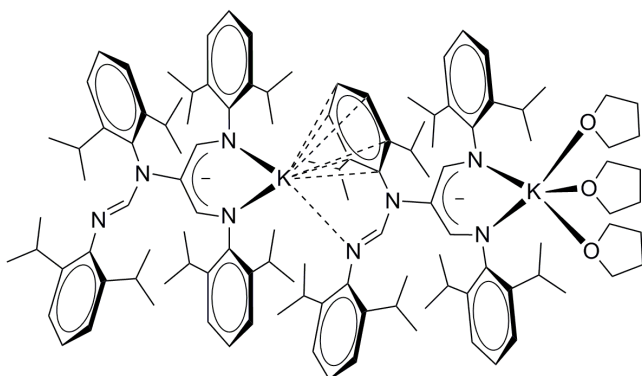


853.99): C, 67.51; H, 8.26; N, 4.92. Found: C, 67.74; H, 7.70; N, 4.91. ¹H NMR (400 MHz, *d*₈-THF, 21 °C): δ = 0.88 – 1.30 (d, 36H, CH(CH₃)₂), 1.76 (m, THF), 2.88 (m, 6H, CH(CH₃)₂), 3.6 (m, THF), 6.24 (t, ³J_{HH} = 7.2, 1H, *para*-Ar), 6.61 – 7.05 (m, 8H, Ar) ppm. ¹³C NMR (100 MHz, *d*₈-THF, 21 °C): It was not possible to get any meaningful information. MS (EI): *m/z* (rel. Int.) = 709 (1%) [M⁺ – 2 THF], 577 (88%) [M⁺ – (C₃H₇, Dipp, THF)], 562 (78%)

[M⁺ – (CH₃, C₃H₇, Dipp, THF)], 534 (93%) [M⁺ – (2 C₃H₇, Dipp, THF)], 162 (100%) [Dipp + H], 824 (1%), 782 (1%), 642 (2%), 630 (55%), 591 (18%), 548 (10%), 500 (18%), 416 (8%), 401 (84%), 385 (91%), 373 (20%), 369 (25%), 355 (23%), 347 (27%), 334 (43%), 284 (30%), 234 (5%), 228 (8%), 214 (37%), 202 (65%), 186 (80%), 177 (52%). IR (ATR): ν = 3059 w, 2956 s, 2926 m, 2865 m, 2666 w, 1627 m, 1589 m, 1526 vs, 1456 s, 1433 vs, 1409 s, 1372 s, 1356 s, 1313 m, 1238 vs, 1215 s, 1183 s, 1141 m, 1092 s, 1057 s, 983 m, 957 m, 931 m, 895 m, 869 w, 839 m, 819 w, 790 s, 771 m, 748 vs, 672 m, 658 m, 636 w, 606 w, 584 w, 530 w, 507 m, 481 w, 435 m, 414 m, 385 w, 264 m, 241 w, 180 m, 125 vs, 65 s, 58 s cm⁻¹. Mp: 180 °C (dec).

[K(DippNCHC{DippNCHN^{Dipp}}CHN^{Dipp})(THF)_{1.5}] (**26**)

Potassium hydride (28 mg, 0.7 mmol) was added to a solution of **2** (527 mg, 1.4 mmol) in 50 mL of THF, and the resulting mixture was stirred overnight at r.t. with a glass-coated stirring



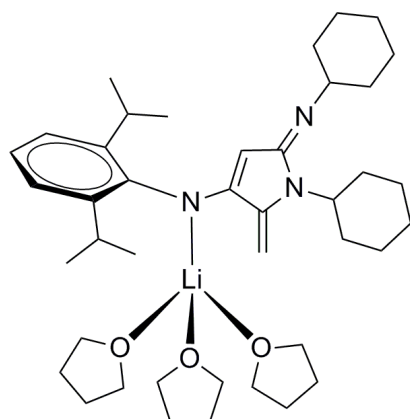
bar. The reaction mixture (turned from yellow to red) was evaporated to dryness in vacuum. *n*-Pentane (50 ml) was added to the residue and the solution was filtered. The filtrate was kept at 5 °C to yield **26** (0.25 g, 40%) as red crystals.

Anal. Calcd for C₁₁₆H₁₆₆K₂N₈O₃ (M_r = 1798.81): C, 77.45; H, 9.30; N, 6.23. Found: C, 77.71; H, 9.47; N, 6.32. ¹H NMR (400 MHz, *d*₈-THF, 22 °C): δ = 0.91, 1.14 (d, ³J_{HH} = 6.8 Hz, 24H, CH(CH₃)₂), 1.04, 1.10, 1.23, 1.26 (d, 24H, CH(CH₃)₂), 1.77 (m, THF), 3.0 – 3.5, 4.1 (m, 8H, CH(CH₃)₂), 3.45 (m, THF), 6.84 (s, br, 2H, NCHC), 6.88 – 7.10 (m, 6H, Ar), 7.62 (d, 4H, *meta*-Ar), 7.98 (t, 2H, *para*-Ar), 8.45 (s,

2H, NCHN) ppm. ^{13}C NMR (100 MHz, d_8 -THF, 21 °C): δ = 24.4 – 26.1 (CH(CH₃)₂), 26.3 (THF), 27.8, 28.1, 28.3, 29.2, 29.4 (CH(CH₃)₂), 68.1 (THF), 119.5 (*para*-Ar), 112.8 (NC(CH₂)₂), 122.2 (*meta*-Ar), 121.4, 122.8, 123.2, 123.4, 126.0 (Ar), 140.7, 141.5, 148.9 (*ortho*-Ar), 140.2, 151.6, 156.2 (*ipso*-Ar) 156.7 (NCHC), 159.0 (NCHN) ppm. MS (EI): m/z (rel. Int.) = 790 (59%) [$\text{M}^+ - 2 \text{ THF}$], 751 (90%) [$\text{M}^+ - (\text{K}, 2 \text{ THF})$], 614 (1%) [$\text{M}^+ - (\text{CH}_3, \text{Dipp}, 3 \text{ THF})$], 521 (100%) [$\text{M}^+ - (\text{C}_3\text{H}_7, \text{CHN}^{\text{Dipp}}, 3 \text{ THF}, \text{K})$], 1000 (1%), 884 (1%), 707 (1%), 614 (1%), 576 (96%), 562 (25%), 469 (2%), 402 (2%), 387 (11%), 373 (10%), 361 (7%), 212 (3%), 200 (7%), 186 (25%). IR (ATR): ν = 3063 w, 3025 w, 2959 s, 2926 m, 2867 m, 1632 vs, 1586 m, 1558 vs, 1463 s, 1443 s, 1400 w, 1383 m, 1361 m, 1306 s, 1277 m, 1254 m, 1237 m, 1182 m, 1161 w, 1096 m, 1058 w, 1043 w, 991 m, 958 w, 933 w, 914 w, 884 w, 843 w, 799 m, 771 w, 753 vs, 696 w, 645 w, 605 w, 558 w, 540 w, 521 w, 487 w, 474 w, 454 w, 437 w, 377 w, 282 m, 236 m, 164 m, 136 m, 103 w, 92 w, 76 w, 69 w, 54 m cm^{-1} . Mp: 145 °C.

[Li(DippN^{Cy-Pyr})(THF)₃] (27)

Lithium (17 mg, 2.4 mmol) was added to a solution of **1** (0.5 g, 1.2 mmol) in 50 mL of THF, and the resulting mixture was stirred at room temperature with a glass-coated stirring bar until



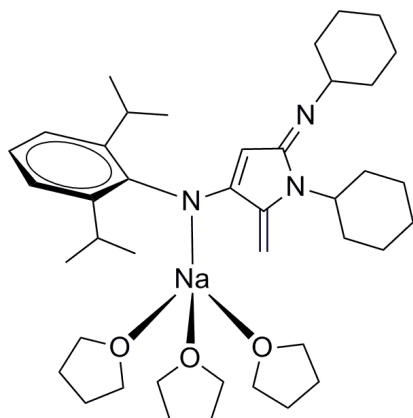
all the lithium was consumed. The reaction mixture (turned from yellow to orange) was transferred into a flask containing **1** (0.5 g, 1.2 mmol), and the intensity of the color increased immediately. The reaction mixture was continued stirring overnight before *N,N'*-dicyclohexylcarbodiimide (0.521 g, 2.5 mmol, slightly in excess) was added. After stirring overnight, the reaction mixture was filtered and the yellow filtrate was then

concentrated in vacuum to an oily liquid before it was kept at -32 °C to yield **27** (1.37 g, 87%) as light yellow crystals. Anal. Calcd for C₄₁H₆₆LiN₃O₃ (655.92): C, 75.08; H, 10.14; N, 6.41. Found: C, 74.41; H, 10.22; N, 6.40. MS (EI): m/z (rel.int.) = 655 (1%) [M^+], 642 (1%) [$\text{M}^+ - \text{CH}$], 612 (80%) [$\text{M}^+ - \text{C}_3\text{H}_7$], 567 (15%) [$\text{M}^+ - 2 \text{ H}, 2 \text{ C}_3\text{H}_7$], 433 (23%) [$\text{DippN}^{\text{Cy-Pyr}} + \text{H}$], 436 (58%) [$\text{M}^+ - (\text{C}_2\text{H}, 2 \text{ C}_6\text{H}_{11}\text{N})$], 160 (70%) [Dipp – H], 527 (1%), 513 (45%), 470 (10%), 408 (100%), 390 (28%), 361 (65%), 340 (14%), 285 (11%), 258 (37%), 202 (96%), 186 (55%). IR (ATR): ν = 3052 w, 2959 s, 2923 vs, 2851 s, 2666 w, 1637 s, 1608 s, 1567 vs, 1517 s, 1490 s, 1446 s, 1413 s, 1379 m, 1363 m, 1345 w, 1306 vs, 1294 vs, 1271 m, 1253 s, 1237 s, 1197 w, 1177 m, 1154 m, 1099 m, 1055 m, 1042 s, 992 w, 980 w, 957 w, 935 w, 888

s, 856 w, 844 w, 798 m, 766 s, 756 s, 737 m, 697 m, 674 m, 615 m, 600 m, 571 m, 548 m, 495 s, 437 vs, 400 s, 354 m, 334 m, 312 w, 283 m, 214 s, 176 w, 161 w, 145 w, 136 w, 111 w, 95 w, 74 w, 57 m cm⁻¹. Mp: 129 °C.

[Na(DippN^{Cy}-Pyr)(THF)₃] (28)

Sodium (55 mg, 2.4 mmol) was added to a solution of **1** (0.5 g, 1.2 mmol) in 50 mL of THF, and the resulting mixture was stirred at room temperature with a glass-coated stirring bar until

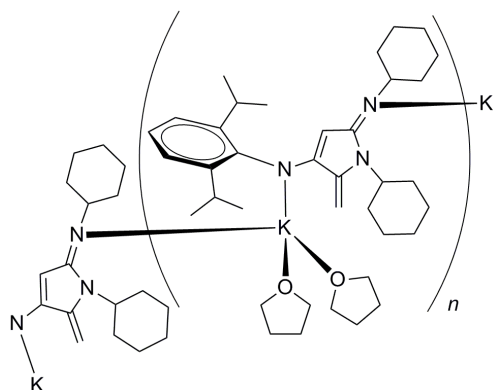


all the sodium was consumed. The reaction mixture (turned from yellow to bright red) was transferred into a flask containing **1** (0.5 g, 1.2 mmol), and the intensity of the color increased immediately. The reaction mixture was continued stirring overnight before *N,N'*-dicyclohexylcarbodiimide (0.521 g, 2.5 mmol, slightly in excess) was added. After stirring overnight, the reaction mixture was filtered and the yellow filtrate was then

concentrated in vacuum to an oily liquid before it was kept at -32 °C to yield **28** (1.5 g, 93%) as light yellow crystals. Anal. Calcd for C₄₁H₆₆N₃NaO₃ (671.97): C, 73.28; H, 9.90; N, 6.25. Found: C, 73.52; H, 10.05; N, 6.25. ¹H NMR (400 MHz, *d*₈-THF, 20 °C): δ = 1.06 (d, ³J_{HH} = 7.2 Hz, 6H, CH(CH₃)₂), 1.11 (d, ³J_{HH} = 6.8 Hz, 6H, CH(CH₃)₂), 1.14 – 1.82, and 2.24 – 2.4 (m, br, 20H, cyclohexyl-CH₂), 1.77 (m, THF), 2.89 (m, 1H, C=NCH), 3.35 (sept, ³J_{HH} = 6.8 Hz, 2H, CH(CH₃)₂), 3.61 (m, THF), 3.73 (s, 1H, CHCCCH₂), 3.78 (s, 1H, CHCCCH₂), 4.06 (s, 1H, CHCCCH₂), 4.23 (m, br, 1H, C₂NCH), 6.78 (t, ³J_{HH} = 7.6 Hz, 1H, *para*-Ar), 6.95 (d, ³J_{HH} = 7.6 Hz, 2H, *meta*-Ar) ppm. ¹³C NMR (100 MHz, *d*₈-THF, 21 °C): δ = 24.7 (CH(CH₃)₂), 25.3 (CH(CH₃)₂), 26.3 (THF), 28.1 (CH(CH₃)₂), 25.8, 27.1, 27.6, 27.8, 29.8, 36.5 (cyclohexyl-CH₂), 51.4 (C₂NCH), 58.3 (C=NCH), 68.2 (THF), 71.0 (CHCCCH₂), 73.2 (CHCCCH₂), 121.4 (*para*-Ar), 123.3 (*meta*-Ar), 143.4 (*ortho*-Ar), 152.3 (CHCCCH₂), 153.3 (*ipso*-Ar), 162.9 (CHCCCH₂), 162.5 (NCN) ppm. MS (EI): *m/z* (rel.int.) = 639 (1%) [M⁺ – 2 H, 2 CH₃], 612 (5%) [M⁺ – 3 CH₃, CH₂], 556 (1%) [M⁺ – C₃H₇, THF], 513 (1%) [M⁺ – 2 C₃H₇, THF], 433 (100%) [DippN^{Cy}-Pyr + H], 162 (70%) [Dipp + H], 459 (1%), 390 (72%), 361 (70%), 308 (80%), 254 (75%), 202 (84%), 186 (62%). IR (ATR): ν = 3063 w, 2957 m, 2927 s, 2852 m, 2665 w, 1637 s, 1609 s, 1587 m, 1551 m, 1492 m, 1446 s, 1409 w, 1379 s, 1309 w, 1282 m, 1254 m, 1204 w, 1182 m, 1152 w, 1117 m, 1094 m, 1059 w, 1019 m, 992 w, 957 w, 936 w, 888 m, 844 w, 802 m, 768 s, 744 m, 716 w, 689 m, 677 m, 648 w, 605 m, 530 m, 502 m, 412 m, 349 s, 285 s, 225 vs, 165 vs, 93 s, 63 s cm⁻¹. Mp: 87 °C.

$$\{[\text{K}(\text{DippN}^{\text{Cy-Pyr}})(\text{THF})_2]_4 \cdot \text{THF}\}_n \quad (29)$$

Potassium (94 mg, 2.4 mmol) was added to a solution of **1** (0.5 g, 1.2 mmol) in 50 mL of THF, and the resulting mixture was stirred at room temperature with a glass-coated stirring

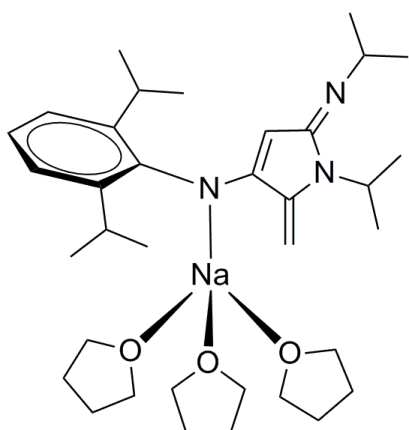


bar until all the potassium was consumed. The reaction mixture (turned from yellow to bright red) was transferred into a flask containing **1** (0.5 g, 1.2 mmol), and the intensity of the color increased immediately. The reaction mixture was continued stirring overnight before *N,N'*-dicyclohexylcarbodiimide (0.521 g, 2.5 mmol, slightly in excess) was added. After stirring

overnight, the reaction mixture was filtered and the yellow filtrate was then concentrated in vacuum to an oily liquid before it was kept at $-32\text{ }^{\circ}\text{C}$ to **29** (1.45 g, 95%) light yellow crystals. Anal. Calcd for $\text{C}_{152}\text{H}_{240}\text{K}_4\text{N}_{12}\text{O}_9$ (2536.00): C, 71.99; H, 9.54; N, 6.63. Found: C, 68.46; H, 9.70; N, 6.44. $^1\text{H NMR}$ (400 MHz, d_8 -THF, $20\text{ }^{\circ}\text{C}$): $\delta = 1.05$ (d, $^3J_{\text{HH}} = 7.2$ Hz, 6H, $\text{CH}(\text{CH}_3)_2$), 1.09 (d, $^3J_{\text{HH}} = 6.4$ Hz, 6H, $\text{CH}(\text{CH}_3)_2$), 1.10 – 1.78, and 2.27 – 2.40 (m, br, 20H, cyclohexyl- CH_2), 1.76 (m, THF), 2.87 (br, 1H, $\text{C}=\text{NCH}$), 3.27 (sept, $^3J_{\text{HH}} = 6.8$ Hz, 2H, $\text{CH}(\text{CH}_3)_2$), 3.6 (m, THF), 3.67 (s, 1H, CHCCCH_2), 3.74 (s, 1H, CHCCCH_2), 4.2 (br, 1H, C_2NCH), 4.30 (s, 1H, CHCCCH_2), 6.7 (t, $^3J_{\text{HH}} = 7.6$ Hz, 1H, *para*-Ar), 6.89 (d, $^3J_{\text{HH}} = 7.6$ Hz, 2H, *meta*-Ar) ppm. $^{13}\text{C NMR}$ (100 MHz, d_8 -THF, 296 K): $\delta = 24.6$ ($\text{CH}(\text{CH}_3)_2$), 25.2 ($\text{CH}(\text{CH}_3)_2$), 26.3 (THF), 25.9, 27.1, 27.6, 27.8, 29.9, 36.6 (cyclohexyl- CH_2), 28.1 ($\text{CH}(\text{CH}_3)_2$), 51.7 (C_2NCH), 58.3 ($\text{C}=\text{NCH}$), 68.2 (THF), 71.8 (CHCCCH_2), 72.1 (CHCCCH_2), 121.5 (*para*-Ar), 123.0 (*meta*-Ar), 142.3 (*ortho*-Ar), 152.5 (CHCCCH_2), 154.0 (*ipso*-Ar), 162.1 (CHCCCH_2), 163.4 (NCN) ppm. **MS** (EI): m/z (rel.int.) = 959 (2%) [$\text{M}^+ - \text{CH}_2$], 876 (15%) [$\text{M}^+ - \text{C}_6\text{H}_{11}\text{N}$], 793 (5%) [$\text{M}^+ - \text{C}_6\text{H}_{11}, \text{C}_6\text{H}_{11}\text{N}$], 779 (6%) [$\text{M}^+ - 2 \text{C}_6\text{H}_{11}\text{N}$], 711 (1%) [$\text{M}^+ - \text{H}, \text{CH}_2, \text{C}_3\text{H}_7, \text{Dipp}, 2 \text{C}_6\text{H}_{11}\text{N}$], 433 (100%) [$\text{DippN}^{\text{Cy-Pyr}} + \text{H}$], 162 (70%) [$\text{Dipp} + \text{H}$], 672 (1%), 594 (4%), 517 (7%), 501 (4%), 390 (66%), 336 (55%), 308 (83%), 257 (77%), 225 (74%), 186 (60%). **IR** (ATR): $\nu = 3061$ w, 2957 m, 2851 m, 2666 w, 1984 w, 1637 s, 1608 s, 1586 m, 1550 m, 1494 m, 1468 m, 1446 m, 1411 w, 1379 m, 1362 m, 1345 m, 1333 m, 1283 m, 1254 m, 1204 w, 1181 m, 1140 w, 1093 m, 1060 m, 1045 w, 1020 m, 992 w, 957 w, 935 w, 887 m, 845 w, 801 m, 768 s, 744 m, 676 m, 657 m, 603 w, 584 w, 531 w, 502 w, 394 m, 350 m, 285 s, 226 s, 165 vs, 136 vs, 91 s, 80 s, 70 s, 60 s cm^{-1} . Mp: $118\text{ }^{\circ}\text{C}$.

[Na(DippN^{iPr}-Pyr)(THF)₃] · THF (30)

Sodium (55 mg, 2.4 mmol) was added to a solution of **1** (0.5 g, 1.2 mmol) in 50 mL of THF, and the resulting mixture was stirred at room temperature with a glass-coated stirring bar until

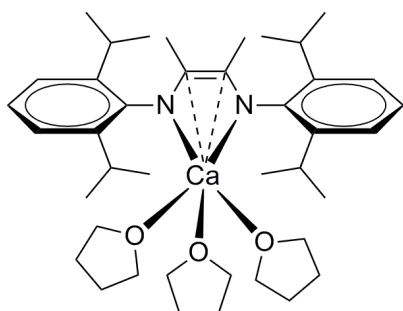


all the potassium was consumed. The reaction mixture (turned from yellow to bright red) was transferred into a flask containing **1** (0.5 g, 1.2 mmol), and the intensity of the color increased immediately. The reaction mixture was continued stirring overnight before *N,N'*-diisopropylcarbodiimide (0.39 mL, 2.5 mmol, slightly in excess) was added. After stirring overnight, the reaction mixture was filtered and the yellow filtrate was then

concentrated in vacuum to an oily liquid before it was kept at -32 °C to yield **30** (1.4 g, 88%) of as light yellow crystals. Anal. Calcd for C₃₉H₆₆N₃NaO₄ (663.95): C, 70.55; H, 10.02; N, 6.33. Found: C, 70.44; H, 10.11; N, 6.57. ¹H NMR (400 MHz, *d*₈-THF, 23 °C): δ = 0.9 (d, ³J_{HH} = 6.4 Hz, 6H, C=NCH(CH₃)₂), 1.07 (d, ³J_{HH} = 7.2 Hz, 6H, CCH(CH₃)₂), 1.13 (d, ³J_{HH} = 6.8 Hz, 6H, CCH(CH₃)₂), 1.27 (d, ³J_{HH} = 7.2 Hz, 6H, C₂NCH(CH₃)₂), 1.77 (m, THF), 3.19 (sept, ³J_{HH} = 6.4 Hz, 1H, C=NCH(CH₃)₂), 3.35 (sept, ³J_{HH} = 6.8 Hz, 2H, CCH(CH₃)₂), 3.61 (m, THF), 3.69 (s, 1H, CCHC), 3.76 (s, 1H, CCH₂), 4.07 (s, 1H, CCH₂), 4.81 (sept, ³J_{HH} = 7.2 Hz, 1H, C₂NCH(CH₃)₂), 6.79 (t, ³J_{HH} = 7.6 Hz, 1H, *para*-Ar), 6.95 (d, ³J_{HH} = 7.6 Hz, 2H, *meta*-Ar) ppm. ¹³C NMR (100 MHz, *d*₈-THF, 23 °C): δ = 19.3 (C₂NCH(CH₃)₂), 24.6 (CCH(CH₃)₂), 25.2 (CCH(CH₃)₂), 25.9 (C=NCH(CH₃)₂), 26.2 (THF), 27.9 (CCH(CH₃)₂), 41.6 (C₂NCH(CH₃)₂), 50.1 (C=NCH(CH₃)₂), 68.2 (THF), 71.2 (CCH₂), 73.1 (CCHC), 121.3 (*para*-Ar), 123.2 (*meta*-Ar), 143.2 (*ortho*-Ar), 151.3 (CCH₂), 153.2 (*ipso*-Ar), 162.1 (CHCCCH₂), 162.4 (NCN) ppm. MS (EI): *m/z* (rel.int.) = 532 (5%) [M⁺ - (CH₂, 3 CH₃)], 473 (1%) [M⁺ - (H, 3 CH₃, THF)], 361 (20%) [M⁺ - CH₂, 3 THF], 354 (100%) [DippN^{iPr}-Pyr + H], 239 (3%) [Na + 3 THF], 177 (40%) [M⁺ - (NaN^{Dipp}, 3 THF)], 162 (98%) [Dipp + H], 532 (1%), 436 (1%), 406 (6%), 310 (8%), 303 (9%), 260 (15%), 254 (14%), 245 (7%), 211 (22%), 202 (29%). IR (ATR): ν = 2961 vs, 2870 m, 1587 vs, 1526 vs, 1458 s, 1357 vs, 1314 vs, 1250 s, 1132 s, 1048 s, 968 m, 941 m, 884 m, 804 s, 767 s, 742 m, 667 m, 571 w, 502 w, 431 w cm⁻¹. Mp: 126 °C.

[Ca(^{Me2}DAD^{Dipp})(THF)₃] (31)

Calcium (100 mg, 2.5 mmol) was added to a solution of **1** (1.0 g, 2.5 mmol) in 100 mL of THF. After addition of iodine (5 mg, 1.97×10^{-2} mmol) the reaction mixture was stirred at r.t.



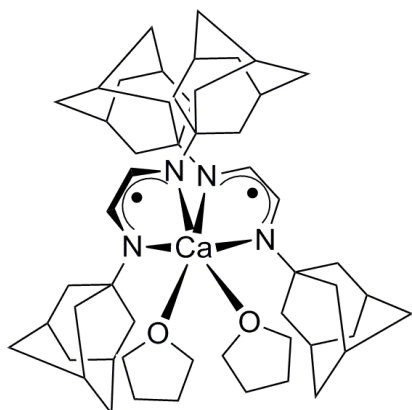
with a glass-coated stirring bar until all the calcium was consumed. The reaction mixture (turned from colorless to bright red) was filtered, and the filtrate was concentrated in vacuum to approximately 30 mL before it was kept at 5 °C to yield **31** (1.5 g, 91%) as red crystals. Anal. calcd for C₄₀H₆₄CaN₂O₃ (M_r = 661.03): C, 72.68; H, 9.76; N, 4.24.

Found: C, 69.05; H, 9.67; N, 4.24. ¹H NMR (400 MHz, *d*₈-THF, 20 °C): δ = 1.07 (d, ³J_{HH} = 6.8 Hz, 12H, CH(CH₃)₂), 1.20 (d, ³J_{HH} = 7.2 Hz, 12H, CH(CH₃)₂), 1.57 (s, 6H, NCCH₃), 1.76 (m, THF), 3.60 (m, THF), 3.74 (sep, ³J_{HH} = 7.2 Hz, 4H, CH(CH₃)₂), 6.41 (t, ³J_{HH} = 7.6 Hz, 2H, *para*-Ar), 6.78 (d, ³J_{HH} = 7.2 Hz, 4H, *meta*-Ar) ppm. ¹³C NMR (100 MHz, *d*₈-THF, 21 °C): δ = 18.6 (NCCH₃), 24.5 (CH(CH₃)₂), 25.8 (CH(CH₃)₂), 26.3 (THF), 27.9 (CH(CH₃)₂), 68.2 (THF), 115.9 (*para*-Ar), 118.6 (NCCH₃), 122.6 (*meta*-Ar), 142.0 (*ortho*-Ar), 154.8 (*ipso*-Ar) ppm. MS (EI): *m/z* (rel. Int.) = 522 (3%) [M⁺ - (CH₃, C₂H₂, C₃H₇, C₄H₆)], 477 (1%) [M⁺ - (3 C₃H₇, C₄H₆)], 433 (1%) [M⁺ - (H, 4 C₃H₇, C₄H₆)], 406 (84%) [Me₂DAD^{Dipp} + 2H], 361 (44%) [Me₂DAD^{Dipp} - C₃H₇], 202 (100%) [Me₂DAD^{Dipp} - (2 CH₃, 4 C₃H₇)], 184 (5%) [Ca(THF)₂], 625 (1%), 555 (1%), 353 (1%), 268 (1%), 231 (13%), 216 (9%), 188 (68%), 175 (27%), 160 (71%). IR (ATR): ν = 3041 w, 2954 vs, 2873 vs, 2702 w, 1665 w, 1580 m, 1550 m, 1452 s, 1416 vs, 1311 vs, 1249 vs, 1104 s, 1026 vs, 934 s, 871 vs, 765 s, 665 m, 631 m, 558 m, 489 w, 440 m cm⁻¹. Mp: 131 °C.

[Ca(^{H2}DAD^{Ad})₂(THF)₂] · THF (32)

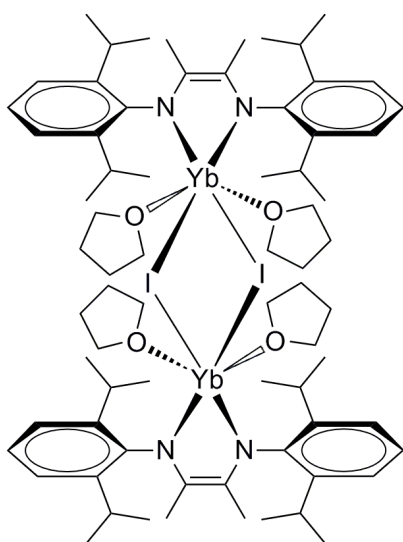
Calcium (64 mg, 1.6 mmol, slightly in excess) was added to a solution of **3** (1.0 g, 3.1 mmol) in 100 mL of THF. After addition of iodine (5 mg, 1.97×10^{-2} mmol), the reaction mixture was stirred at r.t. with a glass-coated stirring bar until all the calcium was consumed. The reaction mixture (turned from colorless to deep green) was filtered, and the filtrate was concentrated in vacuum to approximately 30 mL before it was kept at 5 °C to yield **32** (1.15 g, 82%) as light green crystals. Anal. Calcd for C₅₆H₈₈CaN₄O₃ (M_r = 905.4): C, 74.29; H, 9.80; N, 6.19. Found: C, 74.20; H, 9.79; N, 6.19. ¹H NMR (400 MHz, *d*₈-THF, 23 °C) and ¹³C NMR (100 MHz, *d*₈-THF, 21 °C): because of the paramagnetic properties of the radical anionic DAD, it was not possible to obtain any meaningful ¹H NMR and ¹³C NMR spectra. MS (EI): *m/z* (rel. int.) = 733 (1%) [M⁺ - (C₂H₃, THF)], 697 (1%) [M⁺ - C₁₀H₁₄], 667 (1%)

[M⁺ – (3 H, C₁₁H₁₆N)], 537 (1%) [M⁺ – (2 H, CH₂, C₁₀H₁₅, 2 THF)], 523 (31%) [M⁺ – (2 H, 2 CH₂, C₁₀H₁₅, 2 THF,)], 499 (22%) [M⁺ – (2 CH, CH₂, C₁₀H₁₅, 2 THF)], 388 (4%) [M⁺ – (C₉H₁₂, ^{H2}DAD^{Ad})], 364 (13%) [M⁺ – (^{H2}DAD^{Ad}, THF,)], 350 (72%) [M⁺ – (CH₂, ^{H2}DAD^{Ad}, 2 THF)], 335 (3%) [M⁺ – (H, 2 CH₂, ^{H2}DAD^{Ad}, 2 THF)], 327 (5%) [^{H2}DAD^{Ad} + 3 H], 297 (78%) [^{H2}DAD^{Ad} – C₂H₃], 292 (11%) [M⁺ – 4 C₁₀H₁₅], 189 (3%) [^{H2}DAD^{Ad} – C₁₀H₁₅], 135 (100%) [C₁₀H₁₅], 401 (1%), 374 (6%), 254 (2%), 169 (6%), 164 (7%), 107 (11%), 93 (27%), 79 (27%). **IR** (ATR): ν = 2971 w, 2899 vs, 2846 vs, 2677 w, 2656 w, 1660 w, 1628 w, 1536 w, 1479 w, 1450 m, 1366 w, 1352 w, 1342 w, 1308 m, 1270 w, 1231 m, 1181 w, 1148 w, 1120 w, 1091 m, 1069 w, 1037 m, 982 w, 953 w, 937 w, 907 m, 883 w, 812 w, 770 w, 720 w, 646 w, 619 w, 593 w, 552 w, 523 w, 468 w, 420 m, 410 m, 398 m, 364 m, 293 m, 248 w, 225 w, 197 w, 161 w, 112 w, 96 w, 79 w cm⁻¹. Mp: 274 °C.



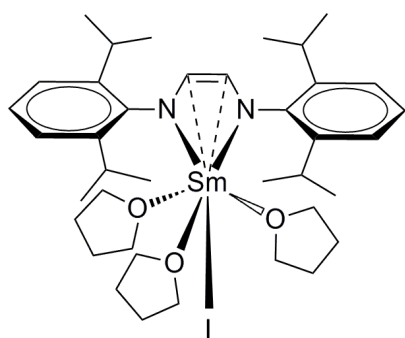
[Yb₂(μ-I)₂(^{Me2}DAD^{Dipp})₂(THF)₄] · THF (33)

Ytterbium (433 mg, 2.5 mmol) was added to a solution of **1** (1.0 g, 2.5 mmol) in 100 mL of THF. The resulting mixture was stirred with iodine (330 mg, 1.3 mmol, slightly in excess) at r.t. with a glass-coated stirring bar until all the ytterbium was consumed. The reaction mixture (turned from yellow to dark red) was evaporated to dryness in vacuum. *n*-Pentane (30 mL) was added to the residue, and the resulting mixture was mixed well before it was filtered. The filtrate was kept at 5 °C to yield **33** (2 g, 90%) as dark red crystals. Anal. Calcd C₇₆H₁₂₀I₂N₄O₅Yb₂ (M_r = 1769.7): C, 51.58; H, 6.83; N, 3.17. Found: C, 51.50; H, 6.78; N, 3.18. **MS** (EI): m/z (rel. int.) = 637 (1%) [M⁺ – (2 C₃H₇, CH₃CCCH₃, THF)], 578 (1%) [M⁺ – (2 THF, I)], 559 (1%) [M⁺ – (8 CH₃, C₃H₇, I)], 524 (1%) [M⁺ – (CH₃CCCH₃, 2 THF, I)], 406 (32%) [^{Me2}DAD^{Dipp} + 2H], 361 (80%) [^{Me2}DAD^{Dipp} – C₃H₇], 202 (98%) [^{Me2}DAD^{Dipp} – (2 CH₃, 4 C₃H₇)], 833 (1%), 795 (1%), 667 (1%), 629 (1%), 599 (1%), 470 (1%), 456 (1%), 428 (1%), 416 (5%), 335(1%), 319(1%), 281 (3%), 266 (5%), 254 (3%), 231 (69%), 214 (9%), 188 (85%), 177 (87%), 162 (100%), 146 (34%).



[Sm(^{H2}DAD^{Dipp})(I)(THF)₃] (34)

Samarium (406 mg, 2.7 mmol) was added to a solution of **2** (1.0 g, 2.7 mmol) in 100 mL of THF. The resulting mixture was stirred with iodine (355 mg, 1.4 mmol, slightly in excess) at



r.t. with a glass-coated stirring bar until all the samarium was consumed. The reaction mixture (turned from yellow to dark blue) was evaporated to dryness in vacuum. *n*-Pentane (30 mL) was added to the residue, and the resulting mixture was mixed well before it was filtered. The filtrate was kept at 5 °C to yield **34** (1.5 g, 92%) as dark blue crystals. Anal.

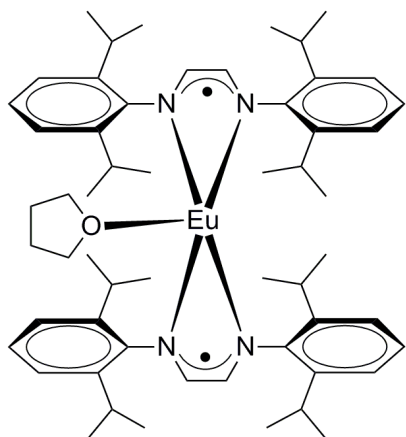
Calcd C₃₈H₆₀IN₂O₃Sm (M_r = 870.16): C, 52.45; H, 6.95; N,

3.22. Found: C, 52.21; H, 6.95; N, 3.24. ¹H NMR (400 MHz, *d*₈-THF, 22 °C): δ = 1.56 (s, br, 24H, CH(CH₃)₂), 1.77 (s, THF), 3.45 (s, THF), 6.64 (s, br, 4H, CH(CH₃)₂), 7.62 (d, ³J_{HH} = 7.6 Hz, 4H, *meta*-Ar), 7.98 (t, ³J_{HH} = 7.6 Hz, 2H, *para*-Ar), 8.55 (s, 2H, NCH) ppm. ¹³C NMR (100 MHz, *d*₈-THF, 23 °C): δ = 25.6 (CH(CH₃)₂), 26.2 (THF), 33.3 (CH(CH₃)₂), 68.1 (THF), 122.4 (*para*-Ar), 125.2 (*meta*-Ar), 130.6 (NCH), 134.2 (*ortho*-Ar), 160.1 (*ipso*-Ar) ppm. MS (EI): *m/z* (rel. int.) = 811 (1%) [M⁺ – 4 CH₃], 528 (100%) [M⁺ – (3 THF, I)], 378 (10%) [^{H2}DAD^{Dipp}], 361 (3%) [^{H2}DAD^{Dipp} – CH₃], 333 (68%) [^{H2}DAD^{Dipp} – C₃H₇], 202 (4%) [^{H2}DAD^{Dipp} – (2 H, 4 C₃H₇)], 160 (7%) [Dipp – H], 896 (1%), 862 (1%), 730 (1%), 674 (1%), 603 (1%), 543 (1%), 392 (5%), 264 (7%), 188 (11%), 174 (18%). IR (ATR): ν = 3062 w, 2960 vs, 2926 m, 2866 m, 1661 m, 1627 w, 1587 w, 1553 w, 1526 w, 1457 s, 1433 s, 1380 m, 1361 m, 1327 m, 1312 m, 1248 s, 1207 m, 1176 m, 1147 w, 1099 m, 993 s, 958 w, 924 m, 885 w, 862 w, 821 m, 796 s, 752 vs, 694 w, 621 w, 579 w, 536 w, 520 w, 465 w, 440 m, 414 m, 363 w, 338 m, 296 m, 273 m, 260 m, 206 w, 162 m, 128 m, 113 m, 84 s, 71 s, 54 vs cm⁻¹. Mp: 105 °C.

[Eu(^{H2}DAD^{Dipp})₂(THF)] (35)

Europium (213 mg, 1.4 mmol, slightly in excess) was added to a solution of **2** (1.0 g, 2.7 mmol) in 100 mL of THF. After addition of iodine (5 mg, 1.97 × 10⁻² mmol), the reaction mixture was stirred at r.t. with a glass-coated stirring bar until all the europium was consumed. The reaction mixture (turned from yellow to deep red) was filtered, and the filtrate was concentrated in vacuum to a black oil. *n*-Pentane (20 mL) was added to the black oil, and the resulting solution was mixed well before it was kept at 5 °C to yield **35** (1.1 g, 83%) as black crystals. Anal. Calcd C₅₆H₈₀EuN₄O (M_r = 977.22): C, 68.83; H, 8.25; N, 5.73. Found: C, 68.85; H, 8.38; N, 5.61. ¹H NMR (400 MHz, *d*₈-THF, 21 °C) and ¹³C NMR (100 MHz, *d*₈-

THF, 21 °C): Because of the strongly paramagnetic nature of the anionic DAD and Eu^{2+} , it was not possible to obtain any meaningful ^1H NMR and ^{13}C NMR spectra. **MS** (EI): m/z (rel.



int.) = 887 (1%) [$\text{M}^+ - 6 \text{CH}_3$], 729 (1%) [$\text{M}^+ - (\text{CH}_3, \text{Dipp}, \text{THF})$], 529 (85%) [$\text{M}^+ - (\text{H}^2\text{DAD}^{\text{Dipp}}, \text{THF})$], 511 (10%) [$\text{M}^+ - (\text{CH}_3, 2 \text{ Dipp}, 2 \text{ C}_3\text{H}_7)$], 378 (9%) [$\text{H}^2\text{DAD}^{\text{Dipp}} + 2\text{H}$], 333 (100%) [$\text{H}^2\text{DAD}^{\text{Dipp}} - \text{C}_3\text{H}_7$], 202 (4%) [$\text{H}^2\text{DAD}^{\text{Dipp}} - (2 \text{ H}, 4 \text{ C}_3\text{H}_7)$], 920 (1%), 792 (1%), 676 (1%), 542 (1%), 452 (2%), 264 (6%), 188 (40%), 174 (52%), 158 (18%). IR (ATR): $\nu = 3054 \text{ w}, 2958 \text{ s}, 2924 \text{ m}, 2865 \text{ m}, 1661 \text{ w}, 1627 \text{ w}, 1588 \text{ w}, 1531 \text{ w}, 1450 \text{ vs}, 1428 \text{ vs}, 1381 \text{ m}, 1360 \text{ m}, 1334 \text{ m}, 1313 \text{ m}, 1256 \text{ vs}, 1197 \text{ m}, 1176 \text{ m}, 1107 \text{ m}, 1051$

$\text{m}, 1036 \text{ m}, 1027 \text{ m}, 957 \text{ w}, 938 \text{ m}, 923 \text{ m}, 878 \text{ m}, 839 \text{ m}, 820 \text{ m}, 794 \text{ s}, 751 \text{ vs}, 684 \text{ m}, 590 \text{ m}, 527 \text{ m}, 484 \text{ m}, 441 \text{ s}, 417 \text{ s}, 334 \text{ s}, 312 \text{ s}, 276 \text{ s}, 147 \text{ vs}, 112 \text{ s}, 89 \text{ s}, 69 \text{ s cm}^{-1}$. Mp: 137 °C.

5. Crystal data and refinement details

X-ray Crystallography

The single-crystal X-ray diffraction data of all the following compounds were collected with a STOE IPDS 2T diffractometer with graphite-monochromated Mo-K α (0.71073) radiation.

Table 15. Crystal data and structure refinement of **4**

Identification code	li0026
Formula Sum	C ₄₀ H ₆₄ Li ₂ N ₂ O ₃
Formula weight	634.81
Crystal size (mm)	0.21 × 0.22 × 0.41
Crystal system	monoclinic
Space group	<i>P</i> 2 ₁
Unit cell parameters	<i>a</i> (Å) 10.733(3) <i>a</i> (°) 90 <i>b</i> (Å) 17.173(6) <i>β</i> (°) 109.2(2) <i>c</i> (Å) 10.982(3) <i>γ</i> (°) 90
Unit cell volume <i>V</i> (Å ³)	1912.1(1)
Molecules per cell <i>Z</i>	2
Crystallographic density ρ_{calcd} (g cm ⁻³)	1.103
Absorption coefficient μ (mm ⁻¹)	0.067
Temperature (°C)	-140
Scan type	ω scan (increment 1.5°, exposure 7 min)
Completeness of dataset	99.9%
θ range of data collection (°)	1.963 ... 25.000
Reflections collected	12434
Independent reflections	6705 (<i>R</i> _{int} = 0.0296)
Independent reflections with $I > 2\sigma(I)$	6177
Solution method	direct methods (SIR-97)
Refinement method	full-matrix least-squares on <i>F</i> ² (SHELXL 2014)
Absorption correction method	none
Range of transmission factors	–
Data / parameters / restraints	6705 / 424 / 1
Goodness of fit (goof) [all data]	1.031
Final R values	
<i>R</i> ₁ [all data, $I \geq 2\sigma(I)$]	0.0439, 0.0391
<i>wR</i> ₂ [all data, $I \geq 2\sigma(I)$]	0.0948, 0.0924
Largest difference peak and hole	0.239 and -0.179 e Å ⁻³
Flack parameter	0.1(4) ^a

Refinement special details: ^a Due to the absence of heavy atoms, the absolute configuration could not be determined reliable.

Table 16. Selected bond lengths [\AA] and angles [$^\circ$] of **4**

Li(1)–N(1)	2.008(4)	C(2)–N(1)	1.418(3)
Li(1)–N(2)	2.03(6)	C(3)–N(2)	1.421(3)
Li(2)–N(1)	2.021(4)	C(1)–C(2)	1.508(4)
Li(2)–N(2)	2.046(5)	C(2)–C(3)	1.363(3)
Li(1)–C(2)	2.260(5)	C(3)–C(4)	1.514(3)
Li(1)–C(3)	2.260(6)	N(1)–Li(1)–N(2)	83.6(2)
Li(1)–O(1)	2.442(6)	N(1)–Li(2)–N(2)	82.9(2)
Li(1)–O(2)	1.895(5)	O(1)–Li(1)–O(2)	107.2(2)
Li(2)–O(3)	1.946(4)	O(1)–Li(2)–O(3)	98.4(2)
Li(2)–O(1)	2.166(5)	Li(1)–O(1)–Li(2)	60.8(2)

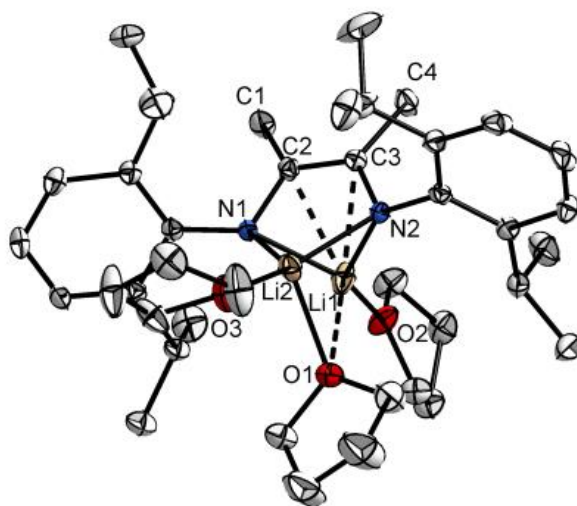
**Figure 51.** Molecular structure of **4** in the crystalline state: Thermal ellipsoids with 50% probability, H atoms omitted for clarity.

Table 17. Crystal data and structure refinement of **5**

Identification code	li0058
Formula Sum	C ₄₄ H ₇₂ N ₂ Na ₂ O ₄
Formula weight	739.01
Crystal size (mm)	0.19 × 0.37 × 0.49
Crystal system	monoclinic
Space group	<i>P</i> 2 ₁ / <i>c</i>
Unit cell parameters	<i>a</i> (Å) 10.06(3) <i>α</i> (°) 90 <i>b</i> (Å) 41.006(1) <i>β</i> (°) 111.9(2) <i>c</i> (Å) 11.385(4) <i>γ</i> (°) 90
Unit cell volume <i>V</i> (Å ³)	4358.1(2)
Molecules per cell <i>Z</i>	4
Crystallographic density ρ_{calcd} (g cm ⁻³)	1.126
Absorption coefficient μ (mm ⁻¹)	0.078
Temperature (°C)	-120
Scan type	ω scan (increment 1.5°, exposure 15 min)
Completeness of dataset	99.8%
θ range of data collection (°)	2.169 ... 25.000
Reflections collected	26731
Independent reflections	7662 (R _{int} = 0.0510)
Independent reflections with $I > 2\sigma(I)$	6121
Solution method	direct methods (SIR-97)
Refinement method	full-matrix least-squares on F^2 (SHELXL 2014)
Absorption correction method	none
Range of transmission factors	–
Data / parameters / restraints	7662 / 515 / 20 ^a
Goodness of fit (gooF) [all data]	1.069
Final R values	
R ₁ [all data, $I \geq 2\sigma(I)$]	0.0837, 0.0684
wR ₂ [all data, $I \geq 2\sigma(I)$]	0.1794, 0.1697
Largest difference peak and hole	0.424 and -0.404 e Å ⁻³
Flack parameter	–

Refinement special details: One THF ligand (C41–C44, O4) is disordered over two positions; site occupancy factors thereof were refined freely. The quality of the structure refinement is limited by moderate disorder of all THF ligands (see *R* values). ^a Restraints on anisotropic displacement parameters of the split THF ligand (DELU commands).

Table 18. Selected bond lengths [\AA] and angles [$^\circ$] of **5**

Na(1)–N(1)	2.388(2)	C(1)–N(1)	1.420(3)
Na(1)–N(2)	2.380(2)	C(2)–N(2)	1.408(4)
Na(2)–N(1)	2.354(2)	C(1)–C(2)	1.372(4)
Na(2)–N(2)	2.385(2)	C(1)–C(3)	1.513(4)
Na(1)–C(1)	2.608(3)	C(2)–C(4)	1.512(4)
Na(1)–C(2)	2.611(2)	N(1)–Na(1)–N(2)	71.5(7)
Na(1)–O(1)	2.344(3)	N(2)–Na(2)–N(1)	72.1(8)
Na(1)–O(2)	2.299(2)	O(1)–Na(1)–O(2)	85.9(9)
Na(2)–O(3)	2.298(4)	O(3)–Na(2)–O(4A)	82.9(4)
Na(2)–O(4A)	2.273(2)		

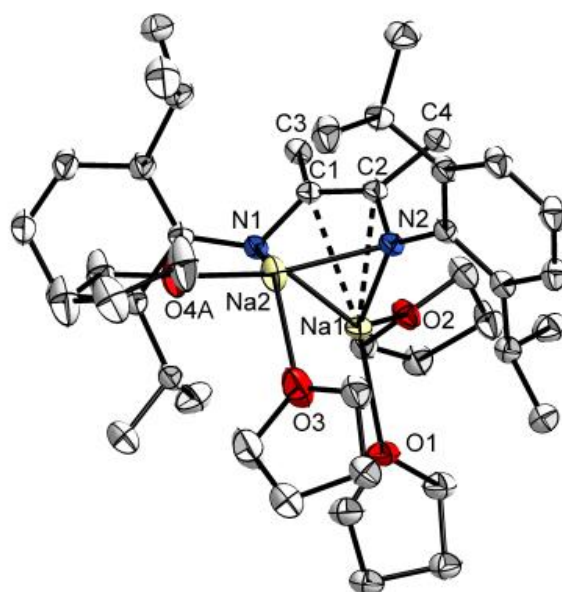


Figure 52. Molecular structure of **5** in the crystalline state : Thermal ellipsoids with 50% probability, H atoms omitted for clarity. The THF ligand with O4 is disordered over two positions (only one situation shown; site occupancy factors: 0.54 : 0.46).

Table 19. Crystal data and structure refinement of **6**

Identification code	li0070
Formula Sum	C ₈₄ H ₁₃₆ K ₄ N ₄ O ₇
Formula weight	1470.36
Crystal size (mm)	0.10 × 0.17 × 0.40
Crystal system	triclinic
Space group	$P\bar{1}$
Unit cell parameters	a (Å) 9.944(4) α (°) 104.4(2) b (Å) 20.126(6) β (°) 98.8(2) c (Å) 23.151(6) γ (°) 102.7(2)
Unit cell volume V (Å ³)	4270.6(2)
Molecules per cell Z	2
Crystallographic density ρ_{calcd} (g cm ⁻³)	1.143
Absorption coefficient μ (mm ⁻¹)	0.260
Temperature (°C)	-120
Scan type	ω scan (increment 1.5°, exposure 13 min)
Completeness of dataset	99.4%
θ range of data collection (°)	1.860 ... 24.999
Reflections collected	32377
Independent reflections	14951 ($R_{\text{int}} = 0.0891$)
Independent reflections with $I > 2\sigma(I)$	11145
Solution method	direct methods (SIR-97)
Refinement method	full-matrix least-squares on F^2 (SHELXL 2014)
Absorption correction method	none
Range of transmission factors	–
Data / parameters / restraints	14951 / 892 / 69 ^a
Goodness of fit (gooF) [all data]	1.027
Final R values	
R ₁ [all data, $I \geq 2\sigma(I)$]	0.0845, 0.0602
wR ₂ [all data, $I \geq 2\sigma(I)$]	0.1631, 0.1491
Largest difference peak and hole	0.571 and -0.456 e Å ⁻³
Flack parameter	–

Refinement special details: The quality of the structure refinement (see R values) is limited by moderate disorder of all THF ligands. ^a Restraints on anisotropic displacements parameters (SIMU and DELU commands) of some THF C atoms (C29–C32, C33–C36, C77–C80).

Table 20. Selected bond lengths [\AA] and angles [$^\circ$] of **6**

K(1)–N(1)	2.681(2)	K(4)–(O4)	2.818(2)
K(1)–N(2)	2.763(3)	K(4)–(O6)	2.712(3)
K(2)–N(1)	2.738(3)	K(4)–(O7)	2.737(3)
K(2)–N(2)	2.767(2)	C(1)–C(2)	1.361(5)
K(3)–N(3)	2.686(2)	C(41)–C(42)	1.364(4)
K(3)–N(4)	2.714(3)	C(1)–N(1)	1.420(4)
K(4)–N(3)	2.726(2)	C(2)–N(2)	1.413(4)
K(4)–N(4)	2.818(2)	C(41)–N(3)	1.407(4)
K(1)–C(1)	2.899(2)	C(42)–N(4)	1.417(4)
K(1)–C(2)	2.935(3)	N(1)–K(1)–N(2)	64.6(8)
K(1)–C(59)	3.121(4)	N(1)–K(2)–N(2)	63.8(6)
K(1)–C(60)	2.965(4)	N(3)–K(3)–N(4)	64.1(7)
K(1)–C(61)	3.268(4)	N(3)–K(4)–N(4)	62.3(6)
K(3)–C(41)	2.955(2)	O(1)–K(2)–O(3)	87.5(8)
K(3)–C(42)	2.961(3)	O(1)–K(2)–O(2)	120.0(8)
K(3)–C(8)	3.284(4)	O(3)–K(2)–O(2)	96.2(8)
K(1)–O(1)	2.826(3)	O(4)–K(3)–O(5)	149.0(8)
K(2)–O(1)	2.879(2)	O(6)–K(4)–O(7)	87.2(8)
K(2)–O(2)	2.738(3)	O(4)–K(4)–O(6)	120.3(7)
K(2)–O(3)	2.739(3)	O(4)–K(4)–O(7)	80.7(7)
K(3)–O(4)	3.165(2)	K(1)–O(1)–K(2)	80.5(8)
K(3)–O(5)	2.652(3)	K(3)–O(4)–K(4)	75.0(5)

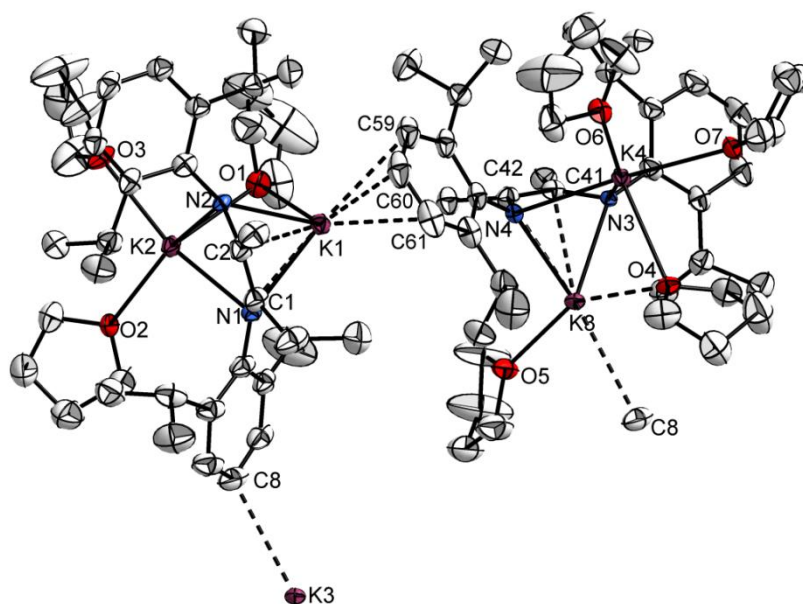
**Figure 53.** Molecular structure of **6** in the crystalline state: Thermal ellipsoids with 30% probability, H atoms omitted for clarity.

Table 21. Crystal data and structure refinement of **7**

Identification code	li0025
Formula Sum	C ₉₂ H ₁₅₂ N ₄ O ₉ Rb ₄
Formula weight	1800.05
Crystal size (mm)	0.14 × 0.20 × 0.45
Crystal system	monoclinic
Space group	P 2 ₁ /c
Unit cell parameters	<i>a</i> (Å) 36.526(7) <i>α</i> (°) 90 <i>b</i> (Å) 12.578(2) <i>β</i> (°) 105.6(2) <i>c</i> (Å) 21.387(5) <i>γ</i> (°) 90
Unit cell volume <i>V</i> (Å ³)	9463.9(3)
Molecules per cell <i>Z</i>	4
Crystallographic density ρ_{calcd} (g cm ⁻³)	1.263
Absorption coefficient μ (mm ⁻¹)	2.110
Temperature (°C)	-140
Scan type	ω scan (increment 1.5°, exposure 10 min)
Completeness of dataset	97.4% ^a
θ range of data collection (°)	1.897 ... 24.999
Reflections collected	48335
Independent reflections	16211 (R _{int} = 0.0720)
Independent reflections with <i>I</i> > 2 σ (<i>I</i>)	11846
Solution method	patterson methods (SHELXS 2013)
Refinement method	full-matrix least-squares on <i>F</i> ² (SHELXL 2014)
Absorption correction method	numerical
Range of transmission factors	0.5507 ... 0.7552
Data / parameters / restraints	16211 / 1056 / 251 ^b
Goodness of fit (goof) [all data]	1.060
Final R values	
R ₁ [all data, <i>I</i> ≥ 2 σ (<i>I</i>)]	0.0834, 0.0527
wR ₂ [all data, <i>I</i> ≥ 2 σ (<i>I</i>)]	0.1279, 0.1148
Largest difference peak and hole	0.756 and -0.554 e Å ⁻³
Flack parameter	–

Refinement special details: ^a Missing data are a result of overlapping reflections due to a very large unit cell. ^b Restraints on C-C and C-O distances and on anisotropic displacement parameters of two THF ligands (O5, C73–C76 and O8, C85–C88) and the non-coordinated THF molecule (O9, C89–C92). Site occupancy factors of the atoms of disordered isopropyl group (C56, C57) and THF ligand (O8, C85–C88) were freely refined, those of C atoms C91 and C92 of the non-coordinated THF molecule were constrained to 0.5.

Table 22. Selected bond lengths [Å] and angles [°] of **7**

Rb(1)–N(1)	2.918(4)	Rb(4)–O(7)	2.916(5)
Rb(1)–N(2)	2.893(3)	Rb(4)–O(8A)	2.843(9)
Rb(2)–N(1)	2.868(3)	C(2)–N(1)	1.411(4)
Rb(2)–N(2)	2.951(4)	C(3)–N(2)	1.414(4)
Rb(3)–N(3)	2.886(4)	C(46)–N(3)	1.404(6)
Rb(3)–N(4)	2.909(4)	C(47)–N(4)	1.407(7)
Rb(4)–N(3)	2.928(4)	C(2)–C(3)	1.367(6)
Rb(4)–N(4)	2.875(4)	C(46)–C(47)	1.362(6)
Rb(1)–C(2)	3.039(4)	N(1)–Rb(1)–N(2)	58.7(8)
Rb(1)–C(3)	3.057(4)	N(1)–Rb(2)–N(2)	58.6(9)
Rb(3)–C(46)	3.039(4)	N(3)–Rb(3)–N(4)	59.8(1)
Rb(3)–C(47)	3.028(4)	N(3)–Rb(4)–N(4)	59.7(1)
Rb(1)–O(1)	2.903(3)	O(2)–Rb(2)–O(3)	74.7(1)
Rb(2)–O(2)	2.891(3)	O(2)–Rb(2)–O(4)	91.5(1)
Rb(2)–O(3)	2.952(4)	O(3)–Rb(2)–O(4)	84.0(1)
Rb(2)–O(4)	2.864(4)	O(6)–Rb(4)–O(7)	82.9(1)
Rb(3)–O(5)	2.869(7)	O(6)–Rb(4)–O(8A)	87.9(2)
Rb(4)–O(6)	2.899(4)	O(7)–Rb(4)–O(8A)	76.3(2)

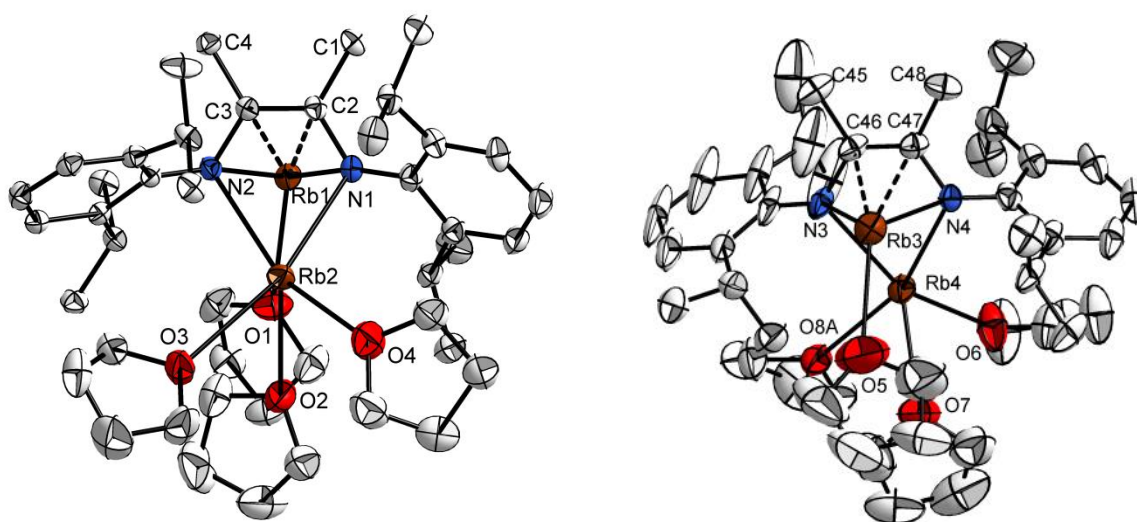


Figure 54. Molecular structure of **7** in the crystalline state: Thermal ellipsoids with 50% probability, H atoms omitted for clarity. Molecule 1 (left) in the asymmetric unit (Symmetry operators to generate equivalent atoms: i $1-x, 0.5+y, 0.5-z$; ii $1-x, -0.5+y, 0.5-z$). Molecule 2 (right) in the asymmetric unit (One isopropyl substituent at the Dipp group attached to N3 and the THF ligand O8 are disordered over two positions. Symmetry operators to generate equivalent atoms: iii $-x, 0.5+y, 0.5-z$, iv $-x, -0.5+y, 0.5-z$).

Table 23. Crystal data and structure refinement of **8**

Identification code	fe0235	
Formula Sum	C ₄₈ H ₈₀ Cs ₂ N ₂ O ₅	
Formula weight	1030.96	
Crystal size (mm)	0.07 x 0.12 x 0.17	
Crystal system	monoclinic	
Space group	C 2/c	
Unit cell parameters	<i>a</i> (Å) 39.16(2)	α (°) 90
	<i>b</i> (Å) 12.227(4)	β (°) 104.4(4)
	<i>c</i> (Å) 21.282(7)	γ (°) 90
Unit cell volume <i>V</i> (Å ³)	9870(8)	
Molecules per cell <i>Z</i>	8	
Crystallographic density ρ_{calcd} (g cm ⁻³)	1.388	
Absorption coefficient μ (mm ⁻¹)	1.521	
Temperature (°C)	-173	
Scan type	ω scan (increment 1.5°, exposure 1 min)	
Completeness of dataset	99.7%	
θ range of data collection (°)	1.943 to 25.199	
Reflections collected	26718	
Independent reflections	8878	
Independent reflections with $I > 2\sigma(I)$	7592	
Solution method	dual-space structure solution (SHELXT 2018/3)	
Refinement method	full-matrix least-squares on F^2 (SHELXL 2018/3)	
Absorption correction method	numerical	
Range of transmission factors	0.8362 to 0.7333	
Data / parameters / restraints	8878 / 756 / 2939	
Goodness of fit (goof) [all data]	1.089	
Final R values		
R ₁ [all data, $I \geq 2\sigma(I)$]	0.0760, 0.0624	
wR ₂ [all data, $I \geq 2\sigma(I)$]	0.1378, 0.1321	
Largest difference peak and hole	0.695 and -1.240 eÅ ⁻³	

Refinement special details: THF ligands with with O1 and O2 are disordered over two positions; THF ligand with O4 is disordered over three positions.

Table 24. Selected bond lengths [\AA] and angles [$^\circ$] of **8**

Cs(1)–N(1)	3.047(4)	C(1)–N(2)	1.413(7)
Cs(1)–N(2)	2.992(4)	C(2)–N(1)	1.397(8)
Cs(2)–N(1)	3.125(5)	C(1)–C(2)	1.334(9)
Cs(2)–N(2)	3.082(6)	C(1)–C(4)	1.519(9)
Cs(2)–C(1)	3.101(7)	C(2)–C(3)	1.515(8)
Cs(2)–C(2)	3.135(7)	N(1)–Cs(1)–N(2)	55.7(1)
Cs(1)–O(2)	3.217(9)	N(1)–Cs(2)–N(2)	54.1(1)
Cs(1)–O(3)	3.003(6)	O(2)–Cs(1)–O(3)	84.8(2)
Cs(1)–O(4)	3.116(2)	O(2)–Cs(1)–O(4)	78.5(5)
Cs(2)–O(1)	3.117(8)	O(3)–Cs(1)–O(4)	69.8(4)

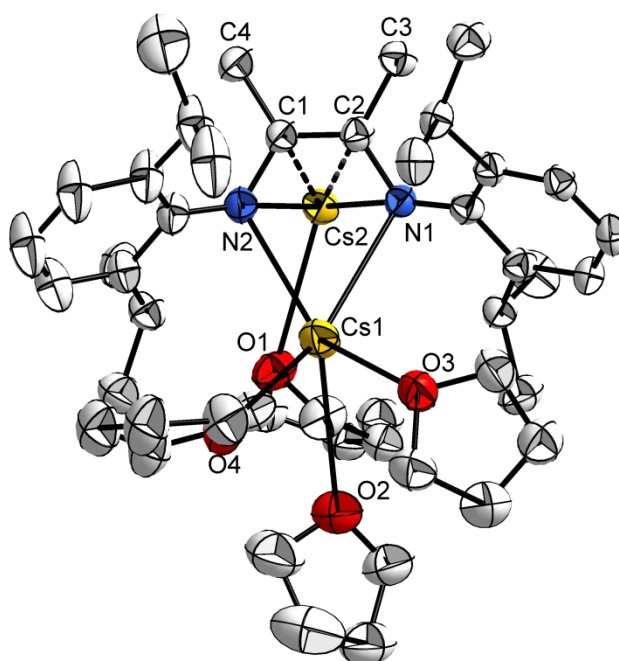
**Figure 55.** Molecular structure of **8** in the crystalline state: Thermal ellipsoids of Rb and N with 50% probability, H atoms omitted for clarity.

Table 25. Crystal data and structure refinement of **9**

Identification code	fe0100
Formula Sum	C _{59.50} H ₉₂ Li ₄ N ₄ O ₃
Formula weight	939.13
Crystal size (mm)	0.07 x 0.10 x 0.16
Crystal system	triclinic
Space group	$P\bar{1}$
Unit cell parameters	a (Å) 12.296(6) α (°) 93.06(5) b (Å) 12.689(7) β (°) 95.75(5) c (Å) 17.358(1) γ (°) 104.34(4)
Unit cell volume V (Å ³)	2602(3)
Molecules per cell Z	2
Crystallographic density ρ_{calcd} (g cm ⁻³)	1.198
Absorption coefficient μ (mm ⁻¹)	0.071
Temperature (°C)	-173
Scan type	ω scan (increment 1.5°, exposure 1 min)
Completeness of dataset	99.0%
θ range of data collection (°)	1.960 to 25.349
Reflections collected	19258
Independent reflections	9447
Independent reflections with $I > 2\sigma(I)$	7630
Solution method	dual-space structure solution (SHELXT 2015)
Refinement method	full-matrix least-squares on F^2 (SHELXL 2015)
Absorption correction method	none
Range of transmission factors	-
Data/parameters/restraints	9447 / 714 / 1551
Goodness of fit (goof) [all data]	1.204
Final R values	
R_1 [all data, $I \geq 2\sigma(I)$]	0.0829, 0.0615
wR_2 [all data, $I \geq 2\sigma(I)$]	0.1207, 0.1134
Largest difference peak and hole	0.225 and -0.207 eÅ ⁻³

Table 26. Selected bond lengths [Å] and angles [°] of **9**

Li(1)–N(1)	2.020(4)	Li(1)–O(1)	1.991(4)
Li(1)–N(2)	2.026(4)	Li(2)–O(3)	2.433(4)
Li(2)–N(1)	2.024(5)	Li(4)–O(2)	1.970(2)
Li(2)–N(3)	2.057(4)	Li(4)–O(3)	2.098(4)
Li(2)–N(4)	2.171(5)	C(1)–N(1)	1.407(3)
Li(3)–N(2)	1.955(4)	C(2)–N(2)	1.406(3)
Li(3)–N(3)	2.218(4)	C(23)–N(3)	1.399(3)
Li(3)–N(4)	2.144(4)	C(24)–N(4)	1.405(3)
Li(4)–N(3)	2.137(4)	C(1)–C(2)	1.355(3)
Li(4)–N(4)	2.157(4)	C(23)–C(24)	1.351(3)
Li(1)–C(1)	2.291(4)	N(1)–Li(1)–N(2)	93.7(2)
Li(1)–C(2)	2.294(4)	N(3)–Li(2)–N(4)	77.6(1)
Li(3)–C(23)	2.208(5)	N(3)–Li(3)–N(4)	74.8(1)
Li(3)–C(24)	2.187(5)	N(3)–Li(4)–N(4)	76.2(1)
Li(4)–C(23)	2.199(4)	O(2)–Li(4)–O(3)	94.7(7)
Li(4)–C(24)	2.191(4)	Li(2)–O(3)–Li(4)	65.1(1)

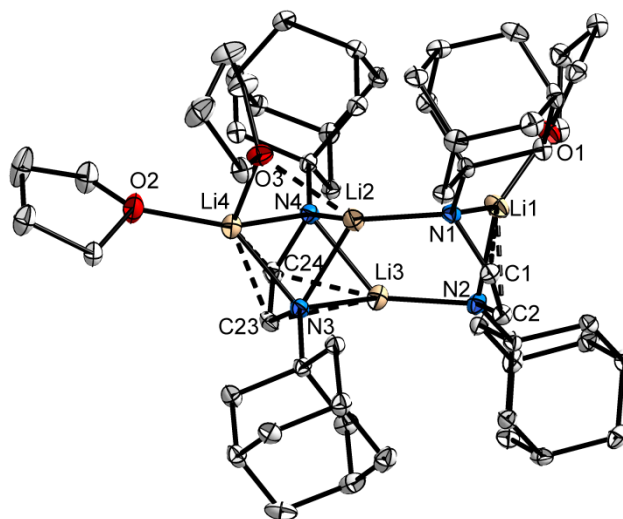
**Figure 56.** Molecular structure of **9** in the crystalline state: Thermal ellipsoids with 30% probability, H atoms omitted for clarity.

Table 27. Crystal data and structure refinement of **11**

Identification	fe0283
Formula Sum	C ₄₀ H ₆₄ KLiN ₂ O ₃
Formula weight	666.97
Crystal size (mm)	0.12 x 0.16 x 0.18 mm
Crystal system	monoclinic
Space group	<i>P</i> 2 ₁ /c
Unit cell parameters	<i>a</i> (Å) 12.906(2) <i>α</i> (°) 90 <i>b</i> (Å) 17.670(3) <i>β</i> (°) 108.0(1) <i>c</i> (Å) 17.953(3) <i>γ</i> (°) 90
Unit cell volume <i>V</i> (Å ³)	3892.8(1)
Molecules per cell <i>Z</i>	4
Crystallographic density ρ_{calcd} (g cm ⁻³)	1.138
Absorption coefficient μ (mm ⁻¹)	0.174
Temperature (°C)	-173
Scan type	ω scan (increment 1.5°, exposure 1 min)
Completeness of dataset	99.4%
θ range of data collection (°)	2.021 to 25.200
Reflections collected	19359
Independent reflections	6971
Independent reflections with $I > 2\sigma(I)$	6079
Solution method	dual-space structure solution (SHELXT 2018/3)
Refinement method	full-matrix least-squares on F^2 (SHELXL 2018/3)
Absorption correction method	none
Data / parameters / restraints	6971 / 572 / 1667
Goodness of fit (goof) [all data]	1.105
Final R values	
R ₁ [all data, $I \geq 2\sigma(I)$]	0.0675, 0.0553
wR ₂ [all data, $I \geq 2\sigma(I)$]	0.1180, 0.1131
Largest difference peak and hole	0.197 and -0.254 eÅ ⁻³

Table 28. Selected bond lengths [\AA] and angles [$^\circ$] of **11**

Li(1)–N(1)	1.924(4)	C(1)–N(1)	1.412(2)
Li(1)–N(2)	1.928(4)	C(2)–N(2)	1.415(3)
K(1)–N(1)	2.838(2)	C(1)–C(2)	1.367(3)
K(1)–N(2)	2.840(2)	C(1)–C(3)	1.508(3)
K(1)–C(1)	2.925(2)	C(2)–C(4)	1.511(3)
K(1)–C(2)	2.920(2)	N(1)–Li(1)–N(2)	89.4(2)
K(1)–O(1A)	2.791(1)	N(1)–K(1)–N(2)	57.0(5)
K(1)–O(1B)	2.605(5)	O(1A)–K(1)–O(1B)	79.7(4)
Li(1)–O(1C)	1.874(1)		

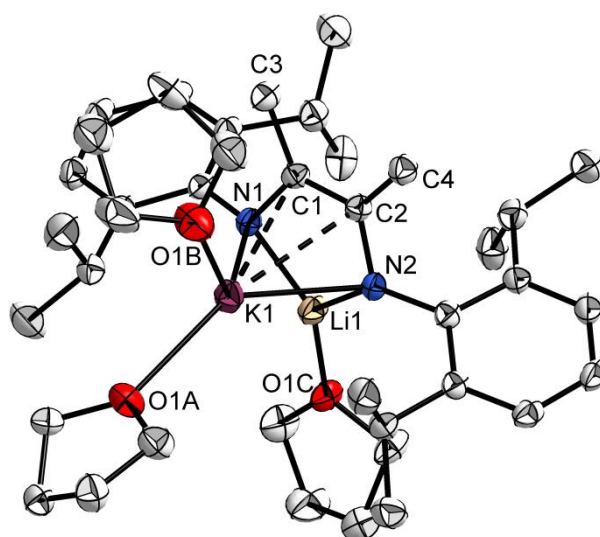
**Figure 57.** Molecular structure of **9** in the crystalline state: Thermal ellipsoids with 30% probability, H atoms omitted for clarity.

Table 29. Crystal data and structure refinement of **12**

Identification code	fe0250
Formula Sum	C ₈₀ H ₁₂₈ Li ₂ N ₄ O ₆ Rb ₂
Formula weight	1426.68
Crystal size (mm)	0.15 x 0.18 x 0.23
Crystal system	monoclinic
Space group	<i>P</i> 2 ₁ /c
Unit cell parameters	<i>a</i> (Å) 20.111(1) <i>α</i> (°) 90 <i>b</i> (Å) 13.173(5) <i>β</i> (°) 95.8(4) <i>c</i> (Å) 29.333(1) <i>γ</i> (°) 90
Unit cell volume <i>V</i> (Å ³)	7731(6)
Molecules per cell <i>Z</i>	4
Crystallographic density ρ_{calcd} (g cm ⁻³)	1.226
Absorption coefficient μ (mm ⁻¹)	1.318
Temperature (°C)	-173
Scan type	ω scan (increment 1.5°, exposure 1 min)
Completeness of dataset	99.2%
θ range of data collection (°)	1.809 to 25.500
Reflections collected	38209
Independent reflections	14264
Independent reflections with $I > 2\sigma(I)$	11237
Solution method	dual-space structure solution (SHELXT 2018/3)
Refinement method	full-matrix least-squares on F^2 (SHELXL 2018/3)
Absorption correction method	numerical
Range of transmission factors	0.7125 to 0.6603
Data / parameters / restraints	14264 / 913 / 1826
Goodness of fit (goof) [all data]	1.030
Final R values	
R ₁ [all data, $I \geq 2\sigma(I)$]	0.0780, 0.0566
wR ₂ [all data, $I \geq 2\sigma(I)$]	0.1268, 0.1182
Largest difference peak and hole	0.635 and -0.543 eÅ ⁻³

Table 30. Selected bond lengths [Å] and angles [°] of **12**

Li(1)–N(1)	1.909(6)	Li(1)–O(1)	1.864(7)
Li(1)–N(2)	1.909(6)	Li(2)–O(3)	1.853(6)
Li(2)–N(3)	1.910(6)	Rb(1)–O(2)	2.891(1)
Li(2)–N(4)	1.899(6)	Rb(2)–O(4)	2.950(3)
Rb(1)–N(1)	3.075(3)	C(1)–N(1)	1.404(4)
Rb(1)–N(2)	2.953(3)	C(2)–N(2)	1.407(4)
Rb(2)–N(3)	3.084(3)	C(29)–N(3)	1.406(4)
Rb(2)–N(4)	3.009(3)	C(30)–N(4)	1.403(4)
Rb(1)–C(1)	3.098(3)	C(1)–C(2)	1.368(4)
Rb(1)–C(2)	3.041(3)	C(29)–C(30)	1.376(4)
Rb(1)–C(47)	3.238(4)	N(1)–Li(1)–N(2)	91.2(3)
Rb(1)–C(48)	3.278(4)	N(3)–Li(2)–N(4)	90.9(3)
Rb(2)–C(29)	3.106(3)	N(1)–Rb(1)–N(2)	53.7(7)
Rb(2)–C(30)	3.056(3)	N(3)–Rb(2)–N(4)	52.9(7)

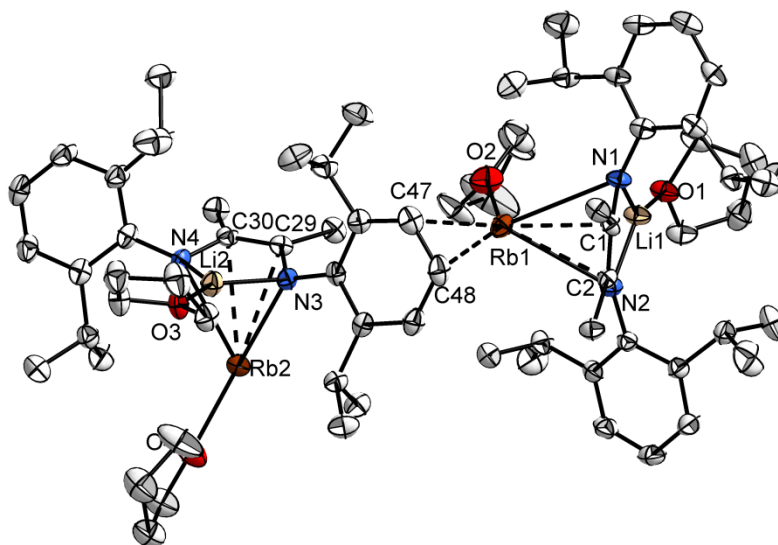
**Figure 58.** Molecular structure of **12** in the crystalline state: Thermal ellipsoids with 50% probability, H atoms omitted for clarity.

Table 31. Crystal data and structure refinement of **15**

Identification code	fe0281
Formula sum	C ₁₀₈ H ₁₆₈ Li ₄ N ₈ Na ₄ O ₅
Formula weight	1778.21
Crystal size (mm)	0.14 x 0.16 x 0.21
Crystal system	monoclinic
Space group	<i>P</i> 2/n
Unit cell parameters	<i>a</i> (Å) 12.104(3) <i>α</i> (°) 90 <i>b</i> (Å) 23.079(6) <i>β</i> (°) 90.3(3) <i>c</i> (Å) 35.954(2) <i>γ</i> (°) 90
Unit cell volume <i>V</i> (Å ³)	10043(6)
Molecules per cell <i>Z</i>	4
Crystallographic density ρ_{calcd} (g cm ⁻³)	1.176
Absorption coefficient μ (mm ⁻¹)	0.085
Temperature (°C)	-173
Scan type	ω scan (increment 1.5°, exposure 1 min)
Completeness of dataset	94.5%
θ range of data collection (°)	1.765 to 25.350
Reflections collected	45527
Independent reflections	17403
Independent reflections with $I > 2\sigma(I)$	13259
Solution method	dual-space structure solution (SHELXT 2018/3)
Refinement method	full-matrix least-squares on F^2 (SHELXL 2018/3)
Absorption correction method	none
Data / parameters / restraints	17403 / 1576 / 4863
Goodness of fit (goof) [all data]	1.227
Final R values	
R ₁ [all data, $I \geq 2\sigma(I)$]	0.1790, 0.1436
wR ₂ [all data, $I \geq 2\sigma(I)$]	0.2850, 0.2700
Largest difference peak and hole	0.422 and -0.387 eÅ ⁻³

Refinement special details: Low completeness, probably not publishable.

Table 32. Selected bond lengths [Å] and angles [°] of **15**

Li(1)–N(1)	1.950(1)	C(2)–N(1)	1.398(8)
Li(1)–N(2)	1.945(1)	C(1)–N(2)	1.377(8)
Li(2)–N(3)	1.949(1)	C(23)–N(4)	1.394(6)
Li(2)–N(4)	1.929(1)	C(24)–N(3)	1.396(7)
Na(1)–N(1)	2.751(5)	C(1)–C(2)	1.368(9)
Na(1)–N(2)	2.857(5)	C(23)–C(24)	1.366(7)
Na(2)–N(1)	2.515(5)	N(1)–Li(1)–N(2)	87.5(4)
Na(2)–N(2)	2.668(5)	N(3)–Li(2)–N(4)	87.3(4)
Na(2)–N(3)	2.680(5)	N(5)–Li(3)–N(6)	87.5(4)
Na(2)–N(4)	2.722(5)	N(7)–Li(4)–N(8)	87.3(4)
Na(1)–C(1)	2.633(6)	N(1)–Na(1)–N(2)	57.4(2)
Na(1)–C(2)	2.579(6)	N(1)–Na(2)–N(2)	62.6(2)
Na(2)–C(1)	2.606(6)	N(3)–Na(2)–N(4)	59.5(1)
Na(2)–C(2)	2.514(6)	N(3)–Na(3)–N(4)	59.6(1)
Na(2)–C(23)	2.530(6)	N(5)–Na(3)–N(6)	59.6(1)
Na(2)–C(24)	2.491(6)	N(5)–Na(4)–N(6)	59.3(1)
Li(1)–O(1A)	1.944(1)	N(7)–Na(4)–N(8)	62.4(2)
Li(2)–O(1B)	2.013(2)	N(7)–Na(5)–N(8)	57.6(1)

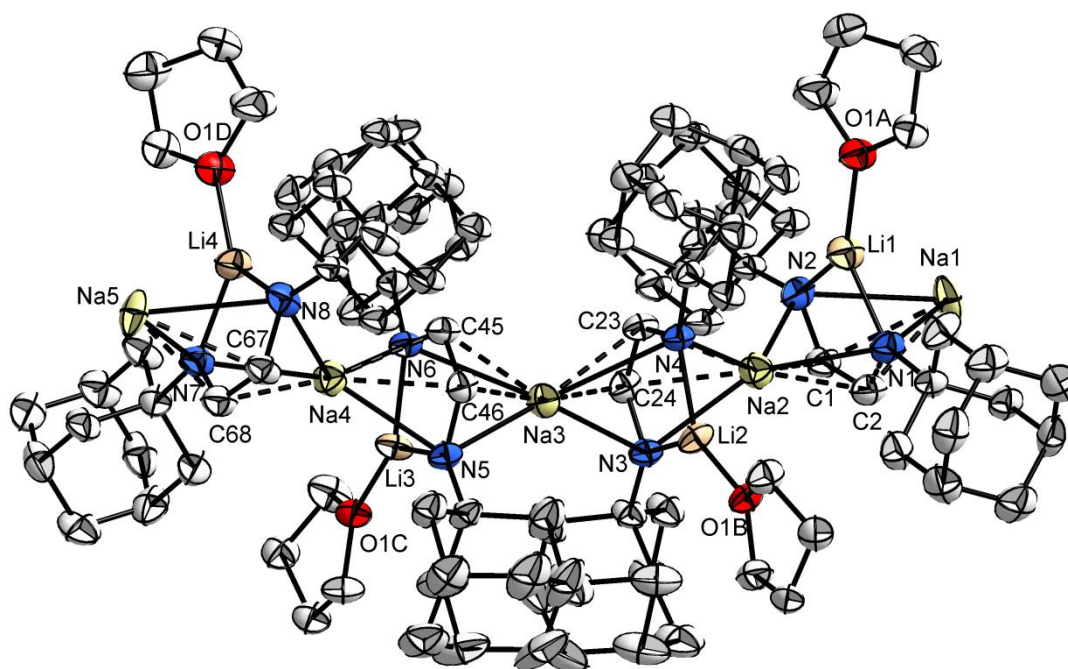
**Figure 59.** Molecular structure of **15** in the crystalline state: Thermal ellipsoids with 50% probability, H atoms omitted for clarity.

Table 33. Crystal data and structure refinement of **16**

Identification code	li0151
Formula Sum	C ₃₂ H ₅₀ LiN ₂ O ₂
Formula weight	501.68
size (mm)	0.19 × 0.27 × 0.37
Crystal system	tetragonal
Space group	<i>P</i> 4 ₃ 2 ₁ 2
Unit cell parameters	<i>a</i> (Å) 10.123(2) <i>α</i> (°) 90 <i>b</i> (Å) = <i>a</i> <i>β</i> (°) 90 <i>c</i> (Å) 30.606(1) <i>γ</i> (°) 90
Unit cell volume <i>V</i> (Å ³)	3136.5(2)
Molecules per cell <i>Z</i>	4
Crystallographic density ρ_{calcd} (g cm ⁻³)	1.062
Absorption coefficient μ (mm ⁻¹)	0.064
Temperature (°C)	-120
Scan type	ω scan (increment 1.5°, exposure 8 min)
Completeness of dataset	99.3%
θ range of data collection (°)	2.119 ... 24.993
Reflections collected	13460
Independent reflections	2735 (<i>R</i> _{int} = 0.0332)
Independent reflections with <i>I</i> > 2 σ (<i>I</i>)	2345
Solution method	direct methods (SIR-97)
Refinement method	full-matrix least-squares on <i>F</i> ² (SHELXL 2016/4)
Absorption correction method	none
Data / parameters / restraints	2735 / 234 / 48 ^a
Goodness of fit (goof) [all data]	1.055
Final R values	
<i>R</i> ₁ [all data, <i>I</i> ≥ 2 σ (<i>I</i>)]	0.0559, 0.0463
<i>wR</i> ₂ [all data, <i>I</i> ≥ 2 σ (<i>I</i>)]	0.1249, 0.1194
Largest difference peak and hole	0.174 and -0.143 e Å ⁻³
Extinction coefficient	0.011(4)
Flack parameter	0.2(6) ^b

Refinement special details: One isopropyl group (C12–C14) and the DME ligand (O, C15, C16) are disordered over each two orientations, site occupancy factors were refined freely. SADI and SIMU restraints ^a were applied on both disordered groups. The absolute configuration cannot be determined reliable due to the absence of heavy atoms. The value of the Flack parameter ^b is meaningless.

Table 34. Selected bond lengths [\AA] and angles [$^\circ$] of **16**

Li–N	2.032(4)	C(1)–C(1')	1.448(3)
Li–N'	2.032(4)	C(1)–C2	1.485(4)
Li–O1	2.146(2)	C(1')–C2'	1.485(4)
Li–O(1')	2.146(2)	N–Li–N'	81.0(8)
C(1)–N	1.329(3)	O–Li–O'	77.5(6)
C(1')–N'	1.329(3)		

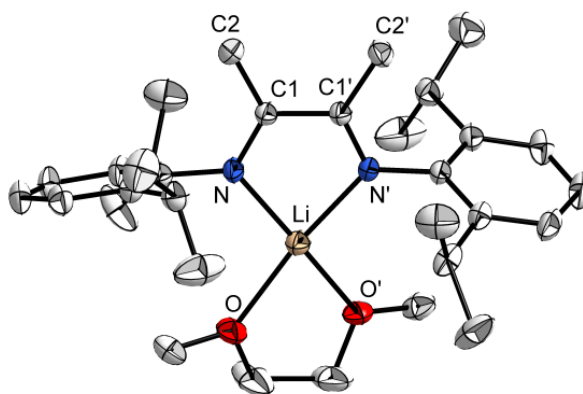
**Figure 60.** Molecular structure of **16** in the crystalline state: Thermal ellipsoids with 50% probability, H atoms omitted for clarity.

Table 35. Crystal data and structure refinement of **19**

Identification code	li0047
Formula Sum	C ₃₀ H ₄₈ LiN ₂ O ₂
Formula weight	475.64
Crystal size (mm)	0.23 × 0.27 × 0.44
Crystal system	triclinic
Space group	$P\bar{1}$
Unit cell parameters	a (Å) 10.675(5) α (°) 95.8(3) b (Å) 11.278(5) β (°) 100.2(3) c (Å) 11.880(5) γ (°) 104.9(3)
Unit cell volume V (Å ³)	1344.0(1)
Molecules per cell Z	2
Crystallographic density ρ_{calcd} (g cm ⁻³)	1.175
Absorption coefficient μ (mm ⁻¹)	0.072
Temperature (°C)	-120
Scan type	ω scan (increment 1.5°, exposure 5 min)
Completeness of dataset	99.6%
θ range of data collection (°)	1.891 ... 24.999
Reflections collected	11763
Independent reflections	4725 (R _{int} = 0.0390)
Independent reflections with $I > 2\sigma(I)$	3669
Solution method	direct methods (SHELXS 2013)
Refinement method	full-matrix least-squares on F^2 (SHELXL 2014)
Absorption correction method	none
Range of transmission factors	–
Data / parameters / restraints	4725 / 316 / 0
Goodness of fit (goof) [all data]	1.027
Final R values	
R ₁ [all data, $I \geq 2\sigma(I)$]	0.0647, 0.0476
wR ₂ [all data, $I \geq 2\sigma(I)$]	0.1266, 0.1190
Largest difference peak and hole	0.423 and -0.274 e Å ⁻³
Flack parameter	–

Table 34. Selected bond lengths [Å] and angles [°] of **19**

Li–N(1)	1.995(3)	C(2)–N(2)	1.328(2)
Li–N(2)	2.010(3)	C(1)–C(2)	1.408(2)
Li–O(1)	1.953(2)	N(1)–Li–N(2)	87.4(1)
Li–O(2)	2.002(3)	O(1)–Li–O(2)	103.7(1)
C(1)–N(1)	1.320(2)		

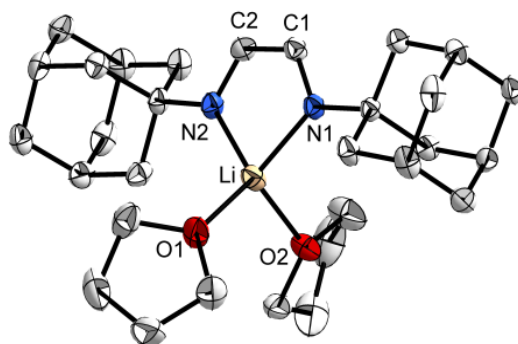
**Figure 61.** Molecular structure of **19** in the crystalline state: Thermal ellipsoids with 50% probability, H atoms omitted for clarity.

Table 36. Crystal data and structure refinement of **20**

Identification code	fe0061
Formula Sum	C ₆₀ H ₈₈ LiN ₄ O ₂
Formula weight	904.28
Crystal size (mm)	0.14 x 0.17 x 0.21 mm
Crystal system	monoclinic
Space group	P2 ₁
Unit cell parameters	a (Å) 10.180(1) α (°) 90 b (Å) 12.816(3) β (°) 102.8(1) c (Å) 21.905(3) γ (°) 90
Unit cell volume V (Å ³)	2786.2(8)
Molecules per cell Z	2
Crystallographic density ρ_{calcd} (g cm ⁻³)	1.078
Absorption coefficient μ (mm ⁻¹)	0.064
Temperature (°C)	-173
Scan type	ω scan (increment 1.5°, exposure 15 min)
Completeness of dataset	99.8%
θ range of data collection (°)	1.853 to 25.500
Reflections collected	23944
Independent reflections	9924
Independent reflections with $I > 2\sigma(I)$	9924
Solution method	dual-space structure solution (SHELXT 2017/1)
Refinement method	full-matrix least-squares on F^2 (SHELXL 2017/1)
Absorption correction method	none
Range of transmission factors	-
Data / parameters / restraints	9924 / 729 / 1383
Goodness of fit (goof) [all data]	1.061
Final R values	
R ₁ [all data, $I \geq 2\sigma(I)$]	0.0661, 0.0514
wR ₂ [all data, $I \geq 2\sigma(I)$]	0.1110, 0.1051
Largest difference peak and hole	0.144 and -0.240 eÅ ⁻³

Refinement special details: THF ligands are disordered over two positions.

Table 38. Selected bond lengths [\AA] and angles [$^\circ$] of **20**

Li(1)–N(1)	2.062(6)	C(35)–N(3)	1.266(4)
Li(1)–N(2)	2.031(6)	C(36)–N(4)	1.276(4)
Li(1)–O(1)	1.977(6)	C(37)–N(4)	1.429(4)
Li(1)–O(2)	1.963(2)	C(49)–N(3)	1.431(4)
C(1)–N(1)	1.330(4)	C(1)–C(2)	1.399(5)
C(2)–N(2)	1.333(4)	C(36)–C(35)	1.462(4)
C(3)–N(1)	1.413(4)	N(1)–Li(1)–N(2)	86.0(2)
C(15)–N(2)	1.411(4)	O(1)–Li(1)–O(2)	105.3(5)

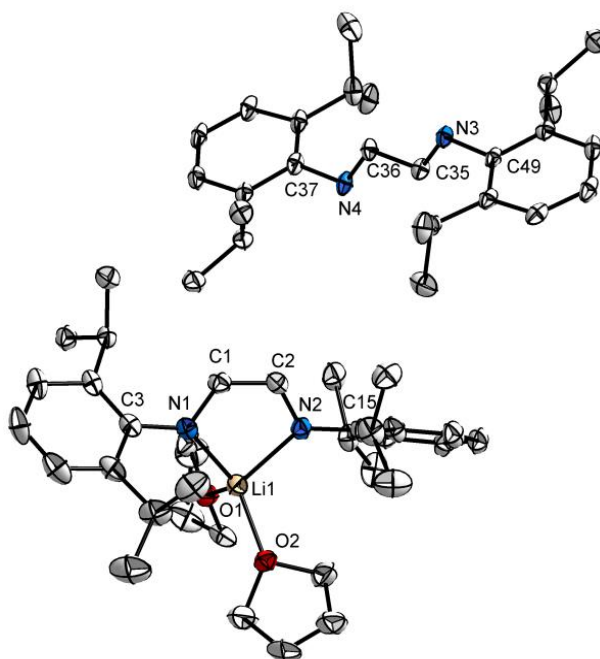
**Figure 62.** Molecular structure of **20** in the crystalline state: Thermal ellipsoids with 50% probability, H atoms omitted for clarity.

Table 39. Crystal data and structure refinement of **22**

Identification code	fe0064
Formula Sum	C ₄₂ H ₆₈ KN ₂ O ₄
Formula weight	704.08
Crystal size (mm)	0.19 x 0.25 x 0.30 mm
Crystal system	monoclinic
Space group	C 2/c
Unit cell parameters	<i>a</i> (Å) 21.802(2) <i>α</i> (°) 90 <i>b</i> (Å) 17.627(9) <i>β</i> (°) 108.9(6) <i>c</i> (Å) 22.871(2) <i>γ</i> (°) 90
Unit cell volume <i>V</i> (Å ³)	8314.6(1)
Molecules per cell <i>Z</i>	8
Crystallographic density ρ_{calcd} (g cm ⁻³)	1.125
Absorption coefficient μ (mm ⁻¹)	0.168
Temperature (°C)	-173
Scan type	ω scan (increment 1.5°, exposure 15 min)
Completeness of dataset	99.5%
θ range of data collection (°)	1.949 to 25.347
Reflections collected	21872
Independent reflections	7507
Independent reflections with $I > 2\sigma(I)$	7507
Solution method	dual-space structure solution (SHELXT 2017/1)
Refinement method	full-matrix least-squares on F^2 (SHELXL 2017/1)
Absorption correction method	none
Range of transmission factors	-
Data / parameters / restraints	7507 / 542 / 1258
Goodness of fit (goof) [all data]	1.075
Final R values	
R ₁ [all data, $I \geq 2\sigma(I)$]	0.0598, 0.0449
wR ₂ [all data, $I \geq 2\sigma(I)$]	0.1032, 0.0973
Largest difference peak and hole	0.252 and -0.226 eÅ ⁻³

Refinement special details: Two THF ligands are disordered over two positions.

Table 40. Selected bond lengths [\AA] and angles [$^\circ$] of **22**

K(1)–N(1)	2.796(1)	C(1)–N(1)	1.326(2)
K(1)–N(2)	2.785(1)	C(2)–N(2)	1.330(2)
K(1)–O(1)	2.795(6)	C(1)–C(2)	1.403(2)
K(1)–O(2)	2.727(2)	N(1)–K(1)–N(2)	62.5(4)
K(1)–O(3)	2.825(1)	O(1)–K(1)–O(3)	114.3(1)
K(1)–O(4)	2.704(8)	O(2)–K(1)–O(4)	148.0(1)

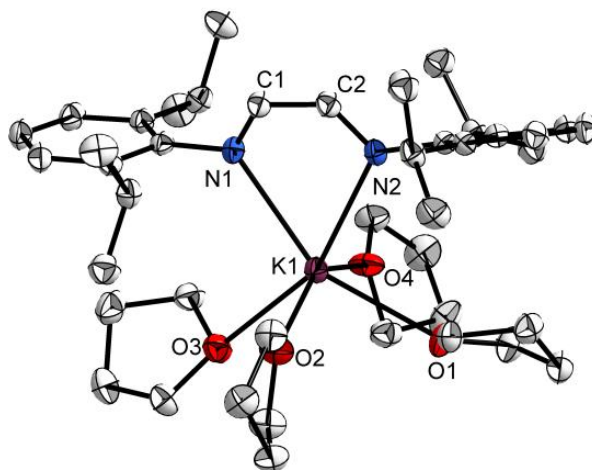
**Figure 63.** Molecular structure of **22** in the crystalline state: Thermal ellipsoids with 50% probability, H atoms omitted for clarity.

Table 41. Crystal data and structure refinement of **23**

Identification code	fe0067
Formula Sum	C ₄₂ H ₆₈ N ₂ O ₄ Rb
Formula weight	750.45
Crystal size (mm)	0.12 x 0.18 x 0.23
Crystal system	monoclinic
Space group	C 2/c
Unit cell parameters	<i>a</i> (Å) 22.260(5) <i>α</i> (°) 90 <i>b</i> (Å) 17.304(2) <i>β</i> (°) 109.0(2) <i>c</i> (Å) 22.979(4) <i>γ</i> (°) 90
Unit cell volume <i>V</i> (Å ³)	8370(3)
Molecules per cell <i>Z</i>	8
Crystallographic density ρ_{calcd} (g cm ⁻³)	1.191
Absorption coefficient μ (mm ⁻¹)	1.223
Temperature (°C)	-173
Scan type	ω scan (increment 1.5°, exposure 15 min)
Completeness of dataset	97.7%
θ range of data collection (°)	1.830 to 25.350
Reflections collected	17876
Independent reflections	7467
Independent reflections with $I > 2\sigma(I)$	7467
Solution method	dual-space structure solution (SHELXT 2017/1)
Refinement method	full-matrix least-squares on F^2 (SHELXL 2017/1)
Absorption correction method	numerical
Range of transmission factors	0.7832 to 0.6803
Data / parameters / restraints	7467 / 1741 / 588
Goodness of fit (goof) [all data]	1.070
Final R values	
R ₁ [all data, $I \geq 2\sigma(I)$]	0.0643, 0.0448
wR ₂ [all data, $I \geq 2\sigma(I)$]	0.0946, 0.0889
Largest difference peak and hole	0.572 and -0.304eÅ ⁻³

Refinement special details: Three THF ligands are disordered over two positions with occupancies from 35% to 63%.

Table 42. Selected bond lengths [\AA] and angles [$^\circ$] of **23**

Rb(1)–N(1)	2.930(2)	C(1)–N(2)	1.327(4)
Rb(1)–N(2)	2.927(2)	C(2)–N(1)	1.324(3)
Rb(1)–O(1)	2.932(2)	C(1)–C(2)	1.395(3)
Rb(1)–O(2)	2.866(2)	N(1)–Rb(1)–N(2)	59.2(6)
Rb(1)–O(3)	3.071(2)	O(1)–Rb(1)–O(3)	121.6(5)
Rb(1)–O(4)	2.890(1)	O(2)–Rb(1)–O(4)	151.9(2)

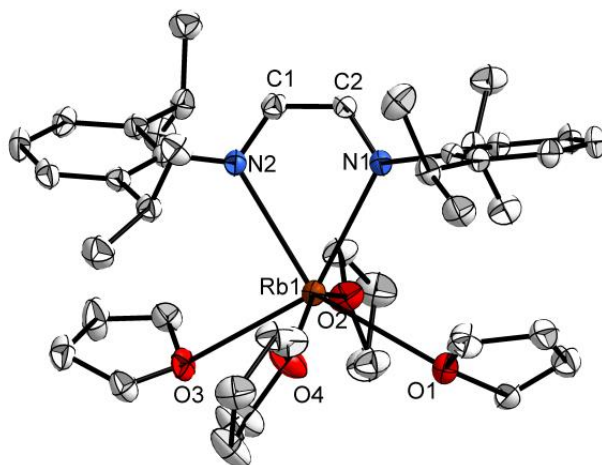
**Figure 64.** Molecular structure of **23** in the crystalline state: Thermal ellipsoids with 50% probability, H atoms omitted for clarity.

Table 43. Crystal data and structure refinement of **25**

Identification code	fe0244
Formula Sum	C ₄₈ H ₇₀ CsN ₃ O ₂
Formula weight	853.98
Crystal system	monoclinic
Space group	<i>P</i> 2 ₁ / <i>c</i>
Unit cell parameters	<i>a</i> (Å) 12.460(5) <i>α</i> (°) 90 <i>b</i> (Å) 22.752(6) <i>β</i> (°) 101.6(2) <i>c</i> (Å) 16.849(5) <i>γ</i> (°) 90
Unit cell volume <i>V</i> (Å ³)	4679(3)
Molecules per cell <i>Z</i>	4
Crystallographic density <i>ρ</i> _{calcd} (g cm ⁻³)	1.217
Absorption coefficient <i>μ</i> (mm ⁻¹)	0.831
Temperature (°C)	-173
Scan type	<i>ω</i> scan (increment 1.5°, exposure 1 min)
Completeness of dataset	99.4%
<i>θ</i> range of data collection (°)	1.865 to 25.350
Reflections collected	22848
Independent reflections	8517
Independent reflections with	<i>I</i> > 2σ(<i>I</i>) 7017
Solution method	dual-space structure solution (SHELXT 2018/3)
Refinement method	full-matrix least-squares on <i>F</i> ² (SHELXL 2018/3)
Data / parameters / restraints	8517 / 499 / 0
Goodness of fit (goof) [all data]	1.137
Final R values	
R ₁ [all data, <i>I</i> ≥ 2σ(<i>I</i>)]	0.0898, 0.0712
wR ₂ [all data, <i>I</i> ≥ 2σ(<i>I</i>)]	0.1654, 0.1556
Largest difference peak and hole	0.901 and -1.958 eÅ ⁻³

Table 44. Selected bond lengths [\AA] and angles [$^\circ$] of **25**

Cs(01)–N(1)	3.153(3)	C(28)–N(3)	1.317(6)
Cs(01)–N(2)	2.994(3)	C(1)–C(2)	1.499(6)
Cs(01)–O(1)	3.041(5)	C(2)–C(27)	1.398(6)
Cs(01)–O(2)	3.295(4)	C(27)–C(28)	1.409(6)
C(1)–N(1)	1.269(6)	N(1)–Cs(01)–N(2)	53.0(9)
C(2)–N(2)	1.322(6)	O(1)–Cs(01)–O(2)	88.0(1)

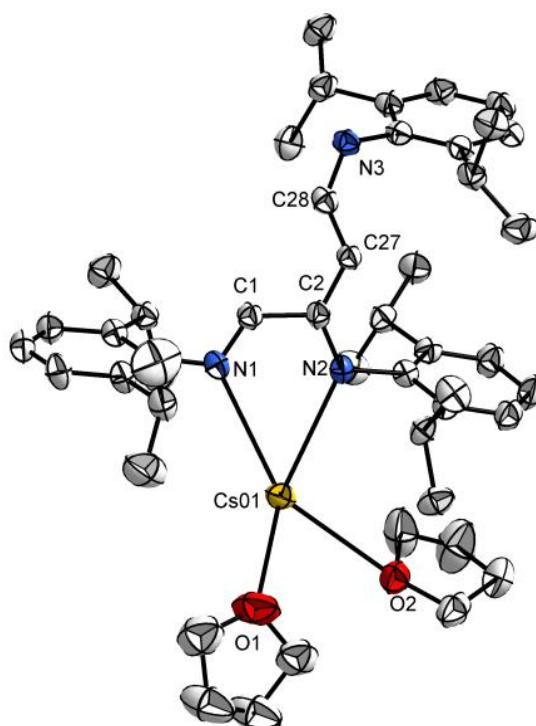
**Figure 65.** Molecular structure of **25** in the crystalline state: Thermal ellipsoids with 50% probability, H atoms omitted for clarity.

Table 45. Crystal data and structure refinement of **26**

Identification code	fe0179
Formula Sum	C ₁₁₆ H ₁₆₆ K ₂ N ₈ O ₃
Formula weight	1798.78
Crystal size (mm)	0.14 x 0.16 x 0.19
Crystal system	orthorhombic
Space group	<i>P</i> 2 ₁ 2 ₁ 2 ₁
Unit cell parameters	<i>a</i> (Å) 19.857(4) <i>α</i> (°) 90 <i>b</i> (Å) 22.351(4) <i>β</i> (°) 90 <i>c</i> (Å) 24.546(5) <i>γ</i> (°) 90
Unit cell volume <i>V</i> (Å ³)	10894(4)
Molecules per cell <i>Z</i>	4
Crystallographic density ρ_{calcd} (g cm ⁻³)	1.097
Absorption coefficient μ (mm ⁻¹)	0.139
Temperature (°C)	-173
Scan type	ω scan (increment 1.5°, exposure 1 min)
Completeness of dataset	99.6%
θ range of data collection (°)	2.002 to 25.349
Reflections collected	32266
Independent reflections	18528
Independent reflections with $I > 2\sigma(I)$	14892
Solution method	dual-space structure solution (SHELXT 2014/5)
Refinement method	full-matrix least-squares on F^2 (SHELXL 2017/1)
Absorption correction method	none
Range of transmission	-
Data / parameters / restraints	18528 / 1360 / 2694
Goodness of fit (goof) [all data]	1.090
Final R values	
R ₁ [all data, $I \geq 2\sigma(I)$]	0.0999, 0.0758
wR ₂ [all data, $I \geq 2\sigma(I)$]	0.1757, 0.1617
Largest difference peak and hole	0.471 and -0.293 eÅ ⁻³

Table 46. Selected bond lengths [Å] and angles [°] of **26**

K(1)–N(1)	2.664(4)	C(28)–N(3)	1.333(8)
K(1)–N(2)	2.728(5)	C(28)–N(4)	1.244(7)
K(1)–N(8)	3.029(4)	C(41)–N(3)	1.439(9)
K(2)–N(5)	2.716(4)	C(53)–N(5)	1.308(6)
K(2)–N(6)	2.720(5)	C(54)–N(7)	1.455(6)
K(1)–C(93)	3.196(5)	C(80)–N(7)	1.350(7)
K(1)–C(94)	3.242(5)	C(80)–N(8)	1.293(6)
K(1)–C(95)	3.281(7)	C(1)–C(2)	1.388(8)
K(1)–C(96)	3.314(6)	C(2)–C(3)	1.396(7)
K(1)–C(97)	3.269(8)	C(53)–C(54)	1.392(7)
K(1)–C(98)	3.232(5)	C(54)–C(55)	1.403(7)
K(2)–O(1)	2.634(1)	N(1)–K(1)–N(2)	69.2(1)
K(2)–O(2)	2.674(7)	N(5)–K(2)–N(6)	67.4(1)
K(2)–O(3)	2.778(1)	O(1)–K(2)–O(2)	80.5(3)
C(1)–N(2)	1.317(6)	O(1)–K(2)–O(3)	92.3(4)
C(2)–N(3)	1.474(6)	O(2)–K(2)–O(3)	93.5(3)
C(3)–N(1)	1.303(6)		

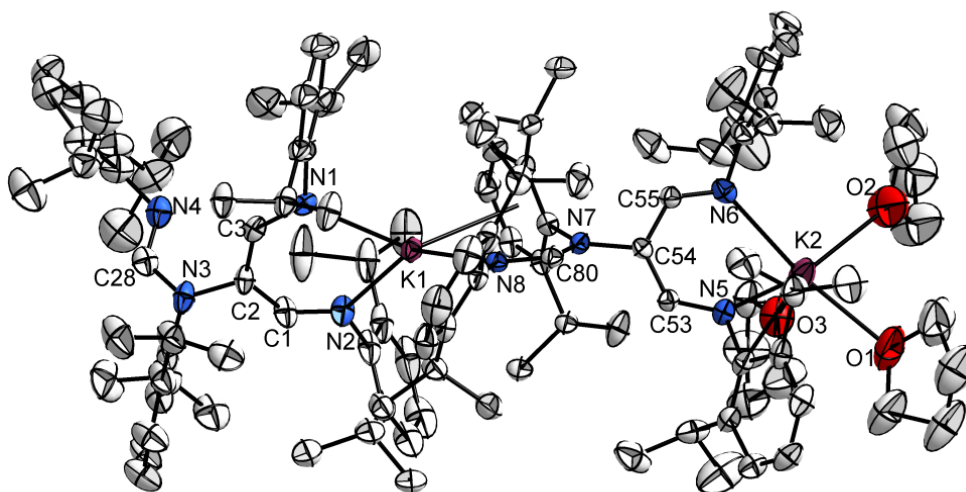
**Figure 66.** Molecular structure of **26** in the crystalline state: Thermal ellipsoids with 50% probability, H atoms omitted for clarity.

Table 47. Crystal data and structure refinement of **27**

Identification code	fe0280
Formula Sum	C ₄₁ H ₆₆ LiN ₃ O ₃
Formula weight	655.90
Crystal size (mm)	0.24 x 0.26 x 0.31 mm
Crystal system	triclinic
Space group	$P\bar{1}$
Unit cell parameters	a (Å) 10.271(4) α (°) 105.5(4) b (Å) 13.706(5) β (°) 91.2(5) c (Å) 15.357(1) γ (°) 110.6(3)
Unit cell volume V (Å ³)	1934.0(2)
Molecules per cell Z	2
Crystallographic density ρ_{calcd} (g cm ⁻³)	1.126
Absorption coefficient μ (mm ⁻¹)	0.069
Temperature (°C)	-173
Scan type	ω scan (increment 1.5°, exposure 1 min)
Completeness of dataset	99.0%
θ range of data collection (°)	1.825 to 25.350
Reflections collected	14172
Independent reflections	7008
Independent reflections with $I > 2\sigma(I)$	5882
Solution method	dual-space structure solution (SHELXT 2018/3)
Refinement method	full-matrix least-squares on F^2 (SHELXL 2018/3)
Absorption correction method	none
Data / parameters / restraints	7008 / 576 / 1287
Goodness of fit (goof) [all data]	1.026
Final R values	
R ₁ [all data, $I \geq 2\sigma(I)$]	0.0727, 0.0597
wR ₂ [all data, $I \geq 2\sigma(I)$]	0.1454, 0.1375
Largest difference peak and hole	0.598 and -0.238 eÅ ⁻³

Table 48. Selected bond lengths [\AA] and angles [$^\circ$] of **27**

Li(1)–N(1)	2.014(3)	C(2)–C(5)	1.326(3)
Li(1)–O(1A)	2.006(7)	C(3)–C(4)	1.436(2)
Li(1)–O(1B)	2.044(1)	C1–N(1)–Li(1)	136.5(2)
Li(1)–O(1C)	2.071(2)	O(1A)–Li(1)–O(1B)	97.6(6)
C(1)–N(1)	1.335(2)	O(1A)–Li(1)–O(1C)	104.3(5)
C(3)–N(2)	1.418(3)	O(1B)–Li(1)–O(1C)	106.1(7)
C(3)–N(3)	1.286(2)	N(1)–Li(1)–O(1A)	114.5(3)
C(1)–C(2)	1.498(3)	N(1)–Li(1)–O(1B)	116.8(5)
C(1)–C(4)	1.380(3)	N(1)–Li(1)–O(1C)	115.3(4)

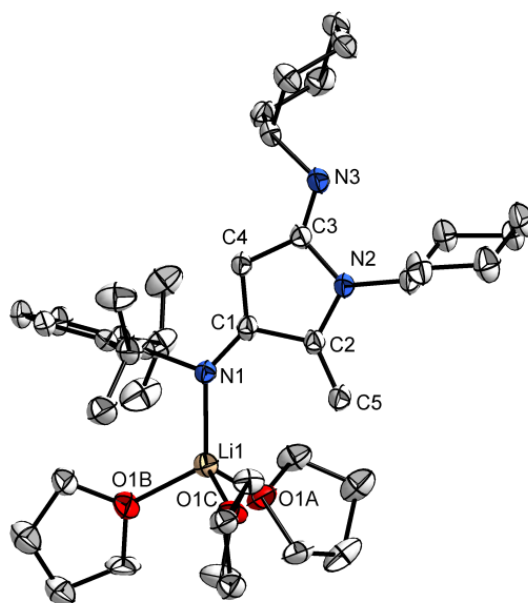
**Figure 67.** Molecular structure of **27** in the crystalline state: Thermal ellipsoids with 50% probability, H atoms omitted for clarity.

Table 49. Crystal data and structure refinement of **28**

Identification code	fe0113
Formula Sum	C ₄₁ H ₆₆ N ₃ NaO ₃
Formula weight	671.95
Crystal size (mm)	0.13 x 0.18 x 0.23
Crystal system	triclinic
Space group	$P\bar{1}$
Unit cell parameters	a (Å) 10.460(3) α (°) 65.3(3) b (Å) 14.046(4) β (°) 84.5(3) c (Å) 15.477(7) γ (°) 70.7(2)
Unit cell volume V (Å ³)	1948.5(1)
Molecules per cell Z	2
Crystallographic density ρ_{calcd} (g cm ⁻³)	1.145
Absorption coefficient μ (mm ⁻¹)	0.081
Temperature (°C)	-173
Scan type	ω scan (increment 1.5°, exposure 1 min)
Completeness of dataset	98.6%
θ range of data collection (°)	2.065 to 25.347
Reflections collected	13872
Independent reflections	7046
Independent reflections with $I > 2\sigma(I)$	70462s
Refinement method	full-matrix least-squares on F^2 (SHELXL 201/4)
Absorption correction method	none
Range of transmission factors	–
Data / parameters / restraints	7046 / 539 / 1127
Goodness of fit (gooF) [all data]	1.101
Final R values	
R ₁ [all data, $I \geq 2\sigma(I)$]	0.0926, 0.0686
wR ₂ [all data, $I \geq 2\sigma(I)$]	0.1398, 0.1302
Largest difference peak and hole	0.390 and -0.218 eÅ ⁻³

Table 50. Selected bond lengths [\AA] and angles [$^\circ$] of **28**

Na(1)–N(1)	2.334(2)	C(4)–C(3)	1.377(4)
Na(1)–O(1A_2)	2.255(1)	C(4)–C(5)	1.437(4)
Na(1)–O(1_2)	2.300(3)	C(3)–N(1)–Na(1)	126.1(2)
Na(1)–O(1B)	2.307(3)	O(1A_2)–Na(1)–O(1_2)	89.3(5)
C(2)–N(2)	1.390(4)	O(1A_2)–Na(1)–O(1B)	121.6(4)
C(3)–N(1)	1.326(4)	O(1_2)–Na(1)–O(1B)	108.0(9)
C(5)–N(2)	1.424(3)	N(1)–Na(1)–O(1B)	109.5(8)
C(5)–N(3)	1.289(4)	N(1)–Na(1)–O(1A_2)	107.3(4)
C(1)–C(2)	1.335(4)	N(1)–Na(1)–O(1_2)	120.8(9)

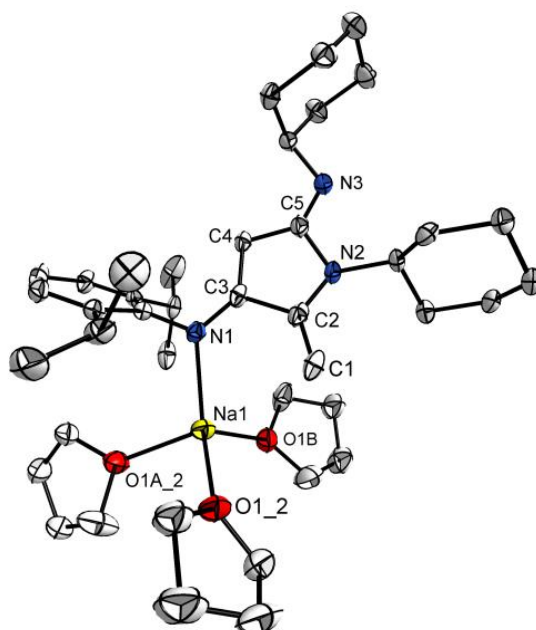
**Figure 68.** Molecular structure of **28** in the crystalline state: Thermal ellipsoids with 50% probability, H atoms omitted for clarity.

Table 51. Crystal data and structure refinement of **29**

Identification code	fe0111
Formula Sum	C ₁₅₂ H ₂₄₀ K ₄ N ₁₂ O ₉
Formula weight	2535.95
Crystal size (mm)	0.11 x 0.17 x 0.27
Crystal system	triclinic
Space group	$P\bar{1}$
Unit cell parameters	a (Å) 10.825(4) α (°) 85.8(3) b (Å) 16.628(5) β (°) 83.5(3) c (Å) 20.510(1) γ (°) 86.5(3)
Unit cell volume V (Å ³)	3653(2)
Molecules per cell Z	1
Crystallographic density ρ_{calcd} (g cm ⁻³)	1.152
Absorption coefficient μ (mm ⁻¹)	0.181
Temperature (°C)	-173
Scan type	ω scan (increment 1.5°, exposure 1 min)
Completeness of dataset	97.6%
θ range of data collection (°)	2.045 to 25.350
Reflections collected	26398
Independent reflections	13038
Independent reflections with $I > 2\sigma(I)$	130382s
Refinement method	full-matrix least-squares on F^2 (SHELXL 2017/1)
Absorption correction method	none
Range of transmission factors	–
Data / parameters / restraints	13038 / 976 / 2428
Goodness of fit (gooF) [all data]	1.041
Final R values	
R ₁ [all data, $I \geq 2\sigma(I)$]	0.0785, 0.0605
wR ₂ [all data, $I \geq 2\sigma(I)$]	0.1511, 0.1413
Largest difference peak and hole	0.588 and -0.432 eÅ ⁻³

Table 52. Selected bond lengths [Å] and angles [°] of **29**

K(1)–N(1_2)	2.734(2)	C(1_3)–C(2_3)	1.326(4)
K(1)–N(3_3)	2.851(2)	C(2_2)–C(3_2)	1.497(3)
K(2)–N(1_3)	2.764(2)	C(2_3)–C(3_3)	1.501(4)
K(2)–N(3_2)	2.814(2)	C(3_2)–C(4_2)	1.385(4)
K(2)–C(6_3)	3.148(3)	C(3_3)–C(4_3)	1.386(3)
K(2)–C(7_3)	3.801(3)	C(4_2)–C(5_2)	1.426(3)
K(1)–O(1_4)	2.682(6)	C(4_3)–C(5_3)	1.416(4)
K(1)–O(1_5)	2.688(2)	C(3_2)–N(1_2)–K(1)	141.8(2)
K(2)–O(1_1)	2.688(1)	C(1_3)–N(1_3)–K(2)	93.8(9)
K(2)–O(1_6)	2.677(2)	C(5_2)–N(3_2)–K(2)	111.1(2)
C(2_2)–N(2_2)	1.400(3)	O(1_4)–K(1)–O(1_5)	87.7(1)
C(2_3)–N(2)	1.406(3)	O(1_1)–K(2)–O(1_6)	144.1(3)
C(3_2)–N(1_2)	1.324(3)	N(1_2)–K(1)–O(1_4)	120.6(1)
C(3_3)–N(1_3)	1.324(3)	N(1_2)–K(1)–O(1_5)	111.0(7)
C(5_2)–N(2_2)	1.420(3)	N(1_3)–K(2)–O(1_1)	110.1(3)
C(5_2)–N(3_2)	1.297(3)	N(1_3)–K(2)–O(1_6)	88.3(6)
C(5_3)–N(2)	1.415(3)	N(3_2)–K(2)–O(1_1)	96.0(3)
C(5_3)–N(3_3)	1.309(3)	N(3_2)–K(2)–O(1_6)	89.0(6)
C(1_2)–C(2_2)	1.327(4)		

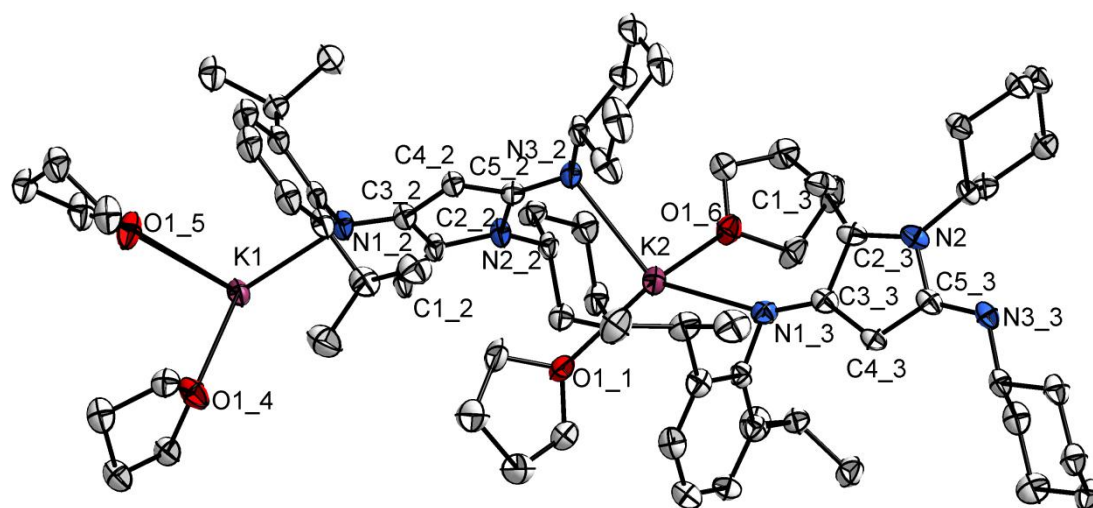
**Figure 69.** Molecular structure of **29** in the crystalline state: Thermal ellipsoids with 50% probability, H atoms omitted for clarity.

Table 53. Crystal data and structure refinement of **30**

Identification code	li0045
Formula Sum	C ₃₉ H ₆₆ N ₃ NaO ₄
Formula weight	663.93
Crystal size (mm)	0.31 × 0.32 × 0.45
Crystal system	monoclinic
Space group	<i>P</i> 2/ <i>c</i>
Unit cell parameters	<i>a</i> (Å) 18.154(5) <i>α</i> (°) 90 <i>b</i> (Å) 12.127(3) <i>β</i> (°) 95.4(2) <i>c</i> (Å) 18.324(4) <i>γ</i> (°) 90
Unit cell volume <i>V</i> (Å ³)	4016.2(2)
Molecules per cell <i>Z</i>	4
Crystallographic density ρ_{calcd} (g cm ⁻³)	1.098
Absorption coefficient μ (mm ⁻¹)	0.079
Temperature (°C)	-120
Scan type	ω scan (increment 1.5°, exposure 8 min)
Completeness of dataset	99.7%
θ range of data collection (°)	2.017... 24.998
Reflections collected	24649
Independent reflections	7056 (R _{int} = 0.0449)
Independent reflections with $I > 2\sigma(I)$	5358
Solution method	direct methods (SHELXS 2013)
Refinement method	full-matrix least-squares on F^2 (SHELXL 2014)
Absorption correction method	none
Range of transmission factors	–
Data / parameters / restraints	7056 / 424 / 0
Goodness of fit (goof) [all data]	1.040
Final R values ^a	
R ₁ [all data, $I \geq 2\sigma(I)$]	0.0922, 0.0723
wR ₂ [all data, $I \geq 2\sigma(I)$]	0.2101, 0.1947
Largest difference peak and hole	0.755 and -0.327 e Å ⁻³
Flack parameter	–

Refinement special details: ^a The quality of the structure refinement (*R* values) is limited by moderate but undefined disorder of all four THF moieties.

Table 54. Selected bond lengths [\AA] and angles [$^\circ$] of **30**

Na–N(1)	2.334(2)	C(14)–C(17)	1.329(4)
Na–O(1)	2.314(3)	C(16)–C(15)	1.425(4)
Na–O(2)	2.301(2)	C(13)–N(1)–Na	132.6(2)
Na–O(3)	2.307(2)	O(1)–Na–O(2)	96.1(9)
C(13)–N(1)	1.325(3)	O(1)–Na–O(3)	95.4(9)
C(14)–N(2)	1.379(4)	O(2)–Na–O(3)	102.83(9)
C(15)–N(2)	1.422(3)	N(1)–Na–O(1)	127.9(9)
C(15)–N(3)	1.287(4)	N(1)–Na–O(2)	116.6(8)
C(13)–C(14)	1.502(3)	N(1)–Na–O(3)	113.7(8)
C(13)–C(16)	1.377(3)		

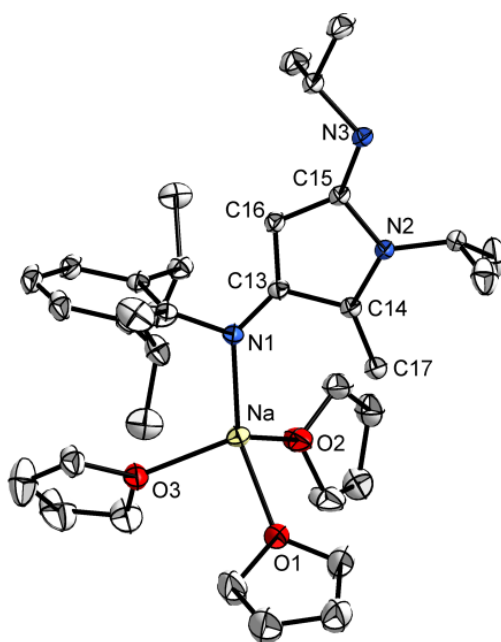
**Figure 70.** Molecular structure of **30** in the crystalline state: Thermal ellipsoids with 50% probability, H atoms omitted for clarity.

Table 55. Crystal data and structure refinement of **31**

Identification code	li0027
Formula Sum	C ₄₀ H ₆₄ CaN ₂ O ₃
Formula weight	661.01
Crystal size (mm)	0.21 × 0.25 × 0.32
Crystal system	orthorhombic
Space group	<i>Pbca</i>
Unit cell parameters	<i>a</i> (Å) 17.937(5) <i>α</i> (°) 90 <i>b</i> (Å) 20.062(4) <i>β</i> (°) 90 <i>c</i> (Å) 20.871(4) <i>γ</i> (°) 90
Unit cell volume <i>V</i> (Å ³)	7510.3(3)
Molecules per cell <i>Z</i>	8
Crystallographic density ρ_{calcd} (g cm ⁻³)	1.169
Absorption coefficient μ (mm ⁻¹)	0.205
Temperature (°C)	-140
Scan type	ω scan (increment 1.5°, exposure 15 min)
Completeness of dataset	99.9%
θ range of data collection (°)	1.809 ... 24.999
Reflections collected	31614
Independent reflections	6604 (R _{int} = 0.0794)
Independent reflections with $I > 2\sigma(I)$	5204
Solution method	patterson methods (SHELXS 2013)
Refinement method	full-matrix least-squares on F^2 (SHELXL 2014)
Absorption correction method	none
Range of transmission factors	–
Data / parameters / restraints	6604 / 415 / 0
Goodness of fit (goof) [all data]	1.050
Final R values	
R ₁ [all data, $I \geq 2\sigma(I)$]	0.0731, 0.0546
wR ₂ [all data, $I \geq 2\sigma(I)$]	0.1513, 0.1389
Largest difference peak and hole	0.374 and -0.388 e Å ⁻³
Flack parameter	–

Table 56. Selected bond lengths [\AA] and angles [$^\circ$] of **31**

Ca–N(1)	2.250(2)	C(3)–N(2)	1.432(3)
Ca–N(2)	2.251(2)	C(1)–C(2)	1.517(3)
Ca–C(2)	2.785(2)	C(2)–C(3)	1.361(3)
Ca–C(3)	2.783(2)	C(3)–C(4)	1.512(3)
Ca–O(1)	2.427(2)	N(1)–Ca–N(2)	80.2(8)
Ca–O(2)	2.426(2)	O(1)–Ca–O(2)	81.7(6)
Ca–O(3)	2.414(2)	O(1)–Ca–O(3)	156.7(6)
C(2)–N(1)	1.427(3)	O(2)–Ca–O(3)	75.9(6)

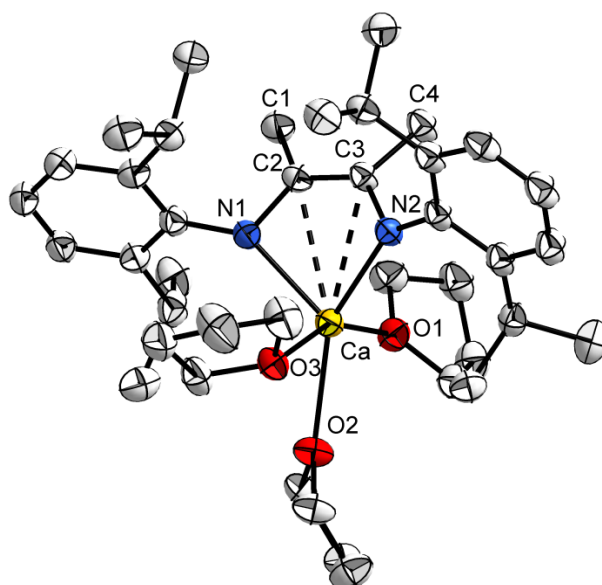
**Figure 71.** Molecular structure of **31** in the crystalline state: Thermal ellipsoids with 50% probability, H atoms omitted for clarity.

Table 57. Crystal data and structure refinement of **32**

Identification code	li0011
formula sum	C ₅₆ H ₈₈ CaN ₄ O ₃
Formula weight	905.38
Crystal size (mm)	0.18 × 0.23 × 0.51
Crystal system	monoclinic
Space group	<i>P</i> 2 ₁ / <i>c</i>
Unit cell parameters	<i>a</i> (Å) 19.727(4) <i>α</i> (°) 90 <i>b</i> (Å) 22.243(4) <i>β</i> (°) 90.1(2) <i>c</i> (Å) 22.619(5) <i>γ</i> (°) 90
Unit cell volume <i>V</i> (Å ³)	9925.0(3)
Molecules per cell <i>Z</i>	8
Crystallographic density ρ_{calcd} (g cm ⁻³)	1.212
Absorption coefficient μ (mm ⁻¹)	0.175
Temperature (°C)	-140
Scan type	ω scan (increment 1.5°, exposure 12 min)
Completeness of dataset	99.9%
θ range of data collection (°)	1.801 ... 26.000
Reflections collected	61149
Independent reflections	19469 (<i>R</i> _{int} = 0.0528)
Independent reflections with <i>I</i> > 2 σ (<i>I</i>)	14678
Solution method	direct methods (SHELXS 2013)
Refinement method	full-matrix least-squares on <i>F</i> ² (SHELXL 2014)
Absorption correction method	none
Range of transmission factors	–
Data / parameters / restraints	19469 / 1399 / 612 ^a
Goodness of fit (gooF) [all data]	1.048
Final R values	
<i>R</i> ₁ [all data, <i>I</i> ≥ 2 σ (<i>I</i>)]	0.0763, 0.0534
<i>wR</i> ₂ [all data, <i>I</i> ≥ 2 σ (<i>I</i>)]	0.1420, 0.1293
Largest difference peak and hole	0.793 and -0.496 e Å ⁻³
Flack parameter	–

Refinement special details: ^a Restraints on C-C distances and anisotropic displacement parameters of the C atoms in the disordered adamantyl groups [(C(26)–C(34), C(56)–C(64), C(87)–C(96)], restraints on C-C and C-O distances and anisotropic displacement parameters of C and O atoms in the solvent THF molecules [O(5), O(6), C(105)–C(112)]. Site occupancy factors of the disordered adamantyl groups were freely refined.

Table 58. Selected bond lengths [Å] and angles [°] of **32**

Ca(1)–N(1)	2.501(2)	C(24)–N(4)	1.327(3)
Ca(1)–N(2)	2.459(2)	C(53)–N(5)	1.317(3)
Ca(1)–N(3)	2.500(2)	C(54)–N(6)	1.334(3)
Ca(1)–N(4)	2.415(2)	C(75)–N(7)	1.333(3)
Ca(2)–N(5)	2.439(2)	C(76)–N(8)	1.330(3)
Ca(2)–N(6)	2.536(2)	C(1)–C(2)	1.406(3)
Ca(2)–N(7)	2.459(2)	C(23)–C(24)	1.396(3)
Ca(2)–N(8)	2.531(2)	C(53)–C(54)	1.404(3)
Ca(1)–O(1)	2.445(2)	C(75)–C(76)	1.399(3)
Ca(1)–O(2)	2.556(2)	N(1)–Ca(1)–N(2)	71.3(1)
Ca(2)–O(3)	2.468(2)	N(3)–Ca(1)–N(4)	71.2(1)
Ca(2)–O(4)	2.491(2)	N(5)–Ca(2)–N(6)	71.4(1)
C(1)–N(1)	1.331(3)	N(7)–Ca(2)–N(8)	70.4(1)
C(2)–N(2)	1.326(3)	O(1)–Ca(1)–O(2)	92.3(1)
C(23)–N(3)	1.326(3)	O(3)–Ca(2)–O(4)	86.5(1)

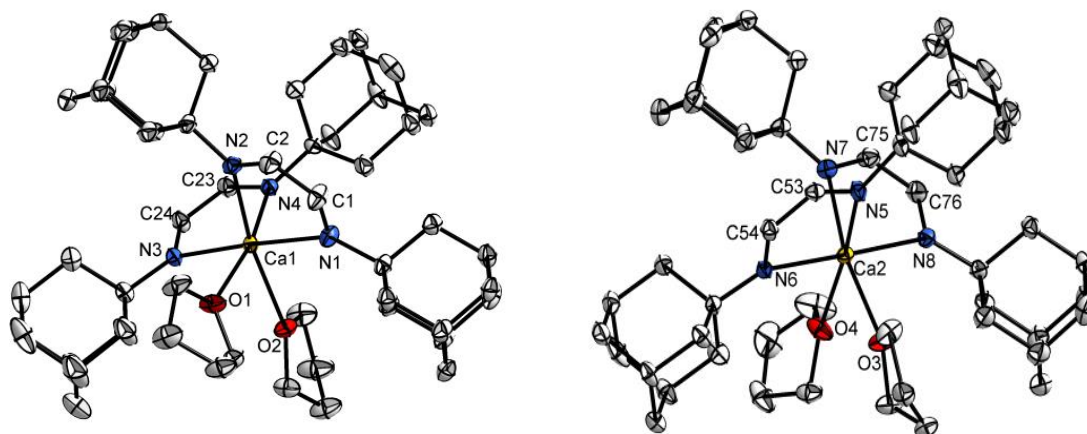
**Figure 72.** Molecular structure of **32** in the crystalline state: Thermal ellipsoids with 50% probability, H atoms omitted for clarity.

Table 59. Crystal data and structure refinement of **33**

Identification code	fe0014_a
Formula Sum	C ₇₆ H ₁₂₀ I ₂ N ₄ O ₅ Yb ₂
Formula weight	1769.5
Crystal size (mm)	0.17 × 0.33 × 0.50
Crystal system	monoclinic
Space group	<i>P</i> 2 ₁ / <i>n</i>
Unit cell parameters	<i>a</i> (Å) 16.047(6) <i>α</i> (°) 90 <i>b</i> (Å) 15.603(4) <i>β</i> (°) 111.50(3) <i>c</i> (Å) 16.242(4) <i>γ</i> (°) 90
Unit cell volume <i>V</i> (Å ³)	3784(2)
Molecules per cell <i>Z</i>	4
Crystallographic density <i>ρ</i> _{calcd} (Mg m ⁻³)	1.630
Absorption coefficient <i>μ</i> (mm ⁻¹)	3.967
Temperature (°C)	-173
Completeness of dataset	98.9%
<i>θ</i> range of data collection (°)	1.876... 29.311
Reflections collected	34307
Independent reflections	10046 (<i>R</i> _{int} = 0.0928)
Refinement method	full-matrix least-squares on <i>F</i> ² (SHELXL 2016/6)
Data / parameters / restraints	10046 / 434 / 664
Goodness of fit (gooF) [all data]	1.161
Final <i>R</i> values <i>a</i>	
<i>R</i> ₁ [all data, <i>I</i> ≥ 2σ (<i>I</i>)]	0.0425, 0.0478
<i>wR</i> ₂ [all data, <i>I</i> ≥ 2σ (<i>I</i>)]	0.1182, 0.1225
Largest difference peak and hole	1.467 and -3.041 e Å ⁻³

Half of the molecule in the asymmetric unit.

Table 60. Selected bond lengths [\AA] and angles [$^\circ$] of **33**

Yb(1)–N(1)	2.426(4)	C(1)–C(2)	1.428(7)
Yb(1)–N(2)	2.462(3)	C(1)–C(3)	1.504(8)
Yb(1)–O(1)	2.468(3)	C(2)–C(4)	1.502(6)
Yb(1)–O(2)	2.467(3)	N(1)–Yb(1)–N(2)	68.1(1)
Yb(1)–I(1)	3.154(9)	O(1)–Yb(1)–O(2)	85.8(1)
C(1)–N(1)	1.345(5)	I(1)–Yb(1)–I(1)	82.3(1)
C(2)–N(2)	1.340(7)		

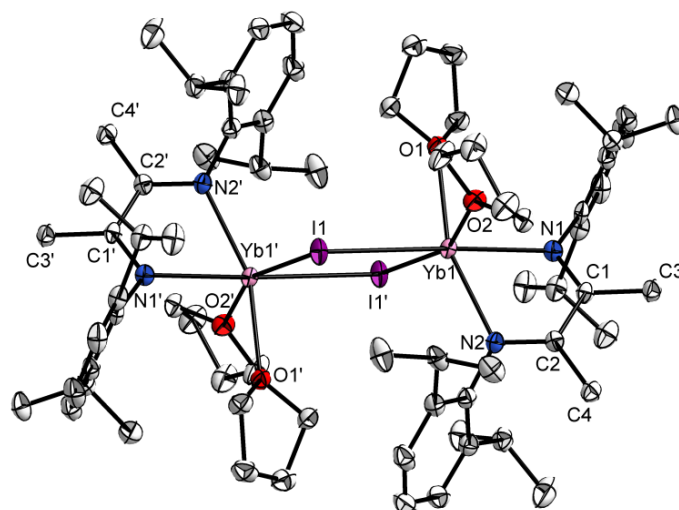
**Figure 73.** Molecular structure of **33** in the crystalline state: Thermal ellipsoids with 50% probability, H atoms omitted for clarity.

Table 61. Crystal data and structure refinement of **34**

Identification code	fe0102
Formula Sum	C ₃₈ H ₆₀ IN ₂ O ₃ Sm
Formula weight	1740.25
Crystal size (mm)	0.14 x 0.19 x 0.25
Crystal system	triclinic
Space group	$P\bar{1}$
Unit cell parameters	a (Å) 12.026(9) α (°) 69.6(5) b (Å) 12.182(7) β (°) 78.9(6) c (Å) 14.687(9) γ (°) 75.9(5)
Unit cell volume V (Å ³)	1942(2)
Molecules per cell Z	2
Crystallographic density ρ_{calcd} (g cm ⁻³)	1.488
Absorption coefficient μ (mm ⁻¹)	2.341
Temperature (°C)	-173
Scan type	ω scan (increment 1.5°, exposure 1 min)
Completeness of dataset	98.3%
θ range of data collection (°)	1.817 to 25.342
Reflections collected	13747
Independent reflections	6958
Independent reflections with $I > 2\sigma(I)$	6366
Structure solution method	dual-space structure solution (SHELXT 2014/5)
Refinement method	full-matrix least-squares on F^2 (SHELXL 2017/1)
Absorption correction method	Numerical
Range of transmission factors	0.5747 to 0.4555
Data/parameters/restraints	6958 / 461 / 884
Goodness of fit (GooF) [all data]	1.113
Final R values	
R_1 [all data, $I \geq 2\sigma(I)$]	0.0605, 0.0560
wR_2 [all data, $I \geq 2\sigma(I)$]	0.1522, 0.1470
Largest difference peak and hole	2.308 and -2.916 eÅ ⁻³

Refinement special details: Large residual density peaks due to inefficient absorption correction. One THF moiety is disordered over two positions.

Table 62. Selected bond lengths [\AA] and angles [$^\circ$] of **34**

Sm–N(1)	2.267(6)	N(2)–C(2)	1.403(8)
Sm–N(2)	2.247(6)	C(1)–C(2)	1.365(1)
Sm–O(1)	2.425(2)	N(1)–Sm(1)–N(2)	80.3(2)
Sm–O(2)	2.495(6)	N(1)–Sm(1)–I(1)	161.1(1)
Sm–O(3)	2.457(5)	N(2)–Sm(1)–I(1)	117.7(2)
Sm–C(1)	2.655(6)	O(1)–Sm(1)–I(1)	73.3(4)
Sm–C(2)	2.662(7)	O(2)–Sm(1)–I(1)	82.3(1)
Sm–I	3.192(3)	O(3)–Sm(1)–I(1)	85.7(1)
N(1)–(C1)	1.378(8)		

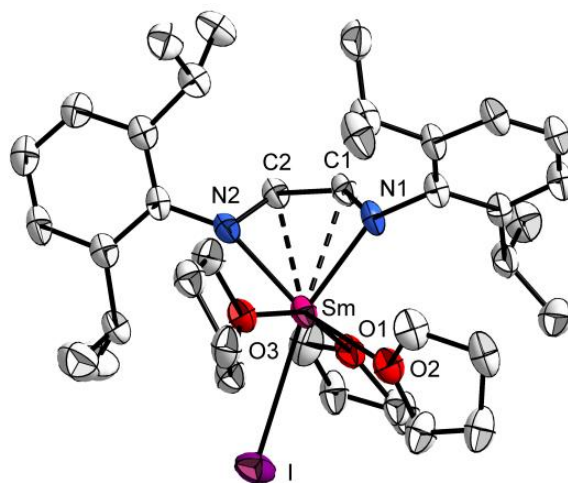
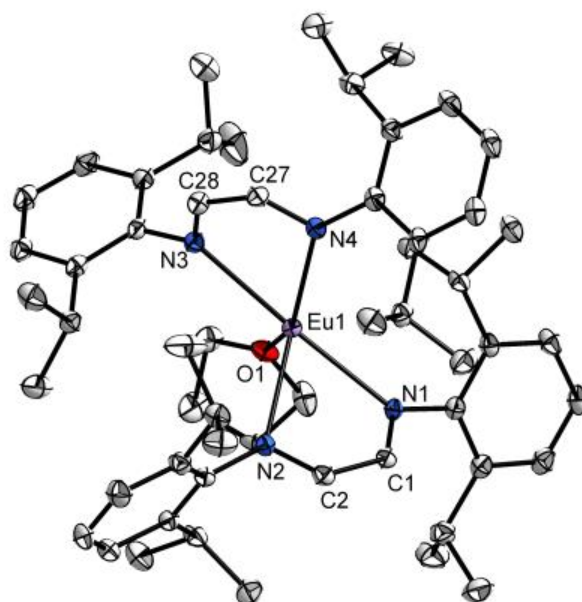
**Figure 74.** Molecular structure of **34** in the crystalline state: Thermal ellipsoids with 50% probability, H atoms omitted for clarity.

Table 63. Crystal data and structure refinement of **35**

Identification code	fe0070
Formula Sum	C ₅₆ H ₈₀ EuN ₄ O
Formula weight	977.22
Crystal size (mm)	0.16 x 0.21 x 0.27
Crystal system	monoclinic
Space group	P 2 ₁ /n
Unit cell parameters	<i>a</i> (Å) 12.910(3) <i>α</i> (°) 90 <i>b</i> (Å) 30.199(8) <i>β</i> (°) 96.2(2) <i>c</i> (Å) 13.210(3) <i>γ</i> (°) 90
Unit cell volume <i>V</i> (Å ³)	5120(2)
Molecules per cell <i>Z</i>	4
Crystallographic density ρ_{calcd} (g cm ⁻³)	1.268
Absorption coefficient μ (mm ⁻¹)	1.266
Temperature (°C)	-173
Scan type	ω scan (increment 1.5°, exposure 1 min)
Completeness of dataset	99.1%
θ range of data collection (°)	2.055 to 29.227
Reflections collected	35357
Independent reflections	13652
independent reflections	6958
independent reflections with $I > 2\sigma(I)$	6366
Solution method	dual-space structure solution (SHELXT 2014/5)
Refinement method	full-matrix least-squares on F^2 (SHELXL 2017/1)
Absorption correction method	numerical
Range of transmission factors	0.7934 to 0.6418
Data / parameters / restraints	13652 / 615 / 1169
Goodness of fit (goof) [all data]	1.092
Final R values	
R ₁ [all data, $I \geq 2\sigma(I)$]	0.0430, 0.0352
wR ₂ [all data, $I \geq 2\sigma(I)$]	0.0753, 0.0725
Largest difference peak and hole	0.545 and -1.111 eÅ ⁻³

Table 64. Selected bond lengths [\AA] and angles [$^\circ$] of **35**

Eu(1)–N(1)	2.573(2)	C(2)–C(1)	1.403(3)
Eu(1)–N(2)	2.536(2)	C(27)–C(28)	1.402(3)
Eu(1)–N(3)	2.552(2)	N(1)–Eu(1)–N(2)	68.3(6)
Eu(1)–N(4)	2.596(2)	N(3)–Eu(1)–N(4)	68.0(6)
Eu(1)–O(1)	2.557(1)	O(1)–Eu(1)–N(2)	98.3(2)
C(1)–N(1)	1.334(3)	O(1)–Eu(1)–N(3)	89.1(3)
C(2)–N(2)	1.332(3)	N(1)–Eu(1)–O(1)	87.6(3)
C(27)–N(4)	1.336(3)	N(4)–Eu(1)–O(1)	141.1(3)
C(28)–N(3)	1.330(3)		

**Figure 75.** Molecular structure of **35** in the crystalline state: Thermal ellipsoids with 50% probability, H atoms omitted for clarity.

6. References

1. G. van Koten, K. Vrieze, *Adv. Organomet. Chem.* **1982**, *21*, 151.
2. H. tom Dieck, K. D. Franz, F. Hohmann, *Chem. Ber.* **1975**, *108*, 163.
3. K. Vrieze, *J. Organomet. Chem.* **1986**, *300*, 307.
4. C. Mealli, A. Ienco, A. D. Phillips, A. Galindo, *Eur. J. Inorg. Chem.* **2007**, 2556.
5. J. Scholz, B. Richter, R. Goddard, C. Krüger, *Chem. Ber.* **1993**, *126*, 57.
6. S. Danièle, C. Drost, B. Gehrhus, S. M. Hawkins, P. B. Hitchcock, M. F. Lappert, P. G. Merle, S. G. Bott, *J. Chem. Soc., Dalton Trans.* **2001**, 3179.
7. I. L. Fedushkin, A. A. Skatova, V. A. Chudakova, G. K. Fukin, *Angew. Chem., Int. Ed.* **2003**, *42*, 3294.
8. I. L. Fedushkin, A. A. Skatova, V. A. Chudakova, V. K. Cherkasov, G. K. Fukin, M. A. Lopatin, *Eur. J. Inorg. Chem.* **2004**, 388.
9. Y. Liu, P. Yang, J. Yu, X. Yang, J. D. Zhang, Z. Chen, H. F. Schaefer, B. Wu, *Organometallics* **2008**, *27*, 5830.
10. P. Yang, X. Yang, J. Yu, Y. Liu, C. Zhang, Y. Deng, B. Wu, *Dalton Trans.* **2009**, 5773.
11. T. K. Panda, H. Kaneko, K. Pal, H. Tsurugi, K. Mashima, *Organometallics* **2010**, *29*, 2610.
12. M. Bhadbhade, G. K. B. Clentsmith, L. D. Field, *Organometallics* **2010**, *29*, 6509.
13. T. Janes, J. M. Rawson, D. Song, *Dalton Trans.* **2013**, *42*, 10640.
14. A. A. Kissel, D. M. Lyubov, T. V. Mahrova, G. K. Fukin, A. V. Cherkasov, T. A. Glukhova, D. Cui, A. A. Trifonov, *Dalton Trans.* **2013**, *42*, 9211.
15. S. Robinson, E. S. Davies, W. Lewis, A. J. Blake, S. T. Liddle, *Dalton Trans.* **2014**, *43*, 4351.
16. S. Harder, J. Brettar, *Angew. Chem., Int. Ed.* **2006**, *45*, 3474.
17. S. Kobayashi, Y. Yamashita, *Acc. Chem. Res.* **2011**, *44*, 58.
18. M. H. Chisholm, J. Gallucci, K. Phomphrai, *Chem. Commun.* **2003**, 48.
19. M. H. Chisholm, J. Gallucci, K. Phomphrai, *Inorg. Chem.* **2004**, *43*, 6717.
20. M. H. Chisholm, *Inorg. Chim. Acta* **2009**, *362*, 4284.
21. M. J. Saly, M. J. Heeg, C. H. Winter, *Inorg. Chem.* **2009**, *48*, 5303.
22. S. Datta, P. W. Roesky, S. Blechert, *Organometallics* **2007**, *26*, 4392.

23. S. Datta, M. T. Gamer, P. W. Roesky, *Organometallics* **2008**, *27*, 1207.
24. W. Clegg, E. K. Cope, A. J. Edwards, F. S. Mair, *Inorg. Chem.* **1998**, *37*, 2317.
25. C. F. Caro, P. B. Hitchcock, M. F. Lappert, *Chem. Commun.* **1999**, 1433.
26. S. Harder, *Organometallics* **2002**, *21*, 3782.
27. M. S. Hill, P. B. Hitchcock, *Chem. Commun.* **2003**, 1758.
28. M. R. Crimmin, I. J. Casely, M. S. Hill, *J. Am. Chem. Soc.* **2005**, *127*, 2042.
29. M. R. Crimmin, M. Arrowsmith, A. G. M. Barrett, I. J. Casely, M. S. Hill, P. A. Procopiou, *J. Am. Chem. Soc.* **2009**, *131*, 9670.
30. S. P. Sarish, A. Jana, P. W. Roesky, T. Schulz, M. John, S. Datta, *Inorg. Chem.* **2010**, *49*, 3816.
31. J. Jenter, R. Köppe, P. W. Roesky, *Organometallics* **2011**, *30*, 1404.
32. M. Rieckhoff, U. Pieper, D. Stalke, F. T. Edelmann, *Angew. Chem., Int. Ed.* **1993**, *32*, 1079.
33. V. Lorenz, B. Neumüller, K.-H. Thiele, *Z. Naturforsch., B: Chem. Sci.* **1995**, *50*, 71.
34. Y. Liu, P. Yang, J. Yu, X. J. Yang, J. D. Zhang, Z. Chen, Z. Chen, H. F. Schaefer, B. Wu, *Organometallics* **2008**, *27*, 5830.
35. Y. Liu, Y. Zhao, X. J. Yang, S. Li, J. Gao, P. Yang, Y. Xia, B. Wu, *Organometallics* **2011**, *30*, 1599.
36. J. Gao, Y. Liu, Y. Zhao, X. -J. Yang, Y. Sui, *Organometallics* **2011**, *30*, 6071.
37. I. L. Fedushkin, A. A. Skatova, V. A. Chudakova, G. K. Fukin, S. Dechert, H. Schumann, *Eur. J. Inorg. Chem.* **2003**, 3336.
38. I. L. Fedushkin, A. A. Skatova, V. A. Chudakova, V. K. Cherkasov, S. Dechert, H. Schumann, *Russ. Chem. Bull., Int. Ed.* **2004**, *53*, 2142.
39. I. L. Fedushkin, A. G. Morozov, O. V. Rassadin, G. K. Fukin, *Chem. Eur. J.* **2005**, *11*, 5749.
40. I. L. Fedushkin, A. A. Skatova, S. Y. Ketkov, O. V. Eremenko, A. V. Piskunov, G. K. Fukin, *Angew. Chem., Int. Ed.* **2007**, *46*, 4302.
41. I. L. Fedushkin, O. V. Eremenko, A. A. Skatova, A. V. Piskunov, G. K. Fukin, S. Y. Ketkov, E. Irran, H. Schumann, *Organometallics* **2009**, *28*, 3863.
42. T. K. Panda, K. Kaneko, O. Michel, K. Pal, H. Tsurugi, K. W. Törnroos, R. Anwender, K. Mashima, *Organometallics* **2012**, *31*, 3178.
43. V. Lorenz, C. G. Hrib, D. Grote, L. Hilfert, M. Krasnopolski, F. T. Edelmann, *Organometallics* **2013**, *32*, 4636.

44. Y. Liu, Y. Zhao, X. -J. Yang, S. Li, J. Gao, P. Yang, Y. Xia, B. Wu, *Organometallics* **2011**, *30*, 1599.
45. K.-H. Thiele, V. Lorenz, G. Thiele, P. Zoenchen, J. Scholz, *Angew. Chem., Int. Ed. Engl.* **1994**, *33*, 1372; *Angew. Chem.* **1994**, *106*, 1461.
46. J. A. C. Clyburne, R. D. Culp, S. Kamepalli, A. H. Cowley, A. Decken, *Inorg. Chem.* **1996**, *35*, 6651.
47. F. S. Mair, R. Manning, R. G. Pritchard, J. E. Warren, *Chem. Commun.* **2001**, 1136.
48. R. J. Baker, R. D. Farley, C. Jones, M. Kloth, D. M. Murphy, *Chem. Commun.* **2002**, 1196.
49. R. J. Baker, A. J. Davis, C. Jones, M. Kloth, *J. Organomet. Chem.* **2002**, *656*, 203.
50. R. J. Baker, C. Jones, M. Kloth, D. P. Mills, *New J. Chem.* **2004**, *28*, 207.
51. R. J. Baker, C. Jones, D. M. Murphy, *Chem. Commun.* **2005**, 1339.
52. X.-J. Yang, J. Yu, Y. Liu, Y. Xie, H. F. Schaefer, Y. Liang, B. Wu, *Chem. Commun.* **2007**, 2363.
53. J. Yu, X.-J. Yang, Y. Liu, Z. Pu, Q.-S. Li, Y. Xie, H. F. Schaefer, B. Wu, *Organometallics* **2008**, *27*, 5800.
54. A. Hinchcliffe, F. S. Mair, E. J. L. McInnes, R. G. Pritchard, J. E. Warren, *Dalton Trans.* **2008**, 222.
55. C. Jones, A. Stasch, W. D. Woodul, *Chem. Commun.* **2009**, 113.
56. Y. Liu, S. Li, X.-J. Yang, P. Yang, B. Wu, *J. Am. Chem. Soc.* **2009**, *131*, 4210.
57. Y. Zhao, Y. Liu, Z. Wang, W. Xu, B. Liu, J.-H. Su, B. Wu, X.-J. Yang, *Chem. Commun.* **2015**, *51*, 1237.
58. Y. Zhao, Y. Li, Q.-S. Li, J.-H. Su, *Dalton Trans.* **2016**, *45*, 246.
59. K. Izod, W. Clegg, S. T. Liddle, *Organometallics*, **2001**, *20*, 367.
60. A. J. Wooles, M. Gregson, O. J. Cooper, A. Middleton-Gear, D. P. Mills, W. Lewis, A. J. Blake, S. T. Liddle, *Organometallics*, **2011**, *30*, 5314.
61. A. J. Wooles, M. Gregson, S. Robinson, O. J. Cooper, D. P. Mills, W. Lewis, A. J. Blake, S. T. Liddle, *Organometallics*, **2011**, *30*, 5326.
62. T. F. Prisner, *Adv. Magn. Opt. Reson.* **1997**, *20*, 245.
63. S. Stoll, G. Jeschke, M. Willer, A. Schweiger, *J. Magn. Reson.* **1998**, *130*, 86.
64. R.-A. Eichel, A. Schweiger, *J. Magn. Reson.* **2001**, *152*, 276.
65. J. Emsley, *The Elements*, Oxford University Press, New York, 1st edn, **1989**.

66. E. K. Cope-Eatough, F. S. Mair, R. G. Pritchard, J. E. Warren, R. J. Woods, *Polyhedron*, **2003** *22*, 1447.
67. T. V. Laine, M. Klinga, A. Maaninen, E. Aitola, M. Leskelä, *Acta Chem. Scand.* **1999**, *53*, 968.
68. B. Zelenay, R. Frutos-Pedreno, J. Markalain-Barta, E. Vega-Isa, A. J. P. White, S. Diez-Gonzalez, *Eur. J. Inorg. Chem.* **2016**, 4649.
69. T. J. Knisley, M. J. Saly, M. J. Heeg, J. L. Roberts, C. H. Winter, *Organometallics* **2011**, *30*, 5010.
70. T. Pugh, S. D. Cosham, J. A. Hamilton, A. J. Kingsley, A. L. Johnson, *Inorg. Chem.* **2013**, *52*, 13719.
71. J. Long, B. G. Shestakov, D. Liu, L. F. Chibotaru, Y. Guari, A. V. Cherkasov, G. K. Fukin, A. A. Trifonov, J. Larionova, *Chem. Commun.* **2017**, *53*, 4706.
72. J. Scholz, A. Dietrich, H. Schumann, K.-H. Thiele, *Chem. Ber.* **1991**, *124*, 1035.
73. K. Mashima, Y. Matsuo, K. Tani, *Organometallics* **1999**, *18*, 1471.
74. F. Amor, P. Gomez-Sal, P. Royo, J. Okuda, *Organometallics* **2000**, *19*, 5168.
75. A. Galindo, A. Ienco, C. Mealli, *New J. Chem.* **2000**, *24*, 73.
76. Y. Matsuo, K. Mashima, K. Tani, *Angew. Chem., Int. Ed.* **2001**, *40*, 960.
77. K. Mashima, A. Nakamura, *J. Organomet. Chem.* **2001**, *621*, 224.
78. Y. Matsuo, K. Mashima, K. Tani, *Organometallics* **2002**, *21*, 138.
79. P. J. Daff, M. Etienne, B. Donnadieu, S. Z. Knottenbelt, J. E. McGrady, *J. Am. Chem. Soc.* **2002**, *124*, 3818.
80. H. Tsurugi, T. Ohno, T. Yamagata, K. Mashima, *Organometallics* **2006**, *25*, 3179.
81. C. Stanciu, M. E. Jones, P. E. Fanwick, M. M. Abu-Omar, *J. Am. Chem. Soc.* **2007**, *129*, 12400.
82. W. Kaim, *Chemtracts* **2007**, *20*, 292.
83. K. A. Kreisel, G. P. A. Yap, K. H. Theopold, *Inorg. Chem.* **2008**, *47*, 5293.
84. H. Tsurugi, T. Ohno, T. Kanayama, R. A. Arteaga-Meller, K. Mashima, *Organometallics* **2009**, *28*, 1950.
85. H. Tsurugi, T. Saito, H. Tanahashi, J. Arnold, K. Mashima, *J. Am. Chem. Soc.* **2011**, *133*, 18673.
86. A. F. Greene, P. Chandrasekaran, Y. Yan, J. T. Mague, J. P. Donahue, *Inorg. Chem.* **2014**, *53*, 308.
87. H. Tanahashi, H. Ikeda, H. Tsurugi, K. Mashima, *Inorg. Chem.* **2016**, *55*, 1446.

88. L. K. Johnson, C. M. Killian, M. Brookhart, *J. Am. Chem. Soc.* **1995**, *117*, 6414.
89. L. K. Johnson, S. Mecking, M. Brookhart, *J. Am. Chem. Soc.* **1996**, *118*, 267.
90. E. Rijnberg, J. Boersma, J. T. B. H. Jastrzebski, M. T. Lakin, A. L. Spek, G. van Koten, *Organometallics* **1997**, *16*, 3158.
91. L. Johansson, O. B. Ryan, M. Tilset, *J. Am. Chem. Soc.* **1999**, *121*, 1974.
92. D. J. Tempel, L. K. Johnson, R. L. Huff, P. S. White, M. Brookhart, *J. Am. Chem. Soc.* **2000**, *122*, 6686.
93. L. Johansson, M. Tilset, J. A. Labinger, J. E. Bercaw, *J. Am. Chem. Soc.* **2001**, *123*, 739.
94. A. H. Zhong, J. A. Labinger, J. E. Bercaw, *J. Am. Chem. Soc.* **2002**, *124*, 1378.
95. C. S. B. Gomes, P. T. Gomes, M. T. Duarte, *J. Organomet. Chem.* **2014**, *760*, 101.
96. V. Yempally, S. J. Kyran, R. K. Raju, W. Y. Fan, E. N. Brothers, D. J. Darensbourg, A. A. Bengali, *Inorg. Chem.* **2014**, *53*, 4081.
97. M. V. Vollmer, C. W. Machan, M. L. Clark, W. E. Antholine, J. Agarwal, H. F. Schaefer III, C. P. Kubiak, J. R. Walensky, *Organometallics* **2015**, *34*, 3.
98. B. Manna, A. V. Desai, N. Kumar, A. Karmakar, S. K. Ghosh, *CrystEngComm* **2015**, *17*, 8796.
99. B. Zelenay, R. Frutos-Pereno, J. Markalain-Barta, E. Vega-Isa, A. J. P. White, S. Diez-Gonzalez, *Eur. J. Inorg. Chem.* **2016**, 4649.
100. F. T. Edelmann, D. M. M. Freckmann, H. Schumann, *Chem. Rev.* **2002**, *102*, 1851.
101. W. E. Piers, D. J. H. Emslie, *Coord. Chem. Rev.* **2002**, *233-234*, 131.
102. A. A. Trifonov, *Russ. Chem. Rev.* **2007**, *76*, 1051.
103. A. Trifonov, in *Olefin upgrading catalysis by nitrogen-based metal complexes*, ed. G. Giambastiani, J. Cámpora, Springer, **2011**, 119.
104. F. G. N. Cloke, *Chem. Soc. Rev.* **1993**, *22*, 17.
105. F. G. N. Cloke, H. C. de Lemos, A. A. Sameh, *J. Chem. Soc., Chem. Commun.* **1986**, 1344.
106. A. Recknagel, M. Noltemeyer, F. T. Edelmann, *J. Organomet. Chem.* **1991**, *410*, 53.
107. H. Görls, B. Neumüller, A. Scholz, J. Scholz, *Angew. Chem., Int. Ed. Engl.* **1995**, *34*, 673.
108. A. A. Trifonov, *Eur. J. Inorg. Chem.* **2007**, 3151.
109. P. Poremba, F. T. Edelmann, *J. Organomet. Chem.* **1997**, *549*, 101.

110. T.V. Petrovskaya, I. L. Fedushkin, V.L. Nevodchikov, M. N. Bochkarev, N.V. Borodina, I. L. Eremenko, S. E. Nefedov, *Russ. Chem. Bull.* **1998**, *47*, 2341.
111. J. Scholz, H. Görls, H. Schumann, H. Weimann, *Organometallics* **2001**, *20*, 4394.
112. A. A. Trifonov, E. A. Fedorova, G. K. Fukin, E. V. Baranov, N. O. Druzhkov, M. N. Bochkarev, *Chem. Eur. J.* **2006**, *12*, 2752.
113. J. A. Moore, A. H. Cowley, J. C. Gordon, *Organometallics*, **2006**, *25*, 5207.
114. A. A. Trifonov, I. A. Borovkov, E. A. Fedorova, G. K. Fukin, J. Larionova, N. O. Druzhkov, V. K. Cherkasov, *Chem. Eur. J.* **2007**, *13*, 4981.
115. M. D. Walter, D. J. Berg, R. A. Andersen, *Organometallics*, **2007**, *26*, 2296.
116. P. Cui, Y. Chen, G. Wang, G. Li, W. Xia, *Organometallics* **2008**, *27*, 4013.
117. T. V. Mahrova, G. K. Fukin, A. V. Cherkasov, A. A. Trifonov, *Russ. Chem. Bull.* **2008**, *57*, 2285.
118. T. V. Mahrova, G. K. Fukin, A. V. Cherkasov, A. A. Trifonov, N. Ajellal, J.-F. Carpentier, *Inorg. Chem.* **2009**, *48*, 4258.
119. H. Kaneko, H. Nagae, H. Tsurugi, K. Mashima, *J. Am. Chem. Soc.* **2011**, *133*, 19626.
120. A. A. Trifonov, B. G. Shestakov, K. A. Lyssenko, J. Larionova, G. K. Fukin, A. V. Cherkasov, *Organometallics* **2011**, *30*, 4882.
121. B. G. Shestakov, T. V. Mahrova, J. Larionova, J. Long, A. V. Cherkasov, G. K. Fukin, K. A. Lyssenko, W. Scherer, C. Hauf, T. V. Magdesieva, O. A. Levitskiy, A. A. Trifonov, *Organometallics* **2015**, *34*, 1177.
122. B. G. Shestakov, T. V. Makhrova, K. A. Lyssenko, A. A. Trifonov, *Russ. Chem. Bull., Int. Ed.* **2013**, *62*, 412.
123. I. L. Fedushkin, A. A. Skatova, D. S. Yambulatov, A. V. Cherkasov, S. V. Demeshko, *Russ. Chem. Bull., Int. Ed.* **2015**, *64*, 38.
124. H. Liao, L. Zhong, Z. Xiao, T. Zheng, H. Gao, Q. Wu, *Chem. Eur. J.* **2016**, *22*, 14048.
125. D. S. Yambulatov, A. A. Skatova, A. V. Cherkasov, I. L. Fedushkin, *Russ. Chem. Bull., Int. Ed.* **2017**, *66*, 1187.
126. I. L. Fedushkin, D. S. Yambulatov, A. A. Skatova, E. V. Baranov, S. Demeshko, A. S. Bogomyakov, V. I. Ovcharenko, E. M. Zueva, *Inorg. Chem.* **2017**, *56*, 9825.
127. T. Sakakura, H.-J. Lautenschläger, M. N. Tanaka, *J. Chem. Soc., Chem. Commun.* **1991**, 40.
128. A. G. Molander, M. J. Julius, *Org. Chem.* **1992**, *57*, 6347.
129. A. G. Molander, W. H. Retsch, *J. Am. Chem. Soc.* **1997**, *119*, 8817.

130. A. G. Molander, E. D. Dowdy, B. C. Noll, *Organometallics* **1998**, *17*, 3754.
131. A. G. Molander, C. P. Corrette, *Organometallics* **1998**, *17*, 5504.
132. A. G. Molander, E. E. J. Knight, *Org. Chem.* **1998**, *63*, 7009.
133. T. I. Gountchev, T. D. Tilley, *Organometallics* **1999**, *18*, 5661.
134. A. R. Muci, J. E. Bercaw, *Tetrahedron Lett.* **2000**, *41*, 7609.
135. A. A. Trifonov, T. P. Spaniol, J. Okuda, *Dalton Trans.* **2004**, *33*, 2245.
136. K. Takaki, K. Sonoda, T. Kousaka, G. Koshiji, T. Shishido, K. Takehira, *Tetrahedron Lett.* **2001**, *42*, 9211.
137. K. Takaki, K. Komeyama, K. Takehira, *Tetrahedron* **2003**, *59*, 10381.
138. Y. Horino, T. Livinghouse, *Organometallics* **2004**, *23*, 12.
139. M. Rastatter, A. Zulys, P. W. Roesky, *Catalysis. Chem. Commun.* **2006**, 874.
140. J. Li, C. Zhao, J. Liu, H. Huang, F. Wang, X. Xu, C. Cui, *Inorg. Chem.* **2016**, *55*, 9105.
141. Y. Shi, J. Li, C. Cui, *Dalton Trans.* **2017**, *46*, 10957.
142. M. D. Hannant, M. Schormann, M. Bochmann, *J. Chem. Soc., Dalton Trans.* **2002**, 4071.
143. F. Stoffelbach, R. Poli, P. Richard, *J. Organomet. Chem.* **2002**, *663*, 269.
144. F. Stoffelbach, P. Richard, R. Poli, T. Jenny, C. Savary, *Inorg. Chim. Acta* **2006**, *359*, 4447.
145. C. Roukoss, S. Fiddy, A. de Mallmann, N. Rendon, J.-M. Basset, E. Kuntz, C. Coperet, *Dalton Trans.* **2007**, 5546.
146. S. Anga, K. Naktode, H. Adimulam, T. K. Panda, *Dalton Trans.* **2014**, *43*, 14876.
147. Y. Liu, L. Yang, *Chin. J. Chem.* **2015**, *33*, 473.
148. H. Nishiyama, H. Ikeda, T. Saito, B. Kriegel, H. Tsurugi, J. Arnold, K. Mashima, *J. Am. Chem. Soc.* **2017**, *139*, 6494.
149. J. Liu, W. Chen, J. Li, C. Cui, *ACS Catal.* **2018**, *8*, 2230.
150. https://pubs.acs.org/doi/suppl/10.1021/acscatal.8b00010/suppl_file/cs8b00010_si_001.pdf
151. K. Kunz, G. Erker, G. Kehr, R. Fröhlich, *Organometallics* **2001**, *20*, 392.
152. C. Glock, H. Görls, M. Westerhausen, *Eur. J. Inorg. Chem.* **2011**, 5288.
153. C. Glock, F. M. Younis, S. Ziemann, H. Görls, W. Imhof, S. Kriek, M. Westerhausen, *Organometallics* **2013**, *32*, 2649.
154. J. Jenter, M. T. Gamer, P. W. Roesky, *Organometallics* **2010**, *29*, 4410.

155. D. Walther, *Z. Chem.* **1974**, *14*, 285.
156. A. Scholz, K.-H. Thiele, J. Scholz, R. Weimann, *J. Organomet. Chem.* **1995**, *501*, 195.
157. Y. Zhao, Y. Liu, Z. Wang, W. Xu, B. Liu, J.-H. Su, B. Wu, X.-J. Yang, *Chem. Commun.* **2015**, *51*, 1237.
158. J. Li, H. Huang, F. Wang, C. Cui, *Organometallics* **2015**, *34*, 683.

7. Liste der Veröffentlichungen

Journals

H. H. Haeri, R. Duraisamy, N. Harmgarth, P. Liebing, V. Lorenz, D. Hinderberger, F. T. Edelmann, *ChemistryOpen* **2018**, 7, 701.